Powder spreading and spreadability in the additive manufacturing of metallic materials: a critical review

Journal of Materials Processing Tech.

Powder spreading and spreadability in the additive manufacturing of metallic materials: a critical review

--Manuscript Draft--

Manuscript Number:	PROTEC-D-22-00722R2
Article Type:	Review Article
Keywords:	Spreadability; Flowability; Laser Powder Bed Fusion (LPBF); Electro Beam Melting (EBM)
Corresponding Author:	Emilio Bassini, Ph.D Politecnico di Torino Torino, ITALY
First Author:	Luigi C. Capozzi
Order of Authors:	Luigi C. Capozzi
	Antonio Sivo
	Emilio Bassini, Ph.D
Abstract:	This review aims to build a coherent picture of the problem of powder spreading and spreadability in metal Additive Manufacturing (AM) because of its impact on ensuring highly consistent production, optimization of the process and reduction of the manufacturing costs. The review shows the current progress in understanding spreading dynamics, the role of powder characteristics, the spreading systems and the testing tools developed for assessing powder spreadability. The problem of finding appropriate quantitative metrics and the recent advances in the use of standardized methods to assess powder spreadability is critically discussed. Attention is given to future trends and research gaps and opportunities.

Cover Letter (this item must contain a statement that the submission is original and is not being submitted for publication

To, 21/03/2022

Dear Dr. Cao,

My name is Emilio Bassini, I'm a researcher working in the Material Science and Technology department at Politecnico di Torino.

I'm writing to you following the Journal of Materials Processing Technology guide for authors regarding the possibility of publishing a review paper on the journal mentioned above.

As anticipated, I'd ask you, as the editor in chief, if the following review could be suitable for JMPT.
The review title is "Powder spreading and spreadability in the additive manufacturing process".

Powder spreading and spreadability is a relatively new topic. However, its importance is growing quickly as researchers in academia and practitioners in the industry are eager to improve the AM process's quality, reliability, and replicability. In this review, after a quick glimpse into powder-based AM manufacturing, we analyze the current state of research and understanding about powder spreading to put together a coherent picture of the current knowledge.
Based on the works published in the literature, we try to rationalize the concept of powder spreadability and give a clear picture of the proposals done by many researchers to quantify spreadability through the definition of new metrics and correlate them with the physical and bulk properties of the powders.

This topic could be suitable and attractive for the journal readership since powder spreadability is closely connected with processing technology related to additive manufacturing. Therefore, we kindly ask you to consider this work for possible consideration for these reasons.

The work consists of ca. 55 pages and contains 112 references. No work from the co-authors of this review was cited; therefore, the **self-citation percentage equals 0.**
Attentions were given to theoretical and practical topics, trying to build a document to help researchers and end-users.
The work also contains many references to the simulation techniques commonly used to assess this physical problem.
The paper underlines which models or experiments provide higher reliability, guiding people involved in the AM field to higher quality standards, providing a more robust knowledge of those phenomena intercurring during each powder layer spreading.

Furthermore, as required in the guide, we would like to mention that all the authors of this work have already published several works concerning the AM world with many citations from the academic catchment.

Finally, since this is a requirement for entering the publishing process on JMPT, I'd like to mention that in 2019, I was able to publish a paper In JMPT regarding the application of the Hot Isostatic Pressing as a near-net-shape processing technology applied to a Nickel-based alloy. The paper DOI is provided below.

The main points contained in this review can be summarized as follows:

- This review aims to discuss powder spreading and spreadability for additive manufacturing purposes intensely.
- In-depth knowledge of spreadability can drastically improve the AM process's quality, reliability, and replicability.
- This review analyzes the current state of research and understanding about powder spreading
- The review aims to give a clear picture of the current knowledge of powder spreadability to help researchers and final users to achieve higher part density and lower superficial roughness.

- The work gives a tool to quantify spreadability using quantitative metrics and correlate them with the physical and bulk properties of the powders.

I want to thank you for your kind attention, and I hope that this paper could be of interest to you and the journal's readership.

The submission is original and was not submitted to any other journal but JMPT for evaluation.

Best regards

Emilio Bassini Ph.D.
Department of Applied Science and Technology
Politecnico di Torino
Corso Duca degli Abruzzi 24,
Torino, Italy

Rebuttal

References were updated according to the AE suggestions and the guide for authors, even if that section is not completely clear. Edits were done manually since the Mendeley template uses parenthesis.

Works are now cited separately every time. The only exception is on page 32, where the paragraph is written in bullet form. Thus a more concise version was preferred.

Declaration of interests

☒The authors declare that they have no known competing financial interests or personal relationships that could have appeared to influence the work reported in this paper.

☐The authors declare the following financial interests/personal relationships which may be considered as potential competing interests:

Powder spreading and spreadability in the additive manufacturing of metallic material: a critical review

Luigi C. Capozzi, Antonio Sivo, Emilio Bassini

Abstract

This review aims to build a coherent picture of the problem of powder spreading and spreadability in metal Additive Manufacturing (AM) because of its impact on ensuring highly consistent production, optimization of the process and reduction of the manufacturing costs. The review shows the current progress in understanding spreading dynamics, the role of powder characteristics, the spreading systems and the testing tools developed for assessing powder spreadability. The problem of finding appropriate quantitative metrics and the recent advances in the use of standardized methods to assess powder spreadability is critically discussed. Attention is given to future trends and research gaps and opportunities.

Keywords:

Spreadability; Flowability; Laser Powder Bed Fusion (LPBF); Electro Beam Melting (EBM);

Introduction

Additive manufacturing (AM) has seen significant growth in the last few years because it is a technology for prototyping or production of metallic components from scratch. ASTM defined AM as *"a process of joining materials to make objects from 3D model data, usually layer upon layer, as opposed to subtractive manufacturing methodologies"*. This technology may generate less waste than traditional processes, the production is distributed, and the printed component can be easily customized as discussed by **Liao and Cooper, (2021)**. On the other hand, **Hu and Mahadevan, (2017)** evidenced that the replicability and the variations in the quality of the final components produced with additive manufacturing are barriers to the massive use of this technology at the industrial level.

In recent years, significant efforts are aimed at developing adequate standards and specifications for AM process, monitoring the process to improve quality and production throughput, increasing the knowledge of raw materials, their behavior during the AM process, and the effect on the final components as discussed by **Frazier (2014)**.

AM community has put forward a great deal of challenges in characterizing and understanding powder materials, their behavior, and processability. In the context of AM technologies that use powder beds, the behavior of powder during the spreading process is not entirely understood. In the recent past, researchers and practitioners have frequently put powder spreading in strong connection with powder flowing or even used the concept of flowability as synonymous with spreadability as discussed in the work of **Zhang et al. (2018)**. Moreover, many tries have been done to correlate standardized measurements to spreadability. Still, they often failed because standardized tests are far from the typical conditions occurring during the powder spreading.

Powder spreading and spreadability is a relatively new topic. Its importance is growing quickly as researchers in academia and practitioners in the industry are eager to improve the quality, reliability, and replicability of the AM process. In this review, after a quick glimpse into powder-based AM manufacturing, we will analyze the current state of research and understanding about powder spreading, trying to put together a coherent picture of the current knowledge. On the basis of the works published in the literature, we will also try to rationalize the concept of powder spreadability and give a clear picture of the proposals done by many researchers to quantify spreadability through the definition of new metrics and correlate them with physical and bulk properties of the powders.

1. Additive manufacturing processes

1.1 Powder-based AM processes

Powder bed fusion (PBF) technology uses a localized heat source to melt or sinter powders that are previously spread over the build platform, finally forming a dense layer; a schematic of PBF equipment is shown in Figure 1. Once a layer has been printed, a new powder layer is spread and then melted or sintered. This process is repeated to fabricate components layer by layer. PBF technology includes selective laser sintering (SLS), selective laser melting (SLM), and electron beam melting (EBM) processes, according to the fact the powder is sintered o melted, and the heat source is a laser or electron beam.

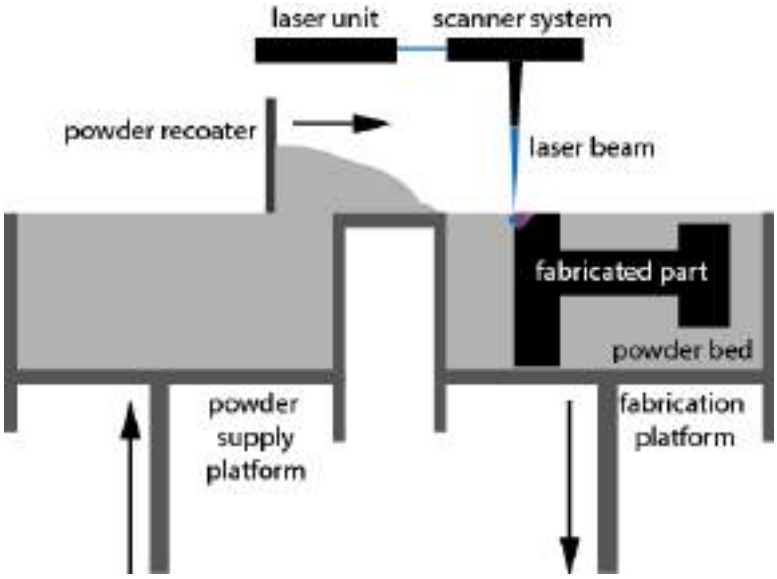

Figure 1 - Illustration of laser powder bed fusion.

In the SLS process, metal powders are spread to form thin bed layers, sintered or partially melted with a high-energy laser, followed by rapid cooling. A high- powered laser selectively melts the metal powder into layers of 20 – 100 µm. After that, a new powder layer is spread, and, again, the heat provided by the laser selectively melts the powders together and with the dense layer below. In SLS, the heat supplied to the powder is tuned in order to avoid powder melting but only sintering**. Bo et al. (2020)** showed that in the SLM process, metal powders are spread to form thin bed layers and melted using a high-energy laser followed by rapid cooling. However, in this case, the heat supplied by the laser is sufficient to melt the metal powder completely. The process is conducted in an inert chamber filled with nitrogen or argon, and the build platform can be heated to reduce the onset of residual thermal stress. The achievable temperature widely varies depending on the machine layout and capabilities. A

postprocessing heat treatment is often required to remove the internal stresses due to thermal changes occurring in the rapid melting and cooling. EBM process uses a focused electron beam within a vacuum chamber to melt the powder layer. The chamber is usually kept up to 700 °C to minimize temperature gradients and reduce the consequent residual stress within the fabricated components. These technologies can produce near net shape components, but SLM results in more accurate components with better surface quality. On the other hand, EBM is faster and produces components with lower residual stresses as reported by **Tan et al. (2017).**

Direct Energy Deposition (DED)

DED, also referred to as blown powder AM (BPAM), involves the introduction of metal powder to a heat source, such as a laser, electron beam or plasma arc, which melts the metal powders or wires together as they are deposited. According t**o Molitch-Hou (2018)**, the first application for DED dates back to 1988.

According to **Sing et al. (2019),** powders result in lower deposition efficiency than metal wires as only a part of the total powder would be melted and bonded to the substrate. Like Electron beam melting, electron beam systems in DED require a vacuum and typically do not have high oxidation issues. On the other hand, laser DED systems require other methods to introduce inert gases. Powder DED machines often have inert gas blown together with the powder from the nozzles, thereby sheathing the melted region, reducing the oxidization rate. Because of the technology's ability to inject metal powder directly into the heat source, often attached to a 4- or 5-axis arm, DED systems are not limited to working onto a flat substrate. Instead, it is possible to print metal onto curved surfaces, such as existing metal structures, e.g. moulds.

For this reason, DED is often used to repair damaged parts, particularly in the aerospace industry. DED machines are also known for producing large components to near net shape before they are machined to their final geometries. This technique requires the powder to flow in a dedicated hose, connecting the feedstock to the nozzle using a different mechanism to powder bed systems. For this reason, this technique is not further detailed in this review.

Besides those techniques which require a heat input to sinter or melt powders, there is also an additive manufacturing technique that does not require any heating source, at least during the printing stage, i.e. binder jetting (BJ). The origin of metal BJ technology dates to 1993 when the Massachusetts Institute of Technology (MIT) developed an inkjet-based process to create three-dimensional objects using metal powders. The process begins by spreading a thin layer of powder, with printheads depositing binder droplets into the powder bed. The printing plate then lowers, and another layer of powder is spread. The process is repeated until the part is complete. Unused powders are efficiently recycled. The as-bound component is referred to as green, a metal casting term that refers to the relatively fragile material used for sand casting moulds. After the printing phase, curing, debinding, and sintering steps must be provided to obtain the final component. Each phase can be slightly different

depending on the processed material and the machine brand. For example, curing can be achieved via ambient air exposure or with the help of thermal or UV curing.

This process, initially designed for metallic powders, was also efficiently applied to ceramic materials as described by **Chen et al. (2022)**, who realized samples made of alumina via BJ.

However, Lecis et al. (2021b) evidenced that powder packing, wettability with the binder and sinterability are essential parameters that must be tailored to achieve desired material properties. At the same time, other authors, such as Roberts et al. (2020), stated that BJ components typically have a low overall density in the green state and high shrinkage and deformation after heat treatment. They also suggested that these properties can be improved by including nanoparticles of the same material in the binder as the nanoparticles can fill the interstices and pore throats between the bed particles.

Similarly to other AM techniques, BJ has several important parameters to tailor before obtaining proper density values. **Mostafaei et al. (2021), for** example, indicated binder saturation and drying time as vital parameters to process WC-Co composites properly.

Mariani et al. (2021) used this technique to fabricate WC-12%Co samples via binder jetting, then sintered in a low-pressure furnace at 1400 °C. The application of BJ span an extensive material range: Lecis et al. (2021a), for example, processed 316L stainless. More specifically, their study showed how this new technology could effectively produce metal parts with mechanical properties comparable with products obtained with traditional techniques and with other additive processes (e.g. Selective Laser Melting).

Romano et al. (2022) demonstrated that BJ can be efficiently used also to additively process materials powders with very low laser absorbance, such as Copper. In this work, a fine high-purity copper powder with a D_{50} of 3.4 µm was used to assess the sintering process in depth.

Even though several AM techniques are available to researchers and end-users, in this review, the authors will focus on powder bed fusion techniques only being the most diffused.

1.2 Powders for AM

A fundamental ingredient of metal AM manufacturing is constituted by the powders used in the process. Each process requires specific powder size and powder size distributions, e.g. SLM requires fine powders, whereas a coarse powder is suitable for EBM. **According to Wang et al. (2022), different** powder systems will also lead to different layer structures when spread over the building platform. For this reason, the main differences among the most diffused systems are reviewed in the following paragraph.

The quality of the final components is influenced, among other many factors, by the shape of the powder, which mainly depends on their producing routes. The most common routes for producing metal powders for additive manufacturing include water atomization, gas atomization, plasma atomization, and plasma rotating electrode process. As shown in Table 1, each process produces powders with different particle shapes and particle size **distributions. The work of Wallner, (2019) showed** that in the water atomization process, the molten metal flow is broken into droplets by a water jet at high velocity and pressure, and the surface tension of the metal droplets gives them a spherical-like shape. These powders present an irregular morphology, which can represent a severe limitation for AM processes. Only a few works deal with powder flowability or spreadability of water atomized (WA) powders. Hoeges et al. (2017), for example, were able to obtain full-dense 316L samples using WA powders but significantly modifying the AM process parameters. According to these authors, 316 L WA powders have a considerably higher avalanche angle than traditional Gas Atomized (GA) ones. Nevertheless, the obtained results proved that WA powders are still usable in SLM systems. GA powders typically have avalanche angles close to 38°, while WA showed 58°.

Conversely, 316L GA and WA powders may show similar behaviour when tested with the Hall and Carney cups. The authors, indeed, noticed that no flow was possible in both systems. These results are directly inherited from the irregularities which characterize WA powders systems. On the other hand, spherical particles can be obtained by using gas atomization. **Sun et al. (2017) de**monstrated that the molten metal flow is perturbed and disintegrated by an inter gas jet at high pressure in the gas atomization process. The resulting particles are spherical with the presence of satellite particles because fine particles dragged by the gas circulating in the atomizing chamber can easily collide with the molten atomized particles. The presence of satellites is not desirable because they decrease powder flowability and spreadability. Plasma atomization consists of the atomization of metal wires by using plasma torches, followed by solidification. The advantage of plasma atomized powders lies in their high sphericity without the presence of satellite particles, in the narrow particle size distribution, and the high purity of the powder, as observed **by Kassym and Perveen, (2020). The** plasma rotating electrode process uses a plasma arc to melt a rod that, rotating rapidly, ejects the molten metal forming spherical particles. The resulting powders possessed a high spherical shape and a narrow particle size distribution.

On the other hand, **Sehhat et al. (2022) increased** powder sphericity by applying the induction plasma spheroidization process to 304L gas atomized powders. The authors reported that dense samples obtained from spheroidized powder have lower tensile strength but higher ductility. In addition, the authors affirmed that mechanical properties changed due to a severe alteration of the powders during the process. Indeed, the spheroidization process caused a strong carbon, nitrogen, and oxygen depletion, leading to a completely different powder microstructure during the re-solidification step. This fact was considered the main reason for reducing the tensile properties. Nevertheless, the process demonstrated to firmly lower the powder avalanche angle and break

energy with respect to as-received ones. Consequently, spheroidized powders have higher flowability than the as-received powder. This data suggests that the as-received material is more cohesive due to its larger asperity.

According to Riener et al. (2021) flowability and spreadability of powders may change with the passing of time depending on storage conditions. The authors underlined that powder, which was stored under humid conditions, results in a lower part density and lower mechanical strength. This deterioration in processability can be reversed by drying the powder in a vacuum drying oven before the SLM process.

Table 1 – Main characteristics of metal powder produces by gas atomization, water atomization, and plasma atomization process (Dawes et al. (2015); Kassym and Perveen, (2020).

Manufacturing process	*Particle size*	*Particle shape*	*Metals*
Water atomization	0–500 μm; wide particle size distribution	Irregular shape Presence of satellite particles	Ni, Co, Fe, Ti, Al
Gas atomization	0–500 μm; wide particle size distribution	Spherical shape Presence of satellite particles	Non-reactive
Plasma atomization	0 – 200 μm; narrow particle size distribution	Higly spherical shape	Ti
Plasma rotating electrode process	0 – 100 μm	Higly spherical shape	Ti

A complete and fruitful characterization of powder to be used in AM process remains a significant challenge because of the complexity of granular systems and their behaviour, see Figure 2, although some examples concerning numerous critical raw materials (CRM) can be found in the work of Popov et al. (2021). Some characteristics are intrinsic of the granular system, i.e. size, morphology, surface/bulk chemistry, and density, and are usually easily assessable. On the other hand, **Leturia et al. (2014) dem**onstrated that the ensemble behaviour not only depends on the physical/chemical characteristics of the powder but also on the external conditions or processing environment, e.g. temperature, humidity, forces applied.

The characterization of metal powders is a fundamental aspect as their behaviour influences the quality of the powder spread layer and, in turn, of the printed component. Researchers, **such as Spierings et al. (2016), and** practitioners usually assess the following characteristics of the powder:

1. Physical, chemical, optical, and thermal properties
2. Ability to form dense packings
3. Ability to easily flow during the spreading process

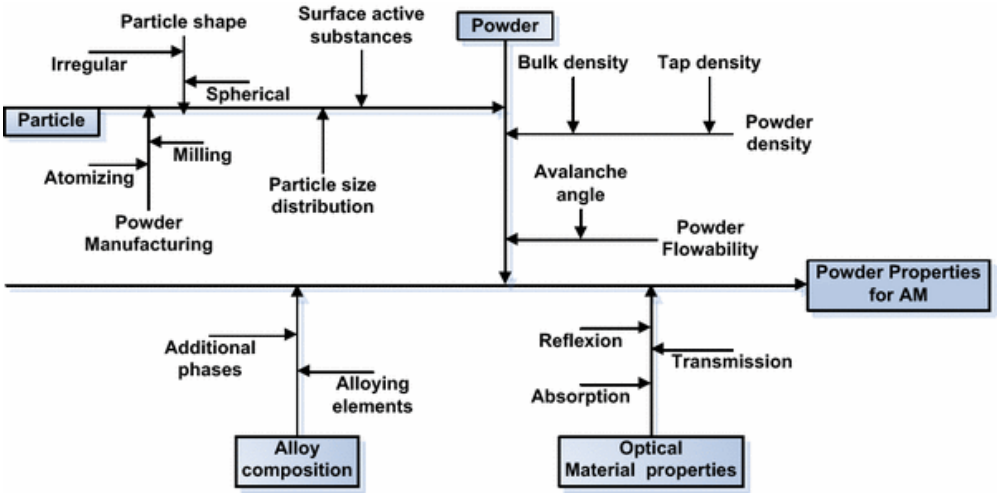

Figure 2 - Ishikawa diagram with influencing parameters for metal powders Spierings et al. (2016)

For example in the work **of Kirchner et al. (2016) the physical properties of different powder for AM application are compared against each others. The authors states that the particle** size distribution and morphology determine the powder flowability and packing density. As a consequence, these quantities control the powder's processability. Among all the observable effects when powders are changed, we can mention the feeding behaviour, the powder bed density and uniformity, or the roughness of the raked layer. These physical variables will affect the printing process parameters, which will be tailored accordingly. For example, finer powders will lead to a lower surface roughness of the samples but lower flowability. Another example comes from the comparison of powders for LPBF and EBM applications. Generally, powders for EBM applications have a larger particle size distribution. Consequently, flowability, apparent and tap density are higher than the SLM powders. Anyway, each system behaves differently and should be carefully analyzed and compared with values coming from literature.

2. Powder spreading

The spreading of powders is a fundamental step in AM and consists of distributing the powder over a large surface using a blade or a roller to form a thin layer before supplying radiant heat able to sinter or melt the layer in specific locations. Powder spreading represents a significant bottleneck in the AM based on powder beds because it strongly determines the quality of the final products.

Since early studies of AM, the spreading of powders has been seen as a fundamental issue in order to obtain metallic parts with good mechanical **properties. Van der Schueren and Kruth, (1995) focused** their attention on three different approaches for spreading the powders based on the use of a blade, a counter rolling cylinder, and, finally, a slot-feed system. They concluded that, contrary to the slot-feed system, both blade and counter rolling cylinder do not require high flow rates of the powder, although high flow rates result in more accurate layer deposition. The dimensional control in the vertical direction was investigated **by Lee et al. (1995). They developed** a model for layer displacement based on powder compressibility and applied load and point out as the results were highly dependent on the materials and particle shape.

It should be pointed out that only in recent years, powders spreadability has started to be studied systematically, using both experiments and simulations. The study of the spreading dynamic has been studied experimentally by the use of visual approaches able to capture the movement of the pile powders. On the other hand, simulations were extensively used as they are able to capture the dynamics of spreading at a smaller scale.

This section will present the basic spreading systems used in AM manufacturing and the main methods used to investigate the problem related to powder spreading.

2.1 Powder spreading systems

Many spreading systems have been employed in AM, such as rollers, comb blades, sweep blades, and moving hoppers. The simplest method to spread powders consists of using a thin blade (or rack) that sweeps and distributes a powder pile along with the building platform, see Figure 3a. The height of the blade gap and the velocity are the only process parameters set in such a system. In this case, powders are subjected to shear stress, but compressive stress is negligible.

In the case of roller type spreaders, the rolling and sliding movement determines a shear flow and, at the same time, exerts compressive stress to the powder. As shown in see Figure 3b, a counter-rotating roller slides along the building platform and rotates in the opposite direction so that the flowability is enhanced by the rotation and, at the same time, the powder is compacted under the roller gap. The main process parameters are the roller gap, its geometry, and its linear and rotational velocity. In the case of forward-rotating rollers (Figure 3c), the compression due to the roller can result in a higher packing density, but, in the case of powders with low flowability or a

relatively high adhesion, the interaction of the roller with the surface of the layer may result in an incomplete or non-uniform spreading or, in the worst cases, in the formation of craters in the layer.

Blades generally produce layers with lower quality and packing density as described in the work of Yang et al. (2017). As Haeri, (2017) suggested, a roller produces more compact and smoother layers because of its larger contact area that allows a gradual particle rearrangement. On the other hand, a blade produces less compact layers with greater roughness because it only drags the particles in its movement and negligible compression. A blade spreader can not be improved simply by increasing its contact area but modifying its head profile, i.e. a super-elliptic profile as can be found in **the work of Haeri, (2017).**

As shown in Figure 3d, a different strategy for spreading powders consists of using a blade and forward-rotating roller simultaneously, although, to our best knowledge, this strategy is not commonly used in the AM. This system might be able to compensate for the lack of compaction due to the use of a blade by using a forward-rotating roller, which in this case could act mainly to compact the powders and not to spread them.

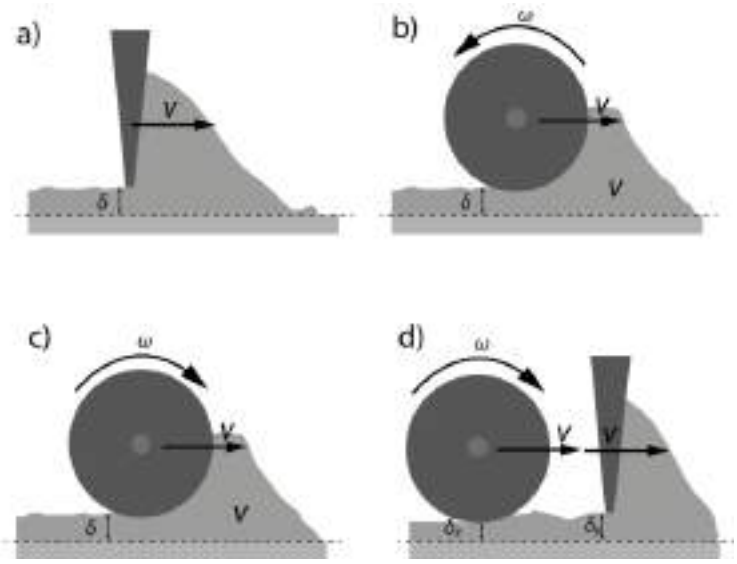

Figure 3. Schematic of AM spreading systems: a) blade, b) counter-rotating roller, c) forward-rotating roller, d) combination of a blade and a forward-rotating roller.

The fundamental AM spreading parameters are the type of spreader, the spreading speed and eventually roller rotation, and the gap height. It is reported that the typical spreading speed of blade spreaders is up to 150 mm/s, whereas, in the case of the roller, the translational velocity is in the range of 5-130 mm/s, and its rotation speed between 250-350 mm/s as suggested by **Oropeza et al. (2021). A**lthough it would be desirable to conduct the spreading as fast as possible to increase productivity, the limitation on the quality of the spread layer imposes a

compromise. The gap height used in the AM equipment is related to the category of AM technology used. As shown in Table 2, the use of laser as a heating source limits the layer thickness to approximately 20 and 100 μm, whereas electron beam can be used to thicker layers from 50 to 200 μm. Of course, the use of different AM technology requires different metals and powders with different size distribution.

In addition, authors like **Wang et al. (2021)** performed discrete element method (DEM) simulations to show differences among spreader geometries. The authors, for example, stated that round and inclined surfaces of blade spreaders allow more particles in the compact region to be deposited compared with vertical blades; thus, the powder layer formed is denser. Furthermore, roller systems have the largest particle motion conflict; thus, powder layers formed are sparse and inhomogeneous with small layer gaps. Finally, they also highlighted that size segregation in blade systems is not as severe as in roller systems.

Similarly, also **Mussatto et al. (2020)** investigated the combined effect of powder morphology, spreading velocity and layer thickness on the powder bed topography uniformity. The authors evidenced that particles sphericity and surface texture influence how much the spreader velocity and the layer thickness may alter the quality of powder bed layers. Secondly, the spreader velocity always impacted the powder bed uniformity, and better uniformity is achieved with spreading velocities $\leq$ 80 mm/s.

Phua et al. (2021) used the Discrete Element Method to assess the recoater geometry and speed effects. More specifically, they compared a toothed and a solid rake noticing that recoater velocity strongly impacts the degree of particle circulation and size segregation. Furthermore, particle circulation was enhanced by the toothed recoater, while solid recoater caused more size segregation.

Table 2 - AM technologies used in processing metal powders.

Category	*Process*	*Heat source / temperature*	*Raw materials (metals)*	*Powder size distribution (approx.)*	*Layer thickness (approx.)*	*Ref.*
Powder-bed fusion	Selective Laser Melting (SLM)	high-intensity laser / above melting point	Iron-based (316L, 420, M2), titanium and titanium based (Ti6Al4V, TiAl), aluminium-based (AlSi, AlCu, AlZn), nickel-based (Inconel 625, 718), copper, niobium, tantalum, bio-material metals–polymers and metals–ceramics combinations	10 – 50 µm	20 – 100 µm	Bo et al. (2020; Chin et al. (2020; Tiwari et al. (2015)
	Selective Laser Sintering (SLS)	high-intensity laser / below melting point				
	Electron Beam Melting (EBM)	Electron Beam / above melting point	Ti grade 2, Ti6Al4V, Inconel 718, CoCrMo; alloys having volatile constituents, e.g. Zn, Mg, Pb, Bi, are not advisable.	40 – 100 µm	50 – 200 µm	Chin et al. (2020; Gokuldoss et al. (2017; Sames et al. (2016)
Directed energy deposition	Powder directed energy deposition	Laser, arc or e-beam / above melting point	Titanium alloy (Ti-22Al-23Nb, Ti-6Al-4V, Ti-6.5Al-3.5Mo-1.5Zr-0.3Si, Ti-5Al-5Mo-4V-1Cr-1Fe), Steel (10V, 15-5 PH, 410, AISI 309Aremet 10, A2, MM10), Nickel based superalloy (CMSX-3, Haynes188, Haynes230, IN600, IN690, IN713, Rene 142, Rene N5), Aluminum alloy (CP Al, 6061, (2024)	20–200 µm	200–800 µm	Chin et al. (2020; Saboori et al. (2017; Sames et al. (2016)

2.2 Testing tools

A standard method for measuring the spreadability of powders in AM process is not currently available. However, many researchers are proposing both tests *in situ* and *ex-situ*. Whereas *in situ* tests are performed directly in the processing apparatus, *ex-situ* tests use novel tools specifically designed to analyze the behaviour of powders during their spreading and quantify the quality of the powder layer generated.

Cordova et al. (2020a) have designed two applicator tools that imitate the shape and the movement of a wire blade presented in a typical AM apparatus. The first tool is called *open applicator* and consists of a blade that slides over a stripe; as the blade slides over a metal strip, the powers flow in the gap fixed to 100 µm and are deposited, forming a layer (Figure 4a). The second tool is called *funnel applicator* because the applicator consists of a blade raised 100 µm over a metal strip and an oblique wall in contact with the strip forming a sort of funnel where the powder flows through before being deposited (Figure 4b). The test consists of weighting and charging an appropriate volume of powder and then moving the applicator at a constant speed of about 200 mm/s (the authors moved the blade manually). The powder spreadability was judged by visual inspection of the layer and measured in terms of relative density. The authors suggested the use of the *open applicator* because it provides conditions more similar to those occurring during the spreading in the processing apparatus and gives results with a smaller deviation than the *funnel applicator*.

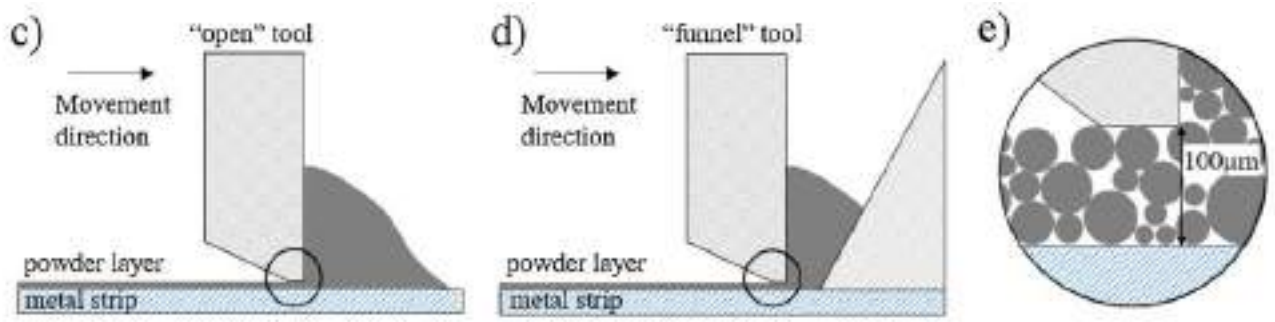

Figure 4. Applicator tools designed by NLR. C) open tool, d) funnel tool, e) Powder flowing through the 100 µm aperture of open and/or funnel tool adapted from Cordova et al. (2020b).

As shown in Figure 5, an automated test machine was built modifying a commercial thin-film applicator with an adjustable height blade that emulates the spreading process in AM equipment according to the works done by **Hulme-Smith et al. (2021) and Mellin et al. (2021)**

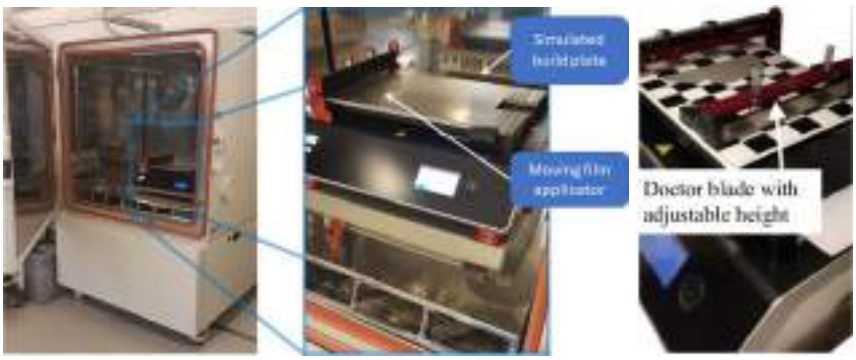

Figure 5 - Automatic powder applicator developed modifying a commercial thin-film applicator and placed in climate chamber Hulme-Smith et al. (2021; Mellin et al. (2021).

A more sophisticated modular powder spreading testbed was designed and fabricated by **Oropeza et al. (2021) to** be used for assessing and testing powder spreadability (Figure 6). The testbed is able to perform multi-layer spreading, uses a roller or blade spreader, has a spreading speed in the range of 0 – 100 mm/s, and a rotation velocity from 0 to 300 rpm, which are the typical range used in AM manufacturing. The use of such an automated testbed can facilitate a systematic study of spreadability because each test requires a small amount of powder.

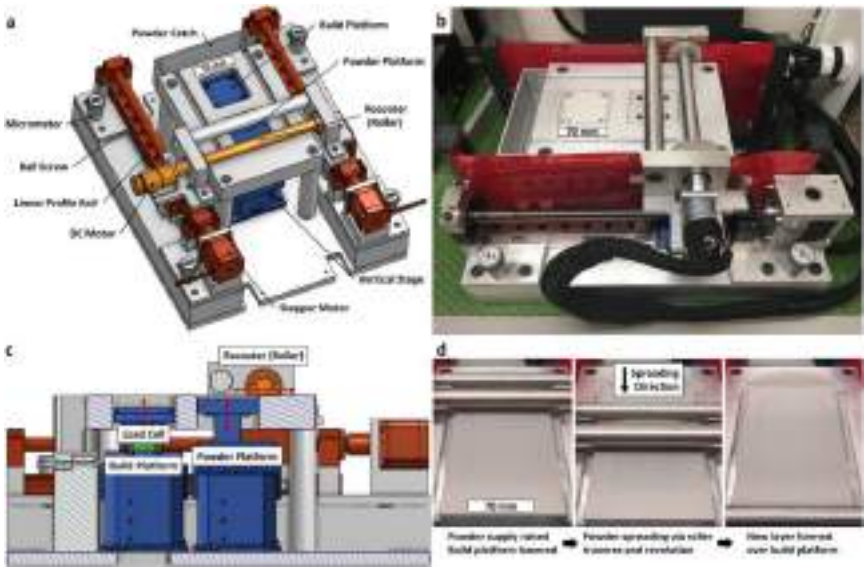

Figure 6 - Mechanized powder spreading testbed developed by Oropeza et al. Oropeza et al. (2021)

Lefebvre et al. (2019) evaluated the spreadability using a Hegman gauge (gauge in the range 0 – 100 μm). It should be pointed out that the Hegman gauge is used to check fineness or the presence of coarse particles in a liquid dispersion, and used in that case to assess powder spreadability. The measurement can assess qualitatively the spreadability by comparing the quality of the spread layer of different samples (Figure 7).

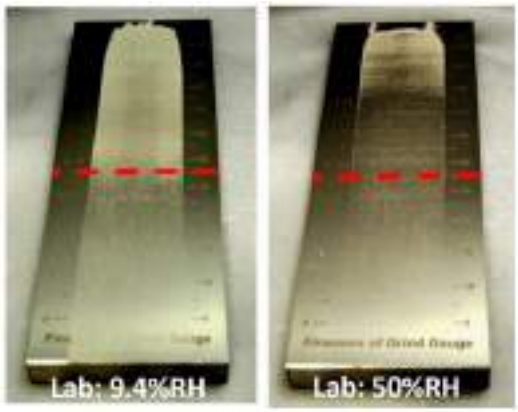

Figure 7 - Spreadability measured by using Hegman gauge (0-100 μm) (Lefebvre et al. (2019).

In **recent years, Chen et al. (2017) attempted** to experimentally capture the dynamics of powder spreading in the additive manufacturing conditions was made by using a visible light camera to measure the dynamic repose

angle (DRA) obtained by moving a powder pile with a blade similar to those used in the manufacturing process. The camera was able to capture the evolution of the angle of repose of the powder pile. The authors showed that, whereas the pile size diminished during spreading, the repose angle remained stable. Powders with small DRA showed better continuity and stability of flow under the blade gap. **Conversely, Escano et al. (2018) used** high-speed x-ray imaging was also used to investigate the evolution of the dynamic repose angle during spreading. Moreover, they were able to visualize the evolution of the surface roughness profile of the powder pile during the spreading process and the formation of powder clusters due to van der Waals cohesion forces or induced by jamming. The formation of these agglomerates can induce irregularities in the shape of the final layer, such as the formation of craters and voids (Figure 8).

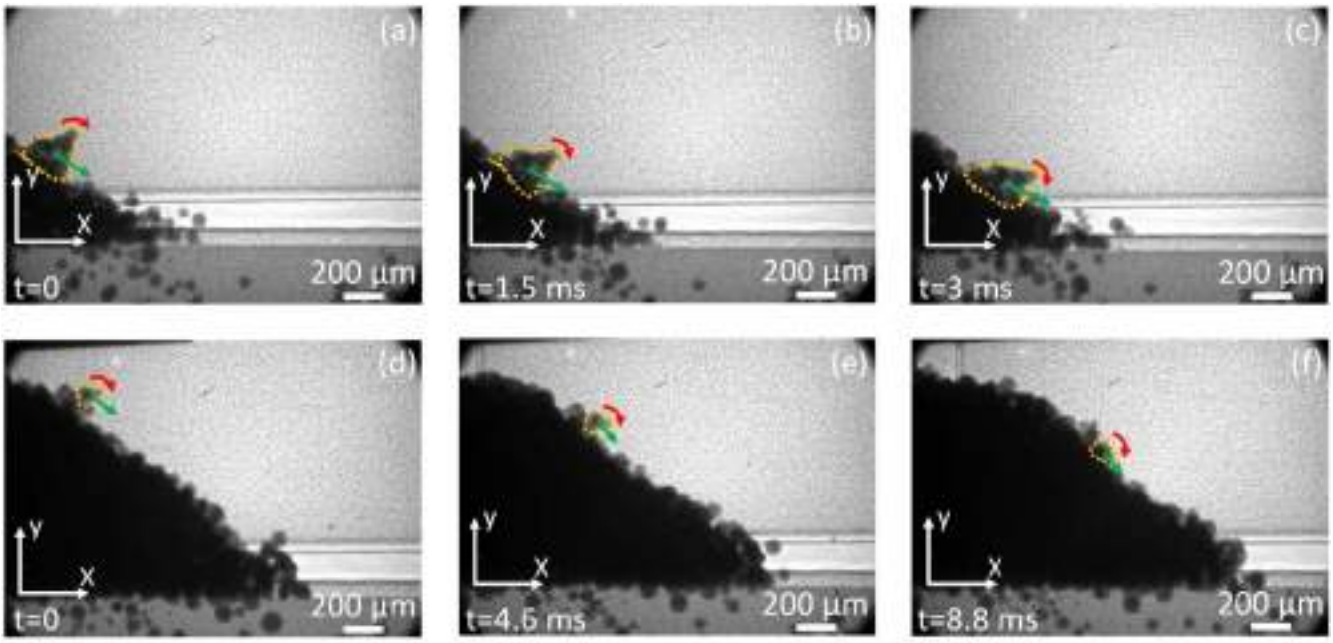

Figure 8 - Dynamic evolution of powder clusters tracked on the surface of the slope during the spreading of 316 L stainless steel powder captures using high-speed x-ray imaging method Escano et al. (2018).

2.3 Numerical methods

The investigation of powder spreading has involved the synergic use of both experiments and simulations. On the one hand, experiments suffer difficulties in a complete characterization of the powders and some lack of replication due to batch-to-batch variability of the feedstock or the non-perfect control of the process conditions. On the other hand, simulations present some limitations, such as the relatively small system size and short simulation times, but also a non-perfect correspondence between the simulated and the real system.

Except for the work **of Shanjani and Toyserkani, (2008), there** are not many examples of using a continuous approach to describe the spreading of powders. They modeled the powder spreading and compaction due to a counter-rotating roller using the assumption of continuum mechanics. The model considered the process of powder spreading similar to the case of a laminar flow of a viscous liquid, where the interaction between the roller and the powder is modeled through a coefficient of friction, and the powder is considered a compressible medium with non-constant density.

On the other hand, the discrete element method (DEM) has been the preferred method for investigating the dynamics of the powder spreading. DEM is a numerical technique proposed **by Cundall and Strack, (1979)** for describing the dynamics of particulate systems, where the continuity assumption fails to describe such systems. DEM is a Lagrangian method that tracks the movement of each particle and its interactions with other particles or the boundaries. Newton's laws of motion for translation and rotation are applied to each particle *i*:

$$m_i \frac{d^2\mathbf{r}_i}{dt^2} = \sum_j \left(\mathbf{F}_{c,ij} +\right) + m_i\mathbf{g}$$

$$I_i \frac{d\boldsymbol{\omega}_i}{dt} = \sum_j \mathbf{T}_{c,ij}$$

where m_i is the mass of the particle i, $\mathbf{r}_i$ its vector position, I_i the moment of inertia, $\boldsymbol{\omega}_i$ the angular velocity, $\mathbf{g}$ is the gravity acceleration vector. Those equations are integrated in time to obtain the temporal evolution of the position, angle, translational velocity, and angular velocity of every particle.

The core of DEM consists of simulating particle- particle and particle- wall interactions by using contact models that are able to calculate contact forces $\mathbf{F}_{c,ij}$ and torques $\mathbf{T}_{c,ij}$ taking into account the position, velocity, and properties of each particle. Usually, these models depend on some physical properties such as Young's modulus and Poisson ratio, but also by the size of the particles and friction behavior. The contact forces are split into the normal and the tangential component to the contact plane and are modeled by using linear viscoelastic models, non- linear viscoelastic models, and hysteretic models as **demonstrated by Blais et al. (2019).**

The simulation of powders in the micron range requires the modeling of adhesive interactions. The main sources of adhesive inter-particle force are capillary effects, electrostatic attraction, and van der Waals interactions. **Li et al. (2016) point**ed out that the metal AM process often requires humidity level to be as low as possible to enhance the densification process, preventing the formation of oxides and hydroxides and the production of hydrogen that can form gaseous pores in the final component.

2.3.1 Characterization of powders and model calibration

DEM parameters require to be calibrated in order to link experiments and simulations; some works from the literature are reported in Table 3. According to Roessler et al. (2019), the calibration tests should be conducted at the same scale and a flow regime close to the actual experiments. As a matter of fact, it is a common practice to scale down the simulations because of the computational costs of DEM. Moreover, Lommen et al. (2014) suggested many other tricks in order to speed up simulations, such as reducing particle stiffness in order to decrease the simulation timestep. The calibration of a parameter can be performed by directly measuring the single property at particle or contact level, such as in the case of particle size, size distribution, and shape. On the other hand, contact parameters are preferably determined using a reverse calibration process, in which the parameters are found indirectly from bulk measurements as found **in the work of Coetzee, (2017). The** calibration can be achieved by using a "trial and error" approach, in which the simulation is repeated with different values of the parameters until a satisfactory match with the experimental results is obtained. In a recent paper, **Richter et al. (2020)** have successfully exploited optimization algorithms and data regression from a design of experiment to tune the DEM parameters. In some cases, previous data from literature are taken as reference values.

A common calibration procedure consists of comparing AOR observed experimentally, and the one obtained varying DEM parameters until a good match between experiment and simulation is reached. Whereas traditionally, DEM simulations try to emulate the flowing of powders from a funnel or a hopper according to the ASTM Flowmeter test. Geer et al. (2018) developed an alternative method, called “cloud method,” which consisted in generating conical heap from the falling under the gravity of a non-contacting cloud of particles. **Meier et al. (2019b) use**d AOR to calibrate the surface energy of metal powders and noted that cohesion influence more the resulting AOR than other DEM parameters, such as stiffness, friction coefficient or the coefficient of restitution. **Desai et al. (2019)** proposed a complex calibration procedure that started over the calibration of friction coefficients using two consecutive AOR virtual experiments and simulations of a virtual rheometer against real tests. Some of these methods are summarized in Table 3.

Table 3 – Calibration method used for powders used in AM.

Authors	Material	Particles			Calibration method	
		Type	Polydispersity	Cohesion	Experimental	Simulation
Geer et al. (2018 Geer et al. (2018)	Gas atomized stainless steel (17-4SS) powder	Spherical	20 – 75 μm	no	AOR obtained from the flow through a fixed funnel	AOR obtained from the flow through a fixed, down-scaled funnel and from clouds of powders
Meier et al, (2019 Meier et al. (2019b)	Ti-6Al-4V	Spherical	20 – 160 μm	yes	AOR obtained from the flow through a fixed funnel	AOR obtained from the flow through a fixed, down-scaled funnel
Desai et al. (2019 Desai et al. (2019)	Ti-6Al-4V	Spherical	Monosized 250 μm	no	AOR + powder rheometer	AOR + powder rheometer

2.3.2 Simulation of the spreading process

The spreading process has been widely explored by using DEM simulations; a comprehensive list is presented in Table 4.

Table 4 – Simulation studies of powder spreading.

Authors	*Powders*	*Spreader*	*Variables studied*	*Metrics*
Mindt et al. (2016	Spherical, polydisperse (15 – 70 µm), non-cohesive, Ti-6Al-4V particles	Flat spreader	Gap thickness	Bed particle fraction,
Haeri et al. (2016	Rods (overlapping multi-sphere method), polydisperse, non-cohesive, polyether ether ketone (PEEK) particles	Roller spreader, flat spreader	Particle shape, gap thickness, roller velocity, blade velocity	Particle shape segregation, bed particle fraction, surface roughness, probability density function (PDF) for the spatial distribution of orientation
Parteli and Pöschel, (2016)	Non-spherical (overlapping multi-sphere method), polydisperse (30 – 100 µm) cohesive, Polymer PA12	Roller spreader	Roller velocity	Gap thickness
Chen et al. Chen et al. (2017)	Spherical, polydisperse (9–140 µm), cohesive, 316L powder	Flat spreader	Cohesion, sliding and rolling friction, particle size, blade height, and velocity	Mass flow rate, dynamic repose angle
Gunasegaram et al. (2017)	Elliptical, polydisperse (37 -183 µm), non-cohesive, Ti-6Al-4V particles	Flat spreader		
Haeri, (2017)	Rods and irregular (overlapping multi-sphere method), polydisperse, non-cohesive, polyether ether ketone (PEEK) particles	From flat to rounded spreaders	Blade velocity, design of blade profile	Bed particle fraction, surface roughness
Nam et al. (2018) (Nan et al., 2018)	Non-spherical (overlapping multi-sphere method), polydisperse (15 – 55 µm) cohesive, gas-atomized 316 L stainless steel particles	Flat spreader	Gap thickness	Particle fraction, Frequency of empty patches, Frequency distribution of jamming
Chen et al. (2019)	Spherical, polydisperse (5 – 80 µm), AISI 316L stainless steel powder	Flat spreader	Particle size, polydispersity, the effect of the wall, cohesion energy	Bed packing fraction, powder flow, percolation
Meier et al. (2019)	Spherical, polydispersed (20 - 44 µm), cohesive, titanium alloy (Ti-6Al-4V) particles	Flat spreader	Gap thickness, cohesion energy	Surface profile, bed packing fraction
Nam and Ghadiri, (2019)	Non-spherical (overlapping multi-sphere method), polydisperse (15 – 55 µm) cohesive, gas-atomized 316 L stainless steel particles	Flat spreader	Gap thickness, blade velocity	Mass flow rate through the gap, Shear band
Gu et al. (2019)	Spherical, polydispersed, cohesive, WC/Inconel 718 composite powders	Flat spreader	Effect of powder bed on thermodynamics and laser processability	
Ma et al. (2020)	Spherical, polydispersed, cohesive powder	Flat spreader	Presence of fine fraction	Packing fraction, coordination number, surface roughness
Fouda and Bayly, (2020)	Spherical, mono-sized (50 µm), non-cohesive titanium alloy (Ti-6Al-4V) particles	Flat spreader	Gap thickness, blade velocity	Bed packing fraction
Chen et al. (2020)	Spherical, polydisperse (5 – 80 µm), cohesive, 316 L stainless steel powder	Counter-rolling spreader	Gap thickness, blade velocity	Mass flow rate through the gap, normal stress on bed, surface profile, bed packing fraction
He et al. (2020)	Spherical, mono-sized (50 µm), cohesive, plasma atomised Ti-6Al-4V particles	Flat spreader		Packing density, surface roughness, density pore, chamber pore
Nam et al. (2020)	Non-spherical (overlapping multi-sphere method), polydisperse (15 – 55 µm) cohesive, gas-atomised 316 L stainless steel particles	Counter-rolling spreader	Roller rotational speed, gap thickness	Particle segregation, mass flow rate of particles through the gap, normalised spread particle volume
Lee et al. (2020)	Spherical, polydisperse (30 -100 µm), cohesive, Co–Cr powder	Flat spreader	Number of layers, spreader velocity,	Height of the layer, dynamic AOR, packing density, particle size distribution
Wang et al. (2020)	Spherical, polydisperse (30 -90 µm), cohesive, Hastelloy X (HX) powder	Roller spreader, flat spreader	Cohesiveness, particle size distribution,	Packing fraction, surface roughness, properties along spreading direction
Yao et al. (2021) Yao et al. (2020)	Spherical, monosizes (34.8, 100, 123.2, 169.4 µm), cohesive, 316 L stainless steel powder	Flat spreader	Particle size, sprading velocity, gap heigh, blade angle	Packing density and its evolution, pore size, particle velocity distribution,

2.3.3 Surrogates and machine learning

The development of surrogates and digital twins is a major trend in research and industrial environment in order to increase process understanding, quantify uncertainty, increase reliability and safety, and, finally, manage product quality. Surrogates and digital twins aim to replicate a manufacturing process, or a part of it, by training machine learning algorithms with data produced by testing data, literature data, and simulation results (Figure 9). Mukherjee and DebRoy, (2019) suggested this approach because it can be beneficial also to the additive manufacturing process to overcome the problem of process replicability due to the complexity of the process itself and the variability of the process variables.

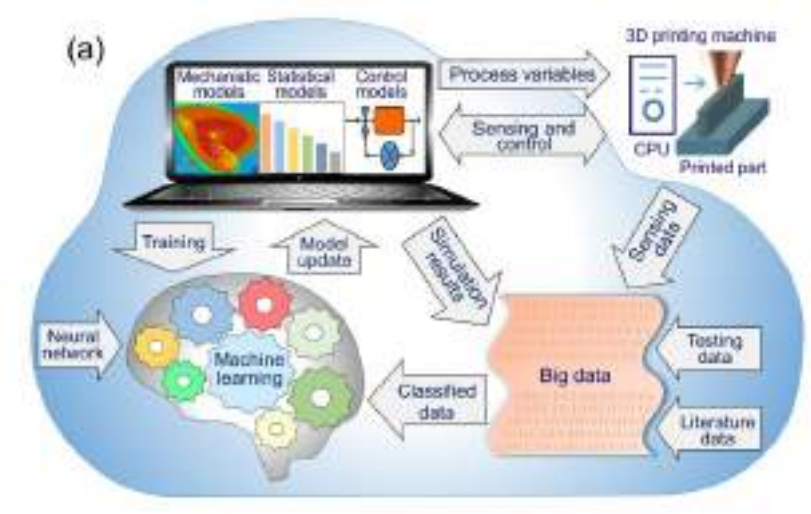

Figure 9 – Schematic representation of the digital twin Mukherjee and DebRoy, (2019).

A three-step approach was proposed by **Desai and Higgs, (2019)** to produce maps correlating roller translational and rotational speed to some spreadability metrics, such as spread throughput, porosity, and layer roughness. The first step consisted in the characterization of powders using a powder rheometer and calibrate DEM powder characteristics against those data. The second step consisted in generating an appropriate design of simulations having as parameters roller translational and rotational speed, performing DEM simulations, and compare their outcome with experimental data. The third step consisted of training a Back Propagation Neural Network (BP-NN) and using it as a surrogate model to create maps that correlate spreader speeds and spread layer properties.

For the sake of easiness, a summary of the techniques mentioned above with relative pros and cons is given below in Table 5:

Table 5 list of in-situ, ex-situ and simulation techniques to determine powder spreadability.

Name	Pros	Cons
Open applicator	Imitate real AM equipment	requires a visual inspection of the layer
Funnel Applicator	Measures powder spreadability	Higher deviation
Modular powder spreading	Totally automated requires only a little powder	-
Hegman gauge	Fast measurement of spreadability	only qualitatively results are achieved
Visible light Camera	Measures the dynamic repose angle of powders	Only a limited amount of information can be obtained
X-ray imaging	Higher resolution, capable of identifying cluster formation	-
Continuous approach	Evaluates powder behaviour based on fluid dynamic Models	Old equations. Not very widespread among researchers and end-users
Discrete approach	simulation of powder-powder interactions	requires a calibration process, high computing power demanding
AI/digital twins	Highly customizable	requires a calibration process, high computing power demanding

3. Powder spreading dynamics

Powder spreading is a complex and articulate process that can be divided into different subprocesses mutually interacting:

1. Avalanching flow due to the horizontal movement of a powder pile imposed by a blade or a roller and convection/circulation of powders within the moving pile;
2. Shear flow in the front and under the gap between the rake and baseplate and in front of the blade;
3. The inertia of the particles that continue to move after being deposited on the substrate.

A general picture of the main problems encountering in the spreading process is shown in Figure 10. If the gap height is not high enough, particles cannot flow through it, impeding the spreading of the powder. A further phenomenon that is usually encountered in the powder spreading is related to the powder size or shape segregation, which means that the particle size/shape distribution within the powder bed differs from the original distribution. Furthermore, the interaction between powder and blade can lead to jamming, resulting in non-uniformity of the powder layer and, in the worst case, in empty patches.

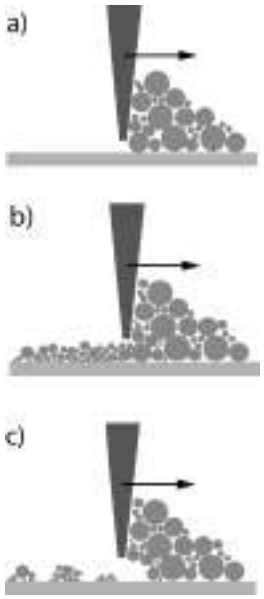

Figure 10 – Schematic of the main problem encountering in powder spreading: a) missing spreading due to small gap size, b) powder size/shape segregation, and c) formation of empty patches due to jamming.

3.1 Blade vs. roller spreader

During spreading, the powder pile moves with the blade/roller and, as the powders are spread into layers, gradually decreases its height. The stress increases with the depth from the slope surface to the bottom, but it drops greatly in the region close to the gap, called the stress-dip region as mentioned in the work of **Chen et al. (2019).** As shown in Figure 11, the powder pile can be divided into three main regions according to the velocity field. While the majority of the powder moves with the rake (relative velocity equal to 0), the front region moves similarly to an avalanche, and the bottom region flows out from the gap between the plate and the rake head. The behavior of the front region is strongly connected only with the powder flowability and not with the powder density of the powder layer. It has been reported that the dynamic angle of repose is not affected by the height of the gap nor by the blade speed as previously described by the same author **Chen et al. (2017).**

On the other hand, the stress-dip region has a substantial impact on the powder deposition. **Chen et al. (2019)** showed that the stress and the mass flow rate in this region directly determine the packing density of the powder layer, whereas the magnitude of their fluctuations determines its uniformity.

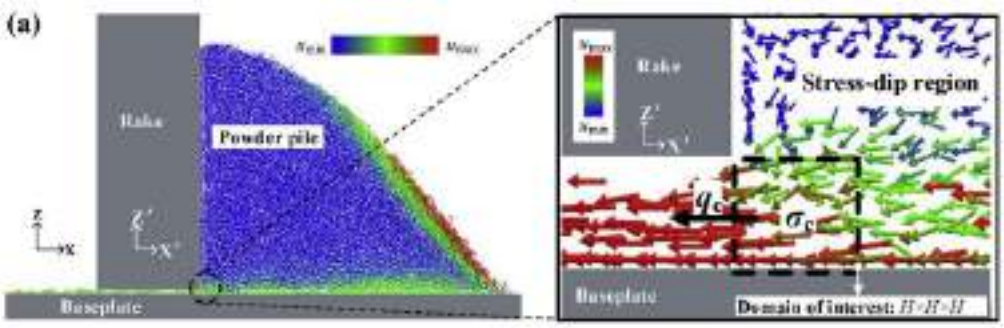

Figure 11. Velocity field of the powder pile Chen et al. (2019).

The effect of blade shearing is exerted on the particles in front of the blade, in a region that is extended in the vertical direction between the baseplate and a height slightly higher than the gap height. As shown in Figure 12a, particle velocity is maximum close to the edges of the blade and minimum close to the baseplate, and its profile follows a universal curve having the sigmoidal shape of a Gauss error function as found in the work **of Nan and Ghadiri, (2019)**. The particles having a velocity lower than the velocity of the blade moves through the gap, are deposited, and forms the powder layer. Furthermore**, Haeri et al. (2016)** explained that in their flowing under the gap, particles are dragged forward because of the contact with the edges of the blade. Nonetheless, **Nan et al. (2018) sho**wed the presence of a jump in particle velocity across the front edge of the blade that is reduced only by rising enough the height of the blade; this behavior is described in Figure 12b,.

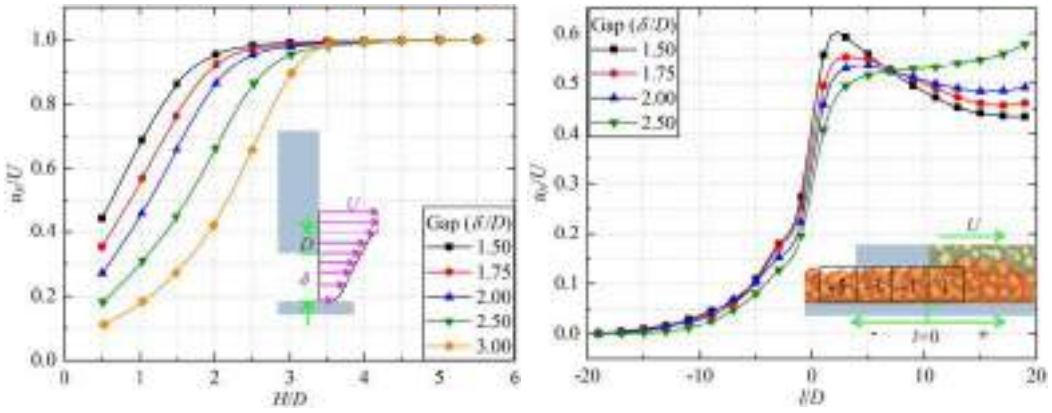

Figure 12 - Variation of particle velocity with H in the region "before blade" for different gaps Nan et al. (2018).

The mass flow rate through the gap increases linearly as the blade speed increases until a critical blade speed is reached and the mass flow rate approaches an asymptotic value, which represents the maximum spreading throughput obtainable using a certain gap height. Whereas the asymptotic value depends on the gap height, the critical velocity appears to be independent of the gap height. This effect has been explained by comparing the gravity inertial timescale, which represents the characteristic falling time of a particle during the spreading process because of the gravity, and the spreading inertial timescale, representing the characteristics time for a blade to pass over a particle at rest. At low blade velocity, the spreading inertial timescale is longer than the gravity inertial timescale, and, consequently, particles have time to fall and pass through the gap. On the other hand, at very high blade speed, when the spreading inertial timescale is much shorter than the gravity inertial timescale, particles cannot reach the gap sufficiently faster, limiting the mass flow rate. The critical velocity is around $5(gD_{90})^{0.5}$, where D_{90} is by number as found in **Nan and Ghadiri, (2019) work.**

Different from the blade, Nan et al. (2020) observed that a roller spreader can translate horizontally and rotate. When the roller does not rotate, the particle velocity field is not dissimilar to the case of a blade, whereas a stronger particle circulation and convection can be noted when the rotation is applied to the roller. In that case, the roller acts as a mixer that moves particles from the bottom to the free surface of the heap and, finally, to the bottom again. Moreover, particles generally not only have larger velocities when the roller system is used, but the forces among particles are more uniformly distributed, enhancing particle rearrangement within the powder bed (Figure 13). As a result, according to **Wang et al. (2020) work, t**he roller spreader seems to produce a smoother powder layer with a higher packing fraction than those obtained with the blade. Finally, as shown **by Lee et al. (2019), the** coordination number in the powder increases from 2.5 to 4 because the roller compresses the particle during the spreading process.

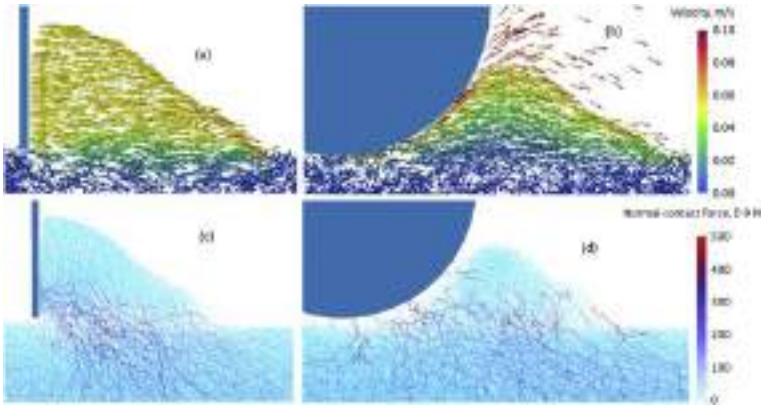

Figure 13 – Velocity vectors in the case of (a) blade and (b) roller spreader. Normal force chains in the case of (c) blade and (d) roller spreader Nan et al. (2020).

3.2 Wall effect and jamming

The presence of the rake and baseplate constraints the particle flow within a small enclosure and induces the presence of voids and discontinuity in the final powder layers. As shown in Figure 14, two mechanisms due to the presence of the spreader rake were identified, i.e. (a) the static wall effect and (b) formation of force-arches and jamming.

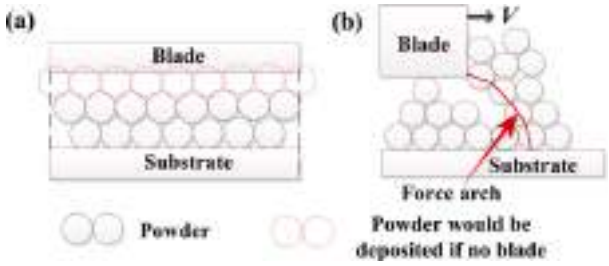

Figure 14 – Schematic illustration of a) wall effect and b) jamming due to force arch Yao et al. (2020).

The static wall effect refers to the reduction of packing fraction generated by vacant sites in the packing due to the presence of walls. In fact, the voids between particles and walls are larger than those between particles. This effect is the typical effect encountering when a discrete medium is confined in a container, and its effect is enhanced as much the characteristic dimension of the container becomes comparable to the dimension of the discrete medium. This effect is particularly important in the spreading process because the gap height is comparable to the powder size. **Karapatis et al. (1999)** provided an analytical expression to estimate the porosity related to the wall effect

Φ_{wall} compared to the total porosity Φ_{total}, assuming an orthorhombic arrangement of monodisperse particles (with a diameter d) in a cylinder (with a diameter D and a height H):

$$\frac{\Phi_{\text{wall}}}{\Phi_{\text{total}}} \approx \frac{d\left(\frac{1}{H}+\frac{4}{D}\right)}{0.8+d\left(\frac{1}{H}+\frac{4}{D}\right)}$$

According to Chen et al. (2019), the static wall effect is negligible if the dimension of the gap is several orders of magnitude bigger than particle size, as $\frac{\Phi_{\text{wall}}}{\Phi_{\text{total}}} \to 0$ for $D \gg d$, but it is relevant otherwise, i.e. $\frac{\Phi_{\text{wall}}}{\Phi_{\text{total}}} \to 1/\left(0.8\frac{H}{D}+1\right)$. The increase of gap height decreases the importance of the static wall effect.

The second effect is related to the movement of the wall and refers to the random formation of force-arches and transient jamming close to the rake, which produces a further reduction section of the passage of the powders. The formation and breakage of these force aches enhances the fluctuation of stress and particle flow and, finally, determine inhomogeneity in the powder layer and empty patches as can be found in Chen et al. (2019); but also in the work of Yao et al. (2020). Transient jamming of particles before the blade is a dynamic phenomenon that consists of the formation and breakage of arches, and its survival time is about 10^{-4} s. The frequency of the jamming phenomena is correlated to the survival time of the jamming events so that the shorter jamming is observed more frequently. Moreover, Nan et al. (2018) noted that the increase of gap height decreases the frequency and the survival time of the jamming events, resulting in more uniform powder spreading.

3.3 Cohesion

It is well known that fine particles exhibit cohesive behavior. Cohesive granular Bond number defined as the ratio of adhesive to gravity forces, $\text{Bo}_g = F_a/mg$, can be used to distinguish cohesive powders ($\text{Bo}_g > 1$), from cohesionless powders ($\text{Bo}_g < 1$). Castellanos, (2005) described the adhesive inter-particle forces which arise from capillary effects, electrostatic attraction, and van der Waals interactions. Cohesive interparticle forces become increasingly relevant compared to gravitational force as particle size decreases as described by Parteli et al. (2014). When the powder humidity level is kept at a low level or remove by vacuum-drying before use, liquid bridges between particles can be considered absent and, consequently, capillary force negligible as found in literature works as the one of Li et al. (2016). Moreover, Meier et al. (2019b), who focused on conductive powders with a diameter below 100 µm, states that electrostatic forces are orders of magnitude lower than van der Waals forces.

DEM simulations have shown the connection between the fluidity of powders through the blade gap while spreading, Bond number Bo_g and particle size. Bond number Bo_g is inversely proportional to the square of the particle size, and a decrease of particle diameter below ~100 µm leads to a sharp increase of Bo_g much above 1.

As Bo_g increases in the range 0 – 3, and particle size decreases until ~ 40 µm, the fluidity of powder increased as well, and the decreasing of particle size can be considered beneficial to powder fluidity. Contrary, further increases of Bo_g above 3 and a decrease of particle size below ~ 40 µm decreased powder fluidity, causes powder agglomeration and reduces the packing density because of the predominance of van del Waal forces as described in the works of Chen et al. (2019), (2017). Cohesiveness can play a double role depending on the magnitude of cohesive forces. In fact, as cohesiveness increases, small particles tend to adhere to larger particles resulting in a more homogeneous layer. In contrast, Wang et al. (2020) noticed that the homogeneity decreases if the cohesive forces exceed a large value because of the difficulties of particles in rearranging themselves under the action of the spreading system. The effect of powder cohesiveness on the quality of powder layers is shown in Figure 15.

Ma et al. (2020) have proposed a simplified expression for the flowability in terms of energy ratio, defined as the ratio of potential energy associated with van der Waals forces and potential energy associated with gravity. According to that definition, flowability is proportional to $1/\gamma_e$, and, in turn, to hR_{eq}^2, where h is the height of the gap and R_{eq}^2 is the equivalent radius.

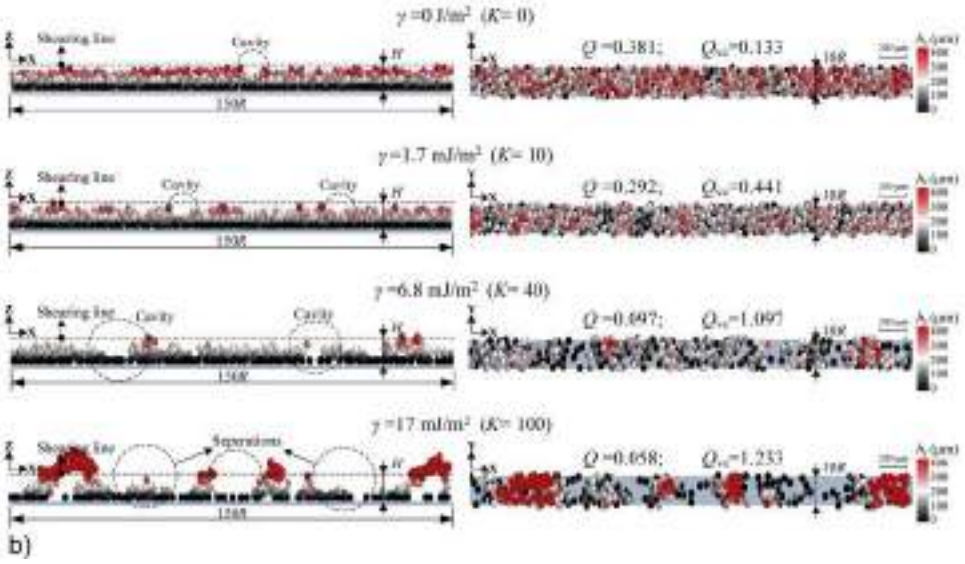

Figure 15 – Effect of powder cohesiveness on the quality of powder layers adapted from Wang et al. (2020)

3.4 Powder segregation

Particle segregation consists of the demixing of the initial powders, leading to spatial non-homogeneity of particle size distribution, shape or other physical properties. Among the many segregation mechanisms, sifting segregation or percolation has been hypothesized to occur during the powder spreading. Percolation consists of the passage of

particles through temporary voids in the powder packing and usually leads to the separation of particles by size. This effect is enhanced in the presence of a powder with a wide particle size distribution because the finer fraction is able to move through the voids formed by the coarser fraction. This effect can lead to a demixing and segregation of the powders, with stratification of the finer fraction on the bottom and the coarser fraction on top.

As **shown by Lee et al. (2020),** during the movement of the blade, coarse particles are segregated to the front surface of the moving pile and, as the spreading proceeds, the particle size distribution changes (Figure 16). The segregation effect due to convection/circulation in the moving heap was also observed in the case of a roller spreader as described by **Nan et al. (2020).**

When percolation leads to segregation, there is no improvement of packing density nor flow rate through the gap between the baseplate and the blade. **Chen et al. (2019) also describ**ed how percolation is a detrimental phenomenon because it could make the use of bimodal powders ineffective. It has been shown that powder segregation has a real impact on the local packing fraction, but contradictory results were obtained concerning the inhomogeneities along the direction of the spreading. In fact, for some studies, the finer fraction is more likely to deposit at the beginning of the spreading process and the coarser at the end, whereases opposite results were found by other researchers like **Muñiz-Lerma et al. (2018).** In that context, the role of cohesion could have played a major role, as the initial agglomerates might be broken by the shear strength during the spreading process and resulting in the deposition of the finer fraction only at the **end. Lee et al. (2020)** also underlined that the spreader velocity can influence segregation because an increase of the rake velocity may lead to a partial remixing of the powders and, finally, resulting in a particle population more similar to the pristine powder.

Segregation was also observed in the case of the roller spreader, and in particular in the case of small gap height (similar to the case of the flat blade) and high rotational speed. In fact**, Nan et al. (2020) evidenced** that high rotational speed enhances particle convection and, finally, triggers segregation mechanisms.

As aforementioned, segregation is also able to separate particles by shape. This effect has been observed with Co–Cr–W–Mo alloy powders. **Pal et al. (2021) also** described how spherical particles easily percolate and were deposited at the starting locations whereas the irregular-shaped particles were found in the ending location.

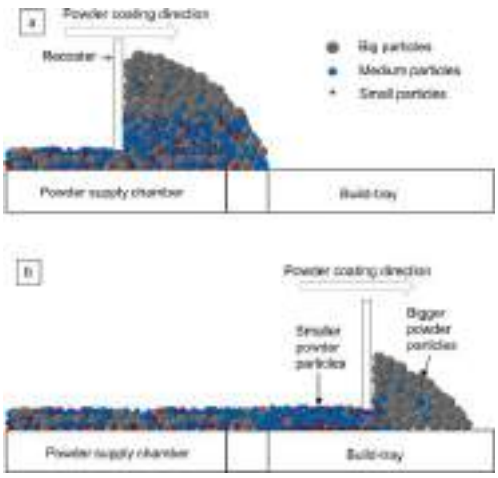

Figure 16 – Schematic of powder spreading: a) powders are collected from the powder supply chamber and b) spread on the build platform Pal et al. (2021).

4. Powder spreadability

4.1 What does spreadability mean?

There is a lack of knowledge and understanding concerning the spreadability of powder in AM manufacturing. American National Standards Institute (ANSI) has put the "spreadability" as a crucial gap in AM process because *"there is no known description of spreadability or standard for how to quantitatively assess powder spreadability"* America Makes and ANSI Additive Manufacturing Standardization, (2017). ISO/ASTM 52900 defines "*spreadability"* as "*the ability of a feedstock material to be spread out in layers that fulfill the requirements for the AM"*. Moreover, it is reported that the draft document ISO/ASTM WK55610 does not explicitly include the concept of spreadability but only of shear and dynamic flow properties and refers to the ASTM standards ASTM D6128, D6682, D6773, and D7891 for shear cell tests and wall friction tests America Makes and ANSI Additive Manufacturing Standardization, (2017).

Desai et al. (2019) defined *spreadability* as "*the ease with which a powder will spread under a set of load conditions"*, in analogy to *powder flowability* defined as "*the ease with which a powder will flow under a set of operating conditions"*. Many authors have strongly associated spreadability with flowability, although high flowability not necessarily implies high spreadability.

The problem concerning spreadability can be resumed as the following:

1. there is not a unique description of spreadability;
2. there is no standard procedure for measure powder spreadability;
3. difficulties in correlating intrinsic powder characteristics with spreadability;
4. difficulties in correlating standardized tests with spreadability.

A highly spreadable powder is such a powder that is able to produce powder layers having the following characteristics:

1. high packing density;
2. layers with a smooth profile;
3. controllable layer thickness;
4. spatial uniformity of its property, i.e. absence of particle agglomerates, voids, and empty patches;
5. allowing high blade speed.

The difficulties arising in understanding and defining powder spreadability and spreading quality are related to the complexity of such a process and the numerous variables involved:

1. Feedstock characteristics: intrinsic properties (materials, size, and size distribution, shape), flowability, and ability to form dense packings;

2. Flow conditions (spreader characteristics, spreader gap height, spreader velocity)
3. Environmental conditions (humidity, temperature, inert gas flow).

4.2 Spreading metrics

Various metrics have been proposed so far for characterizing the quality of the spreading:

- qualitative visual inspection in the work of Snow, (2018);
- percent of coverage as proposed by Meier et al. (2019a; Snow et al. (2019);
- rate of powder deposition by Snow et al. (2019);
- avalanching angle of the powder pile;
- average avalanching angle of the powder pile as found in the work of Snow et al. (2019);
- rate of change of the avalanching angle pile also by Snow et al. (2019).
- powder bed density as suggested by Cordova et al. (2020a)
- surface profile and roughness of the layer as largely debated in the following literature work Chen et al. (2020); Meier et al. (2019a); Snow et al. (2019).

4.2.1 Visual inspection and percent of coverage

Whereas the purely visual inspection of the power layer formed after the spreading of the particles is only a qualitative measure and subject to biases of the operators or judges, the use of an overhead camera and the subsequent image analysis can be used to assess the percentage of the build plate covered by powder. The image of the plate captured after powder spreading is binarized in order to obtain a black/white image. The percentage of coverage is the ratio of white pixels to black pixels. The full description of the technique can be found in the works of **Hulme-Smith et al. (2021) and Snow et al. (2019).** The value obtained from this measure can be an indication of the powder spreadability, in the sense that the higher percentage of coverage indicates the higher spreadability (Figure 17). This metric presented the advantage of being simple to measure, and its interpretation is straightforward. Still, it is not able to give direct information on the uniformity of the powder bed density.

Figure 17. Determination of the percentage of layer coverage by using image analysis Snow et al. (2019).

4.2.2 Metrics based on the dynamic avalanching angle test

An applicator tool that imitates the conditions of powder spreading in AM equipment can be used as a dynamic avalanche angle test. The applicator can be coupled with a simple visible camera as done by **Chen et al. (2017), a** digital microscope as in the work of Snow et al. (2019), or a high-speed, high-energy X-ray imaging system as proposed **by Escano et al. (2018). The** first metric that can be identified in such a test is the deposition rate of the powder. As shown in Figure 18, from the images captured during the test, it can be possible to measure the cross-sectional area of the powder pile *A* and its rate of change *dA/dt*, and finally, the deposition rate as follows:

$$\dot{m} = \rho_a L \frac{dA}{dt}$$

where ρ_a is the apparent density determined by ASTM M212, and L is the width of the metal plate. It should be noted that it is not guaranteed that the apparent density as measured by ASTM M212 corresponds to the apparent density achieved in the powder bed.

Further metrics consisted in measuring the avalanching angle of the powder pile θ (or the time-averaged avalanching angle $\bar{\theta}$) and its rate of change $d\theta/dt$. Those metrics refer to typical variables connected to powder flowability. The powders having high θ, $d\theta/dt$ and $\bar{\theta}$ are considered high flowable powders and result in a powder bed uniformly spread in a thin layer. Contrary, high θ, $d\theta/dt$ and $\bar{\theta}$ are related to powder that exhibited avalanching behavior and poor flowability and, finally resulting in low plate coverage as demonstrated by **Snow et al. (2019).**

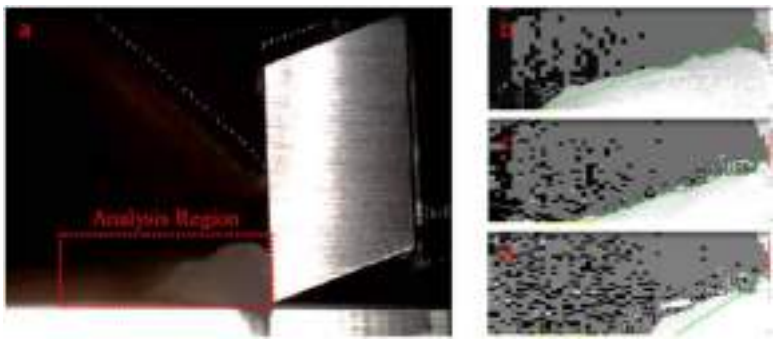

Figure 18 - Avalanching video taken from the digital microscope Snow et al. (2019).

4.2.3 Powder bed density

A measurement of the powder bed density can be performed capturing the metal powder from various location in the powder bed and measuring the density as the ratio of powder mass over the volume:

$$\rho_{PB} = \frac{m_p}{V}$$

Various solutions are reported in the literature to solve the problem of sampling the powder bed. Karapatis et al. 1999) performed simplified tests consisted of depositing the metal powders with a metallic ruler in a cylindrical container, 500-1500 μm depth (depending on the powder size) and having a diameter of 65 mm. Liu et al. (2011) built by SLM a box container with an internal dimension of 30×30×30 mm and weighted the powder within that box. Jacob et al. (2016) developed a special container by using a morphological box, a tool to solve multi-dimensional, non-quantifiable problems through the exclusion of illogical solutions. The container that resulted from such an analysis was constituted of a cylinder with a conical lid whose dimensional characteristics were taken according to **ASTM B212 (2009) standard** for a density cup. Such a container can be used to sample the metal powder from different locations on the build plate. The powder bed density can be determined by weighting the mass of powder captured and V the volume of the cavity (determined by filling the specimen with water).

Cordova et al. (2020a) used the relative density defined as the ratio of the apparent density ρ_{app} and the true density of the material ρ_{true} as a metric to determine the spreadability of powders. The apparent density was defined as the ratio of the mass of powder needed to obtain a layer of length L and the volume of powder bed V; V was determined from the layer length, width and thickness.

X-ray micro-computed tomography was used by **Muñiz-Lerma et al. (2018) to** study the powder spread density (Figure 19).

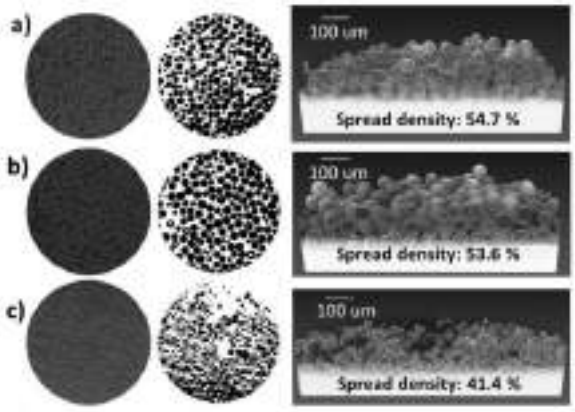

Figure 19 – 2D and 3D image reconstruction obtained using micro-CT scans of three different powders Muñiz-Lerma et al. (2018).

An alternative method to measure the powder-bed density is shown Figure 20. It consists of injecting a UV-curable polymer solution in different locations in the bed, curing the solution to bind the powder, and, finally, using 3D nano computational tomography (3D nano-CT) to measure the density of each sample as d**one by Ali et al. (2018)**. A possible solution consists of 95% Bisphenol-A ethoxylated diacrylate (BAE) and 5% of the photoinitiator Irgacure 819 (5 wt%). The most important parameter to consider is the viscosity of the solution, which should be low enough to allow the spreading of the solution into the powder bed without changing its compaction, but also not too low so that the solution can not bind the powder effectively. The solution can be dispersed using a pneumatic liquid dispensing system placed at an appropriate distance from the bed. Finally, the solution can be cured using a UV lamp and irradiate the system for less than a minute, creating a solid polymeric system that entrapped the metal powder. The sample can be analyzed using a nano-CT scan and, consequently, its three-dimensional structure can be reconstructed, and the powder-bed compaction density can be determined from the ratio of the volume of particles and the total volume the region of interest (ROI) of the sample:

$$\rho_{PB} = \frac{V_p}{V_{ROI}} \times 100$$

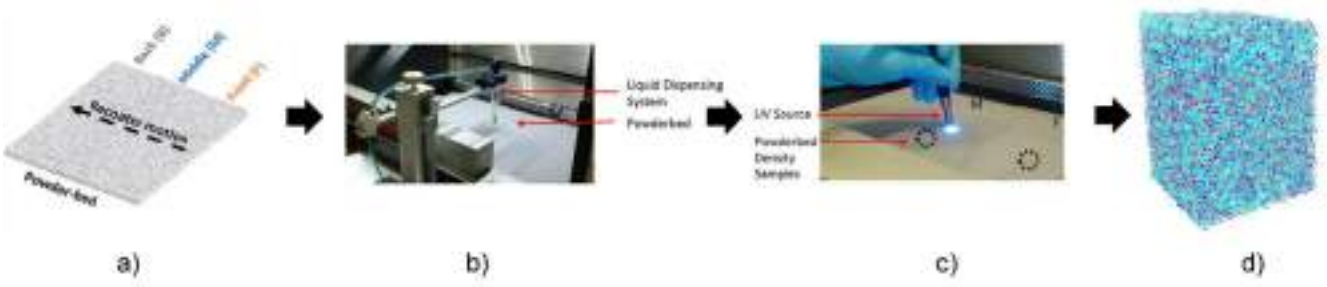

Figure 20. Powder bed density measured after the a) spreading, b) dispersion of UV-curable solution, c) curing the solution and d) perform nano-CT and postprocess the data. Modified after Ali et al. (2018).

4.2.3 Surface profile and roughness of the layer

Since a powder is a discontinuous medium, it forms an irregular profile determined by the shape and the arrangement of the single particles within the powder bed. As shown in Figure 21, the roughness of each spread layer is also determined by the roughness of the previous, fused/sintered layer. Usually, the surface roughness is associated to arithmetical mean deviation as can be read in the **work of He et al. (2020):**

$$R_a = \frac{1}{l}\int_0^l |z(x)|dx$$

where l is the sampling length and $z(x)$ is the vertical deviation from the mean line, i.e. $z(x) = h_b - \bar{h}_b$.

Some authors, as **Meier et al. (2019a), a**ssociated also the standard deviation of the profile heigh to surface roughness in order to evaluate the spatial homogeneity of the layer profile.

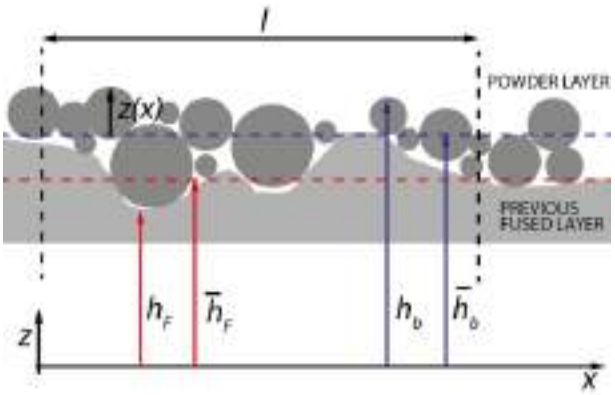

Figure 21 – Illustration of surface roughness.

Whereas surface profile and roughness are easily assessable for numerical simulations as proved by **Meier et al. (2019a), man**y difficulties arise in the experimental investigations because powders tend to modify their arrangement when touched or moved, compromising the reliability of measurements. Laser profilometry can be used to measure the surface roughness in the powder layer because it can be performed in situ and avoid any contact between the powders and the instrument. As shown in Figure 22, the advantage of this technique lies in the ability to capture the surface profile of an extended testing zone (e.g. 64 mm^2), although the resolution of the instrument can limit the capture of the profile of very small particle (e.g. < 10 μm) as described by Chen et al. (2020).

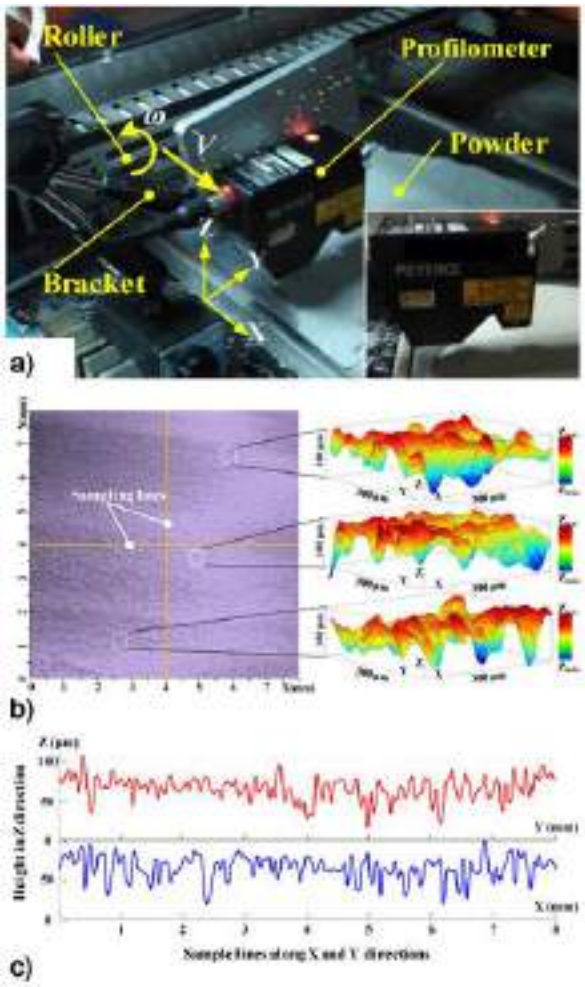

Figure 22 – (a) Experimental setup and example of (b) surface morphology and (c) height profile of a powder layer obtained with laser profilometry tests Chen et al. (2020).

4.3 Spreadability related to standardized tests

Many researchers tried to assess powder spreadability through standardized tests, such as hall flowmeters and powder rheometers, and related them, at least qualitatively, to flowability measurements, see Table 6.

Table 6 – Summary of the standardized tests to access spreadability

Method	*Characterization parameter*	*Link with spreadability*
Rheometer (FT-4)	Basic flow energy (BFE)	Higher its value, lower the spreadability because of the higher flowing resistance Brika et al. (2020); Clayton, (2014); Clayton et al. (2015). Exceptions have been shown Balbaa et al. (2020).
Rheometer (FT-4)	Specific energy (SE)	Higher its value lower the spreadability because of the higher flowing resistance Balbaa et al. (2020); Brika et al. (2020); Clayton et al. (2015)
Rheometer (FT-4)	Conditioned bulk density (CBD)	Higher its value, higher packing density Balbaa et al. (2020); Brika et al. (2020)
Rheometer (FT-4)	Compressibility index (CI)	Lower its value, higher packing density Brika et al. (2020)
Rheometer (FT-4)	Permeability (pressure drop, PD)	Higher permeability (lower PD), higher packing density because of the better ability to release entrapped air Brika et al. (2020)
Rheometer (FT-4)	Aeration energy (AE)	Lower its value, higher powder bed uniformity because of a lower tendency to agglomerate Brika et al. (2020)
Rheometer (FT-4)	Cohesion coefficient (c)	Lower its value, powder bed uniformity because of a lower mechanical interlocking and higher tendency to shear Brika et al. (2020)
Rotating Drum (Revolution powder analyzer)	Avalanche angle (AA)	Higher its value, lower spreadability because of greater resistance to flow Kiani et al. (2020); Snow et al. (2019)
Rotating Drum (Revolution powder analyzer)	Break energy (BE)	Higher its value, lower spreadability because of greater resistance to flow Kiani et al. (2020)
Rotating Drum (Revolution powder analyzer)	Avalanche energy (AE)	Higher its value, lower spreadability because of greater resistance to flow Snow et al. (2019)
Rotating Drum (Revolution powder analyzer)	Avalanche average angle	Higher its value, lower spreadability because of greater resistance to flow Snow et al. (2019)
Rotating Drum (Revolution powder analyzer)	Avalanche surface fractal	Lower its value, better flowability with no agglomeration Sillani et al. (2019)
Hall Flowmeter	Apparent/bulk density (ρ_B)	Poor connection with the lower limit of packing density in the powder layer
Hall Flowmeter	Tap density (ρ_T)	Poor connection with the upper limit of packing density in the powder layer
Hall Flowmeter	Hausner ratio (HR)	Succefful spreading with no lack-of-fusion porosity if HSR < 1.25 Dobson and Starr, (2020)
Hall Flowmeter	Angle of repose (AOR)	Higher the AOR, higher powder cohesion and lower flowability Tan et al. (2017). Higher the AOR, poorer the spreadability Snow et al. (2019). AOR > 40° exhibited poor flowability for high spreading velocities
Hall Flowmeter	Hall flow rate (HF)	Unsuitable method: powders that were not able to flow freely through the funnel were spread without problems Choi et al. (2017; Mitterlehner et al (2021); powders with the same flow rate presented different spreadability Clayton et al. (2015).

4.3.1 Hall flowmeter tests

Many tries have been done for correlating spreadability to Hall flow test as it is cheap and simple to perform. Hall flow test can be used to measure bulk properties such as apparent/bulk ρ_B, tapped density ρ_T and Hausner ratio (HR), the angle of repose (AOR), and the flow rate. However, the limitation in the use of Hall flow tests has been largely demonstrated. In fact, Hall flowmeter measurements are affected by a number of parameters, such as morphology, surface roughness, surface chemistry, size distribution, and environmental conditions as described by **Slotwinski and Garboczi, (2015),** and produce reliable measurements only for free-flowing powders as **confirmed by Clayton, (2014). The** limitation of Hall flow rate measurement has been shown by **Choi et al.**

(2017), which were able to successfully spread two different stainless steel powder samples, where one of them was not able to flow through the Hall flowmeter. Furthermore, Clayton et al. (2015) showed that powders having similar AOR and HF performed differently in an AM process. On **the other hand, some authors as Dobson and Starr, (2020) and Haferkamp et al. (2020) have suggested the use o**f HR as an indicator to understand when the spreading is impeded, and the relationship between flowability, particle size, and interparticle forces.

AOR is usually considered a reliable indicator of powder spreadability. AOR can depict various situations that affect powder spreadability, i.e. AOR < 30° depicts high flowability, whereas AOR > 40° suggests the presence of powder cohesion, see **the work of Tan et al. (2017). As** shown **by Snow et al. (2019) that AOR** can be used to predict the spreading performance. They found that various spreading metrics, i.e. deposition rate, percent of coverage and rate of change of the avalanche angle of a powder pile, have statistical dependencies on AOR, see Figure 23.

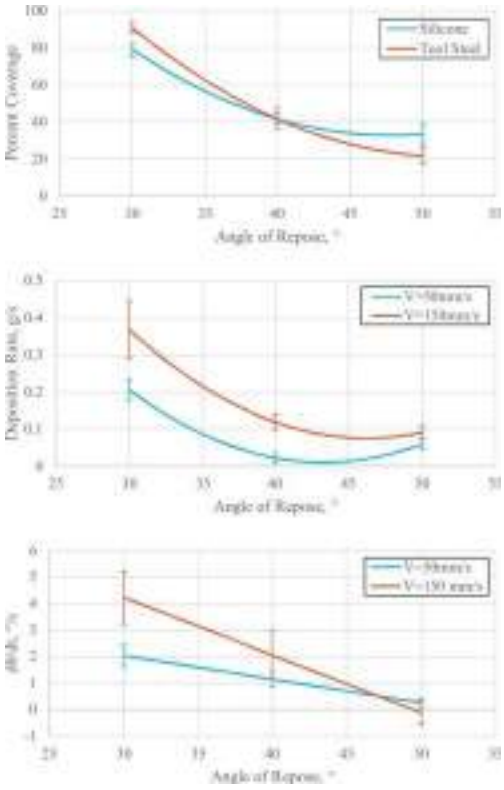

Figure 23 – Spreading metrics as a function of AOR measurements Snow et al. (2019).

4.3.2 Rheometer/FT4 Freeman powder rheometer technique

Powder rheometers offer various tools to characterize powders flow and can provide reliable measurement of bulk properties, such as density, compressibility, and permeability, but also concerning dynamic flow and shear

properties, see Figure 24. Dynamic powder tests consist of determining the axial and rotational forces acting on a rotating blade throughout the whole height of the sample.

Basic flowability energy (BFE) is the energy measured in mJ needed to the blade moving downward in order to displace powders in a specific flow pattern and flow rate in a given volume of powder. BFE is related to the cohesive forces and powder compressibility, and a higher value corresponds to lower powder flowability. Researches tried to qualitatively link BFE to spreadability, arguing that lower BFE values indicate a better spreading performance as suggested by Clayton, (2014); Clayton et al. (2015). Nonetheless, there are examples in the literature where this measurement was not in agreement with the flowability/spreadability exhibited by the powder as in the case of the **work of Balbaa et al. (2020).**

Specific Energy (SE) measures the flowability in a low-stress field and is measured similarly to BFE but with the blade moving upwards. Similar to BFE, **Clayton et al. (2015) su**ggested that higher specific energy was connected to powder more resistant to the motion and, consequently, to lower spreadability.

Conditioned bulk density (CBD) is the bulk density measured with powders with no stresses applied and is considered as an indicator of the packing tendency as **mentioned by Balbaa et al. (2020) but also by Brika et al. (2020). The** compressibility index (CI) is defined as the ratio between density after compression and conditioned bulk density, and it is a measure of the magnitude of interparticle interactions as discussed by Brika et al. (2020). FT4 is able to determine the permeability (pressure drop, PD) of the powder bed, calculating the pressure drop of air passing through the bulk of the sample. The higher the powder permeability, the easier is the release of entrapped air, finally resulting in powder layers with higher packing fraction as documented by **Brika et al. (2020).** Aeration energy (AE) is the energy to displace an aerated powder and gives an indication of the cohesive forces and the mechanical interlocking between particles. As explained in the previous section, high cohesion and mechanical interlocking can be detrimental in the formation of dense and homogeneous powder layers as descriptded in the work of **Brika et al. (2020). A**t the same time the author shows that the cohesion coefficient represents the shear strength at zero normal stress; a low value indicates a high tendency to move from a static state to a dynamic flow.

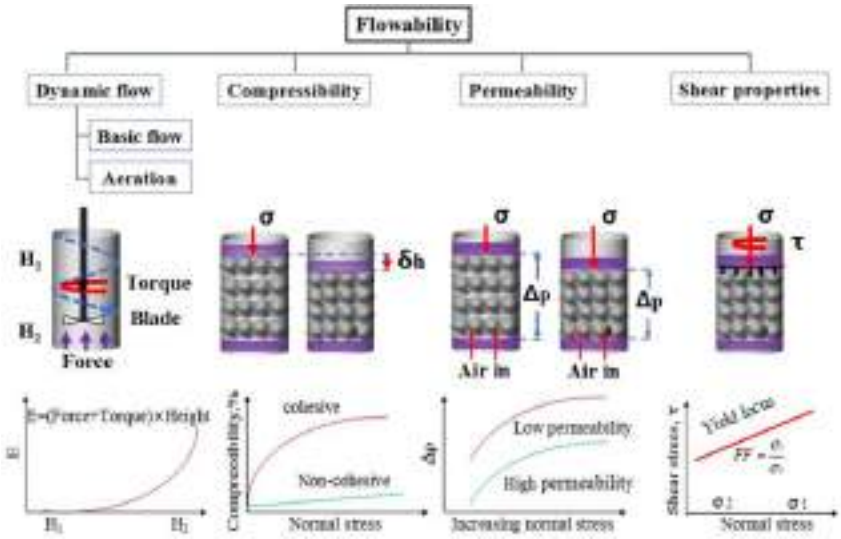

Figure 24 - Schematic diagram of the rheological test available using FT4 Powder Rheometer Wei et al. (2017).

Brika et al. (2020) proposed an index called AMS (AM suitability) to measure the overall suitability of powders from FT4 measurements:

$$\mathrm{AMS} = (\frac{1}{\mathrm{CBD}} + \mathrm{CI} + \mathrm{PD} + \mathrm{SE} + \mathrm{AE} + \mathrm{BFE} + c)/7$$

where ρ_c is the conditioned bulk density, CI the compressibility index, PD the pressure drop, SE the specific energy, AE the aeration energy, BFE the basic flowability energy and *c* the cohesion coefficient; each value is normalized among all the powders studied. According to the authors, the lower the AMS value, the higher is their suitability for AM manufacturing. In contrast, it is reported that the use of FT4 measurements on some spreading metrics was unsuccessful as discussed in the work of **Snow et al. (2019).**

4.3.3 Rotating Drum/Revolution powder analyzer

The core of the Revolution powder analyzer consists of a rotating drum coupled with a digital camera that collects the images of the powder during rotation and, through their analysis, is able to measure the flow properties of powders. Since the instrument measures flowability in low-stress situations, some authors tried to correlate specific measurements obtained with the instrument, such as the avalanche angle, to spreadability.

- Avalanche angle (AA) is the angle obtained from a linear regression of the free powder surface at the incipient occurrence of an avalanche.
- Break energy (BE) is the maximum energy level of the powder before the occurrence of an avalanche and represents the energy required by the powder to start an avalanche.

- Avalanche energy (AE) is the energy released by an avalanche and is calculated by the energy difference between the energy after and before an avalanche **proposed by James, (2019).**

It has been found that the higher AA and BE value, the lower spreadability because of greater resistance to flow. Although further investigations are needed**, Snow et al. (2019) demonstrated** that AA, BE and Avalanche average angle are able to correlate with some spreading metrics, such as the deposition rate, percent of coverage, and rate of change of the avalanche angle of a powder pile.

5. Characteristics that impact spreadability

The complexity of powder spreading lies in the number of variables involved in the process:

1. Feedstock materials;
2. Particle morphology, size and distribution;
3. Moisture influence and pre-treatments;
4. Blade geometry, gap thickness and velocity.

5.1 Feedstock materials and batch-to-batch variability

In AM community is well known that the differences between batches of feedstocks can lead to differences in powder spreading and, consequently, variability in the quality of final products. Testing powders using powder rheometer has highlighted the differences between batches in terms of both basic flowability energy (BFE), which is the energy related to the displacement of powders in a non-gravitational forced flow, and specific energy (SE), which is related to the flowability of unconfined powders. In particular, it has been shown that different batches of powders produced from the same supplier, virtually having the same particle size distribution and resulting in similar angles of repose, exhibited different behavior. Powders with low specific energy showed acceptable behavior, whereas those with high specific energy caused blockages and poor deposition due to the increase of mechanical interlocking and friction as discussed in the work of **Clayton et al. (2015).** Variability was also observed for powders having similar characteristics but produced by different suppliers.

5.2 Particle size, size distribution and shape

The size and shape of particles are fundamental properties to be taken into account as they influence the powder cohesiveness and, finally, flowability and spreadability. It is generally accepted that spherical and smooth powders are preferred because they usually spread in a more uniform powder layer than non-spherical, irregular-shaped powders**. Brika et al. (2020) demonstrated** that a batch of powders produced via gas atomization, which are less regularly shaped, produced higher powder layer porosity than plasma atomized powders, which are more spherical.

Meier et al. (2019a) used DEM simulations to demonstrate that as particle size decreased, and in turn, cohesiveness increased, the quality of powder layer decreased as well, showing the presence of high surface roughness, larger cohesive particle agglomerates, less dense regions, and spatial variations of packing fraction and height profile. Whereas a low packing fraction can be managed in the following process step by changing process parameters accordingly, spatial variations cannot. It has been shown that 10–20 μm can be considered a critical size for powders because, although they sinter fasters, they dramatically reduce the quality of powder layers.

The presence of satellite particles can also be a problem in the spreading process. Satellite particles increase the interparticle friction, decrease flowability, and often cause the inconsistent spread of the powder bed. This condition was observed both in the **work of Mussatto et al. (2020) and Zhao et al. (2020)**.

Particle size distribution is a fundamental aspect to be taken into account because it influences powder flowability and the packing fraction of the power layers after spreading. Depending on the production route of powders, the sieving of specific fractions, or the mixing of powders with different sizes, the powders used in AM can have a narrow size distribution close to monodispersity or be extremely polydisperse. The mixing of multiple powders can lead to multimodal-distributed powders, e.g. bimodal and trimodal powders. The maximum packing fraction (or apparent relative density) of mono-sized powders is about 0.74, whereas the actual value reached in random packing is much lower. In principle, as shown in Figure 25**, Zhu et al. (2007)** demonstrated that the presence of powders having a large ratio of radii can be beneficial to reach the higher packing fraction because finer particles fill the voids between coarser particles.

Generally, a narrower particle size distribution provides better flowability but a lower packing fraction as found in the work of **Averardi et al. (2020). Similar conclusios were found also in the work of Liu et al. (2011).** On the other hand, for wider distribution, if the presence of fine powders is consistent, rheological behavior is affected negatively because of higher inter-particle friction and cohesion as discussed by Brika et al. (2020). In the same year also Kiani et al. (2020) found similar results. Fine powders play a contrasting role; from one hand, the presence of fine powders can increase the packing density as they fill the voids among bigger particles, on the other, a high amount of fine powers below 20 μm can determine agglomeration phenomena and, finally, lack of uniformity in the final powder layers. Dobson and Starr pointed out the importance of fine particulate and showed that a 17-4 PH stainless steel powders having the 30% (on volume basis) of fine particles (below 15 μm) was spread successfully whereas it was not possible to spread the powder when the amount of fine particle was about 55% as demonstrated by Dobson and Starr, (2020).

Some researchers tried to established guidelines on the appropriate particle size distribution to be used in AM. The following rule of thumb for selecting an appropriate particle size distribution was proposed by **Karapatis et al. (1999):**

$$D_{90} < h_{\text{spreader}}, \qquad \frac{D_{50}}{D_{10}} \geq 10, \qquad \frac{D_{90}}{D_{10}} \leq 19$$

which gives a constraint on the maximum size of particles with respect to the spreader clearance and on proportion of finer and coarser fraction, i.e. 50% of the particles should be 10 times bigger than the 10% of the finer fraction and the size ratio between the coarse and the finer fraction should be 1:20. **Spierings and Levy, (2009) pro**posed different requirements for spreading powders in thin layers:

$$\frac{t_{\text{layer}}}{D_{90}} \approx 1.5, \qquad \frac{D_{90}}{D_{10}} \approx 5, \qquad D_{10} > 5\mu\text{m}$$

which indicates that the effective powder layer thickness should be 50% higher than the size of the coarser fraction, the size ratio between the coarse and the finer fraction about 1:5, and the finer fraction about 7.5 times smaller than t_{Layer}, and above 5 μm to avoid powder agglomeration.

The use of bimodal powers can be beneficial to increase the packing fraction of powder layers without compromise the flowability**. Bai et al. (2015)** explained that bimodal powders are usually generated by mixing powders with different mean size and narrow size distribution; similar conclusions were proposed also by **Boley et al. (2016)** When the ratio of radii of the two constituent powders is large enough, i.e. 1:7, and the volume fraction of fine powder is about 0.2-0-4, packing density is usually higher than monomodal powders because finer particles tend to fill the voids left by the coarser fraction.

Ma et al. (2020) simulated the spreading of a metal powder with a size in the range 45 – 150 μm mixed with various quantities (from 0 to 4 % in volume) of a fine powder with particle size ranging between 20 and 40 μm. As shown in Figure 26, an increase of fine fraction from 0 to about 1.5 % lead to an increase of packing fraction and a decrease of surface roughness, whereas higher values of fine fraction result in powder layers with lower packing fraction and higher surface roughness. Those results confirmed the experimental evidence stating that a small amount can increase the quality of the powder layer because the smaller particles fill the voids between the bigger ones, whereas fine particles above a certain amount create problems in the spreading because cohesive forces become significant. Two mechanisms have been used to explain the effect of fine powders. When the fine fraction is in the range 1.5 – 2.5 %, the packing fraction decreases because interlocking and rotational inertia increase, whereas for fine fraction above 2.5 %, the decrease of packing fraction should be attributed to the creation of clusters from the smaller particles under the attractive van der Waals force according to **Ma et al. (2020).**

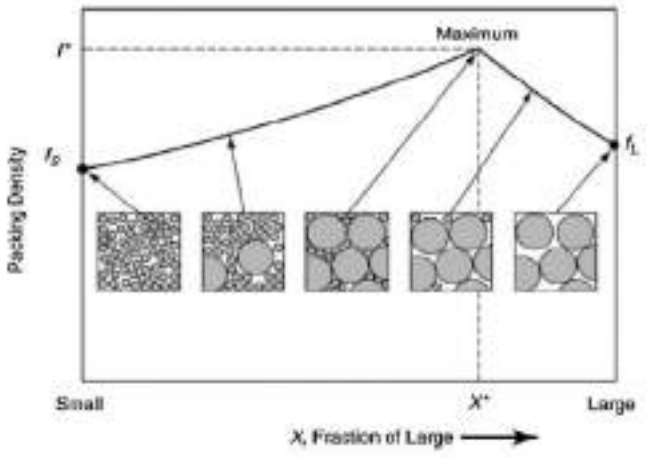

Figure 25 - The schematic of the effects from combinations of different sizes Tan et al. (2017).

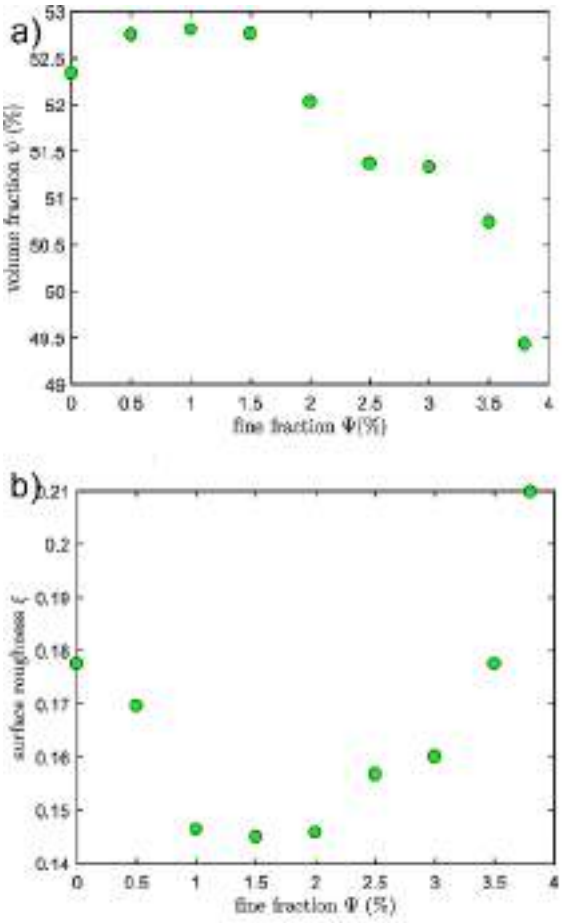

Figure 26 – a) Packing fraction and surface roughness as a function of % of fine fraction Ma et al. (2020).

The effect of different powder shapes has also been investigated. Rod-shaped particles were investigated using various aspect ratio, from 1 (spherical particles) to 2.5, showing that the increase of aspect ratio leads to lower packing density and higher surface roughness. Similar to the case of spherical particles, the spreading of rods is affected by the type of spreader and its velocity. It has been shown that decreasing the spreader velocity can be an effective method for increasing packing density and decrease roughness. Moreover, **Haeri et al. (2016)** affirmed that the spreading performed with a roller type spreader results in high bed quality compared to the flat blade because of its more efficient contact dynamics due to the higher surface of contact and dynamics of a particle flowing through the spreader gap.

A most important undesired effect due to powder segregation is the spatial variation of powder bed properties. As shown **by Ali et al. (2018),** the powder bed density decreases along the moving direction of the recoater. In fact,

as explained in Figure 27, as the recoter moves, the finer particles are deposited first because are able to percolate through the voids that bigger particles form during their movement. Smaller particles are able to better fill the voids and, finally, produce layer with higher packing density. Size segregation lead a change in particle size distribution within the moving heap and, consequently, a change of particle size distribution along the recoater moving direction.

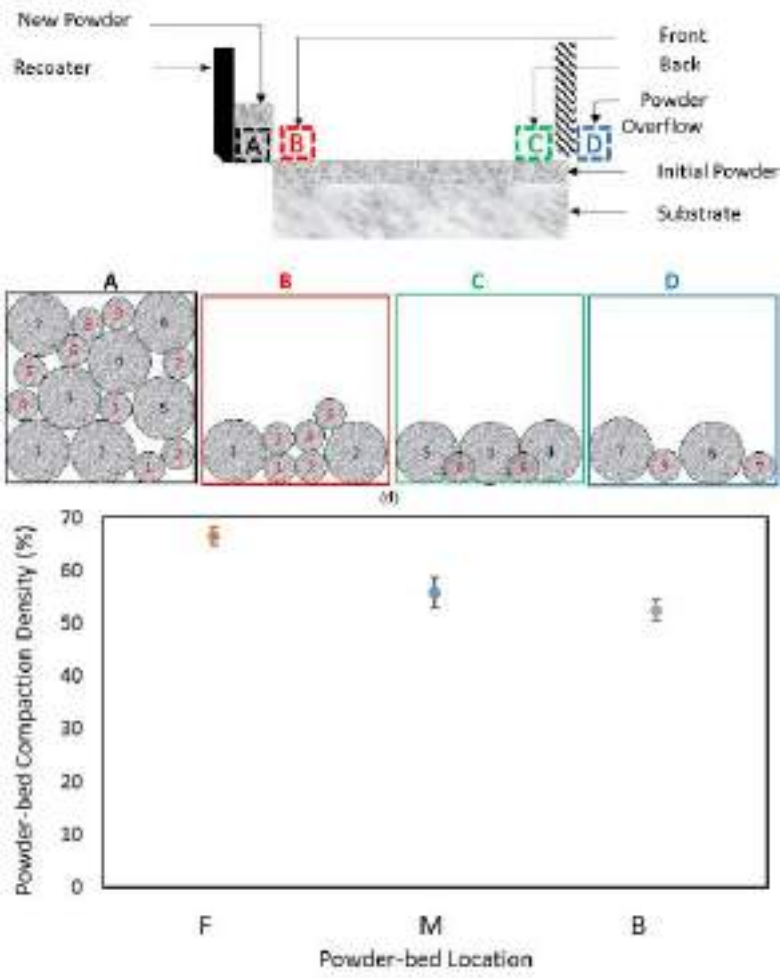

Figure 27 – Powder bed density at different locations, i.e. front (F), middle (M) and back (B) of the bed Ali et al. (2018).

5.3 Humidity

It is well known that humidity can dramatically change the flow behavior and the bulk properties of powders because it causes the formation of liquid bridges between particles, and finally, to interparticle capillary forces as discussed in the works **of Landi et al. (2011) and later by Ma et al. (2019).** Moreover, the moisture adsorbed on

particles can lead to surface modifications, such as the formation of an external oxide layer as demonstrated by Cordova et al. (2020a), that inevitably influence the interactions between particles, e.g. friction and cohesion forces. In AM manufacturing, humidity is considered an important issue, as it can result in poor spreading quality, poor quality of the printed components, and lead to a lack of reproducibility.

As a general **rule, Lefebvre et al. (2020) affirm** that moisture adsorption and desorption depends on RH in the environment and the surface area, but also on the nature of the material**. Engel and Bourell, (2000) observed** that titanium alloy powers exhibit poor flowability/spreadability without a thermal pre-treatment able to reduce moisture adsorbed over the particles. The deeper analysis on plasma atomized titanium powder presented by Lefebvre et al. (2019) demonstrated that the moisture uptake is fast and reversible and showed that there could be a substantial decrease of flowability with the increases of RH. As **shown by Muñiz-Lerma et al. (2018), the** flowability and the apparent density of aluminum powders are affected by RH. Their results suggest that the moisture is adsorbed easily in the presence of a high fraction of fine particles because of their high surface energy, leading to non-uniform spreading. The effect of moisture on the spreading of Inconel 718, Ti6Al4V, AlSi10Mg, Scalmalloy powders was analyzed by **Cordova et al. (2020a). Mitterlehner et al. (2021)** tested nickel-based superalloy powders conditioned at RH 0% and 75%, showing that the humid conditioned power resulted in powder layers with a higher amount of empty patches compared to the dried powder. Moreover, they hypothesize the existence of an RH threshold over which powder layers cannot be dense anymore.

5.4 Powder reuse

Powder spreadability can change in the case of the reuse of powders. The multiple reuses of powders can lead to changes in powders morphology and, consequently, in the flowing behavior during the spreading. **Cordova et al. (2019)** proposed a diagram to be used to decide the feasibility of reusing the powder in a specific application and with a specific material, see Figure 28. In fact, literature data showed that the recyclability of powders is not a straightforward operation, depends on material and particle size distribution, and often lead to contradictory results. **Tang et al. (2015) showe**d that the multiple reuses of Ti-6Al-4V powders with a D_{50} in the other of 70 µm can result in less spherical and rougher particles and, after many cycles, also to the disappearance of satellite particles, but it has also been observed changes in the particle size distributions as suggested **by Strondl et al. (2015).** Unfortunately, research groups reached contradictory conclusions on the effect of recycling on powder flowability/spreadability. On the one hand, it has been claimed that the flowability of reused powders increased because of the reduction of satellite particles and the lower content of moisture due to longer exposure to vacuum as indicated by **Tang et al. (2015),** whereas, on the other, reused powders presented a higher amount of finer particles after recycling and, finally, lower flowability. A similar analysis was conducted using a nickel alloy powder with D_{50} of about 30 µm and led to the conclusion that reused powders contained a larger fraction of coarser particles because a consistent amount of the finer particles is lost during the process. As a result of this

shift in particle size distribution in favor of coarser fractions, used powder exhibited better flowability according **to Strondl et al. (2015). Reused** Inconel 718 powders exhibited lower sphericity compared to virgin powders, and, consequently, the powder bed presented lower apparent and t**apped densities as observed by Chandrasekar et al. (2020) or by Nguyen et al. (2017) i**n an earlier work.

Sutton et al. (2020) found that the density of the powder layer formed by AISI 304L stainless steel powders increases as a result of recycling, and suggested that this effect is due to the increase of flowability/spreadability in reused powder, see Figure 29. In fact, they showed that reused powder exhibited a lower avalanche angle, avalanche energy, and higher conditioned bulk density. The authors suggested that this improvement can be ascribed to the decrease in the number of fine particles and the increase of powder circularity. The shift of particle size distribution towards coarser fraction and the consequent increase of packing density was also observed by **Seyda et al. (2012)** for Ti-6Al-4V powders and S17-4 PH stainless steel **powder by Jacob et al. (2017)**. As suggested by **Sutton et al. (2020),** another reason for the increase of flowability/spreadability can be attributed to the formation of oxides on metals, which might lead to a reduction of friction and surface energy.

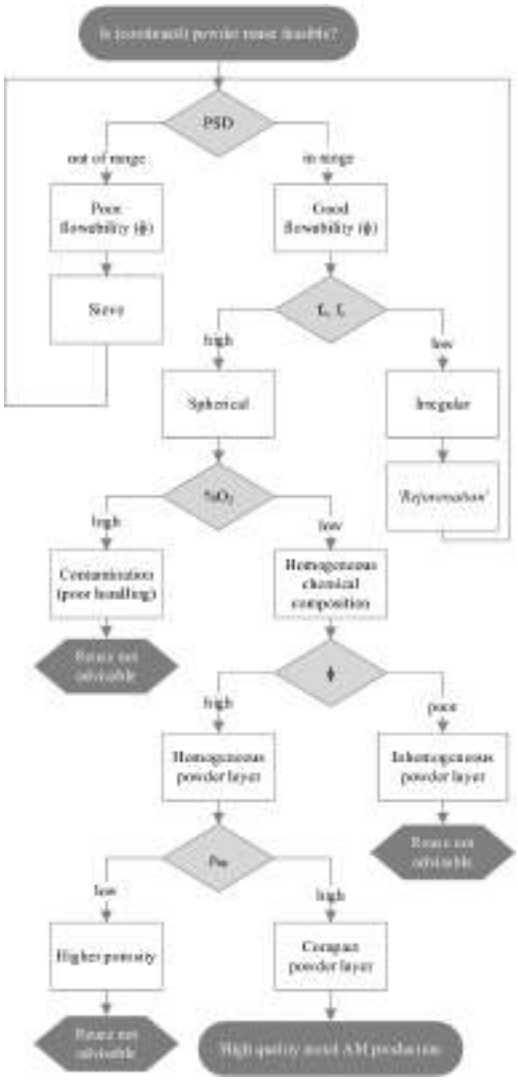

Figure 28 - Reusability decision diagram based on powder properties Cordova et al. (2019).

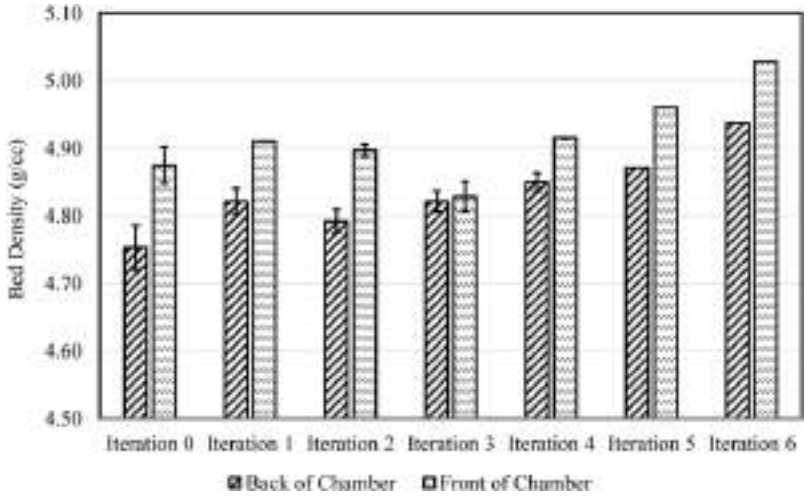

Figure 29 - Powder-bed density measurements at different locations (back and front) for each powder reuse Sutton et al. (2020).

5.5 Powder coating

Coating of metallic powders with nanoparticles can be used as a treatment to reduce the cohesion of fine particles, increase metal powder flowability and bulk powder density. **Gärtner et al. (2021)** demonstrated that nanoparticles act as artificial roughness and are able to distance metal particles, decreasing the value of van der Waals forces and, in turn, particle cohesiveness. Coating is performed by blending in various proportions dried particles and nanoparticles, and ensures that the nanoparticles, seen as guest particles, adhere to the pristine microparticles, which are considered as host particles. As shown in Figure 30a, the size of both the nano-sized guest particles and the micro-sized host particles have a great influence on the overall cohesion behavior of such a system. As shown in Figure 30b, two main mechanisms occur during powder spreading of such particle systems, i.e. (i) the friction and mechanical interlocking between particles, which determine the resistance to flow, and (ii) the reduction of the contact surface, which reduce adhesion between particles and increase the flowability of powders as discussed in the work of **Fereiduni et al. (2019).**

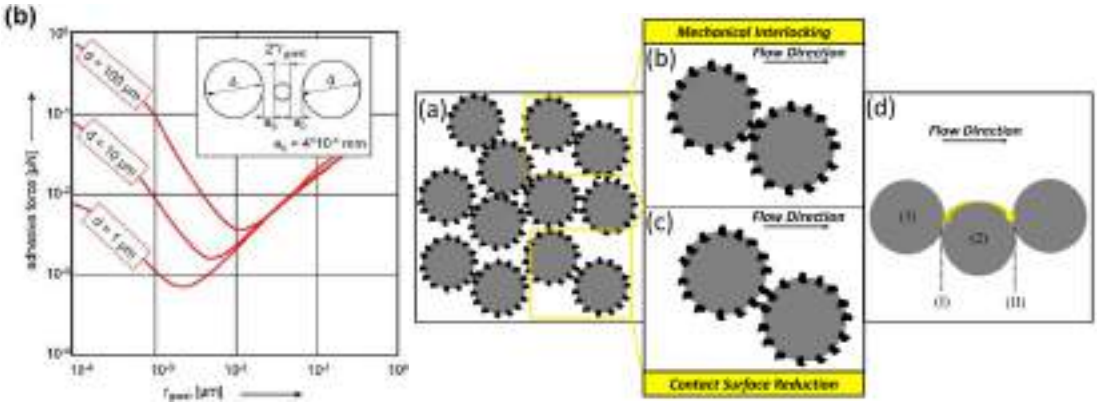

Figure 30 – Adhesive force between host microparticles as a function of nano-sized guest particles radius and for micro-sized host particle diameter Karg et al. (2019) Fereiduni et al. (2019).

Dry coating is a technique for coating powders without the use of any liquid; host and guest particles are blended in a mixer or a mill by suppling high energy in order to produce energetic guest-host collisions, which are responsible for the adhesion of guest nano-sized particles over the surface of the host micro-sized particles as discussed by **Sharma and Setia, (2019). In the context of AM, various systems were testes, i.e. Peng et al. (2018) proposed the coating of fine Inconel 718 microparticles with nano hydrophobic silica or nanocarbon, Karg et al. (2013) proposed the coating of non-spherical powders of allowing close to the eutectic AlSi12, and Karg et al. (2019) demonstrated that the addition of low weight percentage of nanoparticles could lead to more homogenous spreading of powders in thin layers and increase the relative density of LBM samples.**

Wet coating can be seen as an alternative to dry coating. **Streubel et al. (2018)** proposed a procedure that started from the dispersion by ultrasonication of nano-sized powder in water, the laser-irradiation of suspension in jet flowing, mechanical mixing with steel micro-sized powder, and, finally, drying in a furnace.

5.6 Blade geometry, gap clearance and speed

The simplest spreader in AM equipment is constituted by a flat blade. It has been reported by Chen et al. (2017) that the quality of the powder layer decreases as the blade speed increases because the powder tends to dilate, leading to looser flow and creating discontinuity within the layer. The decrease of the gap height triggers the formation of force aches between particles, affecting the continuity and stability of powder flow and, finally, resulting in low-quality **spreading. Beitz et al. (2019) investigate** the effect of three different blade geometries, i.e. flat, slightly round and sharp blades, demonstrating that the flat blade leads to lower roughness and better compaction than the other blades because of its larger horizontal contact surface.

Since the contact dynamics between a flat blade and particles is considered inefficient, some attempts have been made in order to optimize the spreader profile and increase the effectiveness of powder spreading. The use of a super-elliptic edge profile arises from the assumption that a gradual flattening of powders and a larger contact area can reduce the phenomenon of particle dragging and, finally, be beneficial to the spreading. The edge profile was generated using the equation describing superellipse curves $|y/a|^n + |z/b|^n = 1$, where n is responsible for the shape (concave profile for $0 < n < 1$, linear for $n = 1$, convex for $1 < n < 2$, and a rectangle with rounded corners for $n > 2$), a for width and b for height. It has been shown that the concave profile did not produce an improvement in the quality of the final powder layer, whereas the linear profile can increase bed packing fraction for wider profiles. On the other hand, the convex profiles showed the most promising results, especially in the case of n around 5 and **wider edges. Haeri, (2017) noticed that an** optimized profile allows the increase of spreading velocity but limiting, at the same time, the loss in spreading quality.

Generally, the roller outperforms the blade spreader in terms of the quality of the power bed at the same operating conditions as demonstrated by **Haeri et al. (2016). In the** case of counter-rolling spreaders, the increase of spreading velocity reduces the quality of the powder layer because of the increasing of the surface roughness and the decreasing of the packing density. This effect has been explained in terms of two concurrent forces, i.e. the friction force between the particles and the sintered/melted underlying layer and the drag force on particles from the roller. As the roller velocity increases, the drag force exerted on particles from the roller increases as well. At low velocity, the drag force is compensated by the friction force and, consequently, the particles move under the roller, rearrange themselves in a denser packing under the pressure exerted by the roller and, finally, quickly rest because friction opposes the tendency of powder of following the roller. On the other hand, when the drag force is large enough to overcome friction forces, particles do not rest immediately after they passed through the roller gap but flow following the roller movement for a certain distance and, then, deposit on the underlying layer. In this case**, Chen et al. (2020)** affirm that the powder bed shows higher surface roughness and lower packing density.

DEM simulations, performed by **Meier et al. (2019a),** have shown that the quality of powder layers increases with increasing blade gap height, and the optimum value to be set as gap height is equal to two to three times the maximal powder particle diameter. In particular, **Mindt et al. (2016)** observed that powder bed density increased as the blade gap height was increased. On the other hand, **Brika et al. (2020) h**ave obtained experimentally opposite results, as the increase of blade gap height leads to lower powder bed density.

The velocity of the spreader can be an important factor for increasing the productivity of AM process. On the other hand, the choice of a high velocity should be carefully evaluated considering the consequent loss of quality of bed packed layer and reproducibility in that conditions. As shown in Figure 31, the increase of spreader velocity results in powder layers with lower density and higher surface roughness, finally reducing the quality of the powder layer as discussed by **Chen et al. (2020).**

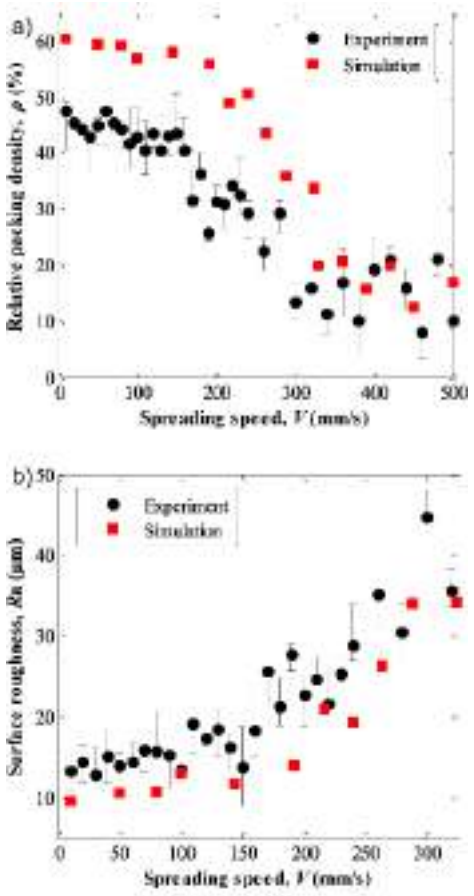

Figure 31 – a) Relative packing density and b) surface roughness as a function of spreading speed Chen et al. (2020).

6. Impact of spreadability on printed component

6.1 Density of the printed component

The density of final parts is affected by the gap height of the recoater/blade used to spread the powders. As shown by many authors, density decreased as the gap height increases. The decrease of density with the increase of spreader gap heights was observed by **Abd- Elghany and Bourell, (2012),** who evaluated the density of the final layer after SLM produced using 304L stainless steel gas atomized powders and three different spreader gap heights. In fact, the spreader can exclude from the spreading the powder fraction having a size above the gap height

so that the smaller the gap height, the finer is the powder fraction spread. The same authors, i.e. **Abd- Elghany and Bourell, (2012)also** mentioned that the consequential exclusion of coarser fraction can be beneficial, as larger particles can form voids due to shrinkage after solidifications, cracks and layer separations at grain boundaries. Similar results were obtained with Ti-6Al-4V alloy powders as can be found in the work of **Brika et al. (2020)**.

Ali et al. (2018) evaluated the differences in the density of printed components along the bed. As shown in Figure 32, density slightly decreases along the recoater moving direction, showing differences of about 0.25%. This difference can be attributed to the non-uniformity of the spreading due to size segregation, which inevitably lead to differences in powder bed density and particle size distribution.

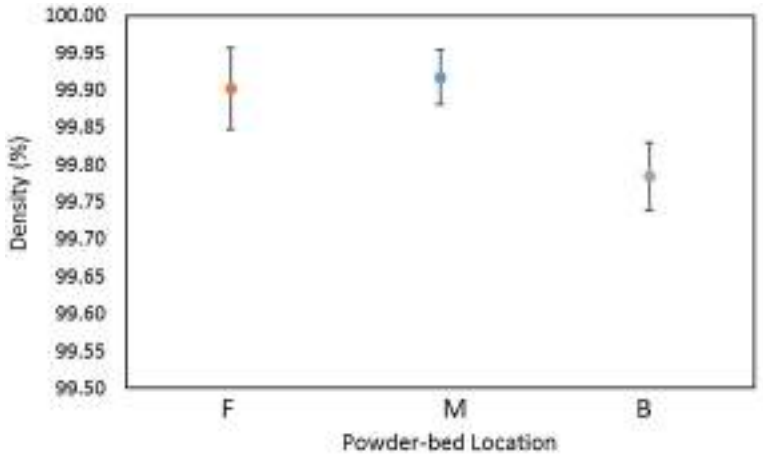

Figure 32 – Density of the printed components at different location,i.e. front (F), middle (M) and back (B) of the bed Ali et al. (2018).

6.2 Surface roughness and dimensional accuracy

The particle size constituting the powder layer has a strong influence on surface roughness. The simulation performed by Lee and Zhang, (2015) showed that the contour of the melt pool is smoother when the powder layer contains a high fraction of fine particles. They also pointed out the importance of packing density on the final quality, as the higher packing fraction results in better surface finish, denser parts without discontinuity and with a smoother surface. Similar to density of printed components, surface roughness is negatively affected when the spreader gap height is increased as **demonstrated by Abd- Elghany and Bourell, (2012).**

Non-uniformity of powder spreading clearly affected the uniformity of surface roughness of the final printed components. **As shown by Ali et al. (2018),** powder segregation during spreading leads to differences in surface roughness of about 20% along the recoater moving direction (Figure 33). These differences can be attributed to the spatial variation of particle size distribution across the build bed.

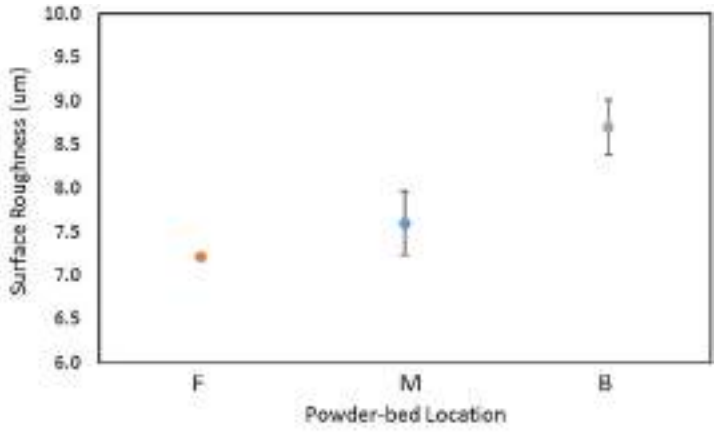

Figure 33 – Surface roughness of the printed components at different locations,i.e. front (F), middle (M) and back (B) of the bed Ali et al. (2018).

Dimensional accuracy is also influenced by the powder spreading**. Balbaa et al. (2020) compared** two powders for L-PBF process, i.e. fine and coarse powders, which exhibited different spreadability. In fact, the fine powder possesses lower flowability (-75%) and packing density (-30%). The less spreadable powder not only resulted in printed components with low density and higher surface roughness but also in poorer dimensional accuracy in both horizontal and building directions. This was explained by the tendency of less spreadable powders to form agglomerates.

6.3 Mechanical properties

In the case of SLM, the mechanical properties of the final components are affected by (i) the rapid melting of particles by the laser beam and their immediate cooling, which could lead to changes in the crystal structures and phases, and (ii) phenomena of incomplete melting, porosity and micro-cracking. The effect of spreader gap height and scanning speed on tensile strength was studied by **Abd- Elghany and Bourell, (2012) for** SLM process. They showed that the increase of gap height and scanning speed decrease, yield strength, ultimate tensile strength and breaking elongation because thicker powder layers presented higher porosity and micro-cracking but also due to a less efficient melting of the powder layer with the layer below. Moreover, the higher surface porosity showed by the thicker layers brought to a decrease of hardness value.

7. Conclusions and future research direction

Powder spreadability is a fundamental aspect of AM manufacturing and requires much more research efforts to be understood and quantified to increase the reliability and repeatability of the process and, consequently, the quality of printed components. Since only in recent years the concept of spreadability has turned on the spotlight and studied systematically. There are still many gaps that need to be addressed:

1. development of standards and metrics quantitatively assess powder spreadability;
2. increasing the understanding of the spreading dynamics;
3. correlate feedstock characteristics to its ability to spreadability;
4. correlate standardized tests (hall flowmeter, rheometers, rotating drums,…) to spreadability;
5. further investigation on the effect of powder spreading on the quality of the final printed components;
6. monitor and control the quality of powder spreading and its variability.

Like many other technological properties, the definition of spreadability is debated, and there is no accordance on how it can be measured. ANSI has inserted spreadability as a gap in AM, as nor unique description nor standards to quantify it is available at the moment. Many spreading metrics have been proposed so far to answer the question "what is a good spreading", but none of them is proved to be effective in the complete quantification of spreadability. Qualitatively, it is considered a powder with good spreadability, the ones that form layers possessing high packing density, spatial uniformity and smooth profile. The main problems in the quantification of powder spreadability lies in the difficulty of generalising the problem to all the possible AM processes and the difficulty of assessing the spread layers directly. Spreading, as an intermediate step in AM process, is not directly assessed but generally evaluated based on the final printed components. More effort should be dedicated to shortening the research gap in this direction and, in particular, to identify the quantitative relation between powders/machine operations and the key properties of the resulting powder layers (e.g. packing density, presence of voids, uniformity), and between the latter and the final printed components.

A clear understanding of the spreading dynamics represents a key factor in achieving quality improvement, replicability, standardization and optimization in AM. Although considerable progress has been made in the past years, the dynamic of spreadability is still not fully understood due to the complexity of the spreading process, which involves the interaction among the spreader, powders, and the surrounding environment. Much effort would need to understand the role of different spreader geometries, material and operational conditions, such as spreader velocity and gap thickness, in their interaction with powders. The research has pointed out as powder characteristics, such as powder friction and cohesion, may play a significant role in the avalanching flow of the powder pile and shear flow in the gap between the spreader and the baseplate during spreading. Although some mechanisms have been identified, the major gap in the research is represented by the fact that the relationship between the occurrence of those mechanisms and powder characteristics is still unclear. From the experimental

standpoint, investigating such a relationship is complicated by the difficulty of a direct assessment of powder spreading.

A further problem is represented by the variability of powder characteristics collected from different batches or vendors. In this sense, the support of first-principle numerical modelling (e.g. DEM, DEM-CFD) for the experimentation can be of advantage to fill this research gap as it direct assesses the spreading phenomena at the particle level and give the experimenter the control of the powder specifications. The problem of the variability of powder characteristics is ubiquitous **Zegzulka, (2020)** and is leading many researchers to explore the causes and possible solutions.

Many efforts have been made in the past to correlate standardized tests such as hall flowmeters, rheometers, and rotating drums to powder spreadability. However, those attempts have only partially addressed this problem and, in some cases, have led to contradictory results. Succeeding in correlating the outcomes from standardised tests with powder spreadability would help identify and choose the appropriate powders to be used in a specific process and with specific process conditions. This represents a big opportunity to increase process/powder understanding and give professionals the suitable instruments to choose the more appropriate materials.

Further investigations on the effect of powder spreading on the quality of the final printed components are needed to design consistent processes. The few papers published call for deepening the investigation of the relationship between powder spreading and mechanical behaviour, microstructure, presence of voids, formation of cracks, and the quality and appearance of the surface of the final products. The complexity of the problem and the number of variables involved require a more systematic and statistical approach, as also mentioned in the work of **Zegzulka et al. (2020).**

None or a few studies have been published concerning monitoring and controlling the quality of powder spreading. The development of new technologies able to measure the quality of powder layers is fundamental in ensuring highly consistent production, optimising the process, and reducing manufacturing costs. There is a broad research space in the development of new in-line devices able to catch specific properties of the layers, such as packing density, layer thickness, uniformity and surface smoothness, during the spreading. At that point, the monitoring and control of the spreading quality would inform an automated algorithm on the energy intensity/duration to be supplied to meet the specifications of the final component.

Furthermore, applying the methods mentioned above for assessing spreadability can be used as a starting point to describe the behaviour of even more complex powder systems. According to the authors' knowledge, only a few papers discuss composite powders' spreadability, for **example, in the work of Lüddecke et al. (2021), where** a nanocomposite powder containing different oxides was investigated. More specifically, stainless steel, tool steel and aluminium alloy powders were reinforced via SiC, graphene, and iron oxide black. The paper's focus was on optimising the printing parameters, and powder spreadability was thoroughly investigated.

Further developments could be achieved by applying Image processing steps. For example **Vakifahmetoglu et al. (2022) rec**ently introduced an image processing algorithm based on Matlab software to examine spreadability as a function of the powder size distribution or other physical properties of the material. Similar efforts could be introduced in the future but using open source programming codes such as python to spread knowledge among researchers and end-users.

Indeed one crucial point to achieve in the future is reducing the complexity of the measurement of powder properties. As long as the adopted techniques become more accessible and faster, their scalability increases and industrialisation becomes possible. This kind of effort was observed in some literary works, e.g. the one from Ahmed et al. (2020), who proposed a simple technique for assessing the powder spreadability.

At the time of this review, all techniques require that powder samples are assessed outside of the printing machine. As a possible future optimization, the aforementioned techniques could be moved directly into the LPBF machines and used online during the printing process. As a further optimization, it would be really interesting to produce a machine routine which optimizes its printing parameters directly from the assessment of the powders using an online feedback system. Knowing in advice the powder properties and tailoring the printing parameters specifically for the processed powders could enhance the layer density obtaining higher densities after the laser melting.

8. References

Abd- Elghany, K., Bourell, D.L., 2012. Property evaluation of 304L stainless steel fabricated by selective laser melting. Rapid Prototyp. J.

Ahmed, M., Pasha, M., Nan, W., Ghadiri, M., 2020. A simple method for assessing powder spreadability for additive manufacturing. Powder Technol. 367, 671–679. https://doi.org/10.1016/j.powtec.2020.04.033

Ali, U., Mahmoodkhani, Y., Shahabad, S.I., Esmaeilizadeh, R., Liravi, F., Sheydaeian, E., Huang, K.Y., Marzbanrad, E., Vlasea, M., Toyserkani, E., 2018. On the measurement of relative powder-bed compaction density in powder-bed additive manufacturing processes. Mater. Des. 155, 495–501.

America Makes, ANSI Additive Manufacturing Standardization, 2017. Standardization roadmap for additive manufacturing. ANSI/National Cent. Def. Manuf. Mach. https//www. ansi. org/standards_activities/standards_boards_ panels/amsc/Default.

Averardi, A., Cola, C., Zeltmann, S.E., Gupta, N., 2020. Effect of particle size distribution on the packing of powder beds: A critical discussion relevant to additive manufacturing. Mater. Today Commun. 24, 100964.

Bai, Y., Wagner, G., Williams, C.B., 2015. Effect of bimodal powder mixture on powder packing density and

sintered density in binder jetting of metals, in: 2015 Annual International Solid Freeform Fabrication Symposium. pp. 758–771.

Balbaa, M.A., Ghasemi, A., Fereiduni, E., Elbestawi, M.A., Jadhav, S.D., Kruth, J.-P., 2020. Role of powder particle size on laser powder bed fusion processability of AlSi10mg alloy. Addit. Manuf. 101630.

Beitz, S., Uerlich, R., Bokelmann, T., Diener, A., Vietor, T., Kwade, A., 2019. Influence of powder deposition on powder bed and specimen properties. Materials (Basel). 12, 297.

Blais, B., Vidal, D., Bertrand, F., Patience, G.S., Chaouki, J., 2019. Experimental Methods in Chemical Engineering: Discrete Element Method—DEM. Can. J. Chem. Eng. 97, 1964–1973.

Bo, S., Wen, S., Yan, C., Wei, Q., Shi, Y., 2020. Selective Laser Melting for Metal and Metal Matrix Composites. Academic Press.

Boley, C.D., Mitchell, S.C., Rubenchik, A.M., Wu, S.S.Q., 2016. Metal powder absorptivity: modeling and experiment. Appl. Opt. 55, 6496–6500.

Brika, S.E., Letenneur, M., Dion, C.A., Brailovski, V., 2020. Influence of particle morphology and size distribution on the powder flowability and laser powder bed fusion manufacturability of Ti-6Al-4V alloy. Addit. Manuf. 31, 100929.

Castellanos, A., 2005. The relationship between attractive interparticle forces and bulk behaviour in dry and uncharged fine powders. Adv. Phys. 54, 263–376.

Chandrasekar, S., Coble, J.B., Yoder, S., Nandwana, P., Dehoff, R.R., Paquit, V.C., Babu, S.S., 2020. Investigating the effect of metal powder recycling in Electron beam Powder Bed Fusion using process log data. Addit. Manuf. 32, 100994.

Chen, H., Chen, Y., Liu, Y., Wei, Q., Shi, Y., Yan, W., 2020. Packing quality of powder layer during counter-rolling-type powder spreading process in additive manufacturing. Int. J. Mach. Tools Manuf. 153, 103553. https://doi.org/10.1016/j.ijmachtools.2020.103553

Chen, H., Wei, Q., Wen, S., Li, Z., Shi, Y., 2017. Flow behavior of powder particles in layering process of selective laser melting: Numerical modeling and experimental verification based on discrete element method. Int. J. Mach. Tools Manuf. 123, 146–159.

Chen, H., Wei, Q., Zhang, Y., Chen, F., Shi, Y., Yan, W., 2019. Powder-spreading mechanisms in powder-bed-based additive manufacturing: Experiments and computational modeling. Acta Mater. 179, 158–171.

Chen, Q., Juste, E., Lasgorceix, M., Petit, F., Leriche, A., 2022. Binder jetting process with ceramic powders: Influence of powder properties and printing parameters. Open Ceram. 9, 100218.

https://doi.org/10.1016/j.oceram.2022.100218

Chin, S.Y., Dikshit, V., Meera Priyadarshini, B., Zhang, Y., 2020. Powder-Based 3D Printing for the Fabrication of Device with Micro and Mesoscale Features. Micromachines 11, 658.

Choi, J.-P., Shin, G.-H., Lee, H.-S., Yang, D.-Y., Yang, S., Lee, C.-W., Brochu, M., Yu, J.-H., 2017. Evaluation of powder layer density for the selective laser melting (SLM) process. Mater. Trans. 58, 294–297.

Clayton, J., 2014. Optimising metal powders for additive manufacturing. Met. Powder Rep. 69, 14–17.

Clayton, J., Millington-Smith, D., Armstrong, B., 2015. The application of powder rheology in additive manufacturing. Jom 67, 544–548.

Coetzee, C.J., 2017. Calibration of the discrete element method. Powder Technol. 310, 104–142.

Cordova, L., Bor, T., de Smit, M., Campos, M., Tinga, T., 2020a. Measuring the spreadability of pre-treated and moisturized powders for laser powder bed fusion. Addit. Manuf. 32, 101082.

Cordova, L., Bor, T., de Smit, M., Carmignato, S., Campos, M., Tinga, T., 2020b. Effects of powder reuse on the microstructure and mechanical behaviour of Al–Mg–Sc–Zr alloy processed by laser powder bed fusion (LPBF). Addit. Manuf. 36. https://doi.org/10.1016/j.addma.2020.101625

Cordova, L., Campos, M., Tinga, T., 2019. Revealing the Effects of Powder Reuse for Selective Laser Melting by Powder Characterization. Jom 71, 1062–1072. https://doi.org/10.1007/s11837-018-3305-2

Cundall, P.A., Strack, O.D.L., 1979. A discrete numerical model for granular assemblies. Geotechnique 29, 47–65.

Dawes, J., Bowerman, R., Trepleton, R., 2015. Introduction to the additive manufacturing powder metallurgy supply chain. Johnson Matthey Technol. Rev. 59, 243–256.

Desai, P.S., Higgs, C.F., 2019. Spreading process maps for powder-bed additive manufacturing derived from physics model-based machine learning. Metals (Basel). 9, 1176.

Desai, P.S., Mehta, A., Dougherty, P.S.M., Higgs III, C.F., 2019. A rheometry based calibration of a first-order DEM model to generate virtual avatars of metal Additive Manufacturing (AM) powders. Powder Technol. 342, 441–456.

Dobson, S.D., Starr, T.L., 2020. Powder characterization and part density for powder bed fusion of 17-4 PH stainless steel. Rapid Prototyp. J.

Engel, B., Bourell, D.L., 2000. Titanium alloy powder preparation for selective laser sintering. Rapid Prototyp. J.

Escano, L.I., Parab, N.D., Xiong, L., Guo, Q., Zhao, C., Fezzaa, K., Everhart, W., Sun, T., Chen, L., 2018.

Revealing particle-scale powder spreading dynamics in powder-bed-based additive manufacturing process by high-speed x-ray imaging. Sci. Rep. 8, 1–11.

Fereiduni, E., Ghasemi, A., Elbestawi, M., 2019. Characterization of Composite Powder Feedstock from Powder Bed Fusion Additive Manufacturing Perspective. Materials (Basel). 12, 3673.

Frazier, W.E., 2014. Metal additive manufacturing: A review. J. Mater. Eng. Perform. 23, 1917–1928. https://doi.org/10.1007/s11665-014-0958-z

Gärtner, E., Jung, H.Y., Peter, N.J., Dehm, G., Jägle, E.A., Uhlenwinkel, V., Mädler, L., 2021. Reducing cohesion of metal powders for additive manufacturing by nanoparticle dry-coating. Powder Technol. 379, 585–595. https://doi.org/10.1016/j.powtec.2020.10.065

Geer, S., Bernhardt-Barry, M.L., Garboczi, E.J., Whiting, J., Donmez, A., 2018. A more efficient method for calibrating discrete element method parameters for simulations of metallic powder used in additive manufacturing. Granul. Matter 20, 77.

Gokuldoss, P.K., Kolla, S., Eckert, J., 2017. Additive manufacturing processes: Selective laser melting, electron beam melting and binder jetting—Selection guidelines. Materials (Basel). 10, 672.

Haeri, S., 2017. Optimisation of blade type spreaders for powder bed preparation in Additive Manufacturing using DEM simulations. Powder Technol. 321, 94–104.

Haeri, S., Wang, Y., Ghita, O., Sun, J., 2016. Discrete element simulation and experimental study of powder spreading process in additive manufacturing. Powder Technol. 306, 45–54.

Haferkamp, L., Spierings, A., Rusch, M., Jermann, D., Spurek, M.A., Wegener, K., 2020. Effect of Particle size of monomodal 316L powder on powder layer density in powder bed fusion. Prog. Addit. Manuf. 1–8.

He, Y., Gardy, J., Hassanpour, A., Bayly, A.E., 2020. A digital-based approach for characterising spread powder layer in additive manufacturing. Mater. Des. 196, 109102.

Hoeges, S., Zwiren, A., Schade, C., 2017. Additive manufacturing using water atomized steel powders. Met. Powder Rep. 72, 111–117. https://doi.org/10.1016/j.mprp.2017.01.004

Hu, Z., Mahadevan, S., 2017. Uncertainty quantification and management in additive manufacturing: current status, needs, and opportunities. Int. J. Adv. Manuf. Technol. 93, 2855–2874.

Hulme-Smith, C.N., Hari, V., Mellin, P., 2021. Spreadability Testing of Powder for Additive Manufacturing. B. Huettenmaenn Monatsh 166, 9–13.

Jacob, G., Donmez, A., Slotwinski, J., Moylan, S., 2016. Measurement of powder bed density in powder bed fusion

additive manufacturing processes. Meas. Sci. Technol. 27, 115601.

Jacob, G., Jacob, G., Brown, C.U., Donmez, M.A., Watson, S.S., Slotwinski, J., 2017. Effects of powder recycling on stainless steel powder and built material properties in metal powder bed fusion processes. US Department of Commerce, National Institute of Standards and Technology ….

James, W.B., 2019. Mercury Scientific Revolution ASTM Paper [WWW Document].

Karapatis, N.P., Egger, G., Gygax, P.E., Glardon, R., 1999. Optimization of powder layer density in selective laser sintering, in: 1999 International Solid Freeform Fabrication Symposium.

Karg, M., Laumer, T., Schmidt, M., 2013. Additive Manufacturing of Gradient and Multimaterial Components, in: Proceedings of the International Conference on Competitive Manufacturing, Stellenbosch, South Africa.

Karg, M.C.H., Munk, A., Ahuja, B., Backer, M.V., Schmitt, J.P., Stengel, C., Kuryntsev, S.V., Schmidt, M., 2019. Expanding particle size distribution and morphology of aluminium-silicon powders for Laser Beam Melting by dry coating with silica nanoparticles. J. Mater. Process. Technol. 264, 155–171.

Kassym, K., Perveen, A., 2020. Atomization processes of metal powders for 3D printing. Mater. Today Proc. 26, 1727–1733.

Kiani, P., Scipioni Bertoli, U., Dupuy, A.D., Ma, K., Schoenung, J.M., 2020. A statistical analysis of powder flowability in metal additive manufacturing. Adv. Eng. Mater. 22, 2000022.

Kirchner, A., Klöden, B., Weißgärber, T., Kieback, B., 2016. Powders for Additive Manufacturing.

Landi, G., Barletta, D., Poletto, M., 2011. Modelling and experiments on the effect of air humidity on the flow properties of glass powders. Powder Technol. 207, 437–443.

Lecis, N., Beltrami, R., Mariani, M., 2021a. Binder jetting 3D printing of 316 stainless steel: Influence of process parameters on microstructural and mechanical properties. Metall. Ital. 113, 31–41.

Lecis, N., Mariani, M., Beltrami, R., Emanuelli, L., Casati, R., Vedani, M., Molinari, A., 2021b. Effects of process parameters, debinding and sintering on the microstructure of 316L stainless steel produced by binder jetting. Mater. Sci. Eng. A 828, 142108. https://doi.org/10.1016/j.msea.2021.142108

Lee, S., Sachs, E., Cima, M., 1995. Layer position accuracy in powder- based rapid prototyping. Rapid Prototyp. J.

Lee, Y., Gurnon, A.K., Bodner, D., Simunovic, S., 2020. Effect of Particle Spreading Dynamics on Powder Bed Quality in Metal Additive Manufacturing. Integr. Mater. Manuf. Innov. 1–13.

Lee, Y., Simunovic, S., Gurnon, K.A., 2019. Quantification of Powder Spreading Process for Metal Additive

Manufacturing. Oak Ridge National Lab.(ORNL), Oak Ridge, TN (United States).

Lee, Y.S., Zhang, W., 2015. Mesoscopic simulation of heat transfer and fluid flow in laser powder bed additive manufacturing, in: International Solid Free Form Fabrication Symposium, Austin. pp. 1154–1165.

Lefebvre, L.-P., Dai, J., Thomas, Y., Daroszewska, M., Martinez-Rubi, Y., 2020. Measurement of Water Content in Metal Powders. Mater. Perform. Charact. 9.

Lefebvre, L.P., Dai, J., Thomas, Y., Martinez-Rubi, Y., 2019. Metal powder flowability: effect of humidity and impact on the reproducibility of the measurements, in: Proceeding of the Additive Manufacturing with Powder Metallurgy Conference. pp. 1–13.

Leturia, M., Benali, M., Lagarde, S., Ronga, I., Saleh, K., 2014. Characterization of flow properties of cohesive powders: A comparative study of traditional and new testing methods. Powder Technol. 253, 406–423.

Li, X.P., O'donnell, K.M., Sercombe, T.B., 2016. Selective laser melting of Al-12Si alloy: Enhanced densification via powder drying. Addit. Manuf. 10, 10–14.

Liao, J., Cooper, D.R., 2021. The Environmental Impacts of Metal Powder Bed Additive Manufacturing. J. Manuf. Sci. Eng. 143.

Liu, B., Wildman, R., Tuck, C., Ashcroft, I., Hague, R., 2011. Investigation the effect of particle size distribution on processing parameters optimisation in selective laser melting process. Addit. Manuf. Res. group, Loughbrgh. Univ. 227–238.

Lommen, S., Schott, D., Lodewijks, G., 2014. DEM speedup: Stiffness effects on behavior of bulk material. Particuology 12, 107–112.

Lüddecke, A., Pannitz, O., Zetzener, H., Sehrt, J.T., Kwade, A., 2021. Powder properties and flowability measurements of tailored nanocomposites for powder bed fusion applications. Mater. Des. 202. https://doi.org/10.1016/j.matdes.2021.109536

Ma, Y., Evans, T.M., Philips, N., Cunningham, N., 2020. Numerical simulation of the effect of fine fraction on the flowability of powders in additive manufacturing. Powder Technol. 360, 608–621.

Ma, Y., Evans, T.M., Philips, N., Cunningham, N., 2019. Modeling the effect of moisture on the flowability of a granular material. Meccanica 54, 667–681. https://doi.org/10.1007/s11012-018-0901-8

Mariani, M., Goncharov, I., Mariani, D., De Gaudenzi, G. Pietro, Popovich, A., Lecis, N., Vedani, M., 2021. Mechanical and microstructural characterization of WC-Co consolidated by binder jetting additive manufacturing. Int. J. Refract. Met. Hard Mater. 100, 105639. https://doi.org/10.1016/j.ijrmhm.2021.105639

Meier, C., Weissbach, R., Weinberg, J., Wall, W.A., Hart, A.J., 2019a. Critical influences of particle size and adhesion on the powder layer uniformity in metal additive manufacturing. J. Mater. Process. Technol. 266, 484–501.

Meier, C., Weissbach, R., Weinberg, J., Wall, W.A., John Hart, A., 2019b. Modeling and characterization of cohesion in fine metal powders with a focus on additive manufacturing process simulations. Powder Technol. 343, 855–866. https://doi.org/10.1016/j.powtec.2018.11.072

Mellin, P., Rashidi, M., Fischer, M., Nyborg, L., Marchetti, L., Hulme-Smith, C., Uhlirsch, M., Strondl, A., 2021. Moisture in Metal Powder and Its Implication for Processability in L-PBF and Elsewhere. BHM Berg-und Hüttenmännische Monatshefte 166, 33–39.

Mindt, H.W., Megahed, M., Lavery, N.P., Holmes, M.A., Brown, S.G.R., 2016. Powder Bed Layer Characteristics: The Overseen First-Order Process Input. Metall. Mater. Trans. A Phys. Metall. Mater. Sci. 47, 3811–3822. https://doi.org/10.1007/s11661-016-3470-2

Mitterlehner, M., Danninger, H., Gierl-Mayer, C., Gschiel, H., 2021. Investigation of the Influence of Powder Moisture on the Spreadability Using the Spreading Tester. BHM Berg- und Hüttenmännische Monatshefte 166, 14–22. https://doi.org/10.1007/s00501-020-01067-x

Molitch-Hou, M., 2018. Overview of additive manufacturing process, in: Additive Manufacturing. Elsevier, pp. 1–38. https://doi.org/10.1016/B978-0-12-812155-9.00001-3

Mostafaei, A., De Vecchis, P.R., Kimes, K.A., Elhassid, D., Chmielus, M., 2021. Effect of binder saturation and drying time on microstructure and resulting properties of sinter-HIP binder-jet 3D-printed WC-Co composites. Addit. Manuf. 46, 102128. https://doi.org/10.1016/j.addma.2021.102128

Mukherjee, T., DebRoy, T., 2019. A digital twin for rapid qualification of 3D printed metallic components. Appl. Mater. Today 14, 59–65.

Muñiz-Lerma, J.A., Nommeots-Nomm, A., Waters, K.E., Brochu, M., 2018. A comprehensive approach to powder feedstock characterization for powder bed fusion additive manufacturing: A case study on AlSi7Mg. Materials (Basel). 11. https://doi.org/10.3390/ma11122386

Mussatto, A., Groarke, R., O'Neill, A., Obeidi, M.A., Delaure, Y., Brabazon, D., 2020. Influences of powder morphology and spreading parameters on the powder bed topography uniformity in powder bed fusion metal additive manufacturing. Addit. Manuf. 101807.

Nan, W., Ghadiri, M., 2019. Numerical simulation of powder flow during spreading in additive manufacturing. Powder Technol. 342, 801–807. https://doi.org/10.1016/j.powtec.2018.10.056

Nan, W., Pasha, M., Bonakdar, T., Lopez, A., Zafar, U., Nadimi, S., Ghadiri, M., 2018. Jamming during particle spreading in additive manufacturing. Powder Technol. 338, 253–262. https://doi.org/10.1016/j.powtec.2018.07.030

Nan, W., Pasha, M., Ghadiri, M., 2020. Numerical simulation of particle flow and segregation during roller spreading process in additive manufacturing. Powder Technol. 364, 811–821.

Nguyen, Q.B., Nai, M.L.S., Zhu, Z., Sun, C.-N., Wei, J., Zhou, W., 2017. Characteristics of inconel powders for powder-bed additive manufacturing. Engineering 3, 695–700.

Oropeza, D., Roberts, R., Hart, A.J., 2021. A modular testbed for mechanized spreading of powder layers for additive manufacturing. Rev. Sci. Instrum. 92, 15114.

Pal, S., Gubeljak, N., Bončina, T., Hudák, R., Toth, T., Zivcak, J., Lojen, G., Leben, N., Drstvenšek, I., 2021. The effects of locations on the build tray on the quality of specimens in powder bed additive manufacturing. Int. J. Adv. Manuf. Technol. 112, 1159–1170. https://doi.org/10.1007/s00170-020-06563-5

Parteli, E.J.R., Schmidt, J., Blümel, C., Wirth, K.-E., Peukert, W., Pöschel, T., 2014. Attractive particle interaction forces and packing density of fine glass powders. Sci. Rep. 4, 6227.

Peng, W., Wang, G., Gigliotti Jr, M.F.X., Singh, P., 2018. Method for treating powder by dry mixing and powder treated thereby.

Phua, A., Doblin, C., Owen, P., Davies, C.H.J., Delaney, G.W., 2021. The effect of recoater geometry and speed on granular convection and size segregation in powder bed fusion. Powder Technol. 394, 632–644. https://doi.org/10.1016/j.powtec.2021.08.058

Popov, V. V, Grilli, M.L., Koptyug, A., Jaworska, L., Katz-Demyanetz, A., Klobčar, D., Balos, S., Postolnyi, B.O., Goel, S., 2021. Powder Bed Fusion Additive Manufacturing Using Critical Raw Materials: A Review. Materials (Basel). 14, 909. https://doi.org/10.3390/ma14040909

Richter, C., Roessler, T., Kunze, G., Katterfeld, A., Will, F., 2020. Development of a standard calibration procedure for the DEM parameters of cohesionless bulk materials–Part II: Efficient optimization-based calibration. Powder Technol. 360, 967–976.

Riener, K., Oswald, S., Winkler, M., Leichtfried, G.J., 2021. Influence of storage conditions and reconditioning of AlSi10Mg powder on the quality of parts produced by laser powder bed fusion (LPBF). Addit. Manuf. 39. https://doi.org/10.1016/j.addma.2021.101896

Roberts, J.W., Sutcliffe, C.J., Green, P.L., Black, K., 2020. Modelling of metallic particle binders for increased part density in binder jet printed components. Addit. Manuf. 34.

https://doi.org/10.1016/j.addma.2020.101244

Roessler, T., Richter, C., Katterfeld, A., Will, F., 2019. Development of a standard calibration procedure for the DEM parameters of cohesionless bulk materials–part I: Solving the problem of ambiguous parameter combinations. Powder Technol. 343, 803–812.

Romano, T., Migliori, E., Mariani, M., Lecis, N., Vedani, M., 2022. Densification behaviour of pure copper processed through cold pressing and binder jetting under different atmospheres. Rapid Prototyp. J. https://doi.org/10.1108/RPJ-09-2021-0243

Saboori, A., Gallo, D., Biamino, S., Fino, P., Lombardi, M., 2017. An overview of additive manufacturing of titanium components by directed energy deposition: microstructure and mechanical properties. Appl. Sci. 7, 883.

Sames, W.J., List, F.A., Pannala, S., Dehoff, R.R., Babu, S.S., 2016. The metallurgy and processing science of metal additive manufacturing. Int. Mater. Rev. 61, 315–360.

Sehhat, M.H., Sutton, A.T., Hung, C., Brown, B., Malley, R.J.O., Park, J., Leu, M.C., 2022. Plasma spheroidization of gas-atomized 304L stainless steel powder for laser powder bed fusion process 1.

Seyda, V., Kaufmann, N., Emmelmann, C., 2012. Investigation of aging processes of Ti-6Al-4 V powder material in laser melting. Phys. Procedia 39, 425–431.

Shanjani, Y., Toyserkani, E., 2008. Material spreading and compaction in powder-based solid freeform fabrication methods: mathematical modeling, in: 19th Annual International Solid Freeform Fabrication Symposium, SFF. pp. 399–410.

Sharma, R., Setia, G., 2019. Mechanical dry particle coating on cohesive pharmaceutical powders for improving flowability-A review. Powder Technol. 356, 458–479.

Sillani, F., Kleijnen, R.G., Vetterli, M., Schmid, M., Wegener, K., 2019. Selective laser sintering and multi jet fusion: Process-induced modification of the raw materials and analyses of parts performance. Addit. Manuf. 27, 32–41.

Sing, S.L., Tey, C.F., Tan, J.H.K., Huang, S., Yeong, W.Y., 2019. 3D printing of metals in rapid prototyping of biomaterials: Techniques in additive manufacturing, Second Edi. ed, Rapid Prototyping of Biomaterials: Techniques in Additive Manufacturing. Elsevier Ltd. https://doi.org/10.1016/B978-0-08-102663-2.00002-2

Slotwinski, J.A., Garboczi, E.J., 2015. Metrology needs for metal additive manufacturing powders. Jom 67, 538–543.

Snow, Z., Martukanitz, R., Joshi, S., 2019. On the development of powder spreadability metrics and feedstock

requirements for powder bed fusion additive manufacturing. Addit. Manuf. 28, 78–86.

Snow, Z.K., 2018. Understanding Powder Spreadability in Powder Bed Fusion Additive Manufacturing.

Spierings, A.B., Levy, G., 2009. Comparison of density of stainless steel 316L parts produced with selective laser melting using different powder grades, in: Proceedings of the Annual International Solid Freeform Fabrication Symposium. Austin, TX, pp. 342–353.

Spierings, A.B., Voegtlin, M., Bauer, T., Wegener, K., 2016. Powder flowability characterisation methodology for powder-bed-based metal additive manufacturing. Prog. Addit. Manuf. 1, 9–20.

Streubel, R., Wilms, M.B., Doñate-Buendía, C., Weisheit, A., Barcikowski, S., Schleifenbaum, J.H., Gökce, B., 2018. Depositing laser-generated nanoparticles on powders for additive manufacturing of oxide dispersed strengthened alloy parts via laser metal deposition. Jpn. J. Appl. Phys. 57, 40310.

Strondl, A., Lyckfeldt, O., Brodin, H., Ackelid, U., 2015. Characterization and control of powder properties for additive manufacturing. Jom 67, 549–554.

Sun, P., Fang, Z.Z., Zhang, Y., Xia, Y., 2017. Review of the methods for production of spherical Ti and Ti alloy powder. Jom 69, 1853–1860.

Sutton, A.T., Kriewall, C.S., Karnati, S., Leu, M.C., Newkirk, J.W., 2020. Characterization of AISI 304L stainless steel powder recycled in the laser powder-bed fusion process. Addit. Manuf. 32, 100981.

Tan, J.H., Wong, W.L.E., Dalgarno, K.W., 2017. An overview of powder granulometry on feedstock and part performance in the selective laser melting process. Addit. Manuf. 18, 228–255.

Tang, H.P., Qian, M., Liu, N., Zhang, X.Z., Yang, G.Y., Wang, J., 2015. Effect of powder reuse times on additive manufacturing of Ti-6Al-4V by selective electron beam melting. Jom 67, 555–563.

Tiwari, S.K., Pande, S., Agrawal, S., Bobade, S.M., 2015. Selection of selective laser sintering materials for different applications. Rapid Prototyp. J.

Vakifahmetoglu, C., Hasdemir, B., Biasetto, L., 2022. Spreadability of Metal Powders for Laser-Powder Bed Fusion via Simple Image Processing Steps. Materials (Basel). 15, 1–13. https://doi.org/10.3390/ma15010205

Van der Schueren, B., Kruth, J.-P., 1995. Powder deposition in selective metal powder sintering. Rapid Prototyp. J.

Wallner, S., 2019. Powder Production Technologies. BHM Berg-und Hüttenmännische Monatshefte 164, 108–111.

Wang, L., Li, E.L., Shen, H., Zou, R.P., Yu, A.B., Zhou, Z.Y., 2020. Adhesion effects on spreading of metal

powders in selective laser melting. Powder Technol. 363, 602–610.

Wang, L., Yu, A., Li, E., Shen, H., Zhou, Z., 2021. Effects of spreader geometry on powder spreading process in powder bed additive manufacturing. Powder Technol. 384, 211–222. https://doi.org/10.1016/j.powtec.2021.02.022

Wang, L., Zhou, Z., Li, E., Shen, H., Yu, A., 2022. Powder deposition mechanism during powder spreading with different spreader geometries in powder bed fusion additive manufacturing. Powder Technol. 395, 802–810. https://doi.org/10.1016/j.powtec.2021.10.017

Wei, W.-H., Wang, L.-Z., Chen, T., Duan, X.-M., Li, W., 2017. Study on the flow properties of Ti-6Al-4V powders prepared by radio-frequency plasma spheroidization. Adv. Powder Technol. 28, 2431–2437.

Yang, L., Hsu, K., Baughman, B., Godfrey, D., Medina, F., Menon, M., Wiener, S., 2017. Additive manufacturing of metals: the technology, materials, design and production. Springer.

Yao, D., An, X., Fu, H., Zhang, H., Yang, X., Zou, Q., Dong, K., 2020. Dynamic investigation on the powder spreading during selective laser melting additive manufacturing. Addit. Manuf. 101707.

Zegzulka, J., Gelnar, D., Jezerska, L., Prokes, R., Rozbroj, J., 2020. Characterization and flowability methods for metal powders. Sci. Rep. 10, 1–19. https://doi.org/10.1038/s41598-020-77974-3

Zhang, Y., Wu, L., Guo, X., Kane, S., Deng, Y., Jung, Y.G., Lee, J.H., Zhang, J., 2018. Additive Manufacturing of Metallic Materials: A Review. J. Mater. Eng. Perform. 27, 1–13. https://doi.org/10.1007/s11665-017-2747-y

Zhao, Y., Aoyagi, K., Daino, Y., Yamanaka, K., Chiba, A., 2020. Significance of powder feedstock characteristics in defect suppression of additively manufactured Inconel 718. Addit. Manuf. 101277.

Zhu, H.H., Fuh, J.Y.H., Lu, L., 2007. The influence of powder apparent density on the density in direct laser-sintered metallic parts. Int. J. Mach. Tools Manuf. 47, 294–298.

Powder spreading and spreadability in the additive manufacturing of metallic material: a critical review

Luigi C. Capozzi, Antonio Sivo, Emilio Bassini

Abstract

This review aims to build a coherent picture of the problem of powder spreading and spreadability in metal Additive Manufacturing (AM) because of its impact on ensuring highly consistent production, optimization of the process and reduction of the manufacturing costs. The review shows the current progress in understanding spreading dynamics, the role of powder characteristics, the spreading systems and the testing tools developed for assessing powder spreadability. The problem of finding appropriate quantitative metrics and the recent advances in the use of standardized methods to assess powder spreadability is critically discussed. Attention is given to future trends and research gaps and opportunities.

Keywords:

Spreadability; Flowability; Laser Powder Bed Fusion (LPBF); Electro Beam Melting (EBM);

Introduction

Additive manufacturing (AM) has seen significant growth in the last few years because it is a technology for prototyping or production of metallic components from scratch. ASTM defined AM as *"a process of joining materials to make objects from 3D model data, usually layer upon layer, as opposed to subtractive manufacturing methodologies"*. This technology may generate less waste than traditional processes, the production is distributed, and the printed component can be easily customized as discussed by Liao and Cooper, (2021). On the other hand, Hu and Mahadevan, (2017) evidenced that the replicability and the variations in the quality of the final components produced with additive manufacturing are barriers to the massive use of this technology at the industrial level.

In recent years, significant efforts are aimed at developing adequate standards and specifications for AM process, monitoring the process to improve quality and production throughput, increasing the knowledge of raw materials, their behavior during the AM process, and the effect on the final components as discussed by Frazier (2014).

AM community has put forward a great deal of challenges in characterizing and understanding powder materials, their behavior, and processability. In the context of AM technologies that use powder beds, the behavior of powder

during the spreading process is not entirely understood. In the recent past, researchers and practitioners have frequently put powder spreading in strong connection with powder flowing or even used the concept of flowability as synonymous with spreadability as discussed in the work of Zhang et al. (2018). Moreover, many tries have been done to correlate standardized measurements to spreadability. Still, they often failed because standardized tests are far from the typical conditions occurring during the powder spreading.

Powder spreading and spreadability is a relatively new topic. Its importance is growing quickly as researchers in academia and practitioners in the industry are eager to improve the quality, reliability, and replicability of the AM process. In this review, after a quick glimpse into powder-based AM manufacturing, we will analyze the current state of research and understanding about powder spreading, trying to put together a coherent picture of the current knowledge. On the basis of the works published in the literature, we will also try to rationalize the concept of powder spreadability and give a clear picture of the proposals done by many researchers to quantify spreadability through the definition of new metrics and correlate them with physical and bulk properties of the powders.

1. Additive manufacturing processes

1.1 Powder-based AM processes

Powder bed fusion (PBF) technology uses a localized heat source to melt or sinter powders that are previously spread over the build platform, finally forming a dense layer; a schematic of PBF equipment is shown in Figure 1. Once a layer has been printed, a new powder layer is spread and then melted or sintered. This process is repeated to fabricate components layer by layer. PBF technology includes selective laser sintering (SLS), selective laser melting (SLM), and electron beam melting (EBM) processes, according to the fact the powder is sintered o melted, and the heat source is a laser or electron beam.

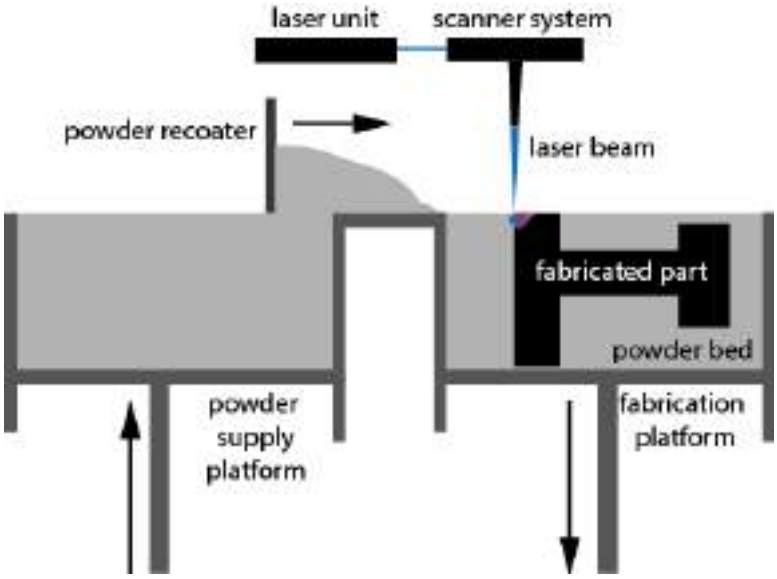

Figure 1 - Illustration of laser powder bed fusion.

In the SLS process, metal powders are spread to form thin bed layers, sintered or partially melted with a high-energy laser, followed by rapid cooling. A high- powered laser selectively melts the metal powder into layers of 20 – 100 μm. After that, a new powder layer is spread, and, again, the heat provided by the laser selectively melts the powders together and with the dense layer below. In SLS, the heat supplied to the powder is tuned in order to avoid powder melting but only sintering. Bo et al. (2020) showed that in the SLM process, metal powders are spread to form thin bed layers and melted using a high-energy laser followed by rapid cooling. However, in this case, the heat supplied by the laser is sufficient to melt the metal powder completely. The process is conducted in an inert chamber filled with nitrogen or argon, and the build platform can be heated to reduce the onset of residual thermal stress. The achievable temperature widely varies depending on the machine layout and capabilities. A

postprocessing heat treatment is often required to remove the internal stresses due to thermal changes occurring in the rapid melting and cooling. EBM process uses a focused electron beam within a vacuum chamber to melt the powder layer. The chamber is usually kept up to 700 °C to minimize temperature gradients and reduce the consequent residual stress within the fabricated components. These technologies can produce near net shape components, but SLM results in more accurate components with better surface quality. On the other hand, EBM is faster and produces components with lower residual stresses as reported by Tan et al. (2017).

1.2 Direct Energy Deposition (DED)

DED, also referred to as blown powder AM (BPAM), involves the introduction of metal powder to a heat source, such as a laser, electron beam or plasma arc, which melts the metal powders or wires together as they are deposited. According to Molitch-Hou (2018), the first application for DED dates back to 1988.

According to Sing et al. (2019), powders result in lower deposition efficiency than metal wires as only a part of the total powder would be melted and bonded to the substrate. Like Electron beam melting, electron beam systems in DED require a vacuum and typically do not have high oxidation issues. On the other hand, laser DED systems require other methods to introduce inert gases. Powder DED machines often have inert gas blown together with the powder from the nozzles, thereby sheathing the melted region, reducing the oxidization rate. Because of the technology's ability to inject metal powder directly into the heat source, often attached to a 4- or 5-axis arm, DED systems are not limited to working onto a flat substrate. Instead, it is possible to print metal onto curved surfaces, such as existing metal structures, e.g. moulds.

For this reason, DED is often used to repair damaged parts, particularly in the aerospace industry. DED machines are also known for producing large components to near net shape before they are machined to their final geometries. This technique requires the powder to flow in a dedicated hose, connecting the feedstock to the nozzle using a different mechanism to powder bed systems. For this reason, this technique is not further detailed in this review.

1.3 Binder Jetting (BJ)

Besides those techniques which require a heat input to sinter or melt powders, there is also an additive manufacturing technique that does not require any heating source, at least during the printing stage, i.e. binder jetting (BJ). The origin of metal BJ technology dates to 1993 when the Massachusetts Institute of Technology (MIT) developed an inkjet-based process to create three-dimensional objects using metal powders. The process begins by spreading a thin layer of powder, with printheads depositing binder droplets into the powder bed. The printing plate then lowers, and another layer of powder is spread. The process is repeated until the part is complete. Unused powders are efficiently recycled. The as-bound component is referred to as green, a metal casting term that refers to the relatively fragile material used for sand casting moulds. After the printing phase, curing,

debinding, and sintering steps must be provided to obtain the final component. Each phase can be slightly different depending on the processed material and the machine brand. For example, curing can be achieved via ambient air exposure or with the help of thermal or UV curing.

This process, initially designed for metallic powders, was also efficiently applied to ceramic materials as described by Chen et al. (2022), who realized samples made of alumina via BJ.

However, Lecis et al. (2021b) evidenced that powder packing, wettability with the binder and sinterability are essential parameters that must be tailored to achieve desired material properties. At the same time, other authors, such as Roberts et al. (2020), stated that BJ components typically have a low overall density in the green state and high shrinkage and deformation after heat treatment. They also suggested that these properties can be improved by including nanoparticles of the same material in the binder as the nanoparticles can fill the interstices and pore throats between the bed particles.

Similarly to other AM techniques, BJ has several important parameters to tailor before obtaining proper density values. Mostafaei et al. (2021), for example, indicated binder saturation and drying time as vital parameters to process WC-Co composites properly.

Mariani et al. (2021) used this technique to fabricate WC-12%Co samples via binder jetting, then sintered in a low-pressure furnace at 1400 °C. The application of BJ span an extensive material range: Lecis et al. (2021a), for example, processed 316L stainless. More specifically, their study showed how this new technology could effectively produce metal parts with mechanical properties comparable with products obtained with traditional techniques and with other additive processes (e.g. Selective Laser Melting).

Romano et al. (2022) demonstrated that BJ can be efficiently used also to additively process materials powders with very low laser absorbance, such as Copper. In this work, a fine high-purity copper powder with a D_{50} of 3.4 µm was used to assess the sintering process in depth.

Even though several AM techniques are available to researchers and end-users, in this review, the authors will focus on powder bed fusion techniques only being the most diffused.

1.4 Powders for AM

A fundamental ingredient of metal AM manufacturing is constituted by the powders used in the process. Each process requires specific powder size and powder size distributions, e.g. SLM requires fine powders, whereas a coarse powder is suitable for EBM. According to Wang et al. (2022), different powder systems will also lead to different layer structures when spread over the building platform. For this reason, the main differences among the most diffused systems are reviewed in the following paragraph.

The quality of the final components is influenced, among other many factors, by the shape of the powder, which mainly depends on their producing routes. The most common routes for producing metal powders for additive manufacturing include water atomization, gas atomization, plasma atomization, and plasma rotating electrode process. As shown in Table 1, each process produces powders with different particle shapes and particle size distributions. The work of Wallner, (2019) showed that in the water atomization process, the molten metal flow is broken into droplets by a water jet at high velocity and pressure, and the surface tension of the metal droplets gives them a spherical-like shape. These powders present an irregular morphology, which can represent a severe limitation for AM processes. Only a few works deal with powder flowability or spreadability of water atomized (WA) powders. Hoeges et al. (2017), for example, were able to obtain full-dense 316L samples using WA powders but significantly modifying the AM process parameters. According to these authors, 316 L WA powders have a considerably higher avalanche angle than traditional Gas Atomized (GA) ones. Nevertheless, the obtained results proved that WA powders are still usable in SLM systems. GA powders typically have avalanche angles close to 38°, while WA showed 58°.

Conversely, 316L GA and WA powders may show similar behaviour when tested with the Hall and Carney cups. The authors, indeed, noticed that no flow was possible in both systems. These results are directly inherited from the irregularities which characterize WA powders systems. On the other hand, spherical particles can be obtained by using gas atomization. Sun et al. (2017) demonstrated that the molten metal flow is perturbed and disintegrated by an inter gas jet at high pressure in the gas atomization process. The resulting particles are spherical with the presence of satellite particles because fine particles dragged by the gas circulating in the atomizing chamber can easily collide with the molten atomized particles. The presence of satellites is not desirable because they decrease powder flowability and spreadability. Plasma atomization consists of the atomization of metal wires by using plasma torches, followed by solidification. The advantage of plasma atomized powders lies in their high sphericity without the presence of satellite particles, in the narrow particle size distribution, and the high purity of the powder, as observed by Kassym and Perveen, (2020). The plasma rotating electrode process uses a plasma arc to melt a rod that, rotating rapidly, ejects the molten metal forming spherical particles. The resulting powders possessed a high spherical shape and a narrow particle size distribution.

On the other hand, Sehhat et al. (2022) increased powder sphericity by applying the induction plasma spheroidization process to 304L gas atomized powders. The authors reported that dense samples obtained from spheroidized powder have lower tensile strength but higher ductility. In addition, the authors affirmed that mechanical properties changed due to a severe alteration of the powders during the process. Indeed, the spheroidization process caused a strong carbon, nitrogen, and oxygen depletion, leading to a completely different powder microstructure during the re-solidification step. This fact was considered the main reason for reducing the tensile properties. Nevertheless, the process demonstrated to firmly lower the powder avalanche angle and break

energy with respect to as-received ones. Consequently, spheroidized powders have higher flowability than the as-received powder. This data suggests that the as-received material is more cohesive due to its larger asperity.

According to Riener et al. (2021) flowability and spreadability of powders may change with the passing of time depending on storage conditions. The authors underlined that powder, which was stored under humid conditions, results in a lower part density and lower mechanical strength. This deterioration in processability can be reversed by drying the powder in a vacuum drying oven before the SLM process.

Table 1 – Main characteristics of metal powder produces by gas atomization, water atomization, and plasma atomization process (Dawes et al. (2015); Kassym and Perveen, (2020).

Manufacturing process	***Particle size***	***Particle shape***	***Metals***
Water atomization	0–500 μm; wide particle size distribution	Irregular shape Presence of satellite particles	Ni, Co, Fe, Ti, Al
Gas atomization	0–500 μm; wide particle size distribution	Spherical shape Presence of satellite particles	Non-reactive
Plasma atomization	0 – 200 μm; narrow particle size distribution	Higly spherical shape	Ti
Plasma rotating electrode process	0 – 100 μm	Higly spherical shape	Ti

A complete and fruitful characterization of powder to be used in AM process remains a significant challenge because of the complexity of granular systems and their behaviour, see Figure 2, although some examples concerning numerous critical raw materials (CRM) can be found in the work of Popov et al. (2021). Some characteristics are intrinsic of the granular system, i.e. size, morphology, surface/bulk chemistry, and density, and are usually easily assessable. On the other hand, Leturia et al. (2014) demonstrated that the ensemble behaviour not only depends on the physical/chemical characteristics of the powder but also on the external conditions or processing environment, e.g. temperature, humidity, forces applied.

The characterization of metal powders is a fundamental aspect as their behaviour influences the quality of the powder spread layer and, in turn, of the printed component. Researchers, such as Spierings et al. (2016), and practitioners usually assess the following characteristics of the powder:

1. Physical, chemical, optical, and thermal properties
2. Ability to form dense packings
3. Ability to easily flow during the spreading process

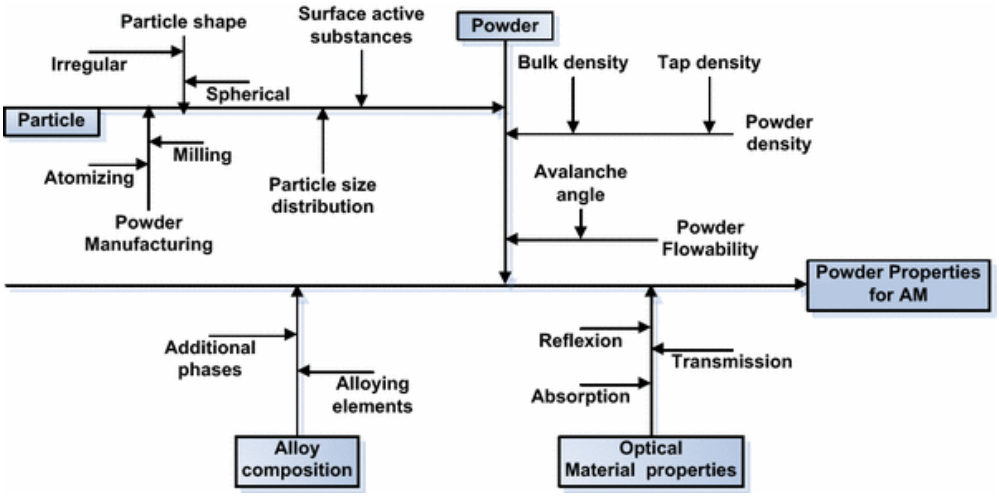

Figure 2 - Ishikawa diagram with influencing parameters for metal powders Spierings et al. (2016)

For example in the work of Kirchner et al. (2016) the physical properties of different powder for AM application are compared against each others. The authors states that the particle size distribution and morphology determine the powder flowability and packing density. As a consequence, these quantities control the powder's processability. Among all the observable effects when powders are changed, we can mention the feeding behaviour, the powder bed density and uniformity, or the roughness of the raked layer. These physical variables will affect the printing process parameters, which will be tailored accordingly. For example, finer powders will lead to a lower surface roughness of the samples but lower flowability. Another example comes from the comparison of powders for LPBF and EBM applications. Generally, powders for EBM applications have a larger particle size distribution. Consequently, flowability, apparent and tap density are higher than the SLM powders. Anyway, each system behaves differently and should be carefully analyzed and compared with values coming from literature.

2. Powder spreading

The spreading of powders is a fundamental step in AM and consists of distributing the powder over a large surface using a blade or a roller to form a thin layer before supplying radiant heat able to sinter or melt the layer in specific locations. Powder spreading represents a significant bottleneck in the AM based on powder beds because it strongly determines the quality of the final products.

Since early studies of AM, the spreading of powders has been seen as a fundamental issue in order to obtain metallic parts with good mechanical properties. Van der Schueren and Kruth, (1995) focused their attention on three different approaches for spreading the powders based on the use of a blade, a counter rolling cylinder, and, finally, a slot-feed system. They concluded that, contrary to the slot-feed system, both blade and counter rolling cylinder do not require high flow rates of the powder, although high flow rates result in more accurate layer deposition. The dimensional control in the vertical direction was investigated by Lee et al. (1995). They developed a model for layer displacement based on powder compressibility and applied load and point out as the results were highly dependent on the materials and particle shape.

It should be pointed out that only in recent years, powders spreadability has started to be studied systematically, using both experiments and simulations. The study of the spreading dynamic has been studied experimentally by the use of visual approaches able to capture the movement of the pile powders. On the other hand, simulations were extensively used as they are able to capture the dynamics of spreading at a smaller scale.

This section will present the basic spreading systems used in AM manufacturing and the main methods used to investigate the problem related to powder spreading.

2.1 Powder spreading systems

Many spreading systems have been employed in AM, such as rollers, comb blades, sweep blades, and moving hoppers. The simplest method to spread powders consists of using a thin blade (or rack) that sweeps and distributes a powder pile along with the building platform, see Figure 3a. The height of the blade gap and the velocity are the only process parameters set in such a system. In this case, powders are subjected to shear stress, but compressive stress is negligible.

In the case of roller type spreaders, the rolling and sliding movement determines a shear flow and, at the same time, exerts compressive stress to the powder. As shown in see Figure 3b, a counter-rotating roller slides along the building platform and rotates in the opposite direction so that the flowability is enhanced by the rotation and, at the same time, the powder is compacted under the roller gap. The main process parameters are the roller gap, its geometry, and its linear and rotational velocity. In the case of forward-rotating rollers (Figure 3c), the compression due to the roller can result in a higher packing density, but, in the case of powders with low flowability or a

relatively high adhesion, the interaction of the roller with the surface of the layer may result in an incomplete or non-uniform spreading or, in the worst cases, in the formation of craters in the layer.

Blades generally produce layers with lower quality and packing density as described in the work of Yang et al. (2017). As Haeri, (2017) suggested, a roller produces more compact and smoother layers because of its larger contact area that allows a gradual particle rearrangement. On the other hand, a blade produces less compact layers with greater roughness because it only drags the particles in its movement and negligible compression. A blade spreader can not be improved simply by increasing its contact area but modifying its head profile, i.e. a super-elliptic profile as can be found in the work of Haeri, (2017).

As shown in Figure 3d, a different strategy for spreading powders consists of using a blade and forward-rotating roller simultaneously, although, to our best knowledge, this strategy is not commonly used in the AM. This system might be able to compensate for the lack of compaction due to the use of a blade by using a forward-rotating roller, which in this case could act mainly to compact the powders and not to spread them.

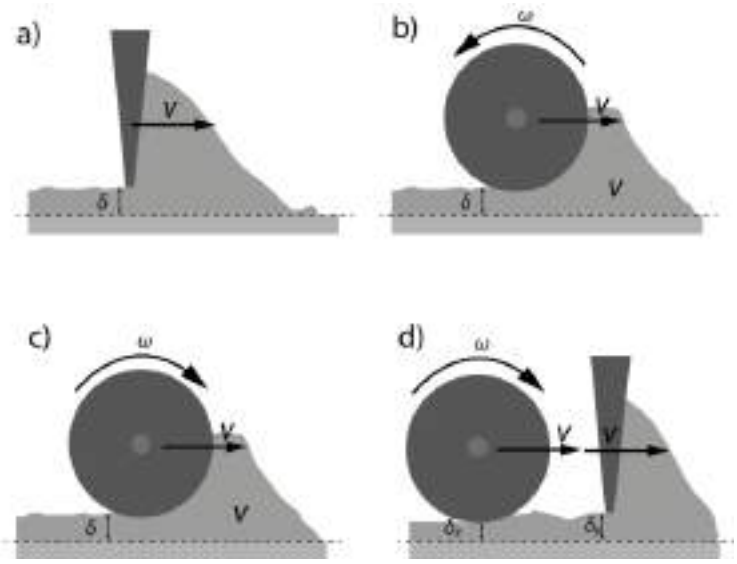

Figure 3. Schematic of AM spreading systems: a) blade, b) counter-rotating roller, c) forward-rotating roller, d) combination of a blade and a forward-rotating roller.

The fundamental AM spreading parameters are the type of spreader, the spreading speed and eventually roller rotation, and the gap height. It is reported that the typical spreading speed of blade spreaders is up to 150 mm/s, whereas, in the case of the roller, the translational velocity is in the range of 5-130 mm/s, and its rotation speed between 250-350 mm/s as suggested by Oropeza et al. (2021). Although it would be desirable to conduct the spreading as fast as possible to increase productivity, the limitation on the quality of the spread layer imposes a

compromise. The gap height used in the AM equipment is related to the category of AM technology used. As shown in Table 2, the use of laser as a heating source limits the layer thickness to approximately 20 and 100 μm, whereas electron beam can be used to thicker layers from 50 to 200 μm. Of course, the use of different AM technology requires different metals and powders with different size distribution.

In addition, authors like Wang et al. (2021) performed discrete element method (DEM) simulations to show differences among spreader geometries. The authors, for example, stated that round and inclined surfaces of blade spreaders allow more particles in the compact region to be deposited compared with vertical blades; thus, the powder layer formed is denser. Furthermore, roller systems have the largest particle motion conflict; thus, powder layers formed are sparse and inhomogeneous with small layer gaps. Finally, they also highlighted that size segregation in blade systems is not as severe as in roller systems.

Similarly, also Mussatto et al. (2020) investigated the combined effect of powder morphology, spreading velocity and layer thickness on the powder bed topography uniformity. The authors evidenced that particles sphericity and surface texture influence how much the spreader velocity and the layer thickness may alter the quality of powder bed layers. Secondly, the spreader velocity always impacted the powder bed uniformity, and better uniformity is achieved with spreading velocities $\leq$ 80 mm/s.

Phua et al. (2021) used the Discrete Element Method to assess the recoater geometry and speed effects. More specifically, they compared a toothed and a solid rake noticing that recoater velocity strongly impacts the degree of particle circulation and size segregation. Furthermore, particle circulation was enhanced by the toothed recoater, while solid recoater caused more size segregation.

Table 2 - AM technologies used in processing metal powders.

Category	*Process*	*Heat source / temperature*	*Raw materials (metals)*	*Powder size distribution (approx.)*	*Layer thickness (approx.)*	*Ref.*
Powder-bed fusion	Selective Laser Melting (SLM)	high-intensity laser / above melting point	Iron-based (316L, 420, M2), titanium and titanium based (Ti6Al4V, TiAl), aluminium-based (AlSi, AlCu, AlZn), nickel-based (Inconel 625, 718), copper, niobium, tantalum, bio-material metals–polymers and metals–ceramics combinations	10 – 50 µm	20 – 100 µm	Bo et al. (2020); Chin et al. (2020); Tiwari et al. (2015)
	Selective Laser Sintering (SLS)	high-intensity laser / below melting point				
	Electron Beam Melting (EBM)	Electron Beam / above melting point	Ti grade 2, Ti6Al4V, Inconel 718, CoCrMo; alloys having volatile constituents, e.g. Zn, Mg, Pb, Bi, are not advisable.	40 – 100 µm	50 – 200 µm	Chin et al. (2020); Gokuldoss et al. (2017); Sames et al. (2016)
Directed energy deposition	Powder directed energy deposition	Laser, arc or e-beam / above melting point	Titanium alloy (Ti-22Al-23Nb, Ti-6Al-4V, Ti-6.5Al-3.5Mo-1.5Zr-0.3Si, Ti-5Al-5Mo-4V-1Cr-1Fe), Steel (10V, 15-5 PH, 410, AISI 309Aremet 10, A2, MM10), Nickel based superalloy (CMSX-3, Haynes188, Haynes230, IN600, IN690, IN713, Rene 142, Rene N5), Aluminum alloy (CP Al, 6061, (2024)	20–200 µm	200–800 µm	Chin et al. (2020); Saboori et al. (2017); Sames et al. (2016)

2.2 Testing tools

A standard method for measuring the spreadability of powders in AM process is not currently available. However, many researchers are proposing both tests *in situ* and *ex-situ*. Whereas *in situ* tests are performed directly in the processing apparatus, *ex-situ* tests use novel tools specifically designed to analyze the behaviour of powders during their spreading and quantify the quality of the powder layer generated.

Cordova et al. (2020a) have designed two applicator tools that imitate the shape and the movement of a wire blade presented in a typical AM apparatus. The first tool is called *open applicator* and consists of a blade that slides over a stripe; as the blade slides over a metal strip, the powers flow in the gap fixed to 100 µm and are deposited, forming a layer (Figure 4a). The second tool is called *funnel applicator* because the applicator consists of a blade raised 100 µm over a metal strip and an oblique wall in contact with the strip forming a sort of funnel where the powder flows through before being deposited (Figure 4b). The test consists of weighting and charging an appropriate volume of powder and then moving the applicator at a constant speed of about 200 mm/s (the authors moved the blade manually). The powder spreadability was judged by visual inspection of the layer and measured in terms of relative density. The authors suggested the use of the *open applicator* because it provides conditions more similar to those occurring during the spreading in the processing apparatus and gives results with a smaller deviation than the *funnel applicator*.

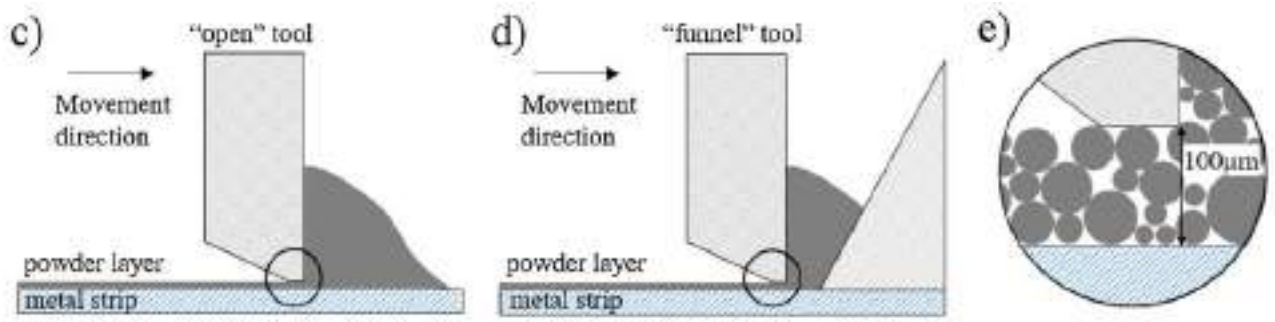

Figure 4. Applicator tools designed by NLR. C) open tool, d) funnel tool, e) Powder flowing through the 100 µm aperture of open and/or funnel tool adapted from Cordova et al. (2020b).

As shown in Figure 5, an automated test machine was built modifying a commercial thin-film applicator with an adjustable height blade that emulates the spreading process in AM equipment according to the works done by Hulme-Smith et al. (2021) and Mellin et al. (2021)

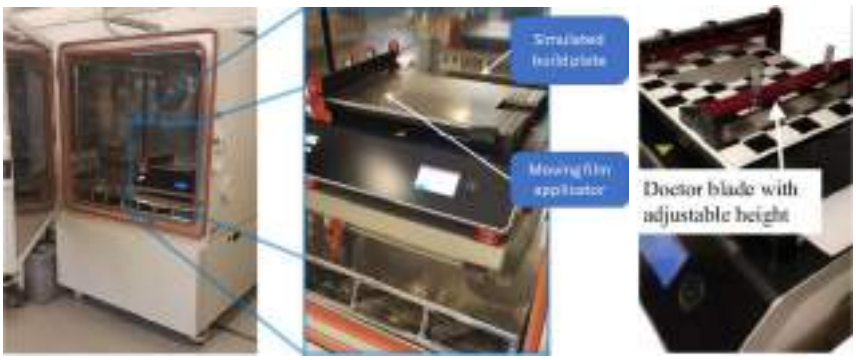

Figure 5 - Automatic powder applicator developed modifying a commercial thin-film applicator and placed in climate chamber Hulme-Smith et al. (2021; Mellin et al. (2021).

A more sophisticated modular powder spreading testbed was designed and fabricated by Oropeza et al. (2021) to be used for assessing and testing powder spreadability (Figure 6). The testbed is able to perform multi-layer spreading, uses a roller or blade spreader, has a spreading speed in the range of 0 – 100 mm/s, and a rotation velocity from 0 to 300 rpm, which are the typical range used in AM manufacturing. The use of such an automated testbed can facilitate a systematic study of spreadability because each test requires a small amount of powder.

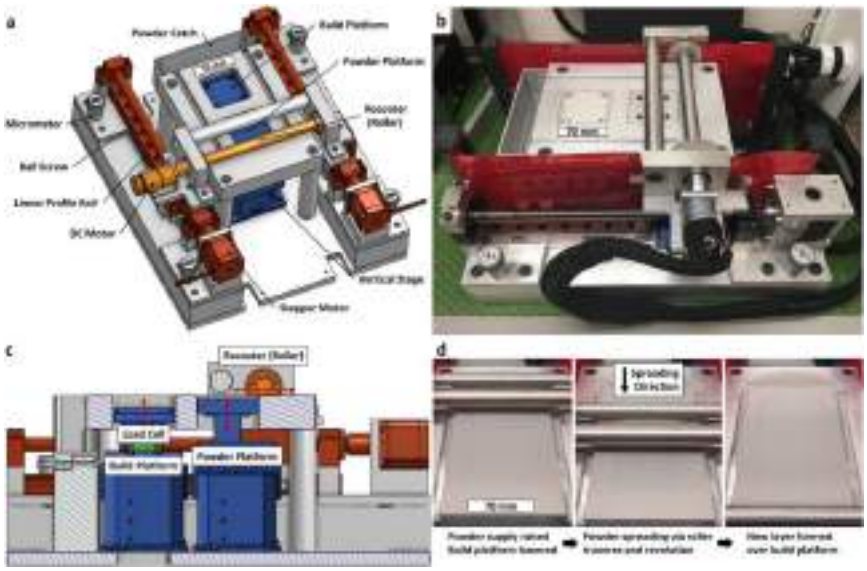

Figure 6 - Mechanized powder spreading testbed developed by Oropeza et al. Oropeza et al. (2021)

Lefebvre et al. (2019) evaluated the spreadability using a Hegman gauge (gauge in the range 0 – 100 μm). It should be pointed out that the Hegman gauge is used to check fineness or the presence of coarse particles in a liquid dispersion, and used in that case to assess powder spreadability. The measurement can assess qualitatively the spreadability by comparing the quality of the spread layer of different samples (Figure 7).

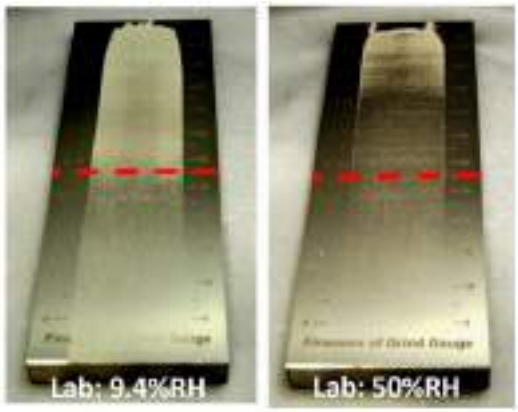

Figure 7 - Spreadability measured by using Hegman gauge (0-100 μm) (Lefebvre et al. (2019).

In recent years, Chen et al. (2017) attempted to experimentally capture the dynamics of powder spreading in the additive manufacturing conditions was made by using a visible light camera to measure the dynamic repose angle

(DRA) obtained by moving a powder pile with a blade similar to those used in the manufacturing process. The camera was able to capture the evolution of the angle of repose of the powder pile. The authors showed that, whereas the pile size diminished during spreading, the repose angle remained stable. Powders with small DRA showed better continuity and stability of flow under the blade gap. Conversely, Escano et al. (2018) used high-speed x-ray imaging was also used to investigate the evolution of the dynamic repose angle during spreading. Moreover, they were able to visualize the evolution of the surface roughness profile of the powder pile during the spreading process and the formation of powder clusters due to van der Waals cohesion forces or induced by jamming. The formation of these agglomerates can induce irregularities in the shape of the final layer, such as the formation of craters and voids (Figure 8).

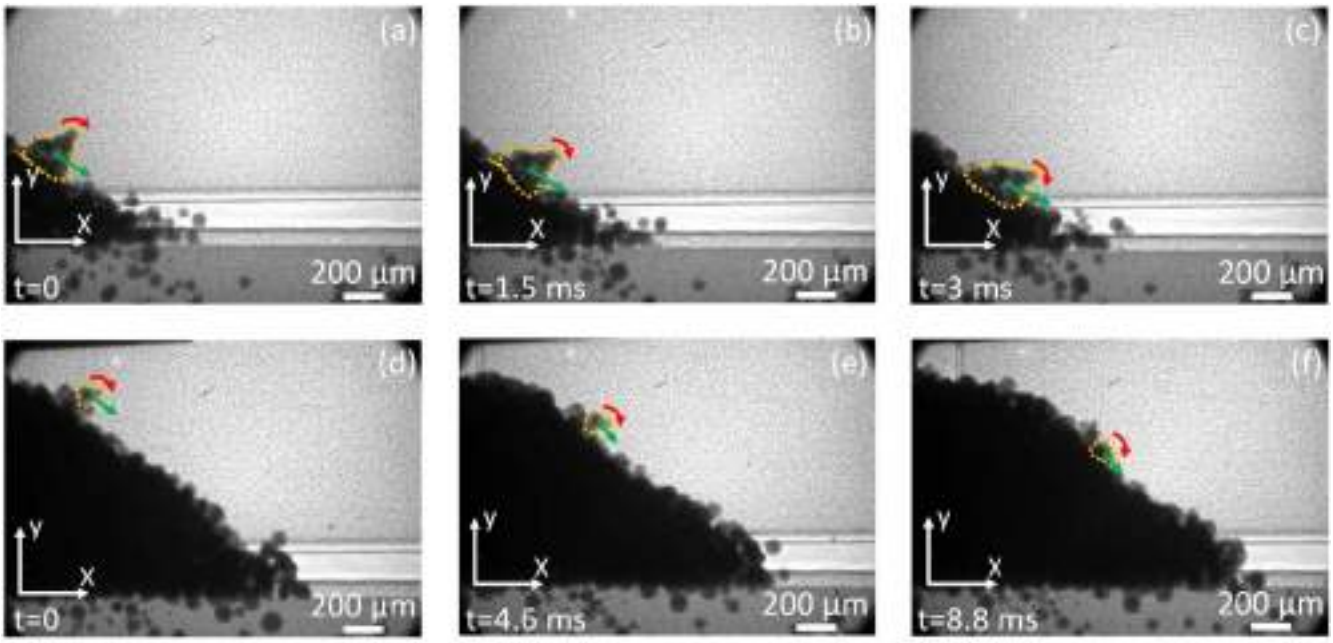

Figure 8 - Dynamic evolution of powder clusters tracked on the surface of the slope during the spreading of 316 L stainless steel powder captures using high-speed x-ray imaging method Escano et al. (2018).

2.3 Numerical methods

The investigation of powder spreading has involved the synergic use of both experiments and simulations. On the one hand, experiments suffer difficulties in a complete characterization of the powders and some lack of replication due to batch-to-batch variability of the feedstock or the non-perfect control of the process conditions. On the other hand, simulations present some limitations, such as the relatively small system size and short simulation times, but also a non-perfect correspondence between the simulated and the real system.

Except for the work of Shanjani and Toyserkani, (2008), there are not many examples of using a continuous approach to describe the spreading of powders. They modeled the powder spreading and compaction due to a counter-rotating roller using the assumption of continuum mechanics. The model considered the process of powder spreading similar to the case of a laminar flow of a viscous liquid, where the interaction between the roller and the powder is modeled through a coefficient of friction, and the powder is considered a compressible medium with non-constant density.

On the other hand, the discrete element method (DEM) has been the preferred method for investigating the dynamics of the powder spreading. DEM is a numerical technique proposed by Cundall and Strack, (1979) for describing the dynamics of particulate systems, where the continuity assumption fails to describe such systems. DEM is a Lagrangian method that tracks the movement of each particle and its interactions with other particles or the boundaries. Newton's laws of motion for translation and rotation are applied to each particle *i*:

$$m_i \frac{d^2\mathbf{r}_i}{dt^2} = \sum_j \left(\mathbf{F}_{c,ij} +\right) + m_i\mathbf{g}$$

$$I_i \frac{d\boldsymbol{\omega}_i}{dt} = \sum_j \mathbf{T}_{c,ij}$$

where m_i is the mass of the particle i, $\mathbf{r}_i$ its vector position, I_i the moment of inertia, $\boldsymbol{\omega}_i$ the angular velocity, $\mathbf{g}$ is the gravity acceleration vector. Those equations are integrated in time to obtain the temporal evolution of the position, angle, translational velocity, and angular velocity of every particle.

The core of DEM consists of simulating particle- particle and particle- wall interactions by using contact models that are able to calculate contact forces $\mathbf{F}_{c,ij}$ and torques $\mathbf{T}_{c,ij}$ taking into account the position, velocity, and properties of each particle. Usually, these models depend on some physical properties such as Young's modulus and Poisson ratio, but also by the size of the particles and friction behavior. The contact forces are split into the normal and the tangential component to the contact plane and are modeled by using linear viscoelastic models, non- linear viscoelastic models, and hysteretic models as demonstrated by Blais et al. (2019).

The simulation of powders in the micron range requires the modeling of adhesive interactions. The main sources of adhesive inter-particle force are capillary effects, electrostatic attraction, and van der Waals interactions. Li et al. (2016) pointed out that the metal AM process often requires humidity level to be as low as possible to enhance the densification process, preventing the formation of oxides and hydroxides and the production of hydrogen that can form gaseous pores in the final component.

2.3.1 Characterization of powders and model calibration

DEM parameters require to be calibrated in order to link experiments and simulations; some works from the literature are reported in Table 3. According to Roessler et al. (2019), the calibration tests should be conducted at the same scale and a flow regime close to the actual experiments. As a matter of fact, it is a common practice to scale down the simulations because of the computational costs of DEM. Moreover, Lommen et al. (2014) suggested many other tricks in order to speed up simulations, such as reducing particle stiffness in order to decrease the simulation timestep. The calibration of a parameter can be performed by directly measuring the single property at particle or contact level, such as in the case of particle size, size distribution, and shape. On the other hand, contact parameters are preferably determined using a reverse calibration process, in which the parameters are found indirectly from bulk measurements as found in the work of Coetzee, (2017). The calibration can be achieved by using a "trial and error" approach, in which the simulation is repeated with different values of the parameters until a satisfactory match with the experimental results is obtained. In a recent paper, Richter et al. (2020) have successfully exploited optimization algorithms and data regression from a design of experiment to tune the DEM parameters. In some cases, previous data from literature are taken as reference values.

A common calibration procedure consists of comparing AOR observed experimentally, and the one obtained varying DEM parameters until a good match between experiment and simulation is reached. Whereas traditionally, DEM simulations try to emulate the flowing of powders from a funnel or a hopper according to the ASTM Flowmeter test. Geer et al. (2018) developed an alternative method, called “cloud method,” which consisted in generating conical heap from the falling under the gravity of a non-contacting cloud of particles. Meier et al. (2019b) used AOR to calibrate the surface energy of metal powders and noted that cohesion influence more the resulting AOR than other DEM parameters, such as stiffness, friction coefficient or the coefficient of restitution. Desai et al. (2019) proposed a complex calibration procedure that started over the calibration of friction coefficients using two consecutive AOR virtual experiments and simulations of a virtual rheometer against real tests. Some of these methods are summarized in Table 3.

Table 3 – Calibration method used for powders used in AM.

Authors	Material	Particles			Calibration method	
		Type	Polydispersity	Cohesion	Experimental	Simulation
Geer et al. (2018 Geer et al. (2018)	Gas atomized stainless steel (17-4SS) powder	Spherical	20 – 75 μm	no	AOR obtained from the flow through a fixed funnel	AOR obtained from the flow through a fixed, down-scaled funnel and from clouds of powders
Meier et al, (2019 Meier et al. (2019b)	Ti-6Al-4V	Spherical	20 – 160 μm	yes	AOR obtained from the flow through a fixed funnel	AOR obtained from the flow through a fixed, down-scaled funnel
Desai et al. (2019 Desai et al. (2019)	Ti-6Al-4V	Spherical	Monosized 250 μm	no	AOR + powder rheometer	AOR + powder rheometer

2.3.2 Simulation of the spreading process

The spreading process has been widely explored by using DEM simulations; a comprehensive list is presented in Table 4.

Table 4 – Simulation studies of powder spreading.

Authors	*Powders*	*Spreader*	*Variables studied*	*Metrics*
Mindt et al. (2016	Spherical, polydisperse (15 – 70 µm), non-cohesive, Ti-6Al-4V particles	Flat spreader	Gap thickness	Bed particle fraction,
Haeri et al. (2016	Rods (overlapping multi-sphere method), polydisperse, non-cohesive, polyether ether ketone (PEEK) particles	Roller spreader, flat spreader	Particle shape, gap thickness, roller velocity, blade velocity	Particle shape segregation, bed particle fraction, surface roughness, probability density function (PDF) for the spatial distribution of orientation
Parteli and Pöschel, (2016)	Non-spherical (overlapping multi-sphere method), polydisperse (30 – 100 µm) cohesive, Polymer PA12	Roller spreader	Roller velocity	Gap thickness
Chen et al. Chen et al. (2017)	Spherical, polydisperse (9–140 µm), cohesive, 316L powder	Flat spreader	Cohesion, sliding and rolling friction, particle size, blade height, and velocity	Mass flow rate, dynamic repose angle
Gunasegaram et al. (2017)	Elliptical, polydisperse (37 -183 µm), non-cohesive, Ti-6Al-4V particles	Flat spreader		
Haeri, (2017)	Rods and irregular (overlapping multi-sphere method), polydisperse, non-cohesive, polyether ether ketone (PEEK) particles	From flat to rounded spreaders	Blade velocity, design of blade profile	Bed particle fraction, surface roughness
Nam et al. (2018) (Nan et al., 2018)	Non-spherical (overlapping multi-sphere method), polydisperse (15 – 55 µm) cohesive, gas-atomized 316 L stainless steel particles	Flat spreader	Gap thickness	Particle fraction, Frequency of empty patches, Frequency distribution of jamming
Chen et al. (2019)	Spherical, polydisperse (5 – 80 µm), AISI 316L stainless steel powder	Flat spreader	Particle size, polydispersity, the effect of the wall, cohesion energy	Bed packing fraction, powder flow, percolation
Meier et al. (2019)	Spherical, polydispersed (20 - 44 µm), cohesive, titanium alloy (Ti-6Al-4V) particles	Flat spreader	Gap thickness, cohesion energy	Surface profile, bed packing fraction
Nam and Ghadiri, (2019)	Non-spherical (overlapping multi-sphere method), polydisperse (15 – 55 µm) cohesive, gas-atomized 316 L stainless steel particles	Flat spreader	Gap thickness, blade velocity	Mass flow rate through the gap, Shear band
Gu et al. (2019)	Spherical, polydispersed, cohesive, WC/Inconel 718 composite powders	Flat spreader	Effect of powder bed on thermodynamics and laser processability	
Ma et al. (2020)	Spherical, polydispersed, cohesive powder	Flat spreader	Presence of fine fraction	Packing fraction, coordination number, surface roughness
Fouda and Bayly, (2020)	Spherical, mono-sized (50 µm), non-cohesive titanium alloy (Ti-6Al-4V) particles	Flat spreader	Gap thickness, blade velocity	Bed packing fraction
Chen et al. (2020)	Spherical, polydisperse (5 – 80 µm), cohesive, 316 L stainless steel powder	Counter-rolling spreader	Gap thickness, blade velocity	Mass flow rate through the gap, normal stress on bed, surface profile, bed packing fraction
He et al. (2020)	Spherical, mono-sized (50 µm), cohesive, plasma atomised Ti-6Al-4V particles	Flat spreader		Packing density, surface roughness, density pore, chamber pore
Nam et al. (2020)	Non-spherical (overlapping multi-sphere method), polydisperse (15 – 55 µm) cohesive, gas-atomised 316 L stainless steel particles	Counter-rolling spreader	Roller rotational speed, gap thickness	Particle segregation, mass flow rate of particles through the gap, normalised spread particle volume
Lee et al. (2020)	Spherical, polydisperse (30 -100 µm), cohesive, Co–Cr powder	Flat spreader	Number of layers, spreader velocity,	Height of the layer, dynamic AOR, packing density, particle size distribution
Wang et al. (2020)	Spherical, polydisperse (30 -90 µm), cohesive, Hastelloy X (HX) powder	Roller spreader, flat spreader	Cohesiveness, particle size distribution,	Packing fraction, surface roughness, properties along spreading direction
Yao et al. (2021) Yao et al. (2020)	Spherical, monosizes (34.8, 100, 123.2, 169.4 µm), cohesive, 316 L stainless steel powder	Flat spreader	Particle size, sprading velocity, gap heigh, blade angle	Packing density and its evolution, pore size, particle velocity distribution,

2.3.3 Surrogates and machine learning

The development of surrogates and digital twins is a major trend in research and industrial environment in order to increase process understanding, quantify uncertainty, increase reliability and safety, and, finally, manage product quality. Surrogates and digital twins aim to replicate a manufacturing process, or a part of it, by training machine learning algorithms with data produced by testing data, literature data, and simulation results (Figure 9). Mukherjee and DebRoy, (2019) suggested this approach because it can be beneficial also to the additive manufacturing process to overcome the problem of process replicability due to the complexity of the process itself and the variability of the process variables.

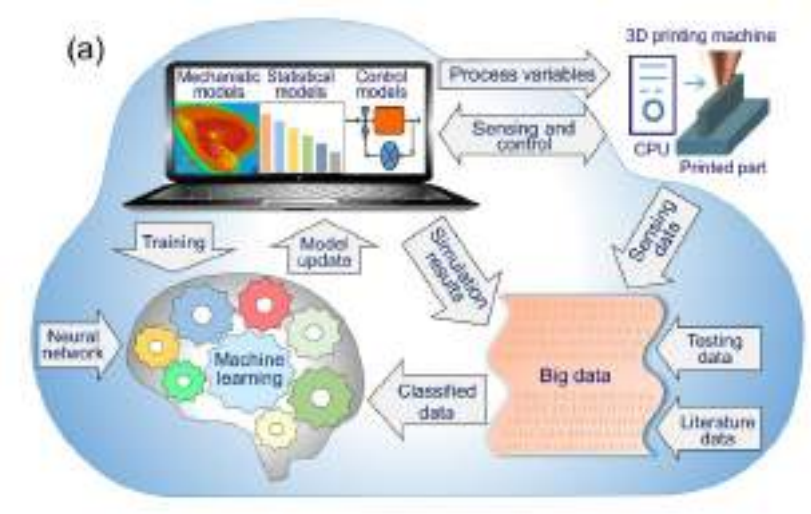

Figure 9 – Schematic representation of the digital twin Mukherjee and DebRoy, (2019).

A three-step approach was proposed by Desai and Higgs, (2019) to produce maps correlating roller translational and rotational speed to some spreadability metrics, such as spread throughput, porosity, and layer roughness. The first step consisted in the characterization of powders using a powder rheometer and calibrate DEM powder characteristics against those data. The second step consisted in generating an appropriate design of simulations having as parameters roller translational and rotational speed, performing DEM simulations, and compare their outcome with experimental data. The third step consisted of training a Back Propagation Neural Network (BP-NN) and using it as a surrogate model to create maps that correlate spreader speeds and spread layer properties.

For the sake of easiness, a summary of the techniques mentioned above with relative pros and cons is given below in Table 5:

Table 5 list of in-situ, ex-situ and simulation techniques to determine powder spreadability.

Name	Pros	Cons
Open applicator	Imitate real AM equipment	requires a visual inspection of the layer
Funnel Applicator	Measures powder spreadability	Higher deviation
Modular powder spreading	Totally automated requires only a little powder	-
Hegman gauge	Fast measurement of spreadability	only qualitatively results are achieved
Visible light Camera	Measures the dynamic repose angle of powders	Only a limited amount of information can be obtained
X-ray imaging	Higher resolution, capable of identifying cluster formation	-
Continuous approach	Evaluates powder behaviour based on fluid dynamic Models	Old equations. Not very widespread among researchers and end-users
Discrete approach	simulation of powder-powder interactions	requires a calibration process, high computing power demanding
AI/digital twins	Highly customizable	requires a calibration process, high computing power demanding

3. Powder spreading dynamics

Powder spreading is a complex and articulate process that can be divided into different subprocesses mutually interacting:

1. Avalanching flow due to the horizontal movement of a powder pile imposed by a blade or a roller and convection/circulation of powders within the moving pile;
2. Shear flow in the front and under the gap between the rake and baseplate and in front of the blade;
3. The inertia of the particles that continue to move after being deposited on the substrate.

A general picture of the main problems encountering in the spreading process is shown in Figure 10. If the gap height is not high enough, particles cannot flow through it, impeding the spreading of the powder. A further phenomenon that is usually encountered in the powder spreading is related to the powder size or shape segregation, which means that the particle size/shape distribution within the powder bed differs from the original distribution. Furthermore, the interaction between powder and blade can lead to jamming, resulting in non-uniformity of the powder layer and, in the worst case, in empty patches.

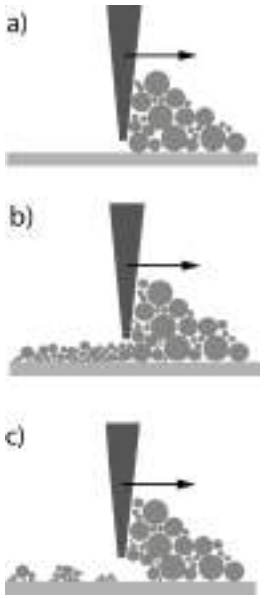

Figure 10 – Schematic of the main problem encountering in powder spreading: a) missing spreading due to small gap size, b) powder size/shape segregation, and c) formation of empty patches due to jamming.

3.1 Blade vs. roller spreader

During spreading, the powder pile moves with the blade/roller and, as the powders are spread into layers, gradually decreases its height. The stress increases with the depth from the slope surface to the bottom, but it drops greatly in the region close to the gap, called the stress-dip region as mentioned in the work of Chen et al. (2019). As shown in Figure 11, the powder pile can be divided into three main regions according to the velocity field. While the majority of the powder moves with the rake (relative velocity equal to 0), the front region moves similarly to an avalanche, and the bottom region flows out from the gap between the plate and the rake head. The behavior of the front region is strongly connected only with the powder flowability and not with the powder density of the powder layer. It has been reported that the dynamic angle of repose is not affected by the height of the gap nor by the blade speed as previously described by the same author Chen et al. (2017).

On the other hand, the stress-dip region has a substantial impact on the powder deposition. Chen et al. (2019) showed that the stress and the mass flow rate in this region directly determine the packing density of the powder layer, whereas the magnitude of their fluctuations determines its uniformity.

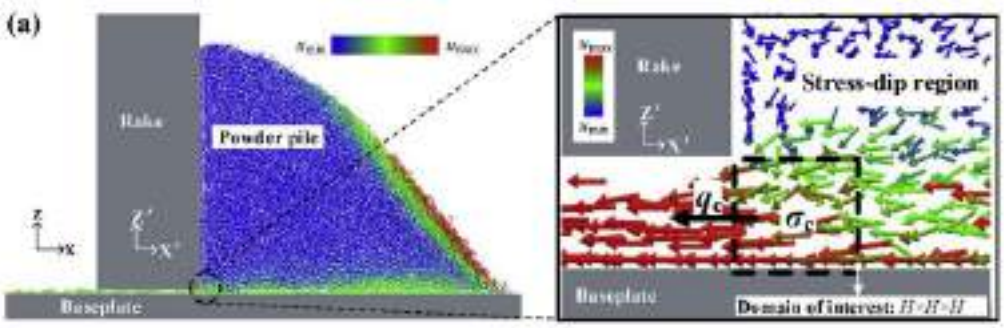

Figure 11. Velocity field of the powder pile Chen et al. (2019).

The effect of blade shearing is exerted on the particles in front of the blade, in a region that is extended in the vertical direction between the baseplate and a height slightly higher than the gap height. As shown in Figure 12a, particle velocity is maximum close to the edges of the blade and minimum close to the baseplate, and its profile follows a universal curve having the sigmoidal shape of a Gauss error function as found in the work of Nan and Ghadiri, (2019). The particles having a velocity lower than the velocity of the blade moves through the gap, are deposited, and forms the powder layer. Furthermore, Haeri et al. (2016) explained that in their flowing under the gap, particles are dragged forward because of the contact with the edges of the blade. Nonetheless, Nan et al. (2018) showed the presence of a jump in particle velocity across the front edge of the blade that is reduced only by rising enough the height of the blade; this behavior is described in Figure 12b,.

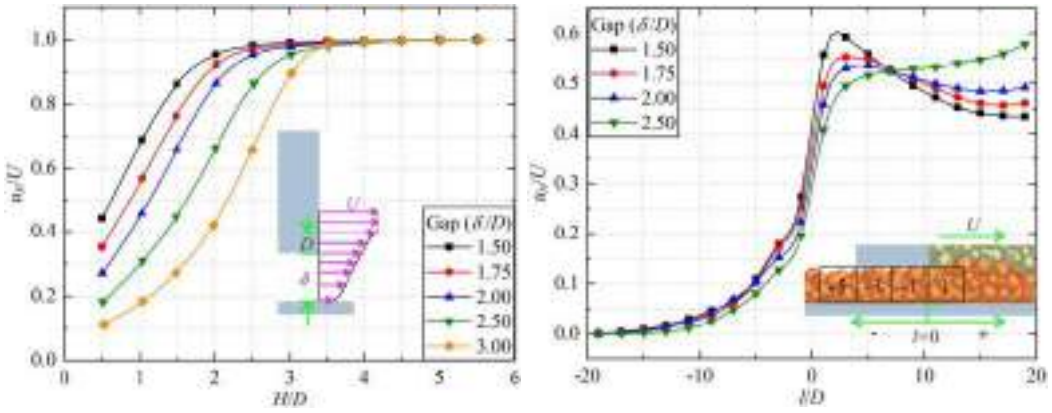

Figure 12 - Variation of particle velocity with H in the region "before blade" for different gaps Nan et al. (2018).

The mass flow rate through the gap increases linearly as the blade speed increases until a critical blade speed is reached and the mass flow rate approaches an asymptotic value, which represents the maximum spreading throughput obtainable using a certain gap height. Whereas the asymptotic value depends on the gap height, the critical velocity appears to be independent of the gap height. This effect has been explained by comparing the gravity inertial timescale, which represents the characteristic falling time of a particle during the spreading process because of the gravity, and the spreading inertial timescale, representing the characteristics time for a blade to pass over a particle at rest. At low blade velocity, the spreading inertial timescale is longer than the gravity inertial timescale, and, consequently, particles have time to fall and pass through the gap. On the other hand, at very high blade speed, when the spreading inertial timescale is much shorter than the gravity inertial timescale, particles cannot reach the gap sufficiently faster, limiting the mass flow rate. The critical velocity is around $5(gD_{90})^{0.5}$, where D_{90} is by number as found in Nan and Ghadiri, (2019) work.

Different from the blade, Nan et al. (2020) observed that a roller spreader can translate horizontally and rotate. When the roller does not rotate, the particle velocity field is not dissimilar to the case of a blade, whereas a stronger particle circulation and convection can be noted when the rotation is applied to the roller. In that case, the roller acts as a mixer that moves particles from the bottom to the free surface of the heap and, finally, to the bottom again. Moreover, particles generally not only have larger velocities when the roller system is used, but the forces among particles are more uniformly distributed, enhancing particle rearrangement within the powder bed (Figure 13). As a result, according to Wang et al. (2020) work, the roller spreader seems to produce a smoother powder layer with a higher packing fraction than those obtained with the blade. Finally, as shown by Lee et al. (2019), the coordination number in the powder increases from 2.5 to 4 because the roller compresses the particle during the spreading process.

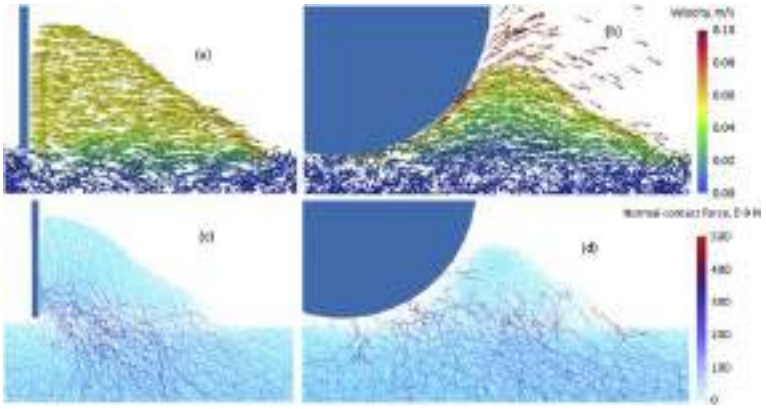

Figure 13 – Velocity vectors in the case of (a) blade and (b) roller spreader. Normal force chains in the case of (c) blade and (d) roller spreader Nan et al. (2020).

3.2 Wall effect and jamming

The presence of the rake and baseplate constraints the particle flow within a small enclosure and induces the presence of voids and discontinuity in the final powder layers. As shown in Figure 14, two mechanisms due to the presence of the spreader rake were identified, i.e. (a) the static wall effect and (b) formation of force-arches and jamming.

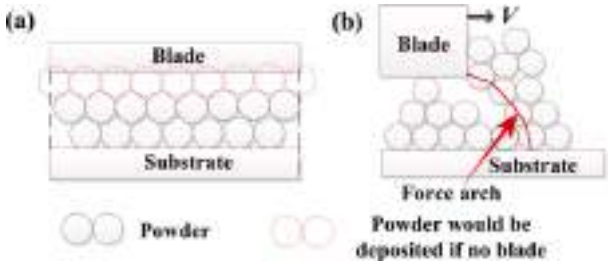

Figure 14 – Schematic illustration of a) wall effect and b) jamming due to force arch Yao et al. (2020).

The static wall effect refers to the reduction of packing fraction generated by vacant sites in the packing due to the presence of walls. In fact, the voids between particles and walls are larger than those between particles. This effect is the typical effect encountering when a discrete medium is confined in a container, and its effect is enhanced as much the characteristic dimension of the container becomes comparable to the dimension of the discrete medium. This effect is particularly important in the spreading process because the gap height is comparable to the powder size. Karapatis et al. (1999) provided an analytical expression to estimate the porosity related to the wall effect

Φ_{wall} compared to the total porosity Φ_{total}, assuming an orthorhombic arrangement of monodisperse particles (with a diameter d) in a cylinder (with a diameter D and a height H):

$$\frac{\Phi_{wall}}{\Phi_{total}} \approx \frac{d\left(\frac{1}{H}+\frac{4}{D}\right)}{0.8+d\left(\frac{1}{H}+\frac{4}{D}\right)}$$

According to Chen et al. (2019), the static wall effect is negligible if the dimension of the gap is several orders of magnitude bigger than particle size, as $\frac{\Phi_{wall}}{\Phi_{total}} \to 0$ for $D \gg d$, but it is relevant otherwise, i.e. $\frac{\Phi_{wall}}{\Phi_{total}} \to 1/\left(0.8\frac{H}{D}+1\right)$. The increase of gap height decreases the importance of the static wall effect.

The second effect is related to the movement of the wall and refers to the random formation of force-arches and transient jamming close to the rake, which produces a further reduction section of the passage of the powders. The formation and breakage of these force aches enhances the fluctuation of stress and particle flow and, finally, determine inhomogeneity in the powder layer and empty patches as can be found in Chen et al. (2019); but also in the work of Yao et al. (2020). Transient jamming of particles before the blade is a dynamic phenomenon that consists of the formation and breakage of arches, and its survival time is about 10^{-4} s. The frequency of the jamming phenomena is correlated to the survival time of the jamming events so that the shorter jamming is observed more frequently. Moreover, Nan et al. (2018) noted that the increase of gap height decreases the frequency and the survival time of the jamming events, resulting in more uniform powder spreading.

3.3 Cohesion

It is well known that fine particles exhibit cohesive behavior. Cohesive granular Bond number defined as the ratio of adhesive to gravity forces, $\mathrm{Bo}_g = F_a/mg$, can be used to distinguish cohesive powders ($\mathrm{Bo}_g > 1$), from cohesionless powders ($\mathrm{Bo}_g < 1$). Castellanos, (2005) described the adhesive inter-particle forces which arise from capillary effects, electrostatic attraction, and van der Waals interactions. Cohesive interparticle forces become increasingly relevant compared to gravitational force as particle size decreases as described by Parteli et al. (2014). When the powder humidity level is kept at a low level or remove by vacuum-drying before use, liquid bridges between particles can be considered absent and, consequently, capillary force negligible as found in literature works as the one of Li et al. (2016). Moreover, Meier et al. (2019b), who focused on conductive powders with a diameter below 100 µm, states that electrostatic forces are orders of magnitude lower than van der Waals forces.

DEM simulations have shown the connection between the fluidity of powders through the blade gap while spreading, Bond number Bo_g and particle size. Bond number Bo_g is inversely proportional to the square of the particle size, and a decrease of particle diameter below ~100 µm leads to a sharp increase of Bo_g much above 1.

As Bo_g increases in the range 0 – 3, and particle size decreases until ~ 40 µm, the fluidity of powder increased as well, and the decreasing of particle size can be considered beneficial to powder fluidity. Contrary, further increases of Bo_g above 3 and a decrease of particle size below ~ 40 µm decreased powder fluidity, causes powder agglomeration and reduces the packing density because of the predominance of van del Waal forces as described in the works of Chen et al. (2019), (2017). Cohesiveness can play a double role depending on the magnitude of cohesive forces. In fact, as cohesiveness increases, small particles tend to adhere to larger particles resulting in a more homogeneous layer. In contrast, Wang et al. (2020) noticed that the homogeneity decreases if the cohesive forces exceed a large value because of the difficulties of particles in rearranging themselves under the action of the spreading system. The effect of powder cohesiveness on the quality of powder layers is shown in Figure 15.

Ma et al. (2020) have proposed a simplified expression for the flowability in terms of energy ratio, defined as the ratio of potential energy associated with van der Waals forces and potential energy associated with gravity. According to that definition, flowability is proportional to $1/\gamma_e$, and, in turn, to hR_{eq}^2, where h is the height of the gap and R_{eq}^2 is the equivalent radius.

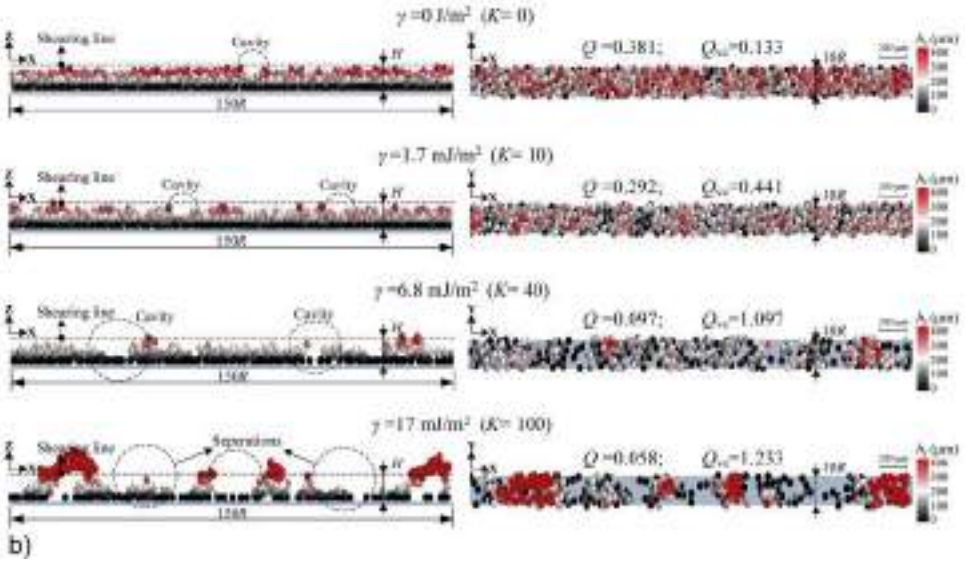

Figure 15 – Effect of powder cohesiveness on the quality of powder layers adapted from Wang et al. (2020)

3.4 Powder segregation

Particle segregation consists of the demixing of the initial powders, leading to spatial non-homogeneity of particle size distribution, shape or other physical properties. Among the many segregation mechanisms, sifting segregation or percolation has been hypothesized to occur during the powder spreading. Percolation consists of the passage of

particles through temporary voids in the powder packing and usually leads to the separation of particles by size. This effect is enhanced in the presence of a powder with a wide particle size distribution because the finer fraction is able to move through the voids formed by the coarser fraction. This effect can lead to a demixing and segregation of the powders, with stratification of the finer fraction on the bottom and the coarser fraction on top.

As shown by Lee et al. (2020), during the movement of the blade, coarse particles are segregated to the front surface of the moving pile and, as the spreading proceeds, the particle size distribution changes (Figure 16). The segregation effect due to convection/circulation in the moving heap was also observed in the case of a roller spreader as described by Nan et al. (2020).

When percolation leads to segregation, there is no improvement of packing density nor flow rate through the gap between the baseplate and the blade. Chen et al. (2019) also described how percolation is a detrimental phenomenon because it could make the use of bimodal powders ineffective. It has been shown that powder segregation has a real impact on the local packing fraction, but contradictory results were obtained concerning the inhomogeneities along the direction of the spreading. In fact, for some studies, the finer fraction is more likely to deposit at the beginning of the spreading process and the coarser at the end, whereases opposite results were found by other researchers like Muñiz-Lerma et al. (2018). In that context, the role of cohesion could have played a major role, as the initial agglomerates might be broken by the shear strength during the spreading process and resulting in the deposition of the finer fraction only at the end. Lee et al. (2020) also underlined that the spreader velocity can influence segregation because an increase of the rake velocity may lead to a partial remixing of the powders and, finally, resulting in a particle population more similar to the pristine powder.

Segregation was also observed in the case of the roller spreader, and in particular in the case of small gap height (similar to the case of the flat blade) and high rotational speed. In fact, Nan et al. (2020) evidenced that high rotational speed enhances particle convection and, finally, triggers segregation mechanisms.

As aforementioned, segregation is also able to separate particles by shape. This effect has been observed with Co–Cr–W–Mo alloy powders. Pal et al. (2021) also described how spherical particles easily percolate and were deposited at the starting locations whereas the irregular-shaped particles were found in the ending location.

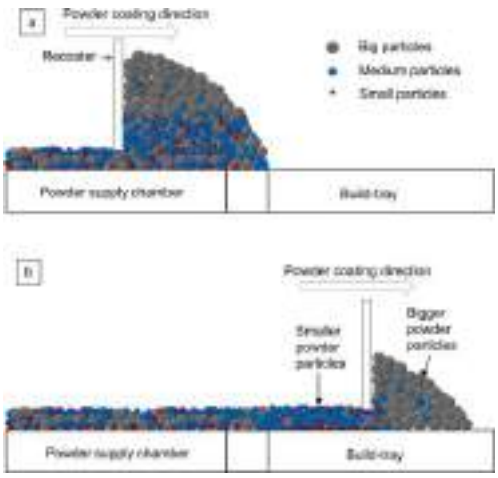

Figure 16 – Schematic of powder spreading: a) powders are collected from the powder supply chamber and b) spread on the build platform Pal et al. (2021).

4. Powder spreadability

4.1 What does spreadability mean?

There is a lack of knowledge and understanding concerning the spreadability of powder in AM manufacturing. American National Standards Institute (ANSI) has put the "spreadability" as a crucial gap in AM process because *"there is no known description of spreadability or standard for how to quantitatively assess powder spreadability"* America Makes and ANSI Additive Manufacturing Standardization, (2017). ISO/ASTM 52900 defines "*spreadability"* as "*the ability of a feedstock material to be spread out in layers that fulfill the requirements for the AM"*. Moreover, it is reported that the draft document ISO/ASTM WK55610 does not explicitly include the concept of spreadability but only of shear and dynamic flow properties and refers to the ASTM standards ASTM D6128, D6682, D6773, and D7891 for shear cell tests and wall friction tests America Makes and ANSI Additive Manufacturing Standardization, (2017).

Desai et al. (2019) defined *spreadability* as "*the ease with which a powder will spread under a set of load conditions"*, in analogy to *powder flowability* defined as "*the ease with which a powder will flow under a set of operating conditions"*. Many authors have strongly associated spreadability with flowability, although high flowability not necessarily implies high spreadability.

The problem concerning spreadability can be resumed as the following:

1. there is not a unique description of spreadability;
2. there is no standard procedure for measure powder spreadability;
3. difficulties in correlating intrinsic powder characteristics with spreadability;
4. difficulties in correlating standardized tests with spreadability.

A highly spreadable powder is such a powder that is able to produce powder layers having the following characteristics:

1. high packing density;
2. layers with a smooth profile;
3. controllable layer thickness;
4. spatial uniformity of its property, i.e. absence of particle agglomerates, voids, and empty patches;
5. allowing high blade speed.

The difficulties arising in understanding and defining powder spreadability and spreading quality are related to the complexity of such a process and the numerous variables involved:

1. Feedstock characteristics: intrinsic properties (materials, size, and size distribution, shape), flowability, and ability to form dense packings;

2. Flow conditions (spreader characteristics, spreader gap height, spreader velocity)
3. Environmental conditions (humidity, temperature, inert gas flow).

4.2 Spreading metrics

Various metrics have been proposed so far for characterizing the quality of the spreading:

- qualitative visual inspection in the work of Snow, (2018);
- percent of coverage as proposed by Meier et al. (2019a; Snow et al. (2019);
- rate of powder deposition by Snow et al. (2019);
- avalanching angle of the powder pile;
- average avalanching angle of the powder pile as found in the work of Snow et al. (2019);
- rate of change of the avalanching angle pile also by Snow et al. (2019).
- powder bed density as suggested by Cordova et al. (2020a)
- surface profile and roughness of the layer as largely debated in the following literature work Chen et al. (2020); Meier et al. (2019a); Snow et al. (2019).

4.2.1 Visual inspection and percent of coverage

Whereas the purely visual inspection of the power layer formed after the spreading of the particles is only a qualitative measure and subject to biases of the operators or judges, the use of an overhead camera and the subsequent image analysis can be used to assess the percentage of the build plate covered by powder. The image of the plate captured after powder spreading is binarized in order to obtain a black/white image. The percentage of coverage is the ratio of white pixels to black pixels. The full description of the technique can be found in the works of Hulme-Smith et al. (2021) and Snow et al. (2019). The value obtained from this measure can be an indication of the powder spreadability, in the sense that the higher percentage of coverage indicates the higher spreadability (Figure 17). This metric presented the advantage of being simple to measure, and its interpretation is straightforward. Still, it is not able to give direct information on the uniformity of the powder bed density.

Figure 17. Determination of the percentage of layer coverage by using image analysis Snow et al. (2019).

4.2.2 Metrics based on the dynamic avalanching angle test

An applicator tool that imitates the conditions of powder spreading in AM equipment can be used as a dynamic avalanche angle test. The applicator can be coupled with a simple visible camera as done by Chen et al. (2017), a digital microscope as in the work of Snow et al. (2019), or a high-speed, high-energy X-ray imaging system as proposed by Escano et al. (2018). The first metric that can be identified in such a test is the deposition rate of the powder. As shown in Figure 18, from the images captured during the test, it can be possible to measure the cross-sectional area of the powder pile *A* and its rate of change *dA/dt*, and finally, the deposition rate as follows:

$$\dot{m} = \rho_a L \frac{dA}{dt}$$

where ρ_a is the apparent density determined by ASTM M212, and L is the width of the metal plate. It should be noted that it is not guaranteed that the apparent density as measured by ASTM M212 corresponds to the apparent density achieved in the powder bed.

Further metrics consisted in measuring the avalanching angle of the powder pile θ (or the time-averaged avalanching angle $\bar{\theta}$) and its rate of change $d\theta/dt$. Those metrics refer to typical variables connected to powder flowability. The powders having high θ, $d\theta/dt$ and $\bar{\theta}$ are considered high flowable powders and result in a powder bed uniformly spread in a thin layer. Contrary, high θ, $d\theta/dt$ and $\bar{\theta}$ are related to powder that exhibited avalanching behavior and poor flowability and, finally resulting in low plate coverage as demonstrated by Snow et al. (2019).

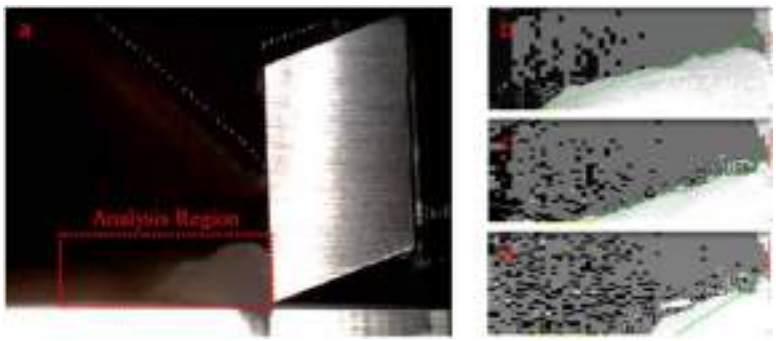

Figure 18 - Avalanching video taken from the digital microscope Snow et al. (2019).

4.2.3 Powder bed density

A measurement of the powder bed density can be performed capturing the metal powder from various location in the powder bed and measuring the density as the ratio of powder mass over the volume:

$$\rho_{PB} = \frac{m_p}{V}$$

Various solutions are reported in the literature to solve the problem of sampling the powder bed. Karapatis et al. (1999) performed simplified tests consisted of depositing the metal powders with a metallic ruler in a cylindrical container, 500-1500 μm depth (depending on the powder size) and having a diameter of 65 mm. Liu et al. (2011) built by SLM a box container with an internal dimension of 30×30×30 mm and weighted the powder within that box. Jacob et al. (2016) developed a special container by using a morphological box, a tool to solve multi-dimensional, non-quantifiable problems through the exclusion of illogical solutions. The container that resulted from such an analysis was constituted of a cylinder with a conical lid whose dimensional characteristics were taken according to ASTM B212 (2009) standard for a density cup. Such a container can be used to sample the metal powder from different locations on the build plate. The powder bed density can be determined by weighting the mass of powder captured and V the volume of the cavity (determined by filling the specimen with water).

Cordova et al. (2020a) used the relative density defined as the ratio of the apparent density ρ_{app} and the true density of the material ρ_{true} as a metric to determine the spreadability of powders. The apparent density was defined as the ratio of the mass of powder needed to obtain a layer of length L and the volume of powder bed V; V was determined from the layer length, width and thickness.

X-ray micro-computed tomography was used by Muñiz-Lerma et al. (2018) to study the powder spread density (Figure 19).

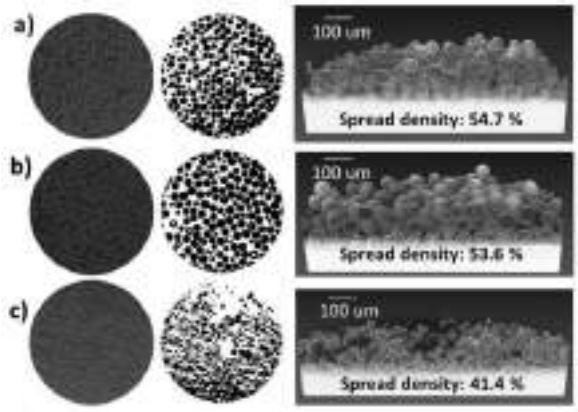

Figure 19 – 2D and 3D image reconstruction obtained using micro-CT scans of three different powders Muñiz-Lerma et al. (2018).

An alternative method to measure the powder-bed density is shown Figure 20. It consists of injecting a UV-curable polymer solution in different locations in the bed, curing the solution to bind the powder, and, finally, using 3D nano computational tomography (3D nano-CT) to measure the density of each sample as done by Ali et al. (2018). A possible solution consists of 95% Bisphenol-A ethoxylated diacrylate (BAE) and 5% of the photoinitiator Irgacure 819 (5 wt%). The most important parameter to consider is the viscosity of the solution, which should be low enough to allow the spreading of the solution into the powder bed without changing its compaction, but also not too low so that the solution can not bind the powder effectively. The solution can be dispersed using a pneumatic liquid dispensing system placed at an appropriate distance from the bed. Finally, the solution can be cured using a UV lamp and irradiate the system for less than a minute, creating a solid polymeric system that entrapped the metal powder. The sample can be analyzed using a nano-CT scan and, consequently, its three-dimensional structure can be reconstructed, and the powder-bed compaction density can be determined from the ratio of the volume of particles and the total volume the region of interest (ROI) of the sample:

$$\rho_{PB} = \frac{V_p}{V_{ROI}} \times 100$$

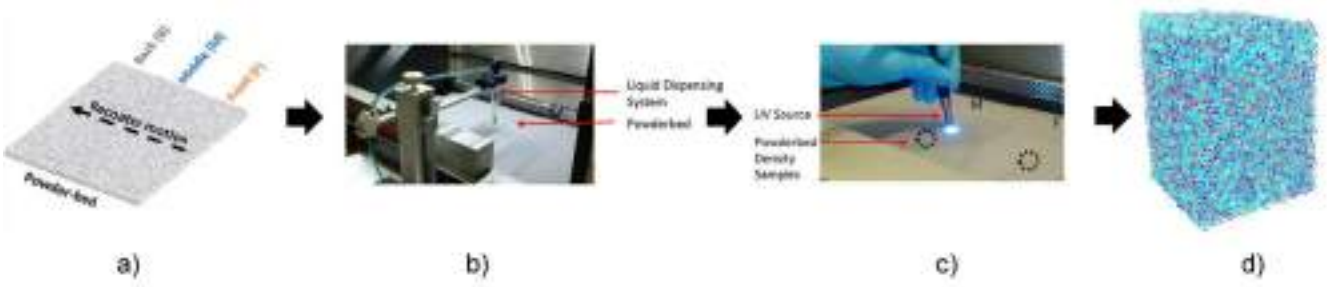

Figure 20. Powder bed density measured after the a) spreading, b) dispersion of UV-curable solution, c) curing the solution and d) perform nano-CT and postprocess the data. Modified after Ali et al. (2018).

4.2.3 Surface profile and roughness of the layer

Since a powder is a discontinuous medium, it forms an irregular profile determined by the shape and the arrangement of the single particles within the powder bed. As shown in Figure 21, the roughness of each spread layer is also determined by the roughness of the previous, fused/sintered layer. Usually, the surface roughness is associated to arithmetical mean deviation as can be read in the work of He et al. (2020):

$$R_a = \frac{1}{l}\int_0^l |z(x)|dx$$

where l is the sampling length and $z(x)$ is the vertical deviation from the mean line, i.e. $z(x) = h_b - \bar{h}_b$.

Some authors, as Meier et al. (2019a), associated also the standard deviation of the profile heigh to surface roughness in order to evaluate the spatial homogeneity of the layer profile.

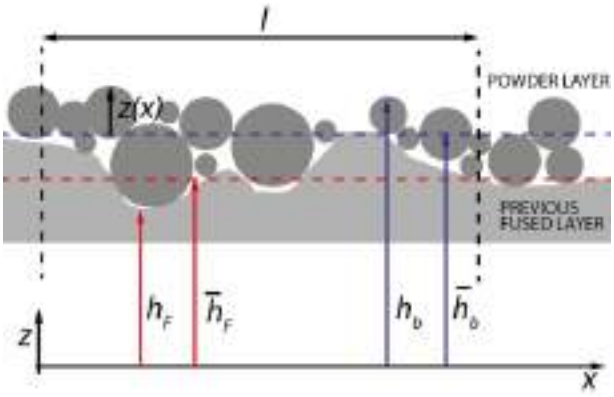

Figure 21 – Illustration of surface roughness.

Whereas surface profile and roughness are easily assessable for numerical simulations as proved by Meier et al. (2019a), many difficulties arise in the experimental investigations because powders tend to modify their arrangement when touched or moved, compromising the reliability of measurements. Laser profilometry can be used to measure the surface roughness in the powder layer because it can be performed in situ and avoid any contact between the powders and the instrument. As shown in Figure 22, the advantage of this technique lies in the ability to capture the surface profile of an extended testing zone (e.g. 64 mm^2), although the resolution of the instrument can limit the capture of the profile of very small particle (e.g. < 10 μm) as described by Chen et al. (2020).

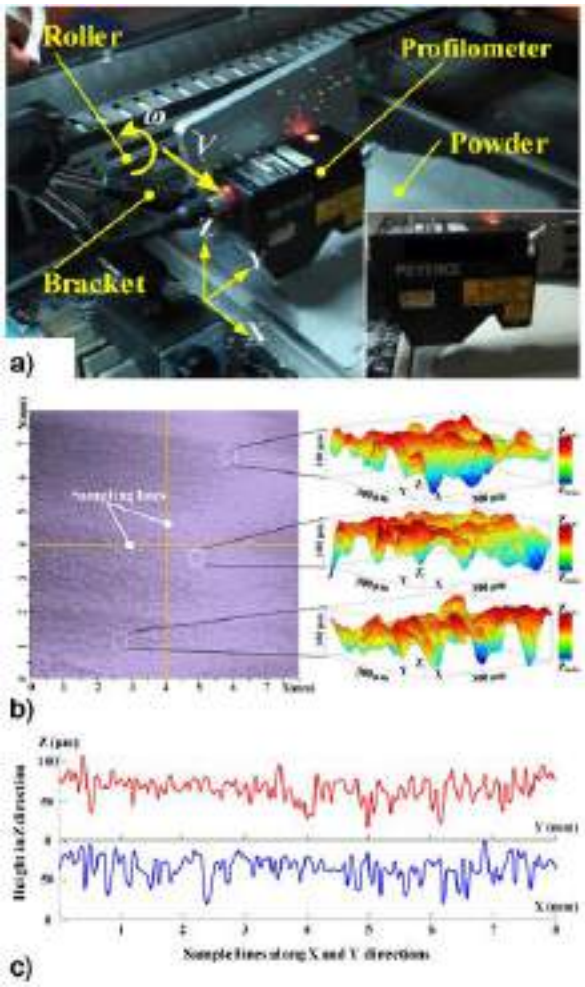

Figure 22 – (a) Experimental setup and example of (b) surface morphology and (c) height profile of a powder layer obtained with laser profilometry tests Chen et al. (2020).

4.3 Spreadability related to standardized tests

Many researchers tried to assess powder spreadability through standardized tests, such as hall flowmeters and powder rheometers, and related them, at least qualitatively, to flowability measurements, see Table 6.

Table 6 – Summary of the standardized tests to access spreadability

Method	***Characterization parameter***	***Link with spreadability***
Rheometer (FT-4)	Basic flow energy (BFE)	Higher its value, lower the spreadability because of the higher flowing resistance Brika et al. (2020); Clayton, (2014); Clayton et al. (2015). Exceptions have been shown Balbaa et al. (2020).
Rheometer (FT-4)	Specific energy (SE)	Higher its value lower the spreadability because of the higher flowing resistance Balbaa et al. (2020); Brika et al. (2020); Clayton et al. (2015)
Rheometer (FT-4)	Conditioned bulk density (CBD)	Higher its value, higher packing density Balbaa et al. (2020); Brika et al. (2020)
Rheometer (FT-4)	Compressibility index (CI)	Lower its value, higher packing density Brika et al. (2020)
Rheometer (FT-4)	Permeability (pressure drop, PD)	Higher permeability (lower PD), higher packing density because of the better ability to release entrapped air Brika et al. (2020)
Rheometer (FT-4)	Aeration energy (AE)	Lower its value, higher powder bed uniformity because of a lower tendency to agglomerate Brika et al. (2020)
Rheometer (FT-4)	Cohesion coefficient (c)	Lower its value, powder bed uniformity because of a lower mechanical interlocking and higher tendency to shear Brika et al. (2020)
Rotating Drum (Revolution powder analyzer)	Avalanche angle (AA)	Higher its value, lower spreadability because of greater resistance to flow Kiani et al. (2020); Snow et al. (2019)
Rotating Drum (Revolution powder analyzer)	Break energy (BE)	Higher its value, lower spreadability because of greater resistance to flow Kiani et al. (2020)
Rotating Drum (Revolution powder analyzer)	Avalanche energy (AE)	Higher its value, lower spreadability because of greater resistance to flow Snow et al. (2019)
Rotating Drum (Revolution powder analyzer)	Avalanche average angle	Higher its value, lower spreadability because of greater resistance to flow Snow et al. (2019)
Rotating Drum (Revolution powder analyzer)	Avalanche surface fractal	Lower its value, better flowability with no agglomeration Sillani et al. (2019)
Hall Flowmeter	Apparent/bulk density (ρ_B)	Poor connection with the lower limit of packing density in the powder layer
Hall Flowmeter	Tap density (ρ_T)	Poor connection with the upper limit of packing density in the powder layer
Hall Flowmeter	Hausner ratio (HR)	Succefful spreading with no lack-of-fusion porosity if HSR < 1.25 Dobson and Starr, (2020)
Hall Flowmeter	Angle of repose (AOR)	Higher the AOR, higher powder cohesion and lower flowability Tan et al. (2017). Higher the AOR, poorer the spreadability Snow et al. (2019). AOR > 40° exhibited poor flowability for high spreading velocities
Hall Flowmeter	Hall flow rate (HF)	Unsuitable method: powders that were not able to flow freely through the funnel were spread without problems Choi et al. (2017; Mitterlehner et al (2021); powders with the same flow rate presented different spreadability Clayton et al. (2015).

4.3.1 Hall flowmeter tests

Many tries have been done for correlating spreadability to Hall flow test as it is cheap and simple to perform. Hall flow test can be used to measure bulk properties such as apparent/bulk ρ_B, tapped density ρ_T and Hausner ratio (HR), the angle of repose (AOR), and the flow rate. However, the limitation in the use of Hall flow tests has been largely demonstrated. In fact, Hall flowmeter measurements are affected by a number of parameters, such as morphology, surface roughness, surface chemistry, size distribution, and environmental conditions as described by Slotwinski and Garboczi, (2015), and produce reliable measurements only for free-flowing powders as confirmed by Clayton, (2014). The limitation of Hall flow rate measurement has been shown by Choi et al. (2017),

which were able to successfully spread two different stainless steel powder samples, where one of them was not able to flow through the Hall flowmeter. Furthermore, Clayton et al. (2015) showed that powders having similar AOR and HF performed differently in an AM process. On the other hand, some authors as Dobson and Starr, (2020) and Haferkamp et al. (2020) have suggested the use of HR as an indicator to understand when the spreading is impeded, and the relationship between flowability, particle size, and interparticle forces.

AOR is usually considered a reliable indicator of powder spreadability. AOR can depict various situations that affect powder spreadability, i.e. AOR < 30° depicts high flowability, whereas AOR > 40° suggests the presence of powder cohesion, see the work of Tan et al. (2017). As shown by Snow et al. (2019) that AOR can be used to predict the spreading performance. They found that various spreading metrics, i.e. deposition rate, percent of coverage and rate of change of the avalanche angle of a powder pile, have statistical dependencies on AOR, see Figure 23.

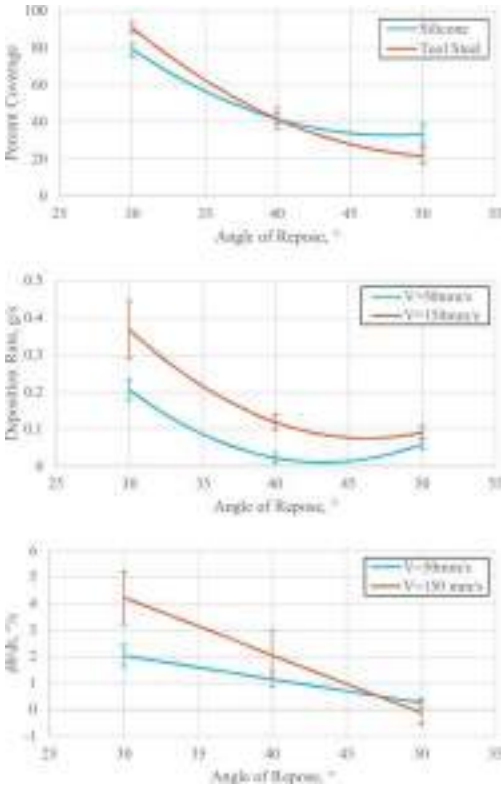

Figure 23 – Spreading metrics as a function of AOR measurements Snow et al. (2019).

4.3.2 Rheometer/FT4 Freeman powder rheometer technique

Powder rheometers offer various tools to characterize powders flow and can provide reliable measurement of bulk properties, such as density, compressibility, and permeability, but also concerning dynamic flow and shear

properties, see Figure 24. Dynamic powder tests consist of determining the axial and rotational forces acting on a rotating blade throughout the whole height of the sample.

Basic flowability energy (BFE) is the energy measured in mJ needed to the blade moving downward in order to displace powders in a specific flow pattern and flow rate in a given volume of powder. BFE is related to the cohesive forces and powder compressibility, and a higher value corresponds to lower powder flowability. Researches tried to qualitatively link BFE to spreadability, arguing that lower BFE values indicate a better spreading performance as suggested by Clayton, (2014); Clayton et al. (2015). Nonetheless, there are examples in the literature where this measurement was not in agreement with the flowability/spreadability exhibited by the powder as in the case of the work of Balbaa et al. (2020).

Specific Energy (SE) measures the flowability in a low-stress field and is measured similarly to BFE but with the blade moving upwards. Similar to BFE, Clayton et al. (2015) suggested that higher specific energy was connected to powder more resistant to the motion and, consequently, to lower spreadability.

Conditioned bulk density (CBD) is the bulk density measured with powders with no stresses applied and is considered as an indicator of the packing tendency as mentioned by Balbaa et al. (2020) but also by Brika et al. (2020). The compressibility index (CI) is defined as the ratio between density after compression and conditioned bulk density, and it is a measure of the magnitude of interparticle interactions as discussed by Brika et al. (2020). FT4 is able to determine the permeability (pressure drop, PD) of the powder bed, calculating the pressure drop of air passing through the bulk of the sample. The higher the powder permeability, the easier is the release of entrapped air, finally resulting in powder layers with higher packing fraction as documented by Brika et al. (2020). Aeration energy (AE) is the energy to displace an aerated powder and gives an indication of the cohesive forces and the mechanical interlocking between particles. As explained in the previous section, high cohesion and mechanical interlocking can be detrimental in the formation of dense and homogeneous powder layers as descriptded in the work of Brika et al. (2020). At the same time the author shows that the cohesion coefficient represents the shear strength at zero normal stress; a low value indicates a high tendency to move from a static state to a dynamic flow.

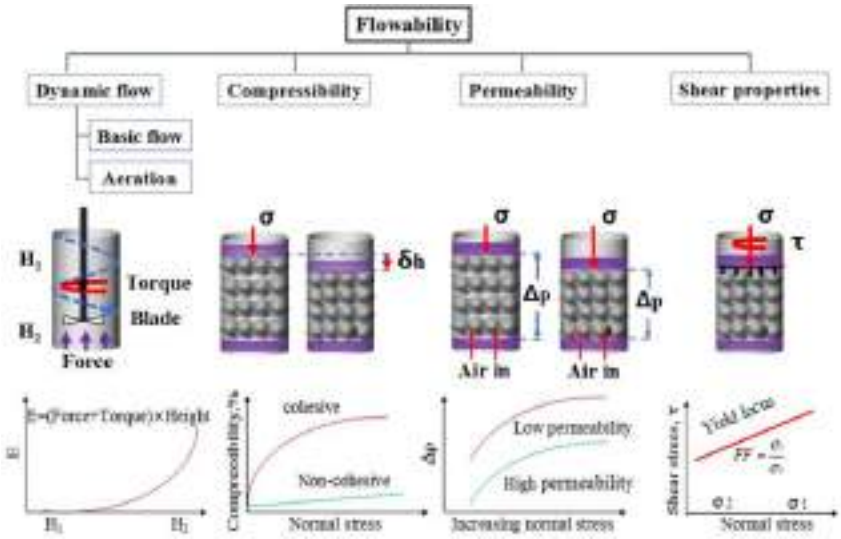

Figure 24 - Schematic diagram of the rheological test available using FT4 Powder Rheometer Wei et al. (2017).

Brika et al. (2020) proposed an index called AMS (AM suitability) to measure the overall suitability of powders from FT4 measurements:

$$\mathrm{AMS} = (\frac{1}{\mathrm{CBD}} + \mathrm{CI} + \mathrm{PD} + \mathrm{SE} + \mathrm{AE} + \mathrm{BFE} + c)/7$$

where ρ_c is the conditioned bulk density, CI the compressibility index, PD the pressure drop, SE the specific energy, AE the aeration energy, BFE the basic flowability energy and c the cohesion coefficient; each value is normalized among all the powders studied. According to the authors, the lower the AMS value, the higher is their suitability for AM manufacturing. In contrast, it is reported that the use of FT4 measurements on some spreading metrics was unsuccessful as discussed in the work of Snow et al. (2019).

4.3.3 Rotating Drum/Revolution powder analyzer

The core of the Revolution powder analyzer consists of a rotating drum coupled with a digital camera that collects the images of the powder during rotation and, through their analysis, is able to measure the flow properties of powders. Since the instrument measures flowability in low-stress situations, some authors tried to correlate specific measurements obtained with the instrument, such as the avalanche angle, to spreadability.

- Avalanche angle (AA) is the angle obtained from a linear regression of the free powder surface at the incipient occurrence of an avalanche.
- Break energy (BE) is the maximum energy level of the powder before the occurrence of an avalanche and represents the energy required by the powder to start an avalanche.

- Avalanche energy (AE) is the energy released by an avalanche and is calculated by the energy difference between the energy after and before an avalanche proposed by James, (2019).

It has been found that the higher AA and BE value, the lower spreadability because of greater resistance to flow. Although further investigations are needed, Snow et al. (2019) demonstrated that AA, BE and Avalanche average angle are able to correlate with some spreading metrics, such as the deposition rate, percent of coverage, and rate of change of the avalanche angle of a powder pile.

5. Characteristics that impact spreadability

The complexity of powder spreading lies in the number of variables involved in the process:

1. Feedstock materials;
2. Particle morphology, size and distribution;
3. Moisture influence and pre-treatments;
4. Blade geometry, gap thickness and velocity.

5.1 Feedstock materials and batch-to-batch variability

In AM community is well known that the differences between batches of feedstocks can lead to differences in powder spreading and, consequently, variability in the quality of final products. Testing powders using powder rheometer has highlighted the differences between batches in terms of both basic flowability energy (BFE), which is the energy related to the displacement of powders in a non-gravitational forced flow, and specific energy (SE), which is related to the flowability of unconfined powders. In particular, it has been shown that different batches of powders produced from the same supplier, virtually having the same particle size distribution and resulting in similar angles of repose, exhibited different behavior. Powders with low specific energy showed acceptable behavior, whereas those with high specific energy caused blockages and poor deposition due to the increase of mechanical interlocking and friction as discussed in the work of Clayton et al. (2015). Variability was also observed for powders having similar characteristics but produced by different suppliers.

5.2 Particle size, size distribution and shape

The size and shape of particles are fundamental properties to be taken into account as they influence the powder cohesiveness and, finally, flowability and spreadability. It is generally accepted that spherical and smooth powders are preferred because they usually spread in a more uniform powder layer than non-spherical, irregular-shaped powders. Brika et al. (2020) demonstrated that a batch of powders produced via gas atomization, which are less regularly shaped, produced higher powder layer porosity than plasma atomized powders, which are more spherical.

Meier et al. (2019a) used DEM simulations to demonstrate that as particle size decreased, and in turn, cohesiveness increased, the quality of powder layer decreased as well, showing the presence of high surface roughness, larger cohesive particle agglomerates, less dense regions, and spatial variations of packing fraction and height profile. Whereas a low packing fraction can be managed in the following process step by changing process parameters accordingly, spatial variations cannot. It has been shown that 10–20 μm can be considered a critical size for powders because, although they sinter fasters, they dramatically reduce the quality of powder layers.

The presence of satellite particles can also be a problem in the spreading process. Satellite particles increase the interparticle friction, decrease flowability, and often cause the inconsistent spread of the powder bed. This condition was observed both in the work of Mussatto et al. (2020) and Zhao et al. (2020).

Particle size distribution is a fundamental aspect to be taken into account because it influences powder flowability and the packing fraction of the power layers after spreading. Depending on the production route of powders, the sieving of specific fractions, or the mixing of powders with different sizes, the powders used in AM can have a narrow size distribution close to monodispersity or be extremely polydisperse. The mixing of multiple powders can lead to multimodal-distributed powders, e.g. bimodal and trimodal powders. The maximum packing fraction (or apparent relative density) of mono-sized powders is about 0.74, whereas the actual value reached in random packing is much lower. In principle, as shown in Figure 25, Zhu et al. (2007) demonstrated that the presence of powders having a large ratio of radii can be beneficial to reach the higher packing fraction because finer particles fill the voids between coarser particles.

Generally, a narrower particle size distribution provides better flowability but a lower packing fraction as found in the work of Averardi et al. (2020). Similar conclusios were found also in the work of Liu et al. (2011). On the other hand, for wider distribution, if the presence of fine powders is consistent, rheological behavior is affected negatively because of higher inter-particle friction and cohesion as discussed by Brika et al. (2020). In the same year also Kiani et al. (2020) found similar results. Fine powders play a contrasting role; from one hand, the presence of fine powders can increase the packing density as they fill the voids among bigger particles, on the other, a high amount of fine powers below 20 μm can determine agglomeration phenomena and, finally, lack of uniformity in the final powder layers. Dobson and Starr pointed out the importance of fine particulate and showed that a 17-4 PH stainless steel powders having the 30% (on volume basis) of fine particles (below 15 μm) was spread successfully whereas it was not possible to spread the powder when the amount of fine particle was about 55% as demonstrated by Dobson and Starr, (2020).

Some researchers tried to established guidelines on the appropriate particle size distribution to be used in AM. The following rule of thumb for selecting an appropriate particle size distribution was proposed by Karapatis et al. (1999):

$$D_{90} < h_{\text{spreader}}, \qquad \frac{D_{50}}{D_{10}} \geq 10, \qquad \frac{D_{90}}{D_{10}} \leq 19$$

which gives a constraint on the maximum size of particles with respect to the spreader clearance and on proportion of finer and coarser fraction, i.e. 50% of the particles should be 10 times bigger than the 10% of the finer fraction and the size ratio between the coarse and the finer fraction should be 1:20. Spierings and Levy, (2009) proposed different requirements for spreading powders in thin layers:

$$\frac{t_{\text{layer}}}{D_{90}} \approx 1.5, \qquad \frac{D_{90}}{D_{10}} \approx 5, \qquad D_{10} > 5\mu\text{m}$$

which indicates that the effective powder layer thickness should be 50% higher than the size of the coarser fraction, the size ratio between the coarse and the finer fraction about 1:5, and the finer fraction about 7.5 times smaller than t_{Layer}, and above 5 μm to avoid powder agglomeration.

The use of bimodal powers can be beneficial to increase the packing fraction of powder layers without compromise the flowability. Bai et al. (2015) explained that bimodal powders are usually generated by mixing powders with different mean size and narrow size distribution; similar conclusions were proposed also by Boley et al. (2016) When the ratio of radii of the two constituent powders is large enough, i.e. 1:7, and the volume fraction of fine powder is about 0.2-0-4, packing density is usually higher than monomodal powders because finer particles tend to fill the voids left by the coarser fraction.

Ma et al. (2020) simulated the spreading of a metal powder with a size in the range 45 – 150 μm mixed with various quantities (from 0 to 4 % in volume) of a fine powder with particle size ranging between 20 and 40 μm. As shown in Figure 26, an increase of fine fraction from 0 to about 1.5 % lead to an increase of packing fraction and a decrease of surface roughness, whereas higher values of fine fraction result in powder layers with lower packing fraction and higher surface roughness. Those results confirmed the experimental evidence stating that a small amount can increase the quality of the powder layer because the smaller particles fill the voids between the bigger ones, whereas fine particles above a certain amount create problems in the spreading because cohesive forces become significant. Two mechanisms have been used to explain the effect of fine powders. When the fine fraction is in the range 1.5 – 2.5 %, the packing fraction decreases because interlocking and rotational inertia increase, whereas for fine fraction above 2.5 %, the decrease of packing fraction should be attributed to the creation of clusters from the smaller particles under the attractive van der Waals force according to Ma et al. (2020).

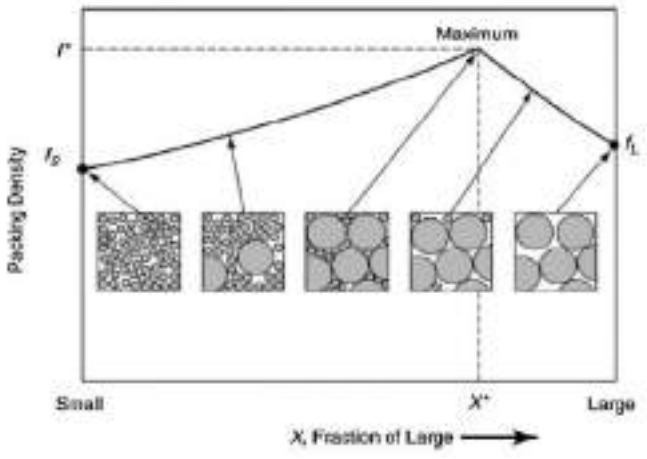

Figure 25 - The schematic of the effects from combinations of different sizes Tan et al. (2017).

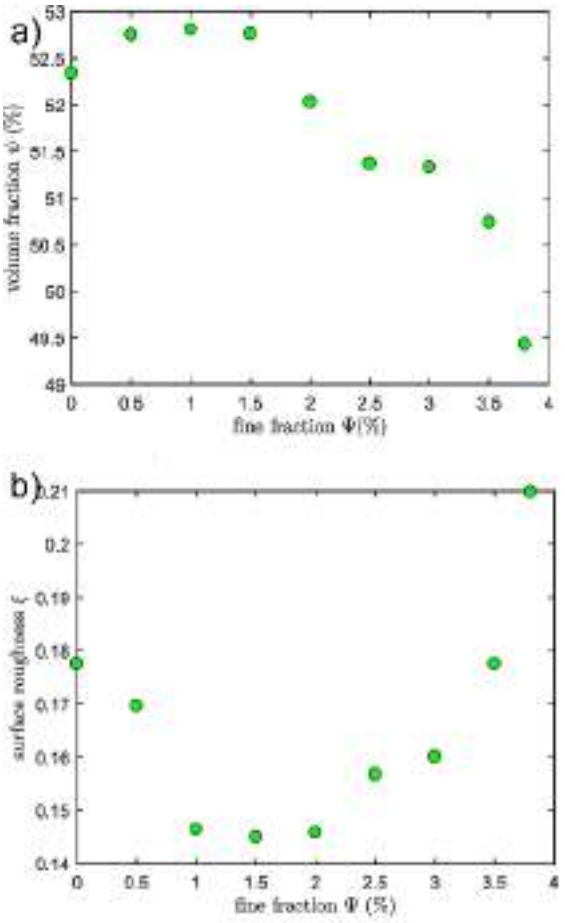

Figure 26 – a) Packing fraction and surface roughness as a function of % of fine fraction Ma et al. (2020).

The effect of different powder shapes has also been investigated. Rod-shaped particles were investigated using various aspect ratio, from 1 (spherical particles) to 2.5, showing that the increase of aspect ratio leads to lower packing density and higher surface roughness. Similar to the case of spherical particles, the spreading of rods is affected by the type of spreader and its velocity. It has been shown that decreasing the spreader velocity can be an effective method for increasing packing density and decrease roughness. Moreover, Haeri et al. (2016) affirmed that the spreading performed with a roller type spreader results in high bed quality compared to the flat blade because of its more efficient contact dynamics due to the higher surface of contact and dynamics of a particle flowing through the spreader gap.

A most important undesired effect due to powder segregation is the spatial variation of powder bed properties. As shown by Ali et al. (2018), the powder bed density decreases along the moving direction of the recoater. In fact,

as explained in Figure 27, as the recoter moves, the finer particles are deposited first because are able to percolate through the voids that bigger particles form during their movement. Smaller particles are able to better fill the voids and, finally, produce layer with higher packing density. Size segregation lead a change in particle size distribution within the moving heap and, consequently, a change of particle size distribution along the recoater moving direction.

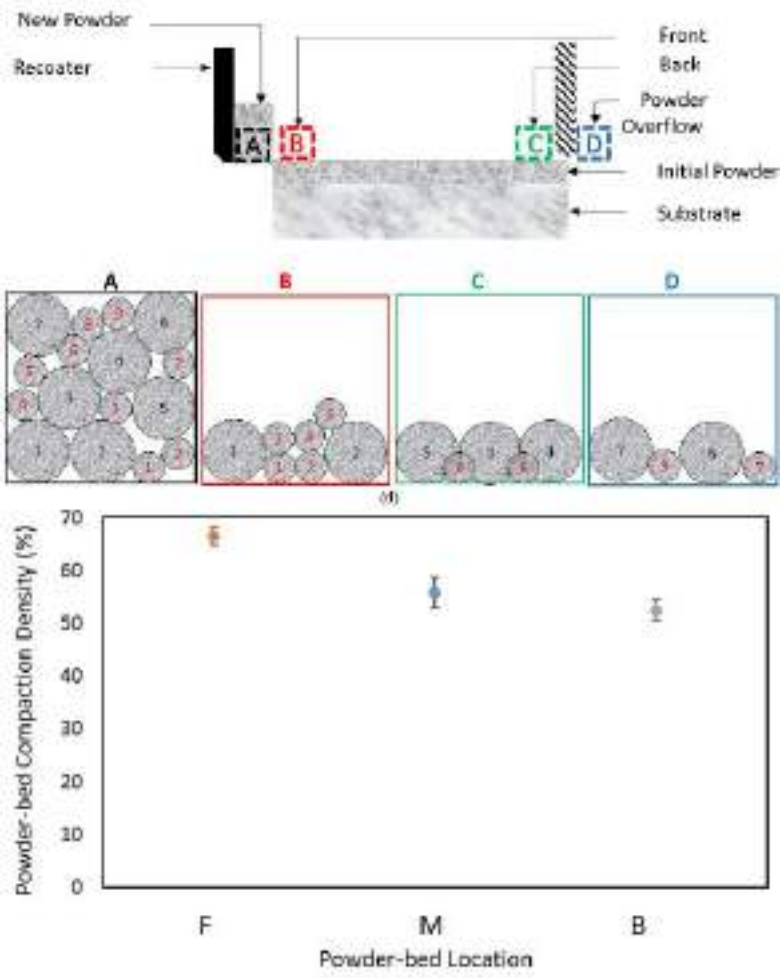

Figure 27 – Powder bed density at different locations, i.e. front (F), middle (M) and back (B) of the bed Ali et al. (2018).

5.3 Humidity

It is well known that humidity can dramatically change the flow behavior and the bulk properties of powders because it causes the formation of liquid bridges between particles, and finally, to interparticle capillary forces as discussed in the works of Landi et al. (2011) and later by Ma et al. (2019). Moreover, the moisture adsorbed on

particles can lead to surface modifications, such as the formation of an external oxide layer as demonstrated by Cordova et al. (2020a), that inevitably influence the interactions between particles, e.g. friction and cohesion forces. In AM manufacturing, humidity is considered an important issue, as it can result in poor spreading quality, poor quality of the printed components, and lead to a lack of reproducibility.

As a general rule, Lefebvre et al. (2020) affirm that moisture adsorption and desorption depends on RH in the environment and the surface area, but also on the nature of the material. Engel and Bourell, (2000) observed that titanium alloy powers exhibit poor flowability/spreadability without a thermal pre-treatment able to reduce moisture adsorbed over the particles. The deeper analysis on plasma atomized titanium powder presented by Lefebvre et al. (2019) demonstrated that the moisture uptake is fast and reversible and showed that there could be a substantial decrease of flowability with the increases of RH. As shown by Muñiz-Lerma et al. (2018), the flowability and the apparent density of aluminum powders are affected by RH. Their results suggest that the moisture is adsorbed easily in the presence of a high fraction of fine particles because of their high surface energy, leading to non-uniform spreading. The effect of moisture on the spreading of Inconel 718, Ti6Al4V, AlSi10Mg, Scalmalloy powders was analyzed by Cordova et al. (2020a). Mitterlehner et al. (2021) tested nickel-based superalloy powders conditioned at RH 0% and 75%, showing that the humid conditioned power resulted in powder layers with a higher amount of empty patches compared to the dried powder. Moreover, they hypothesize the existence of an RH threshold over which powder layers cannot be dense anymore.

5.4 Powder reuse

Powder spreadability can change in the case of the reuse of powders. The multiple reuses of powders can lead to changes in powders morphology and, consequently, in the flowing behavior during the spreading. Cordova et al. (2019) proposed a diagram to be used to decide the feasibility of reusing the powder in a specific application and with a specific material, see Figure 28. In fact, literature data showed that the recyclability of powders is not a straightforward operation, depends on material and particle size distribution, and often lead to contradictory results. Tang et al. (2015) showed that the multiple reuses of Ti-6Al-4V powders with a D_{50} in the other of 70 µm can result in less spherical and rougher particles and, after many cycles, also to the disappearance of satellite particles, but it has also been observed changes in the particle size distributions as suggested by Strondl et al. (2015). Unfortunately, research groups reached contradictory conclusions on the effect of recycling on powder flowability/spreadability. On the one hand, it has been claimed that the flowability of reused powders increased because of the reduction of satellite particles and the lower content of moisture due to longer exposure to vacuum as indicated by Tang et al. (2015), whereas, on the other, reused powders presented a higher amount of finer particles after recycling and, finally, lower flowability. A similar analysis was conducted using a nickel alloy powder with D_{50} of about 30 µm and led to the conclusion that reused powders contained a larger fraction of coarser particles because a consistent amount of the finer particles is lost during the process. As a result of this

shift in particle size distribution in favor of coarser fractions, used powder exhibited better flowability according to Strondl et al. (2015). Reused Inconel 718 powders exhibited lower sphericity compared to virgin powders, and, consequently, the powder bed presented lower apparent and tapped densities as observed by Chandrasekar et al. (2020) or by Nguyen et al. (2017) in an earlier work.

Sutton et al. (2020) found that the density of the powder layer formed by AISI 304L stainless steel powders increases as a result of recycling, and suggested that this effect is due to the increase of flowability/spreadability in reused powder, see Figure 29. In fact, they showed that reused powder exhibited a lower avalanche angle, avalanche energy, and higher conditioned bulk density. The authors suggested that this improvement can be ascribed to the decrease in the number of fine particles and the increase of powder circularity. The shift of particle size distribution towards coarser fraction and the consequent increase of packing density was also observed by Seyda et al. (2012) for Ti-6Al-4V powders and S17-4 PH stainless steel powder by Jacob et al. (2017). As suggested by Sutton et al. (2020), another reason for the increase of flowability/spreadability can be attributed to the formation of oxides on metals, which might lead to a reduction of friction and surface energy.

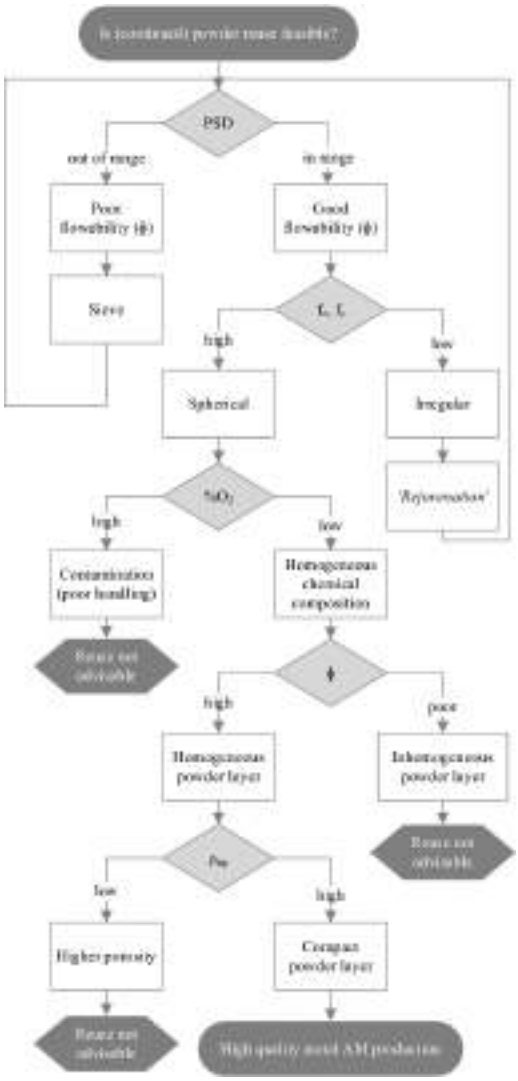

Figure 28 - Reusability decision diagram based on powder properties Cordova et al. (2019).

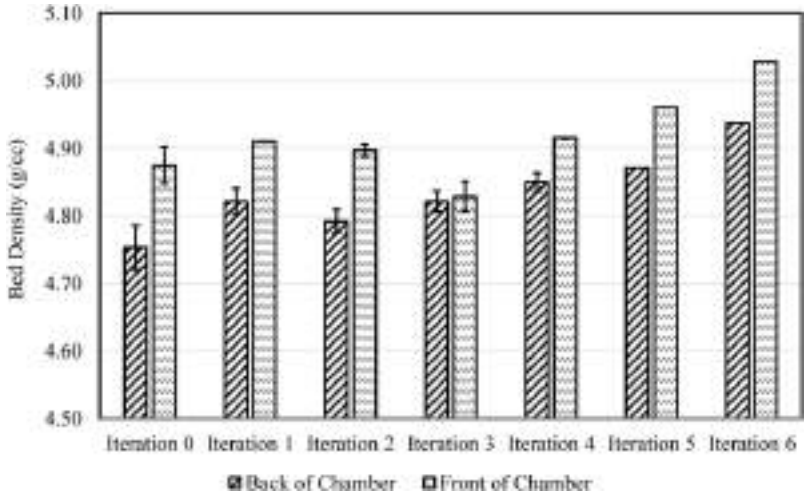

Figure 29 - Powder-bed density measurements at different locations (back and front) for each powder reuse Sutton et al. (2020).

5.5 Powder coating

Coating of metallic powders with nanoparticles can be used as a treatment to reduce the cohesion of fine particles, increase metal powder flowability and bulk powder density. Gärtner et al. (2021) demonstrated that nanoparticles act as artificial roughness and are able to distance metal particles, decreasing the value of van der Waals forces and, in turn, particle cohesiveness. Coating is performed by blending in various proportions dried particles and nanoparticles, and ensures that the nanoparticles, seen as guest particles, adhere to the pristine microparticles, which are considered as host particles. As shown in Figure 30a, the size of both the nano-sized guest particles and the micro-sized host particles have a great influence on the overall cohesion behavior of such a system. As shown in Figure 30b, two main mechanisms occur during powder spreading of such particle systems, i.e. (i) the friction and mechanical interlocking between particles, which determine the resistance to flow, and (ii) the reduction of the contact surface, which reduce adhesion between particles and increase the flowability of powders as discussed in the work of Fereiduni et al. (2019).

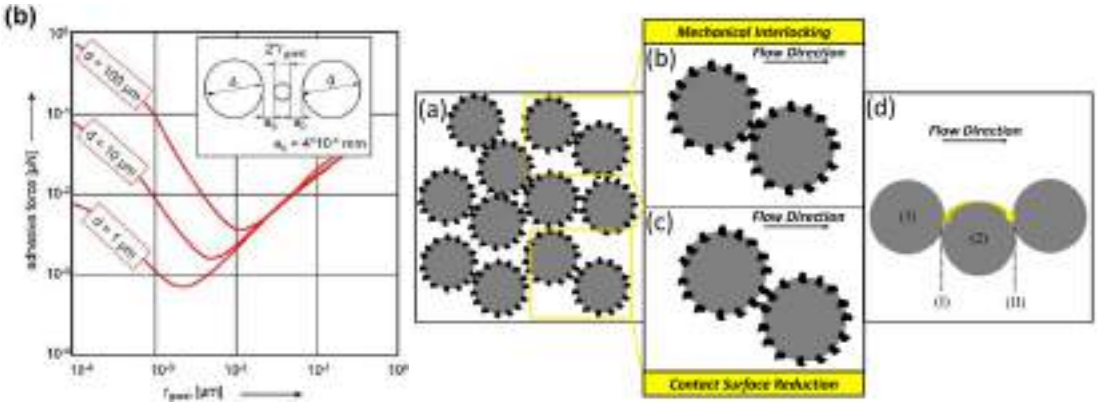

Figure 30 – Adhesive force between host microparticles as a function of nano-sized guest particles radius and for micro-sized host particle diameter Karg et al. (2019) Fereiduni et al. (2019).

Dry coating is a technique for coating powders without the use of any liquid; host and guest particles are blended in a mixer or a mill by suppling high energy in order to produce energetic guest-host collisions, which are responsible for the adhesion of guest nano-sized particles over the surface of the host micro-sized particles as discussed by Sharma and Setia, (2019). In the context of AM, various systems were testes, i.e. Peng et al. (2018) proposed the coating of fine Inconel 718 microparticles with nano hydrophobic silica or nanocarbon, Karg et al. (2013) proposed the coating of non-spherical powders of allowing close to the eutectic AlSi12, and Karg et al. (2019) demonstrated that the addition of low weight percentage of nanoparticles could lead to more homogenous spreading of powders in thin layers and increase the relative density of LBM samples.

Wet coating can be seen as an alternative to dry coating. Streubel et al. (2018) proposed a procedure that started from the dispersion by ultrasonication of nano-sized powder in water, the laser-irradiation of suspension in jet flowing, mechanical mixing with steel micro-sized powder, and, finally, drying in a furnace.

5.6 Blade geometry, gap clearance and speed

The simplest spreader in AM equipment is constituted by a flat blade. It has been reported by Chen et al. (2017) that the quality of the powder layer decreases as the blade speed increases because the powder tends to dilate, leading to looser flow and creating discontinuity within the layer. The decrease of the gap height triggers the formation of force aches between particles, affecting the continuity and stability of powder flow and, finally, resulting in low-quality spreading. Beitz et al. (2019) investigate the effect of three different blade geometries, i.e. flat, slightly round and sharp blades, demonstrating that the flat blade leads to lower roughness and better compaction than the other blades because of its larger horizontal contact surface.

Since the contact dynamics between a flat blade and particles is considered inefficient, some attempts have been made in order to optimize the spreader profile and increase the effectiveness of powder spreading. The use of a super-elliptic edge profile arises from the assumption that a gradual flattening of powders and a larger contact area can reduce the phenomenon of particle dragging and, finally, be beneficial to the spreading. The edge profile was generated using the equation describing superellipse curves $|y/a|^n + |z/b|^n = 1$, where n is responsible for the shape (concave profile for $0 < n < 1$, linear for $n = 1$, convex for $1 < n < 2$, and a rectangle with rounded corners for $n > 2$), a for width and b for height. It has been shown that the concave profile did not produce an improvement in the quality of the final powder layer, whereas the linear profile can increase bed packing fraction for wider profiles. On the other hand, the convex profiles showed the most promising results, especially in the case of n around 5 and wider edges. Haeri, (2017) noticed that an optimized profile allows the increase of spreading velocity but limiting, at the same time, the loss in spreading quality.

Generally, the roller outperforms the blade spreader in terms of the quality of the power bed at the same operating conditions as demonstrated by Haeri et al. (2016). In the case of counter-rolling spreaders, the increase of spreading velocity reduces the quality of the powder layer because of the increasing of the surface roughness and the decreasing of the packing density. This effect has been explained in terms of two concurrent forces, i.e. the friction force between the particles and the sintered/melted underlying layer and the drag force on particles from the roller. As the roller velocity increases, the drag force exerted on particles from the roller increases as well. At low velocity, the drag force is compensated by the friction force and, consequently, the particles move under the roller, rearrange themselves in a denser packing under the pressure exerted by the roller and, finally, quickly rest because friction opposes the tendency of powder of following the roller. On the other hand, when the drag force is large enough to overcome friction forces, particles do not rest immediately after they passed through the roller gap but flow following the roller movement for a certain distance and, then, deposit on the underlying layer. In this case, Chen et al. (2020)affirm that the powder bed shows higher surface roughness and lower packing density.

DEM simulations, performed by Meier et al. (2019a), have shown that the quality of powder layers increases with increasing blade gap height, and the optimum value to be set as gap height is equal to two to three times the maximal powder particle diameter. In particular, Mindt et al. (2016) observed that powder bed density increased as the blade gap height was increased. On the other hand, Brika et al. (2020) have obtained experimentally opposite results, as the increase of blade gap height leads to lower powder bed density.

The velocity of the spreader can be an important factor for increasing the productivity of AM process. On the other hand, the choice of a high velocity should be carefully evaluated considering the consequent loss of quality of bed packed layer and reproducibility in that conditions. As shown in Figure 31, the increase of spreader velocity results in powder layers with lower density and higher surface roughness, finally reducing the quality of the powder layer as discussed by Chen et al. (2020).

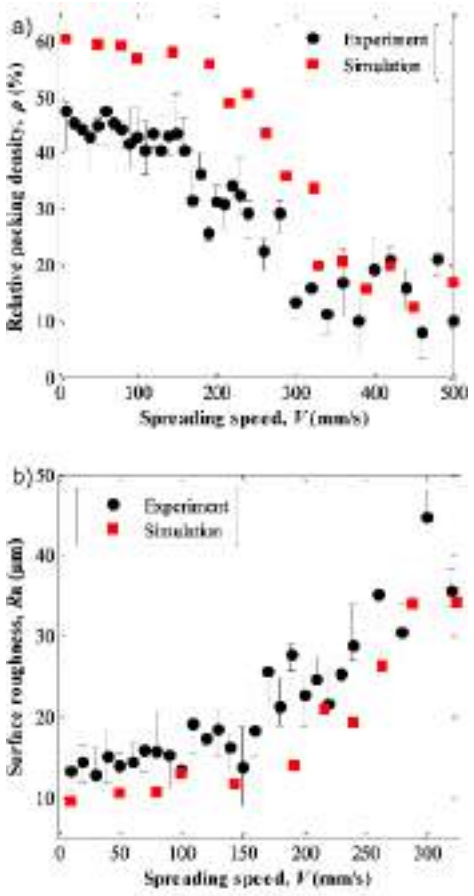

Figure 31 – a) Relative packing density and b) surface roughness as a function of spreading speed Chen et al. (2020).

6. Impact of spreadability on printed component

6.1 Density of the printed component

The density of final parts is affected by the gap height of the recoater/blade used to spread the powders. As shown by many authors, density decreased as the gap height increases. The decrease of density with the increase of spreader gap heights was observed by Abd- Elghany and Bourell, (2012), who evaluated the density of the final layer after SLM produced using 304L stainless steel gas atomized powders and three different spreader gap heights. In fact, the spreader can exclude from the spreading the powder fraction having a size above the gap height

so that the smaller the gap height, the finer is the powder fraction spread. The same authors, i.e. Abd- Elghany and Bourell, (2012)also mentioned that the consequential exclusion of coarser fraction can be beneficial, as larger particles can form voids due to shrinkage after solidifications, cracks and layer separations at grain boundaries. Similar results were obtained with Ti-6Al-4V alloy powders as can be found in the work of Brika et al. (2020).

Ali et al. (2018) evaluated the differences in the density of printed components along the bed. As shown in Figure 32, density slightly decreases along the recoater moving direction, showing differences of about 0.25%. This difference can be attributed to the non-uniformity of the spreading due to size segregation, which inevitably lead to differences in powder bed density and particle size distribution.

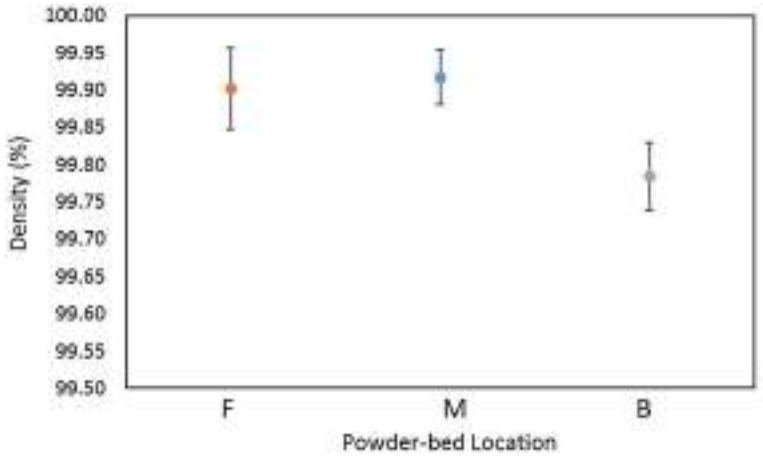

Figure 32 – Density of the printed components at different location,i.e. front (F), middle (M) and back (B) of the bed Ali et al. (2018).

6.2 Surface roughness and dimensional accuracy

The particle size constituting the powder layer has a strong influence on surface roughness. The simulation performed by Lee and Zhang, (2015) showed that the contour of the melt pool is smoother when the powder layer contains a high fraction of fine particles. They also pointed out the importance of packing density on the final quality, as the higher packing fraction results in better surface finish, denser parts without discontinuity and with a smoother surface. Similar to density of printed components, surface roughness is negatively affected when the spreader gap height is increased as demonstrated by Abd- Elghany and Bourell, (2012).

Non-uniformity of powder spreading clearly affected the uniformity of surface roughness of the final printed components. As shown by Ali et al. (2018), powder segregation during spreading leads to differences in surface roughness of about 20% along the recoater moving direction (Figure 33). These differences can be attributed to the spatial variation of particle size distribution across the build bed.

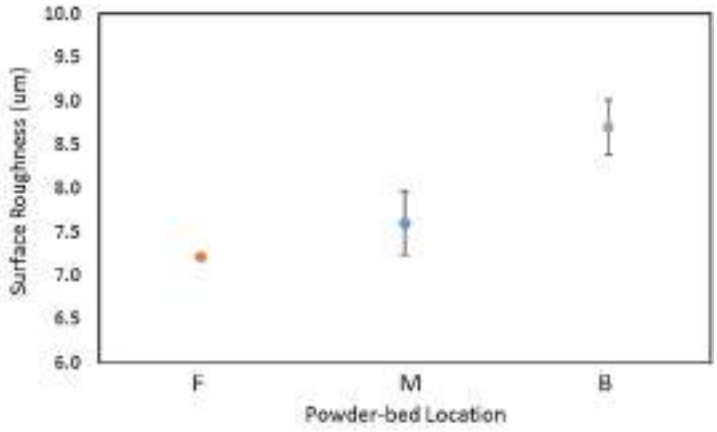

Figure 33 – Surface roughness of the printed components at different locations,i.e. front (F), middle (M) and back (B) of the bed Ali et al. (2018).

Dimensional accuracy is also influenced by the powder spreading. Balbaa et al. (2020) compared two powders for L-PBF process, i.e. fine and coarse powders, which exhibited different spreadability. In fact, the fine powder possesses lower flowability (-75%) and packing density (-30%). The less spreadable powder not only resulted in printed components with low density and higher surface roughness but also in poorer dimensional accuracy in both horizontal and building directions. This was explained by the tendency of less spreadable powders to form agglomerates.

6.3 Mechanical properties

In the case of SLM, the mechanical properties of the final components are affected by (i) the rapid melting of particles by the laser beam and their immediate cooling, which could lead to changes in the crystal structures and phases, and (ii) phenomena of incomplete melting, porosity and micro-cracking. The effect of spreader gap height and scanning speed on tensile strength was studied by Abd- Elghany and Bourell, (2012) for SLM process. They showed that the increase of gap height and scanning speed decrease, yield strength, ultimate tensile strength and breaking elongation because thicker powder layers presented higher porosity and micro-cracking but also due to a less efficient melting of the powder layer with the layer below. Moreover, the higher surface porosity showed by the thicker layers brought to a decrease of hardness value.

7. Conclusions and future research direction

Powder spreadability is a fundamental aspect of AM manufacturing and requires much more research efforts to be understood and quantified to increase the reliability and repeatability of the process and, consequently, the quality

of printed components. Since only in recent years the concept of spreadability has turned on the spotlight and studied systematically. There are still many gaps that need to be addressed:

1. development of standards and metrics quantitatively assess powder spreadability;
2. increasing the understanding of the spreading dynamics;
3. correlate feedstock characteristics to its ability to spreadability;
4. correlate standardized tests (hall flowmeter, rheometers, rotating drums,…) to spreadability;
5. further investigation on the effect of powder spreading on the quality of the final printed components;
6. monitor and control the quality of powder spreading and its variability.

Like many other technological properties, the definition of spreadability is debated, and there is no accordance on how it can be measured. ANSI has inserted spreadability as a gap in AM, as nor unique description nor standards to quantify it is available at the moment. Many spreading metrics have been proposed so far to answer the question "what is a good spreading", but none of them is proved to be effective in the complete quantification of spreadability. Qualitatively, it is considered a powder with good spreadability, the ones that form layers possessing high packing density, spatial uniformity and smooth profile. The main problems in the quantification of powder spreadability lies in the difficulty of generalising the problem to all the possible AM processes and the difficulty of assessing the spread layers directly. Spreading, as an intermediate step in AM process, is not directly assessed but generally evaluated based on the final printed components. More effort should be dedicated to shortening the research gap in this direction and, in particular, to identify the quantitative relation between powders/machine operations and the key properties of the resulting powder layers (e.g. packing density, presence of voids, uniformity), and between the latter and the final printed components.

A clear understanding of the spreading dynamics represents a key factor in achieving quality improvement, replicability, standardization and optimization in AM. Although considerable progress has been made in the past years, the dynamic of spreadability is still not fully understood due to the complexity of the spreading process, which involves the interaction among the spreader, powders, and the surrounding environment. Much effort would need to understand the role of different spreader geometries, material and operational conditions, such as spreader velocity and gap thickness, in their interaction with powders. The research has pointed out as powder characteristics, such as powder friction and cohesion, may play a significant role in the avalanching flow of the powder pile and shear flow in the gap between the spreader and the baseplate during spreading. Although some mechanisms have been identified, the major gap in the research is represented by the fact that the relationship between the occurrence of those mechanisms and powder characteristics is still unclear. From the experimental standpoint, investigating such a relationship is complicated by the difficulty of a direct assessment of powder spreading.

A further problem is represented by the variability of powder characteristics collected from different batches or vendors. In this sense, the support of first-principle numerical modelling (e.g. DEM, DEM-CFD) for the experimentation can be of advantage to fill this research gap as it direct assesses the spreading phenomena at the particle level and give the experimenter the control of the powder specifications. The problem of the variability of powder characteristics is ubiquitous Zegzulka, (2020) and is leading many researchers to explore the causes and possible solutions.

Many efforts have been made in the past to correlate standardized tests such as hall flowmeters, rheometers, and rotating drums to powder spreadability. However, those attempts have only partially addressed this problem and, in some cases, have led to contradictory results. Succeeding in correlating the outcomes from standardised tests with powder spreadability would help identify and choose the appropriate powders to be used in a specific process and with specific process conditions. This represents a big opportunity to increase process/powder understanding and give professionals the suitable instruments to choose the more appropriate materials.

Further investigations on the effect of powder spreading on the quality of the final printed components are needed to design consistent processes. The few papers published call for deepening the investigation of the relationship between powder spreading and mechanical behaviour, microstructure, presence of voids, formation of cracks, and the quality and appearance of the surface of the final products. The complexity of the problem and the number of variables involved require a more systematic and statistical approach, as also mentioned in the work of Zegzulka et al. (2020).

None or a few studies have been published concerning monitoring and controlling the quality of powder spreading. The development of new technologies able to measure the quality of powder layers is fundamental in ensuring highly consistent production, optimising the process, and reducing manufacturing costs. There is a broad research space in the development of new in-line devices able to catch specific properties of the layers, such as packing density, layer thickness, uniformity and surface smoothness, during the spreading. At that point, the monitoring and control of the spreading quality would inform an automated algorithm on the energy intensity/duration to be supplied to meet the specifications of the final component.

Furthermore, applying the methods mentioned above for assessing spreadability can be used as a starting point to describe the behaviour of even more complex powder systems. According to the authors' knowledge, only a few papers discuss composite powders' spreadability, for example, in the work of Lüddecke et al. (2021), where a nanocomposite powder containing different oxides was investigated. More specifically, stainless steel, tool steel and aluminium alloy powders were reinforced via SiC, graphene, and iron oxide black. The paper's focus was on optimising the printing parameters, and powder spreadability was thoroughly investigated.

Further developments could be achieved by applying Image processing steps. For example Vakifahmetoglu et al. (2022) recently introduced an image processing algorithm based on Matlab software to examine spreadability as

a function of the powder size distribution or other physical properties of the material. Similar efforts could be introduced in the future but using open source programming codes such as python to spread knowledge among researchers and end-users.

Indeed, one crucial point to achieve in the future is reducing the complexity of the measurement of powder properties. As long as the adopted techniques become more accessible and faster, their scalability increases and industrialisation becomes possible. This kind of effort was observed in some literary works, e.g. the one from Ahmed et al. (2020), who proposed a simple technique for assessing the powder spreadability.

At the time of this review, all techniques require that powder samples are assessed outside of the printing machine. As a possible future optimization, the aforementioned techniques could be moved directly into the LPBF machines and used online during the printing process. As a further optimization, it would be really interesting to produce a machine routine which optimizes its printing parameters directly from the assessment of the powders using an online feedback system. Knowing in advice the powder properties and tailoring the printing parameters specifically for the processed powders could enhance the layer density obtaining higher densities after the laser melting.

8. References

Abd- Elghany, K., Bourell, D.L., 2012. Property evaluation of 304L stainless steel fabricated by selective laser melting. Rapid Prototyp. J.

Ahmed, M., Pasha, M., Nan, W., Ghadiri, M., 2020. A simple method for assessing powder spreadability for additive manufacturing. Powder Technol. 367, 671–679. https://doi.org/10.1016/j.powtec.2020.04.033

Ali, U., Mahmoodkhani, Y., Shahabad, S.I., Esmaeilizadeh, R., Liravi, F., Sheydaeian, E., Huang, K.Y., Marzbanrad, E., Vlasea, M., Toyserkani, E., 2018. On the measurement of relative powder-bed compaction density in powder-bed additive manufacturing processes. Mater. Des. 155, 495–501.

America Makes, ANSI Additive Manufacturing Standardization, 2017. Standardization roadmap for additive manufacturing. ANSI/National Cent. Def. Manuf. Mach. https//www. ansi. org/standards_activities/standards_boards_ panels/amsc/Default.

Averardi, A., Cola, C., Zeltmann, S.E., Gupta, N., 2020. Effect of particle size distribution on the packing of powder beds: A critical discussion relevant to additive manufacturing. Mater. Today Commun. 24, 100964.

Bai, Y., Wagner, G., Williams, C.B., 2015. Effect of bimodal powder mixture on powder packing density and sintered density in binder jetting of metals, in: 2015 Annual International Solid Freeform Fabrication Symposium. pp. 758–771.

Balbaa, M.A., Ghasemi, A., Fereiduni, E., Elbestawi, M.A., Jadhav, S.D., Kruth, J.-P., 2020. Role of powder particle size on laser powder bed fusion processability of AlSi10mg alloy. Addit. Manuf. 101630.

Beitz, S., Uerlich, R., Bokelmann, T., Diener, A., Vietor, T., Kwade, A., 2019. Influence of powder deposition on powder bed and specimen properties. Materials (Basel). 12, 297.

Blais, B., Vidal, D., Bertrand, F., Patience, G.S., Chaouki, J., 2019. Experimental Methods in Chemical Engineering: Discrete Element Method—DEM. Can. J. Chem. Eng. 97, 1964–1973.

Bo, S., Wen, S., Yan, C., Wei, Q., Shi, Y., 2020. Selective Laser Melting for Metal and Metal Matrix Composites. Academic Press.

Boley, C.D., Mitchell, S.C., Rubenchik, A.M., Wu, S.S.Q., 2016. Metal powder absorptivity: modeling and experiment. Appl. Opt. 55, 6496–6500.

Brika, S.E., Letenneur, M., Dion, C.A., Brailovski, V., 2020. Influence of particle morphology and size distribution on the powder flowability and laser powder bed fusion manufacturability of Ti-6Al-4V alloy. Addit. Manuf. 31, 100929.

Castellanos, A., 2005. The relationship between attractive interparticle forces and bulk behaviour in dry and uncharged fine powders. Adv. Phys. 54, 263–376.

Chandrasekar, S., Coble, J.B., Yoder, S., Nandwana, P., Dehoff, R.R., Paquit, V.C., Babu, S.S., 2020. Investigating the effect of metal powder recycling in Electron beam Powder Bed Fusion using process log data. Addit. Manuf. 32, 100994.

Chen, H., Chen, Y., Liu, Y., Wei, Q., Shi, Y., Yan, W., 2020. Packing quality of powder layer during counter-rolling-type powder spreading process in additive manufacturing. Int. J. Mach. Tools Manuf. 153, 103553. https://doi.org/10.1016/j.ijmachtools.2020.103553

Chen, H., Wei, Q., Wen, S., Li, Z., Shi, Y., 2017. Flow behavior of powder particles in layering process of selective laser melting: Numerical modeling and experimental verification based on discrete element method. Int. J. Mach. Tools Manuf. 123, 146–159.

Chen, H., Wei, Q., Zhang, Y., Chen, F., Shi, Y., Yan, W., 2019. Powder-spreading mechanisms in powder-bed-based additive manufacturing: Experiments and computational modeling. Acta Mater. 179, 158–171.

Chen, Q., Juste, E., Lasgorceix, M., Petit, F., Leriche, A., 2022. Binder jetting process with ceramic powders: Influence of powder properties and printing parameters. Open Ceram. 9, 100218. https://doi.org/10.1016/j.oceram.2022.100218

Chin, S.Y., Dikshit, V., Meera Priyadarshini, B., Zhang, Y., 2020. Powder-Based 3D Printing for the Fabrication

of Device with Micro and Mesoscale Features. Micromachines 11, 658.

Choi, J.-P., Shin, G.-H., Lee, H.-S., Yang, D.-Y., Yang, S., Lee, C.-W., Brochu, M., Yu, J.-H., 2017. Evaluation of powder layer density for the selective laser melting (SLM) process. Mater. Trans. 58, 294–297.

Clayton, J., 2014. Optimising metal powders for additive manufacturing. Met. Powder Rep. 69, 14–17.

Clayton, J., Millington-Smith, D., Armstrong, B., 2015. The application of powder rheology in additive manufacturing. Jom 67, 544–548.

Coetzee, C.J., 2017. Calibration of the discrete element method. Powder Technol. 310, 104–142.

Cordova, L., Bor, T., de Smit, M., Campos, M., Tinga, T., 2020a. Measuring the spreadability of pre-treated and moisturized powders for laser powder bed fusion. Addit. Manuf. 32, 101082.

Cordova, L., Bor, T., de Smit, M., Carmignato, S., Campos, M., Tinga, T., 2020b. Effects of powder reuse on the microstructure and mechanical behaviour of Al–Mg–Sc–Zr alloy processed by laser powder bed fusion (LPBF). Addit. Manuf. 36. https://doi.org/10.1016/j.addma.2020.101625

Cordova, L., Campos, M., Tinga, T., 2019. Revealing the Effects of Powder Reuse for Selective Laser Melting by Powder Characterization. Jom 71, 1062–1072. https://doi.org/10.1007/s11837-018-3305-2

Cundall, P.A., Strack, O.D.L., 1979. A discrete numerical model for granular assemblies. Geotechnique 29, 47–65.

Dawes, J., Bowerman, R., Trepleton, R., 2015. Introduction to the additive manufacturing powder metallurgy supply chain. Johnson Matthey Technol. Rev. 59, 243–256.

Desai, P.S., Higgs, C.F., 2019. Spreading process maps for powder-bed additive manufacturing derived from physics model-based machine learning. Metals (Basel). 9, 1176.

Desai, P.S., Mehta, A., Dougherty, P.S.M., Higgs III, C.F., 2019. A rheometry based calibration of a first-order DEM model to generate virtual avatars of metal Additive Manufacturing (AM) powders. Powder Technol. 342, 441–456.

Dobson, S.D., Starr, T.L., 2020. Powder characterization and part density for powder bed fusion of 17-4 PH stainless steel. Rapid Prototyp. J.

Engel, B., Bourell, D.L., 2000. Titanium alloy powder preparation for selective laser sintering. Rapid Prototyp. J.

Escano, L.I., Parab, N.D., Xiong, L., Guo, Q., Zhao, C., Fezzaa, K., Everhart, W., Sun, T., Chen, L., 2018. Revealing particle-scale powder spreading dynamics in powder-bed-based additive manufacturing process by high-speed x-ray imaging. Sci. Rep. 8, 1–11.

Fereiduni, E., Ghasemi, A., Elbestawi, M., 2019. Characterization of Composite Powder Feedstock from Powder Bed Fusion Additive Manufacturing Perspective. Materials (Basel). 12, 3673.

Frazier, W.E., 2014. Metal additive manufacturing: A review. J. Mater. Eng. Perform. 23, 1917–1928. https://doi.org/10.1007/s11665-014-0958-z

Gärtner, E., Jung, H.Y., Peter, N.J., Dehm, G., Jägle, E.A., Uhlenwinkel, V., Mädler, L., 2021. Reducing cohesion of metal powders for additive manufacturing by nanoparticle dry-coating. Powder Technol. 379, 585–595. https://doi.org/10.1016/j.powtec.2020.10.065

Geer, S., Bernhardt-Barry, M.L., Garboczi, E.J., Whiting, J., Donmez, A., 2018. A more efficient method for calibrating discrete element method parameters for simulations of metallic powder used in additive manufacturing. Granul. Matter 20, 77.

Gokuldoss, P.K., Kolla, S., Eckert, J., 2017. Additive manufacturing processes: Selective laser melting, electron beam melting and binder jetting—Selection guidelines. Materials (Basel). 10, 672.

Haeri, S., 2017. Optimisation of blade type spreaders for powder bed preparation in Additive Manufacturing using DEM simulations. Powder Technol. 321, 94–104.

Haeri, S., Wang, Y., Ghita, O., Sun, J., 2016. Discrete element simulation and experimental study of powder spreading process in additive manufacturing. Powder Technol. 306, 45–54.

Haferkamp, L., Spierings, A., Rusch, M., Jermann, D., Spurek, M.A., Wegener, K., 2020. Effect of Particle size of monomodal 316L powder on powder layer density in powder bed fusion. Prog. Addit. Manuf. 1–8.

He, Y., Gardy, J., Hassanpour, A., Bayly, A.E., 2020. A digital-based approach for characterising spread powder layer in additive manufacturing. Mater. Des. 196, 109102.

Hoeges, S., Zwiren, A., Schade, C., 2017. Additive manufacturing using water atomized steel powders. Met. Powder Rep. 72, 111–117. https://doi.org/10.1016/j.mprp.2017.01.004

Hu, Z., Mahadevan, S., 2017. Uncertainty quantification and management in additive manufacturing: current status, needs, and opportunities. Int. J. Adv. Manuf. Technol. 93, 2855–2874.

Hulme-Smith, C.N., Hari, V., Mellin, P., 2021. Spreadability Testing of Powder for Additive Manufacturing. B. Huettenmaenn Monatsh 166, 9–13.

Jacob, G., Donmez, A., Slotwinski, J., Moylan, S., 2016. Measurement of powder bed density in powder bed fusion additive manufacturing processes. Meas. Sci. Technol. 27, 115601.

Jacob, G., Jacob, G., Brown, C.U., Donmez, M.A., Watson, S.S., Slotwinski, J., 2017. Effects of powder recycling

on stainless steel powder and built material properties in metal powder bed fusion processes. US Department of Commerce, National Institute of Standards and Technology ….

James, W.B., 2019. Mercury Scientific Revolution ASTM Paper [WWW Document].

Karapatis, N.P., Egger, G., Gygax, P.E., Glardon, R., 1999. Optimization of powder layer density in selective laser sintering, in: 1999 International Solid Freeform Fabrication Symposium.

Karg, M., Laumer, T., Schmidt, M., 2013. Additive Manufacturing of Gradient and Multimaterial Components, in: Proceedings of the International Conference on Competitive Manufacturing, Stellenbosch, South Africa.

Karg, M.C.H., Munk, A., Ahuja, B., Backer, M.V., Schmitt, J.P., Stengel, C., Kuryntsev, S.V., Schmidt, M., 2019. Expanding particle size distribution and morphology of aluminium-silicon powders for Laser Beam Melting by dry coating with silica nanoparticles. J. Mater. Process. Technol. 264, 155–171.

Kassym, K., Perveen, A., 2020. Atomization processes of metal powders for 3D printing. Mater. Today Proc. 26, 1727–1733.

Kiani, P., Scipioni Bertoli, U., Dupuy, A.D., Ma, K., Schoenung, J.M., 2020. A statistical analysis of powder flowability in metal additive manufacturing. Adv. Eng. Mater. 22, 2000022.

Kirchner, A., Klöden, B., Weißgärber, T., Kieback, B., 2016. Powders for Additive Manufacturing.

Landi, G., Barletta, D., Poletto, M., 2011. Modelling and experiments on the effect of air humidity on the flow properties of glass powders. Powder Technol. 207, 437–443.

Lecis, N., Beltrami, R., Mariani, M., 2021a. Binder jetting 3D printing of 316 stainless steel: Influence of process parameters on microstructural and mechanical properties. Metall. Ital. 113, 31–41.

Lecis, N., Mariani, M., Beltrami, R., Emanuelli, L., Casati, R., Vedani, M., Molinari, A., 2021b. Effects of process parameters, debinding and sintering on the microstructure of 316L stainless steel produced by binder jetting. Mater. Sci. Eng. A 828, 142108. https://doi.org/10.1016/j.msea.2021.142108

Lee, S., Sachs, E., Cima, M., 1995. Layer position accuracy in powder- based rapid prototyping. Rapid Prototyp. J.

Lee, Y., Gurnon, A.K., Bodner, D., Simunovic, S., 2020. Effect of Particle Spreading Dynamics on Powder Bed Quality in Metal Additive Manufacturing. Integr. Mater. Manuf. Innov. 1–13.

Lee, Y., Simunovic, S., Gurnon, K.A., 2019. Quantification of Powder Spreading Process for Metal Additive Manufacturing. Oak Ridge National Lab.(ORNL), Oak Ridge, TN (United States).

Lee, Y.S., Zhang, W., 2015. Mesoscopic simulation of heat transfer and fluid flow in laser powder bed additive

manufacturing, in: International Solid Free Form Fabrication Symposium, Austin. pp. 1154–1165.

Lefebvre, L.-P., Dai, J., Thomas, Y., Daroszewska, M., Martinez-Rubi, Y., 2020. Measurement of Water Content in Metal Powders. Mater. Perform. Charact. 9.

Lefebvre, L.P., Dai, J., Thomas, Y., Martinez-Rubi, Y., 2019. Metal powder flowability: effect of humidity and impact on the reproducibility of the measurements, in: Proceeding of the Additive Manufacturing with Powder Metallurgy Conference. pp. 1–13.

Leturia, M., Benali, M., Lagarde, S., Ronga, I., Saleh, K., 2014. Characterization of flow properties of cohesive powders: A comparative study of traditional and new testing methods. Powder Technol. 253, 406–423.

Li, X.P., O'donnell, K.M., Sercombe, T.B., 2016. Selective laser melting of Al-12Si alloy: Enhanced densification via powder drying. Addit. Manuf. 10, 10–14.

Liao, J., Cooper, D.R., 2021. The Environmental Impacts of Metal Powder Bed Additive Manufacturing. J. Manuf. Sci. Eng. 143.

Liu, B., Wildman, R., Tuck, C., Ashcroft, I., Hague, R., 2011. Investigation the effect of particle size distribution on processing parameters optimisation in selective laser melting process. Addit. Manuf. Res. group, Loughbrgh. Univ. 227–238.

Lommen, S., Schott, D., Lodewijks, G., 2014. DEM speedup: Stiffness effects on behavior of bulk material. Particuology 12, 107–112.

Lüddecke, A., Pannitz, O., Zetzener, H., Sehrt, J.T., Kwade, A., 2021. Powder properties and flowability measurements of tailored nanocomposites for powder bed fusion applications. Mater. Des. 202. https://doi.org/10.1016/j.matdes.2021.109536

Ma, Y., Evans, T.M., Philips, N., Cunningham, N., 2020. Numerical simulation of the effect of fine fraction on the flowability of powders in additive manufacturing. Powder Technol. 360, 608–621.

Ma, Y., Evans, T.M., Philips, N., Cunningham, N., 2019. Modeling the effect of moisture on the flowability of a granular material. Meccanica 54, 667–681. https://doi.org/10.1007/s11012-018-0901-8

Mariani, M., Goncharov, I., Mariani, D., De Gaudenzi, G. Pietro, Popovich, A., Lecis, N., Vedani, M., 2021. Mechanical and microstructural characterization of WC-Co consolidated by binder jetting additive manufacturing. Int. J. Refract. Met. Hard Mater. 100, 105639. https://doi.org/10.1016/j.ijrmhm.2021.105639

Meier, C., Weissbach, R., Weinberg, J., Wall, W.A., Hart, A.J., 2019a. Critical influences of particle size and adhesion on the powder layer uniformity in metal additive manufacturing. J. Mater. Process. Technol. 266, 484–501.

Meier, C., Weissbach, R., Weinberg, J., Wall, W.A., John Hart, A., 2019b. Modeling and characterization of cohesion in fine metal powders with a focus on additive manufacturing process simulations. Powder Technol. 343, 855–866. https://doi.org/10.1016/j.powtec.2018.11.072

Mellin, P., Rashidi, M., Fischer, M., Nyborg, L., Marchetti, L., Hulme-Smith, C., Uhlirsch, M., Strondl, A., 2021. Moisture in Metal Powder and Its Implication for Processability in L-PBF and Elsewhere. BHM Berg-und Hüttenmännische Monatshefte 166, 33–39.

Mindt, H.W., Megahed, M., Lavery, N.P., Holmes, M.A., Brown, S.G.R., 2016. Powder Bed Layer Characteristics: The Overseen First-Order Process Input. Metall. Mater. Trans. A Phys. Metall. Mater. Sci. 47, 3811–3822. https://doi.org/10.1007/s11661-016-3470-2

Mitterlehner, M., Danninger, H., Gierl-Mayer, C., Gschiel, H., 2021. Investigation of the Influence of Powder Moisture on the Spreadability Using the Spreading Tester. BHM Berg- und Hüttenmännische Monatshefte 166, 14–22. https://doi.org/10.1007/s00501-020-01067-x

Molitch-Hou, M., 2018. Overview of additive manufacturing process, in: Additive Manufacturing. Elsevier, pp. 1–38. https://doi.org/10.1016/B978-0-12-812155-9.00001-3

Mostafaei, A., De Vecchis, P.R., Kimes, K.A., Elhassid, D., Chmielus, M., 2021. Effect of binder saturation and drying time on microstructure and resulting properties of sinter-HIP binder-jet 3D-printed WC-Co composites. Addit. Manuf. 46, 102128. https://doi.org/10.1016/j.addma.2021.102128

Mukherjee, T., DebRoy, T., 2019. A digital twin for rapid qualification of 3D printed metallic components. Appl. Mater. Today 14, 59–65.

Muñiz-Lerma, J.A., Nommeots-Nomm, A., Waters, K.E., Brochu, M., 2018. A comprehensive approach to powder feedstock characterization for powder bed fusion additive manufacturing: A case study on AlSi7Mg. Materials (Basel). 11. https://doi.org/10.3390/ma11122386

Mussatto, A., Groarke, R., O'Neill, A., Obeidi, M.A., Delaure, Y., Brabazon, D., 2020. Influences of powder morphology and spreading parameters on the powder bed topography uniformity in powder bed fusion metal additive manufacturing. Addit. Manuf. 101807.

Nan, W., Ghadiri, M., 2019. Numerical simulation of powder flow during spreading in additive manufacturing. Powder Technol. 342, 801–807. https://doi.org/10.1016/j.powtec.2018.10.056

Nan, W., Pasha, M., Bonakdar, T., Lopez, A., Zafar, U., Nadimi, S., Ghadiri, M., 2018. Jamming during particle spreading in additive manufacturing. Powder Technol. 338, 253–262. https://doi.org/10.1016/j.powtec.2018.07.030

Nan, W., Pasha, M., Ghadiri, M., 2020. Numerical simulation of particle flow and segregation during roller spreading process in additive manufacturing. Powder Technol. 364, 811–821.

Nguyen, Q.B., Nai, M.L.S., Zhu, Z., Sun, C.-N., Wei, J., Zhou, W., 2017. Characteristics of inconel powders for powder-bed additive manufacturing. Engineering 3, 695–700.

Oropeza, D., Roberts, R., Hart, A.J., 2021. A modular testbed for mechanized spreading of powder layers for additive manufacturing. Rev. Sci. Instrum. 92, 15114.

Pal, S., Gubeljak, N., Bončina, T., Hudák, R., Toth, T., Zivcak, J., Lojen, G., Leben, N., Drstvenšek, I., 2021. The effects of locations on the build tray on the quality of specimens in powder bed additive manufacturing. Int. J. Adv. Manuf. Technol. 112, 1159–1170. https://doi.org/10.1007/s00170-020-06563-5

Parteli, E.J.R., Schmidt, J., Blümel, C., Wirth, K.-E., Peukert, W., Pöschel, T., 2014. Attractive particle interaction forces and packing density of fine glass powders. Sci. Rep. 4, 6227.

Peng, W., Wang, G., Gigliotti Jr, M.F.X., Singh, P., 2018. Method for treating powder by dry mixing and powder treated thereby.

Phua, A., Doblin, C., Owen, P., Davies, C.H.J., Delaney, G.W., 2021. The effect of recoater geometry and speed on granular convection and size segregation in powder bed fusion. Powder Technol. 394, 632–644. https://doi.org/10.1016/j.powtec.2021.08.058

Popov, V. V, Grilli, M.L., Koptyug, A., Jaworska, L., Katz-Demyanetz, A., Klobčar, D., Balos, S., Postolnyi, B.O., Goel, S., 2021. Powder Bed Fusion Additive Manufacturing Using Critical Raw Materials: A Review. Materials (Basel). 14, 909. https://doi.org/10.3390/ma14040909

Richter, C., Roessler, T., Kunze, G., Katterfeld, A., Will, F., 2020. Development of a standard calibration procedure for the DEM parameters of cohesionless bulk materials–Part II: Efficient optimization-based calibration. Powder Technol. 360, 967–976.

Riener, K., Oswald, S., Winkler, M., Leichtfried, G.J., 2021. Influence of storage conditions and reconditioning of AlSi10Mg powder on the quality of parts produced by laser powder bed fusion (LPBF). Addit. Manuf. 39. https://doi.org/10.1016/j.addma.2021.101896

Roberts, J.W., Sutcliffe, C.J., Green, P.L., Black, K., 2020. Modelling of metallic particle binders for increased part density in binder jet printed components. Addit. Manuf. 34. https://doi.org/10.1016/j.addma.2020.101244

Roessler, T., Richter, C., Katterfeld, A., Will, F., 2019. Development of a standard calibration procedure for the DEM parameters of cohesionless bulk materials–part I: Solving the problem of ambiguous parameter

combinations. Powder Technol. 343, 803–812.

Romano, T., Migliori, E., Mariani, M., Lecis, N., Vedani, M., 2022. Densification behaviour of pure copper processed through cold pressing and binder jetting under different atmospheres. Rapid Prototyp. J. https://doi.org/10.1108/RPJ-09-2021-0243

Saboori, A., Gallo, D., Biamino, S., Fino, P., Lombardi, M., 2017. An overview of additive manufacturing of titanium components by directed energy deposition: microstructure and mechanical properties. Appl. Sci. 7, 883.

Sames, W.J., List, F.A., Pannala, S., Dehoff, R.R., Babu, S.S., 2016. The metallurgy and processing science of metal additive manufacturing. Int. Mater. Rev. 61, 315–360.

Sehhat, M.H., Sutton, A.T., Hung, C., Brown, B., Malley, R.J.O., Park, J., Leu, M.C., 2022. Plasma spheroidization of gas-atomized 304L stainless steel powder for laser powder bed fusion process 1.

Seyda, V., Kaufmann, N., Emmelmann, C., 2012. Investigation of aging processes of Ti-6Al-4 V powder material in laser melting. Phys. Procedia 39, 425–431.

Shanjani, Y., Toyserkani, E., 2008. Material spreading and compaction in powder-based solid freeform fabrication methods: mathematical modeling, in: 19th Annual International Solid Freeform Fabrication Symposium, SFF. pp. 399–410.

Sharma, R., Setia, G., 2019. Mechanical dry particle coating on cohesive pharmaceutical powders for improving flowability-A review. Powder Technol. 356, 458–479.

Sillani, F., Kleijnen, R.G., Vetterli, M., Schmid, M., Wegener, K., 2019. Selective laser sintering and multi jet fusion: Process-induced modification of the raw materials and analyses of parts performance. Addit. Manuf. 27, 32–41.

Sing, S.L., Tey, C.F., Tan, J.H.K., Huang, S., Yeong, W.Y., 2019. 3D printing of metals in rapid prototyping of biomaterials: Techniques in additive manufacturing, Second Edi. ed, Rapid Prototyping of Biomaterials: Techniques in Additive Manufacturing. Elsevier Ltd. https://doi.org/10.1016/B978-0-08-102663-2.00002-2

Slotwinski, J.A., Garboczi, E.J., 2015. Metrology needs for metal additive manufacturing powders. Jom 67, 538–543.

Snow, Z., Martukanitz, R., Joshi, S., 2019. On the development of powder spreadability metrics and feedstock requirements for powder bed fusion additive manufacturing. Addit. Manuf. 28, 78–86.

Snow, Z.K., 2018. Understanding Powder Spreadability in Powder Bed Fusion Additive Manufacturing.

Spierings, A.B., Levy, G., 2009. Comparison of density of stainless steel 316L parts produced with selective laser melting using different powder grades, in: Proceedings of the Annual International Solid Freeform Fabrication Symposium. Austin, TX, pp. 342–353.

Spierings, A.B., Voegtlin, M., Bauer, T., Wegener, K., 2016. Powder flowability characterisation methodology for powder-bed-based metal additive manufacturing. Prog. Addit. Manuf. 1, 9–20.

Streubel, R., Wilms, M.B., Doñate-Buendía, C., Weisheit, A., Barcikowski, S., Schleifenbaum, J.H., Gökce, B., 2018. Depositing laser-generated nanoparticles on powders for additive manufacturing of oxide dispersed strengthened alloy parts via laser metal deposition. Jpn. J. Appl. Phys. 57, 40310.

Strondl, A., Lyckfeldt, O., Brodin, H., Ackelid, U., 2015. Characterization and control of powder properties for additive manufacturing. Jom 67, 549–554.

Sun, P., Fang, Z.Z., Zhang, Y., Xia, Y., 2017. Review of the methods for production of spherical Ti and Ti alloy powder. Jom 69, 1853–1860.

Sutton, A.T., Kriewall, C.S., Karnati, S., Leu, M.C., Newkirk, J.W., 2020. Characterization of AISI 304L stainless steel powder recycled in the laser powder-bed fusion process. Addit. Manuf. 32, 100981.

Tan, J.H., Wong, W.L.E., Dalgarno, K.W., 2017. An overview of powder granulometry on feedstock and part performance in the selective laser melting process. Addit. Manuf. 18, 228–255.

Tang, H.P., Qian, M., Liu, N., Zhang, X.Z., Yang, G.Y., Wang, J., 2015. Effect of powder reuse times on additive manufacturing of Ti-6Al-4V by selective electron beam melting. Jom 67, 555–563.

Tiwari, S.K., Pande, S., Agrawal, S., Bobade, S.M., 2015. Selection of selective laser sintering materials for different applications. Rapid Prototyp. J.

Vakifahmetoglu, C., Hasdemir, B., Biasetto, L., 2022. Spreadability of Metal Powders for Laser-Powder Bed Fusion via Simple Image Processing Steps. Materials (Basel). 15, 1–13. https://doi.org/10.3390/ma15010205

Van der Schueren, B., Kruth, J.-P., 1995. Powder deposition in selective metal powder sintering. Rapid Prototyp. J.

Wallner, S., 2019. Powder Production Technologies. BHM Berg-und Hüttenmännische Monatshefte 164, 108–111.

Wang, L., Li, E.L., Shen, H., Zou, R.P., Yu, A.B., Zhou, Z.Y., 2020. Adhesion effects on spreading of metal powders in selective laser melting. Powder Technol. 363, 602–610.

Wang, L., Yu, A., Li, E., Shen, H., Zhou, Z., 2021. Effects of spreader geometry on powder spreading process in

powder bed additive manufacturing. Powder Technol. 384, 211–222. https://doi.org/10.1016/j.powtec.2021.02.022

Wang, L., Zhou, Z., Li, E., Shen, H., Yu, A., 2022. Powder deposition mechanism during powder spreading with different spreader geometries in powder bed fusion additive manufacturing. Powder Technol. 395, 802–810. https://doi.org/10.1016/j.powtec.2021.10.017

Wei, W.-H., Wang, L.-Z., Chen, T., Duan, X.-M., Li, W., 2017. Study on the flow properties of Ti-6Al-4V powders prepared by radio-frequency plasma spheroidization. Adv. Powder Technol. 28, 2431–2437.

Yang, L., Hsu, K., Baughman, B., Godfrey, D., Medina, F., Menon, M., Wiener, S., 2017. Additive manufacturing of metals: the technology, materials, design and production. Springer.

Yao, D., An, X., Fu, H., Zhang, H., Yang, X., Zou, Q., Dong, K., 2020. Dynamic investigation on the powder spreading during selective laser melting additive manufacturing. Addit. Manuf. 101707.

Zegzulka, J., Gelnar, D., Jezerska, L., Prokes, R., Rozbroj, J., 2020. Characterization and flowability methods for metal powders. Sci. Rep. 10, 1–19. https://doi.org/10.1038/s41598-020-77974-3

Zhang, Y., Wu, L., Guo, X., Kane, S., Deng, Y., Jung, Y.G., Lee, J.H., Zhang, J., 2018. Additive Manufacturing of Metallic Materials: A Review. J. Mater. Eng. Perform. 27, 1–13. https://doi.org/10.1007/s11665-017-2747-y

Zhao, Y., Aoyagi, K., Daino, Y., Yamanaka, K., Chiba, A., 2020. Significance of powder feedstock characteristics in defect suppression of additively manufactured Inconel 718. Addit. Manuf. 101277.

Zhu, H.H., Fuh, J.Y.H., Lu, L., 2007. The influence of powder apparent density on the density in direct laser-sintered metallic parts. Int. J. Mach. Tools Manuf. 47, 294–298.

Figure_01

Click here to access/download;Figure;Figure 1.png

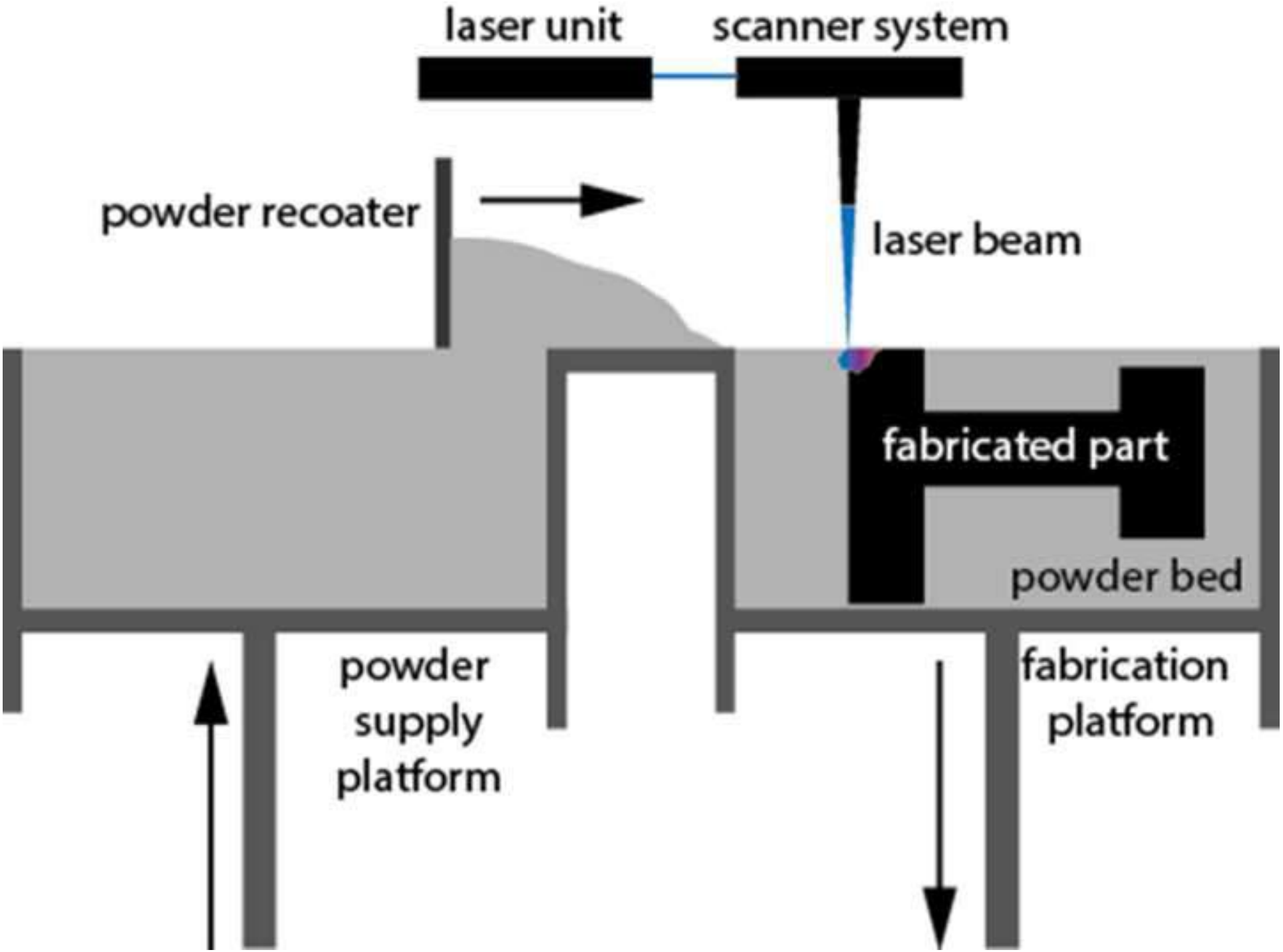

Fig_02

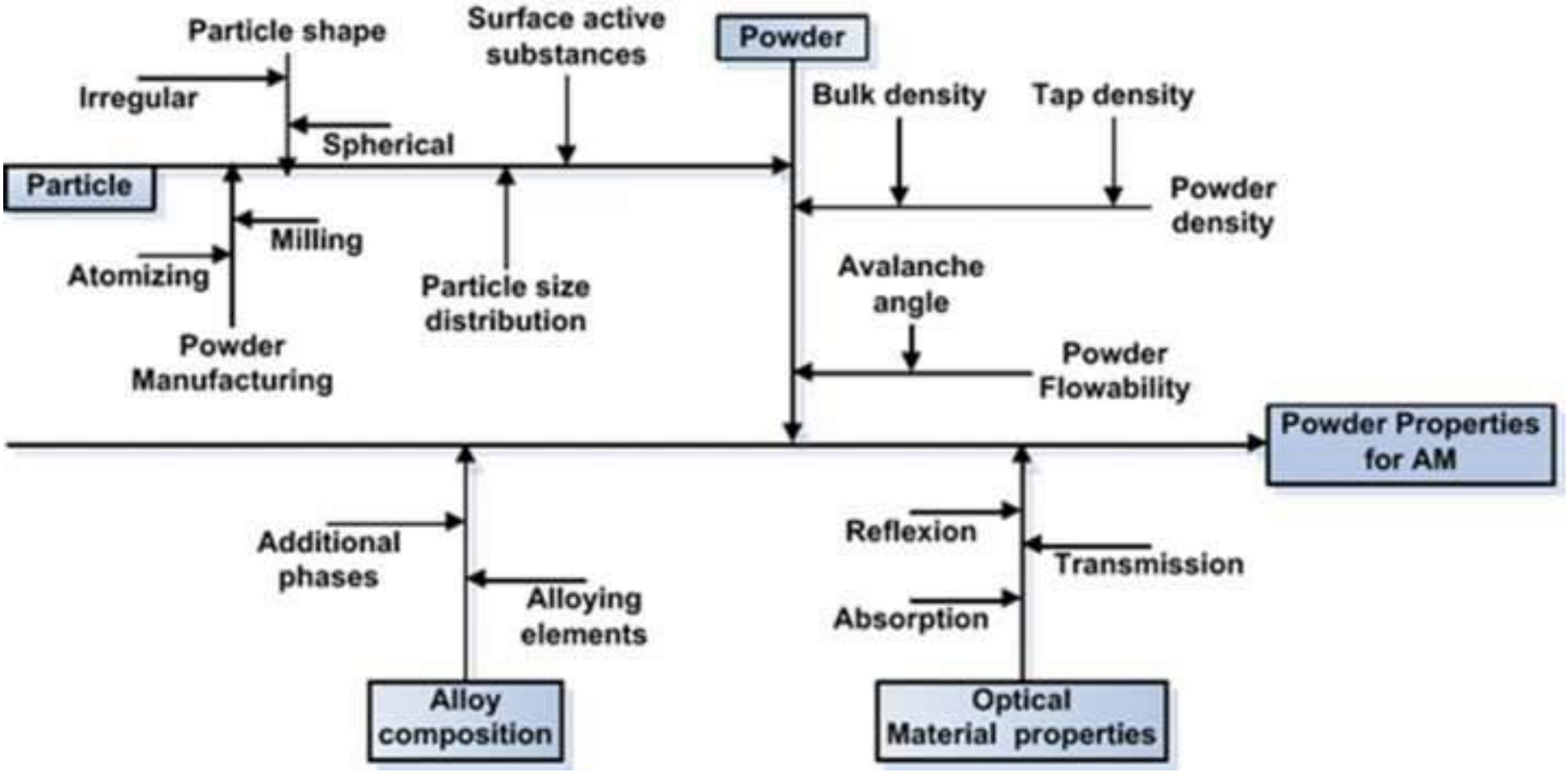

Fig_03

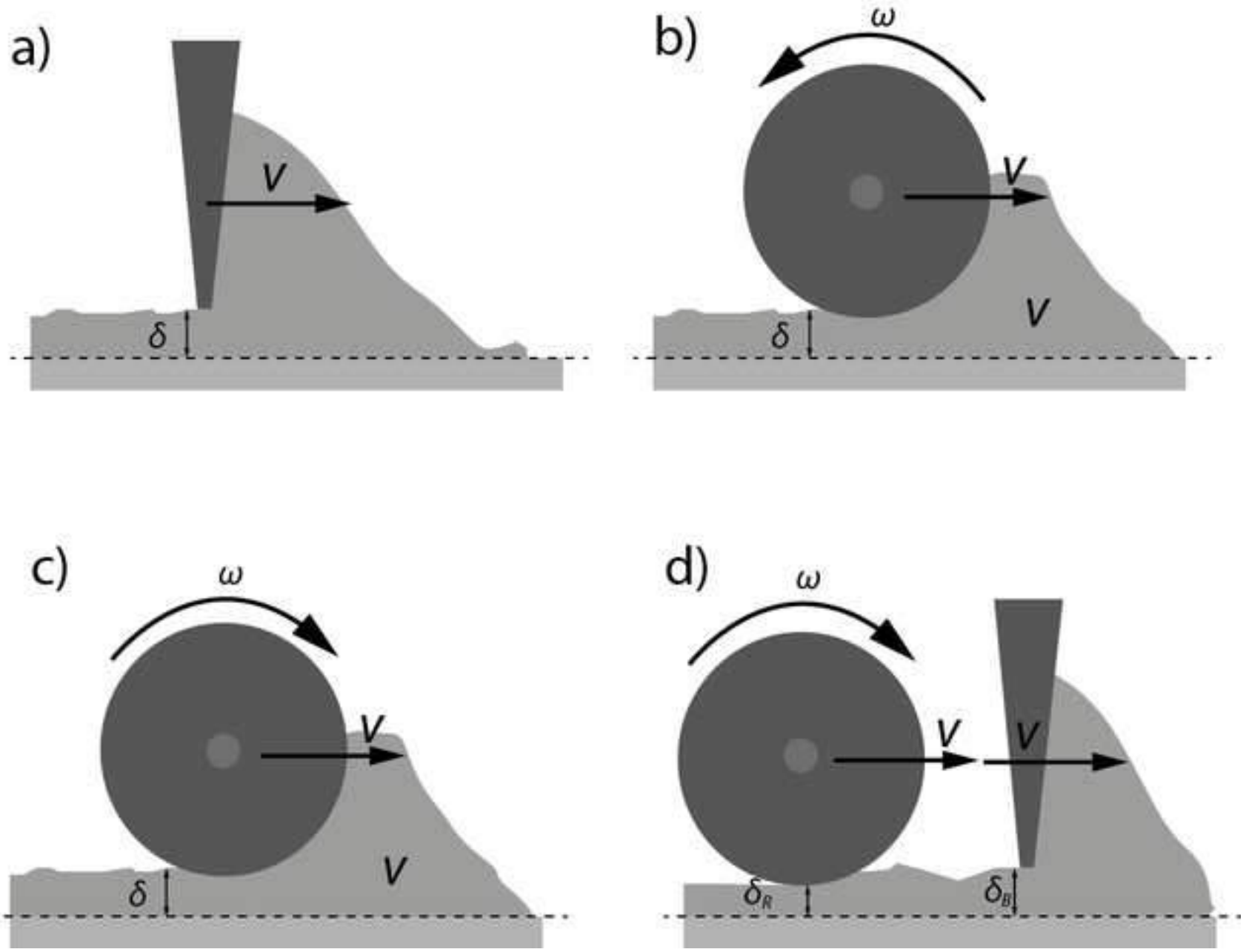

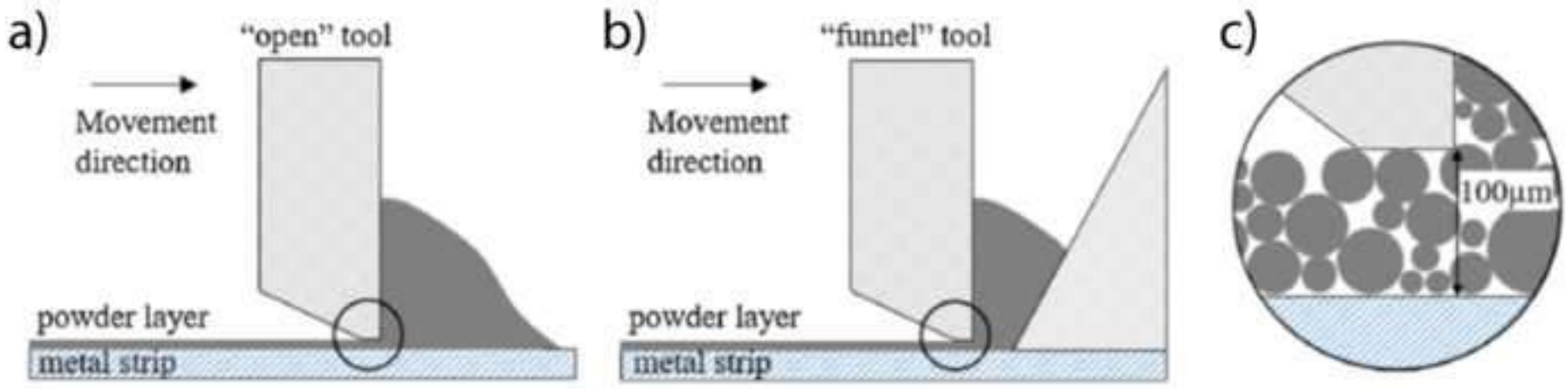

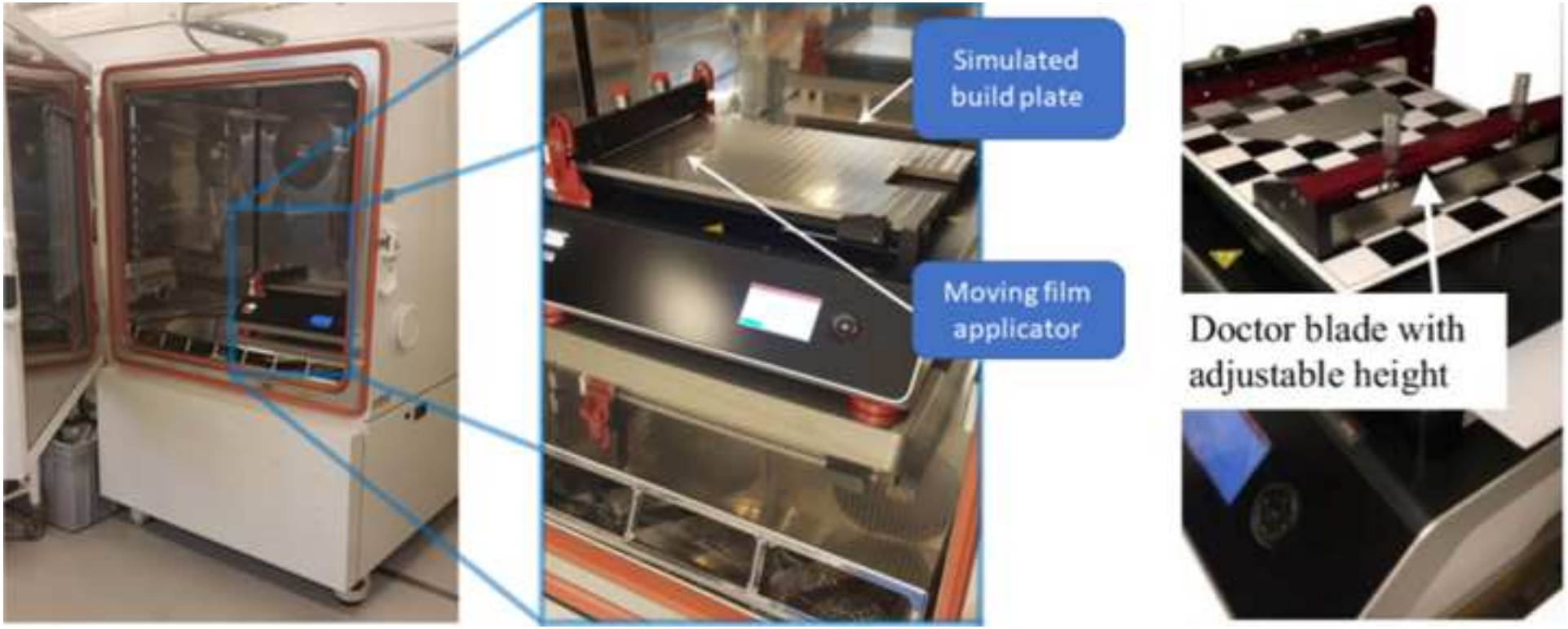

Fig_06

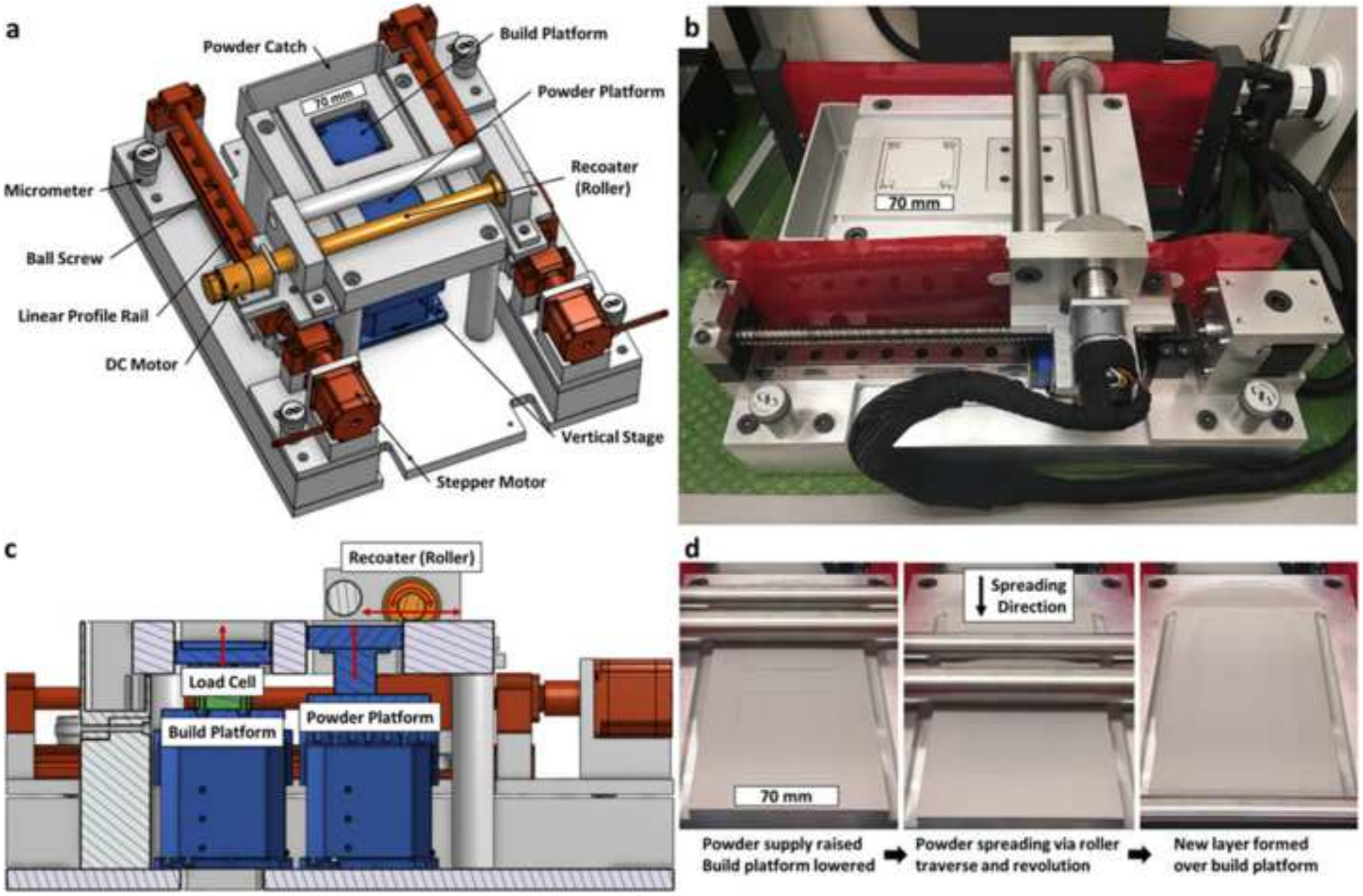

Fig_07

Click here to access/download;Figure;Figure 7.png

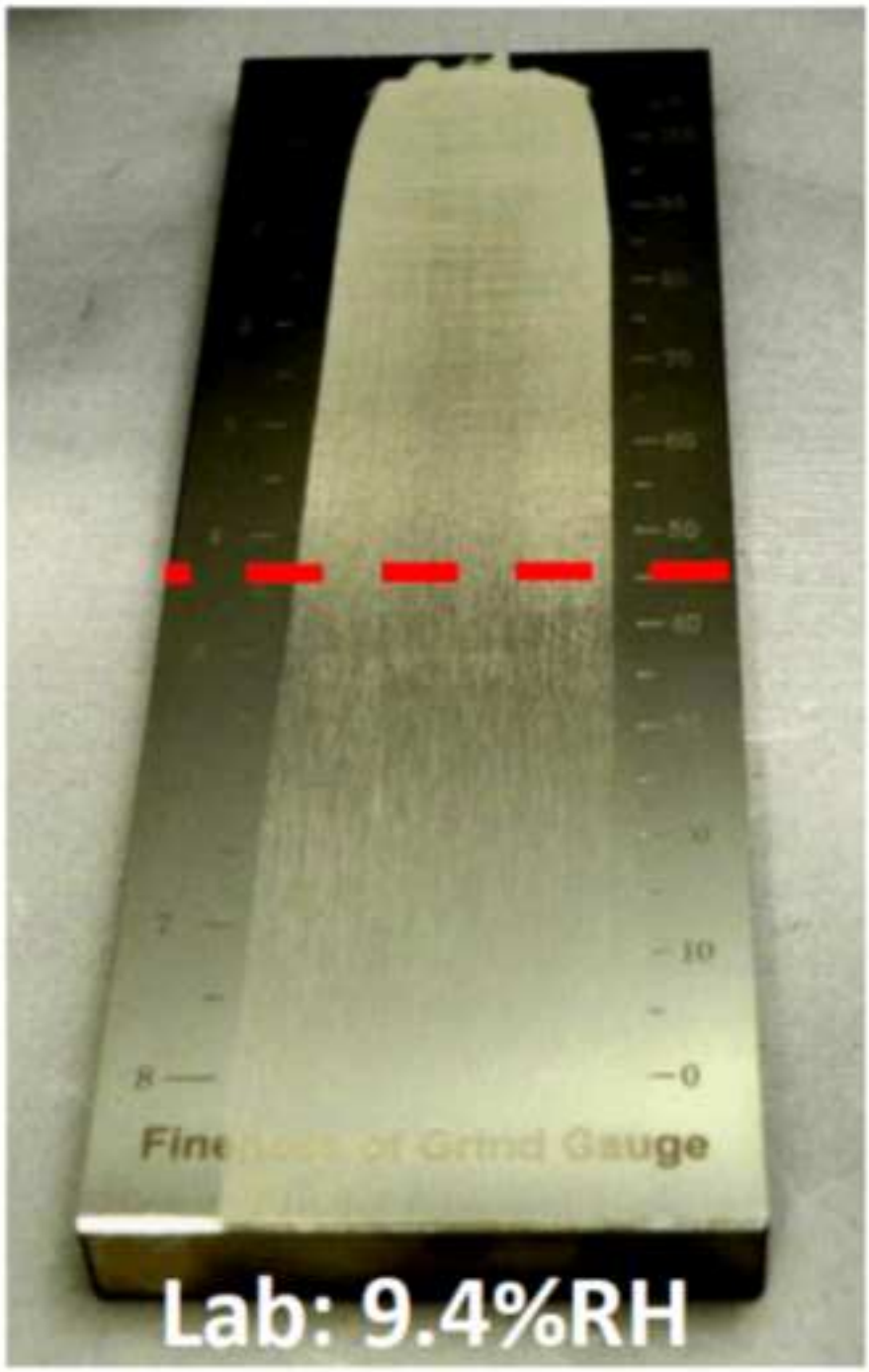

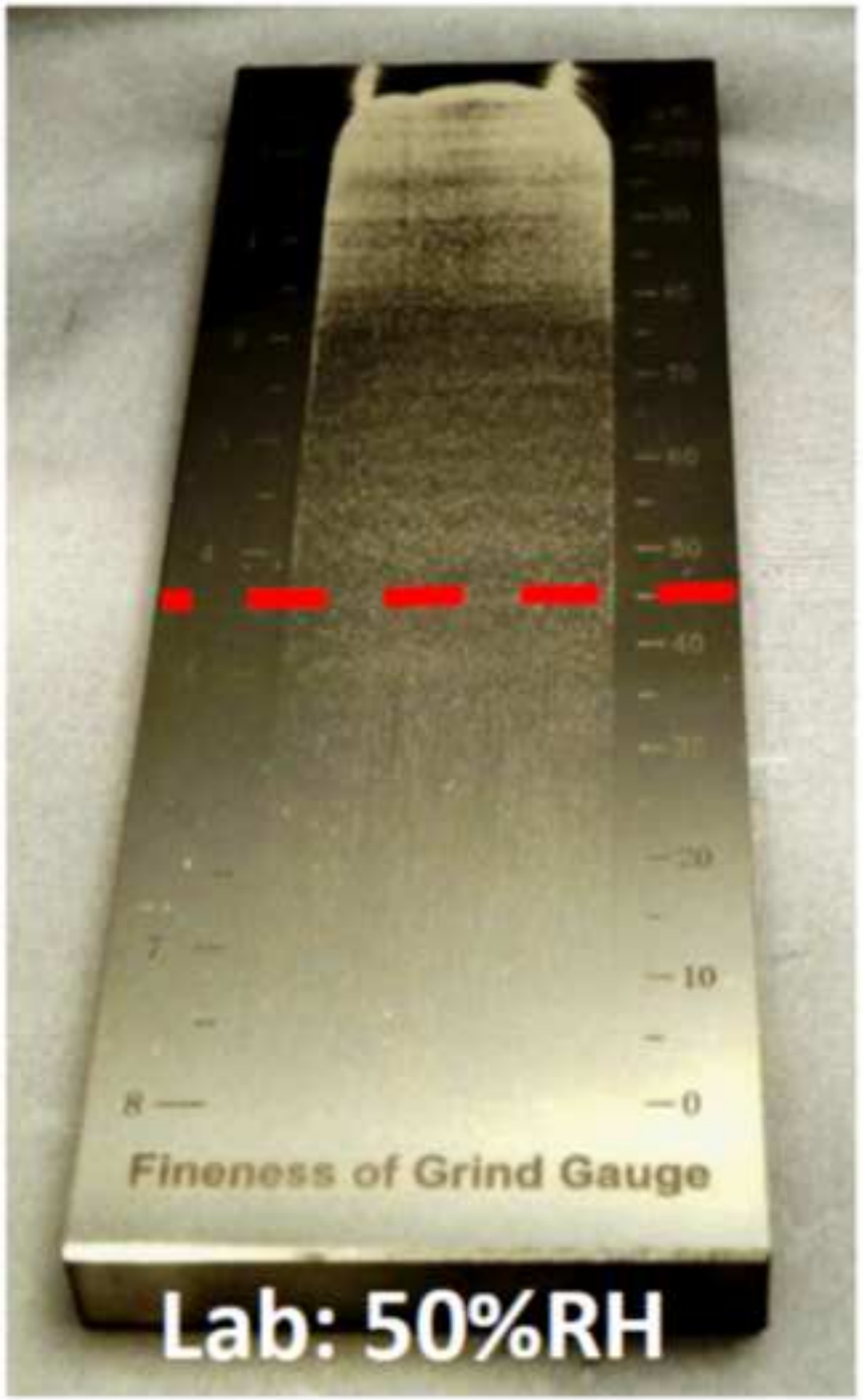

Fig_08

Click here to access/download;Figure;Figure 8.png

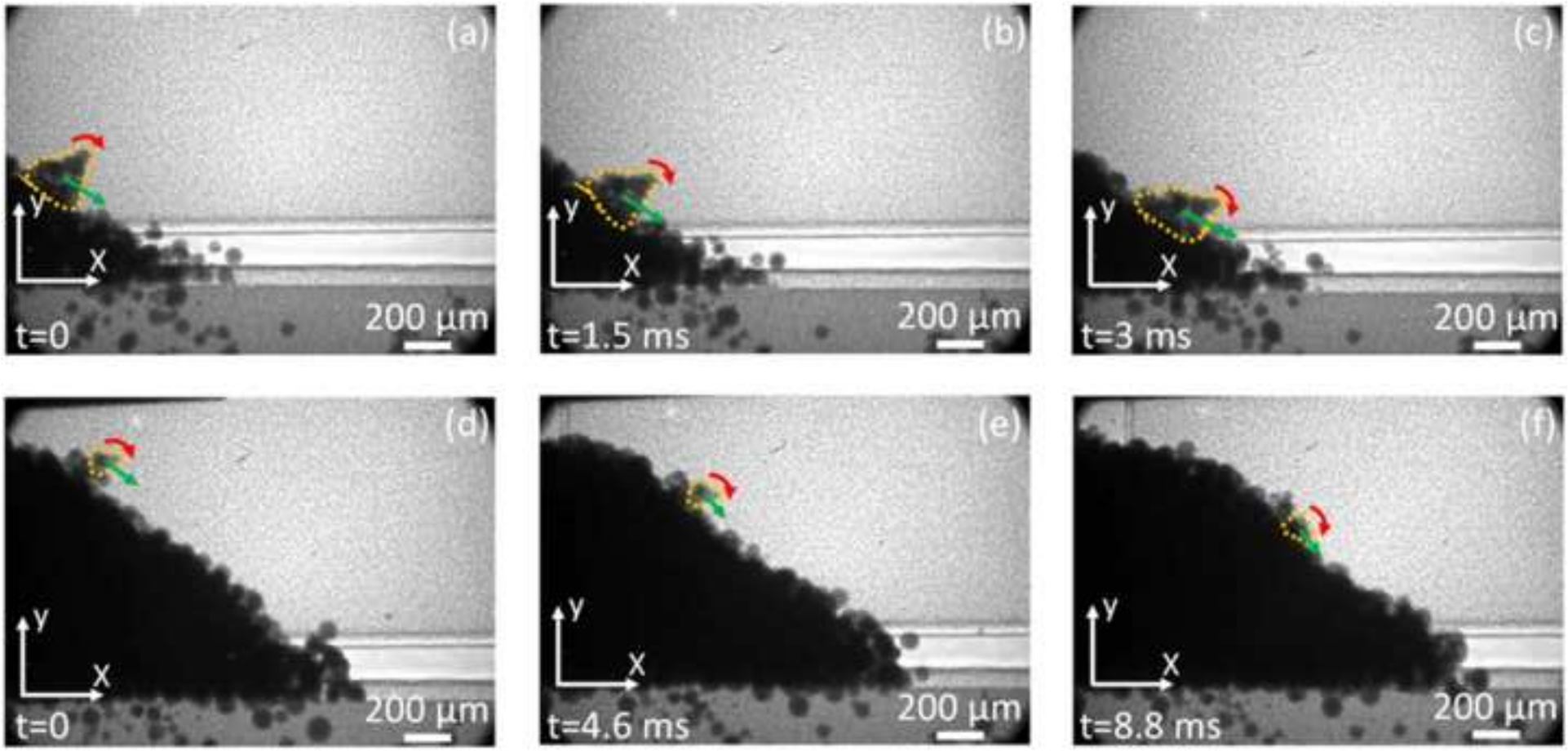

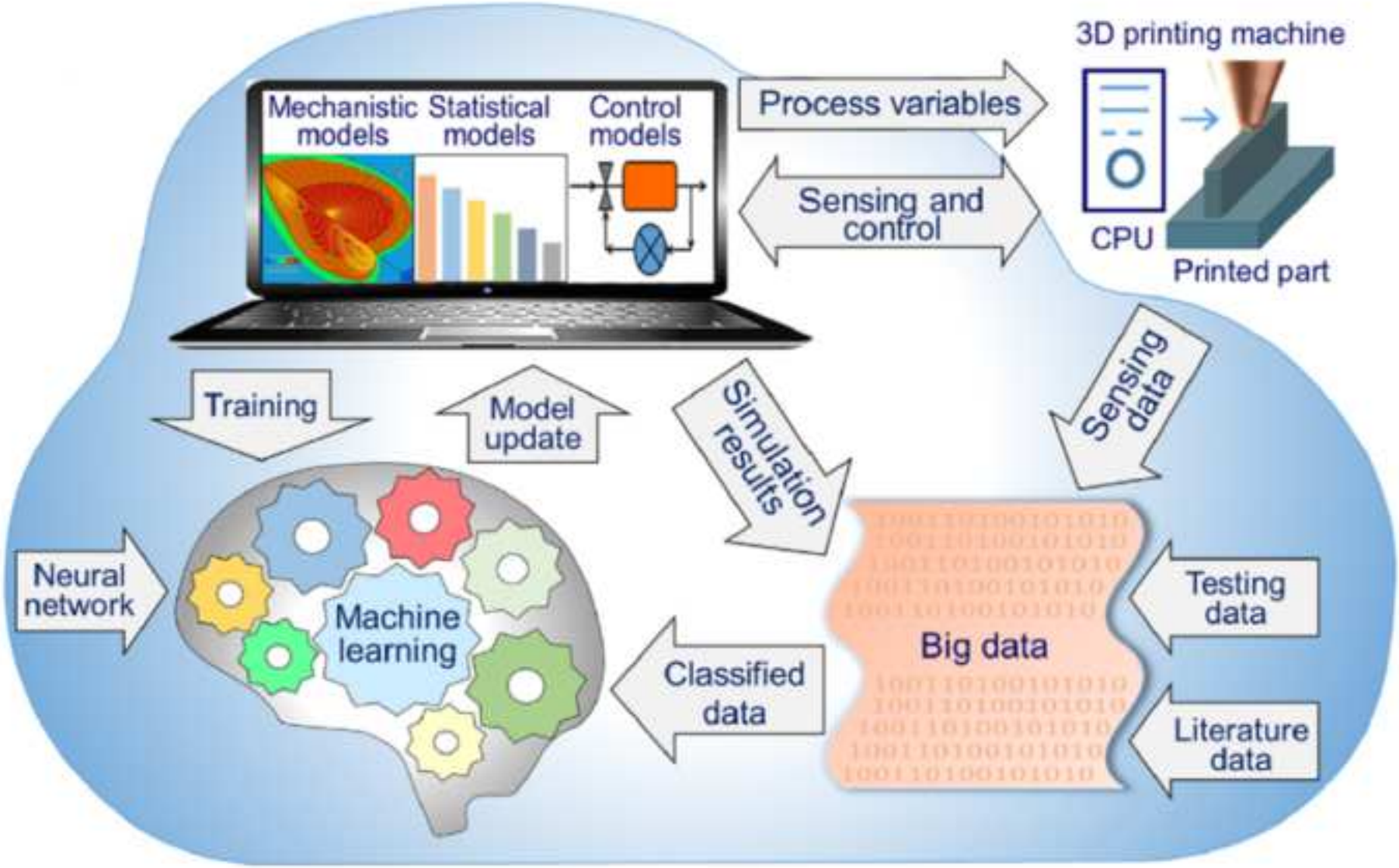

Fig_10

Click here to access/download;Figure;Figure 10.png

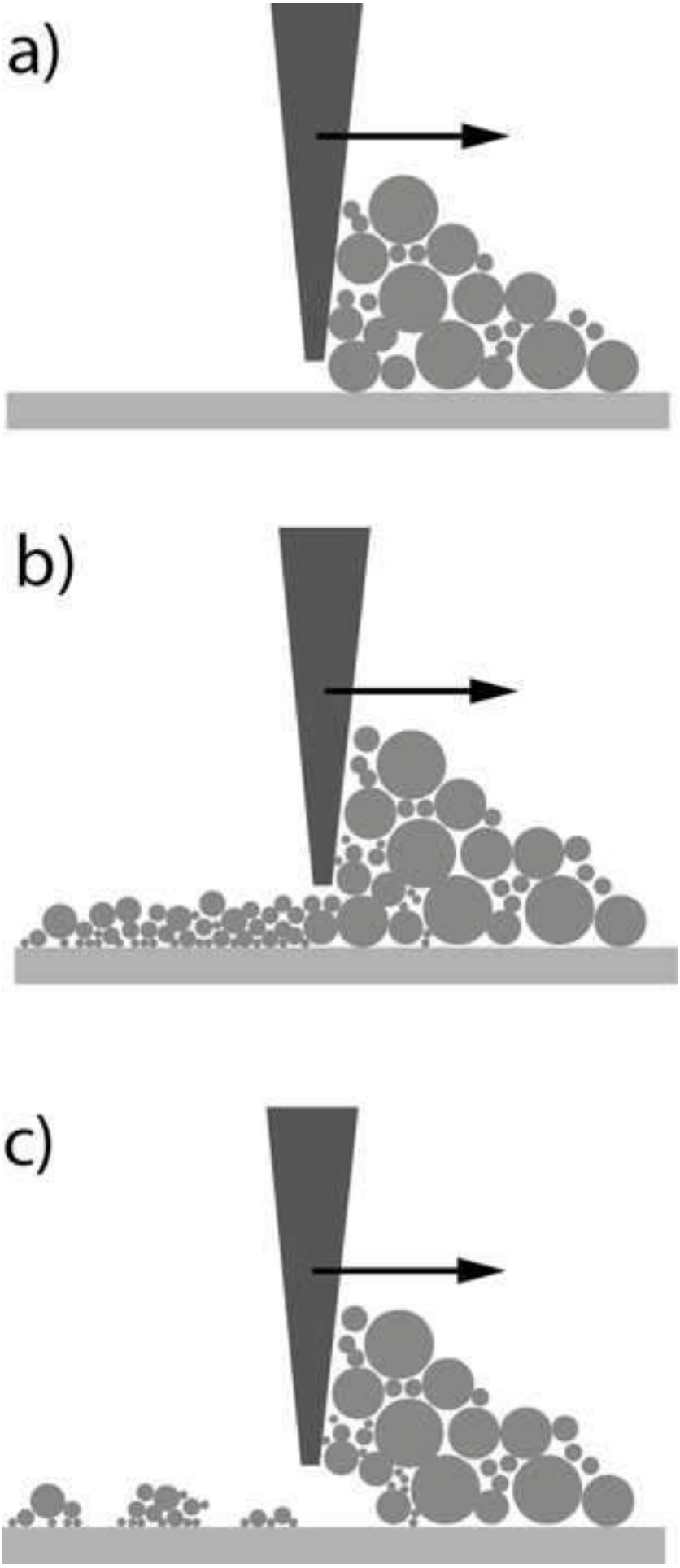

Fig_11

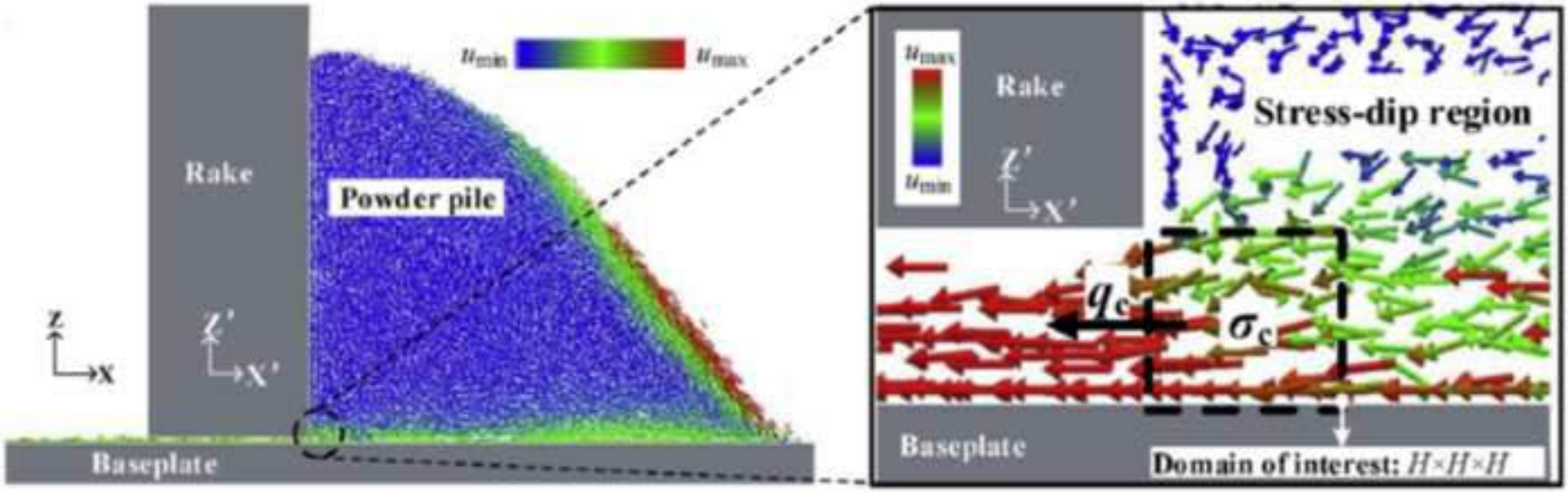

Fig_12

Click here to access/download;Figure;Figure 12.png

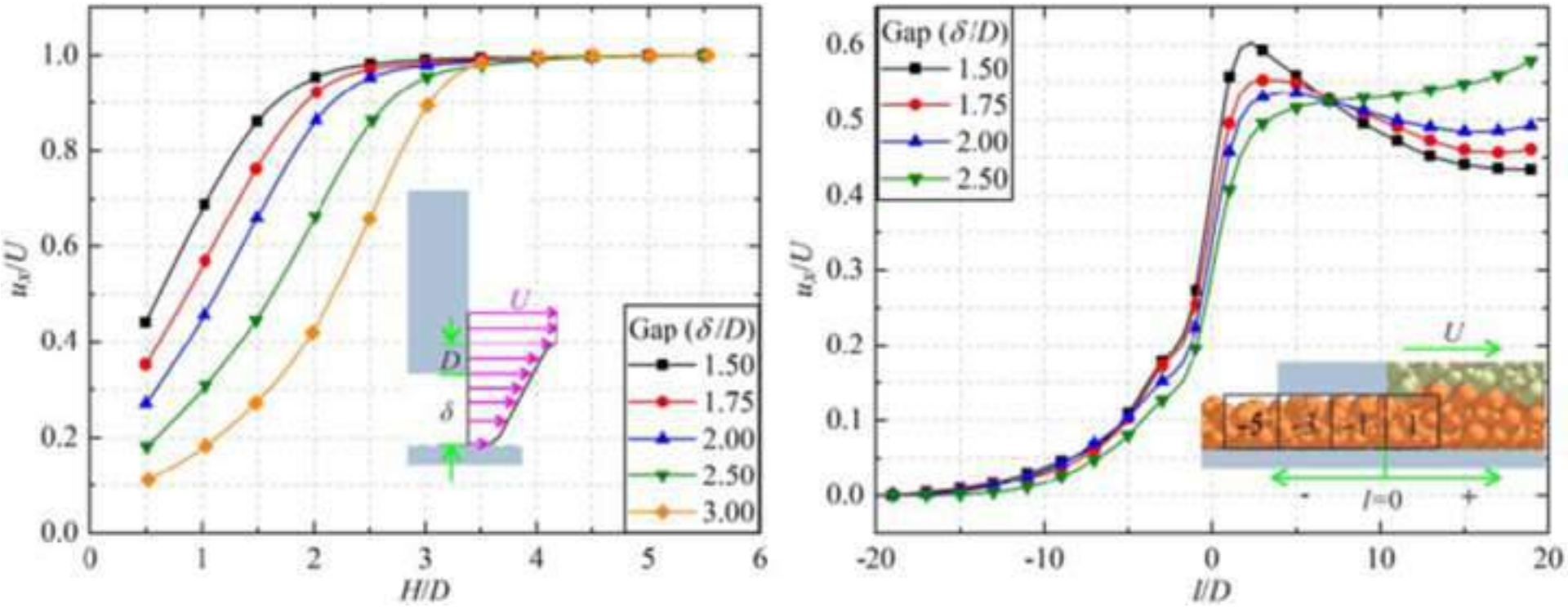

Fig_13

Click here to access/download;Figure;Figure 13.png

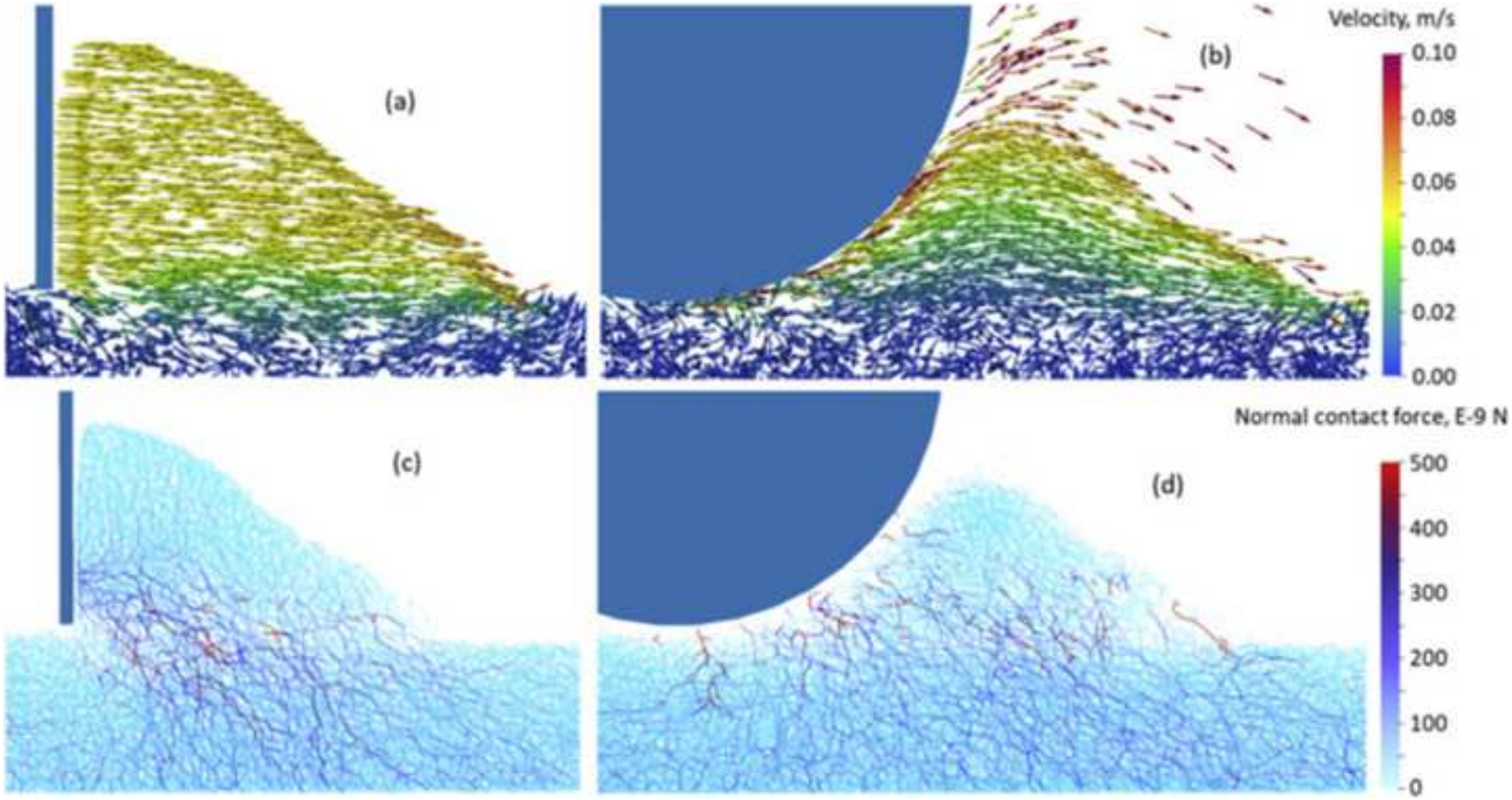

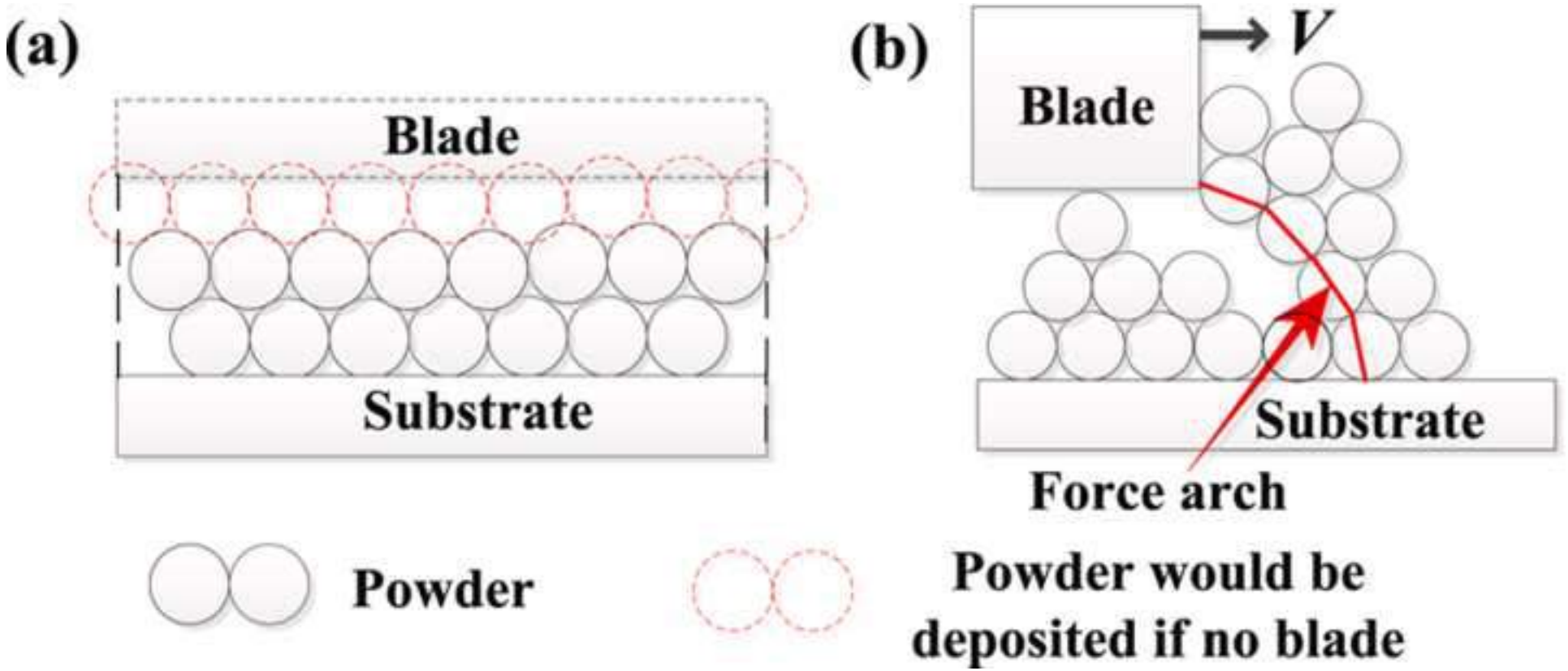

Fig_15

Click here to access/download;Figure;Figure 15.png

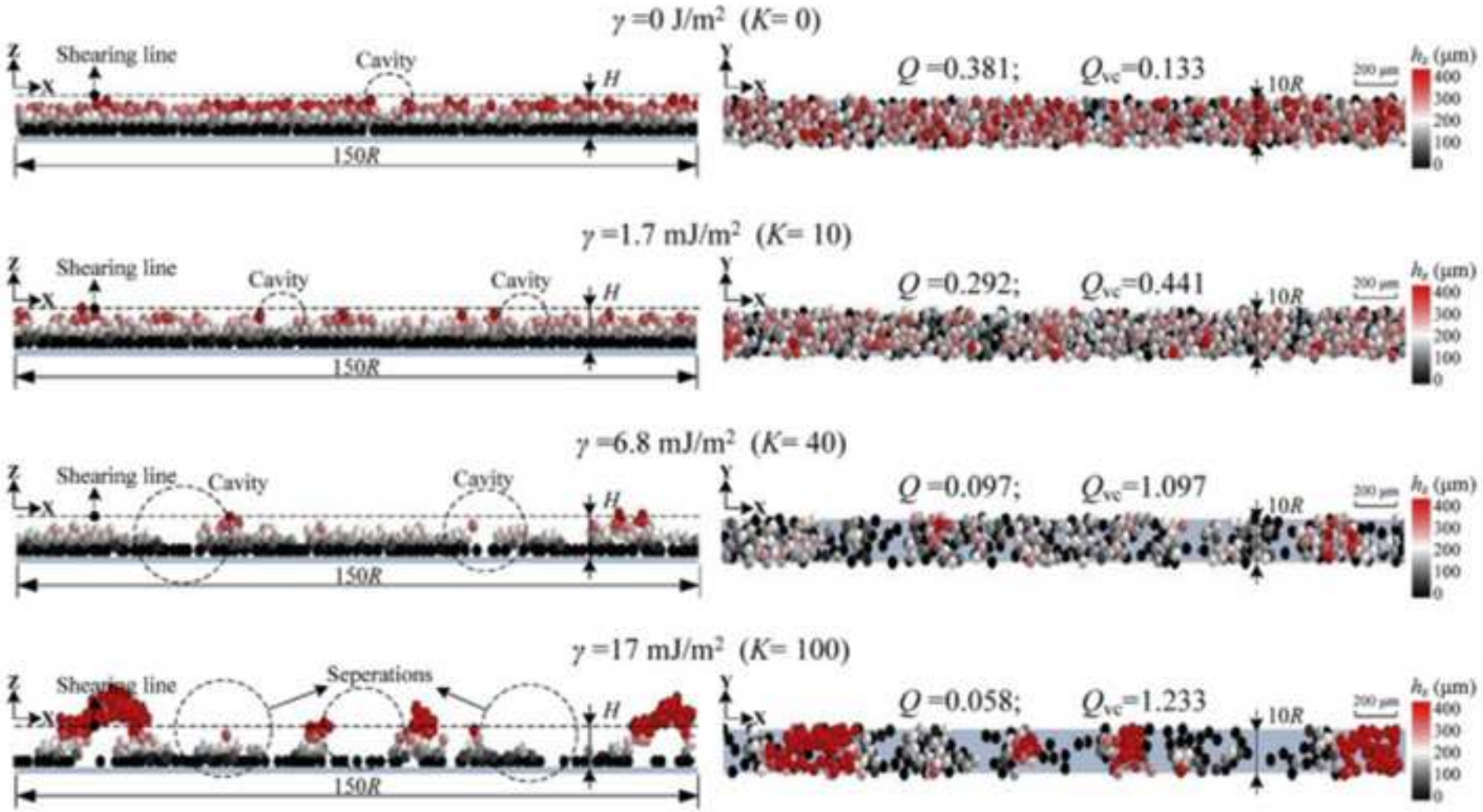

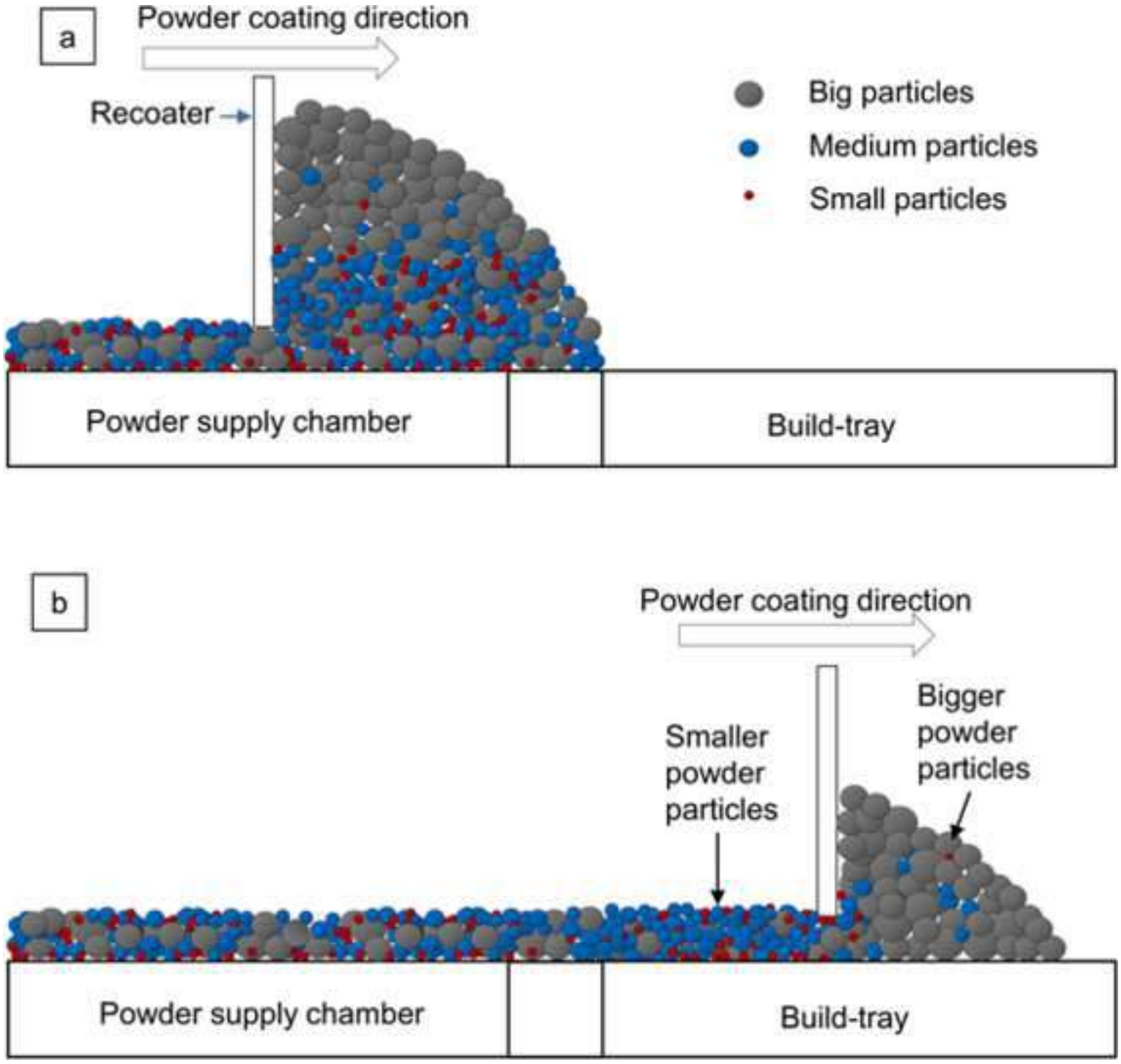

Fig_17

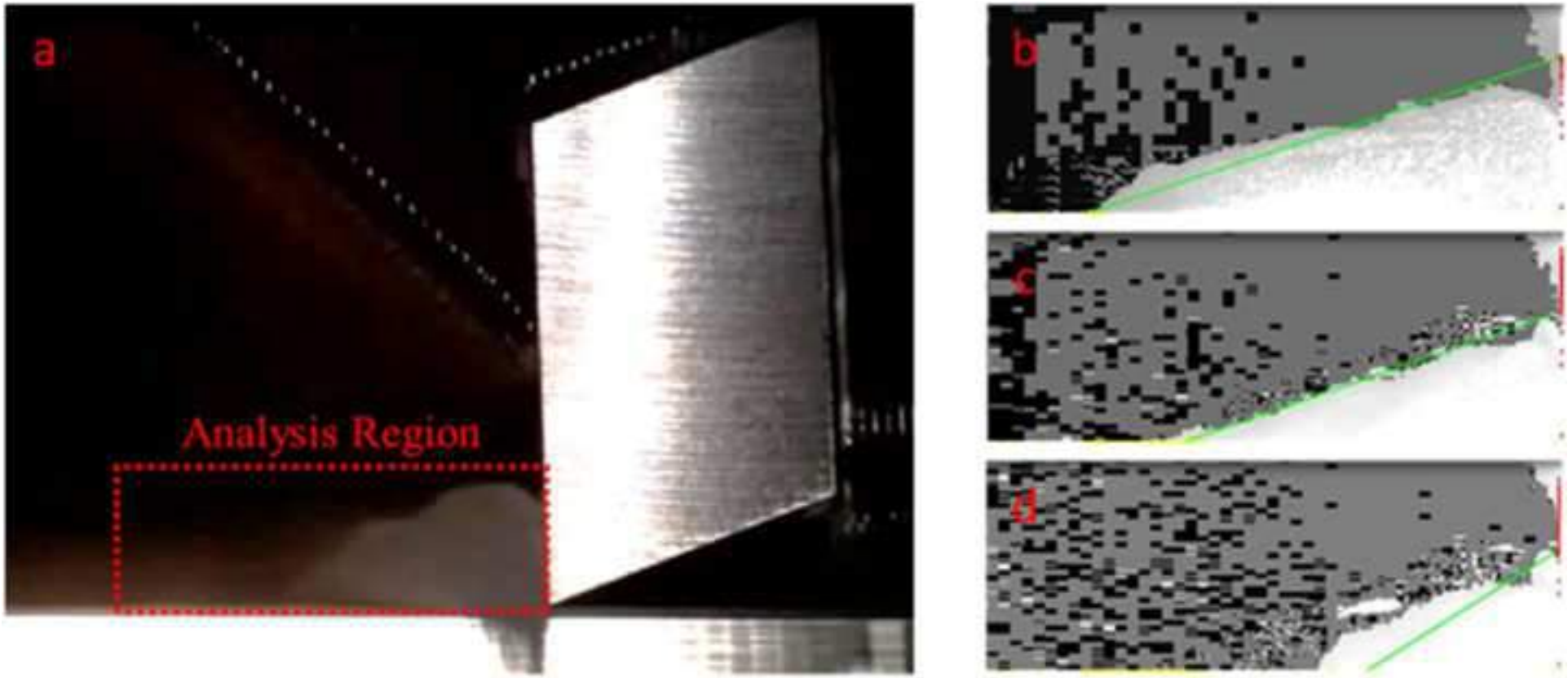

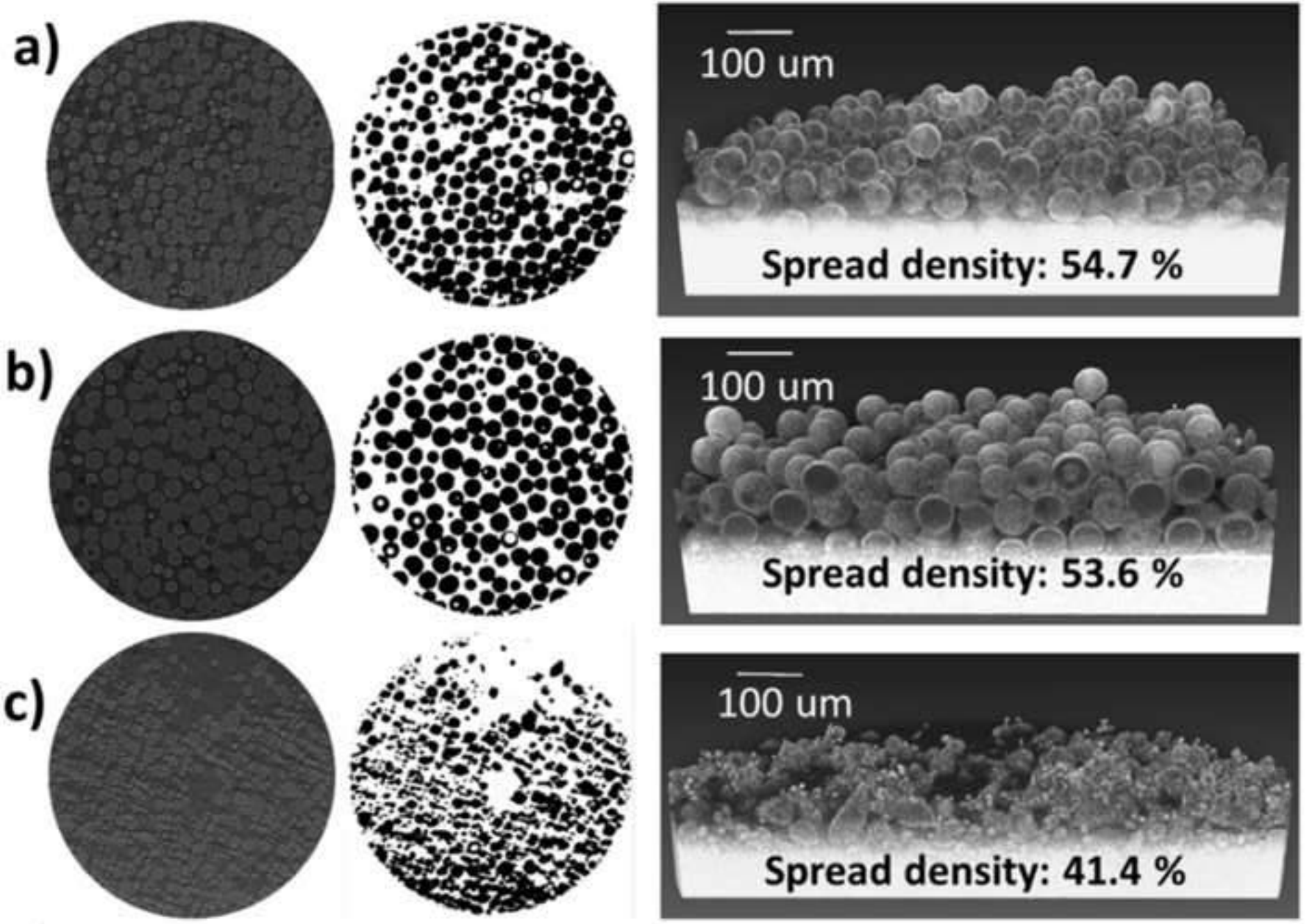

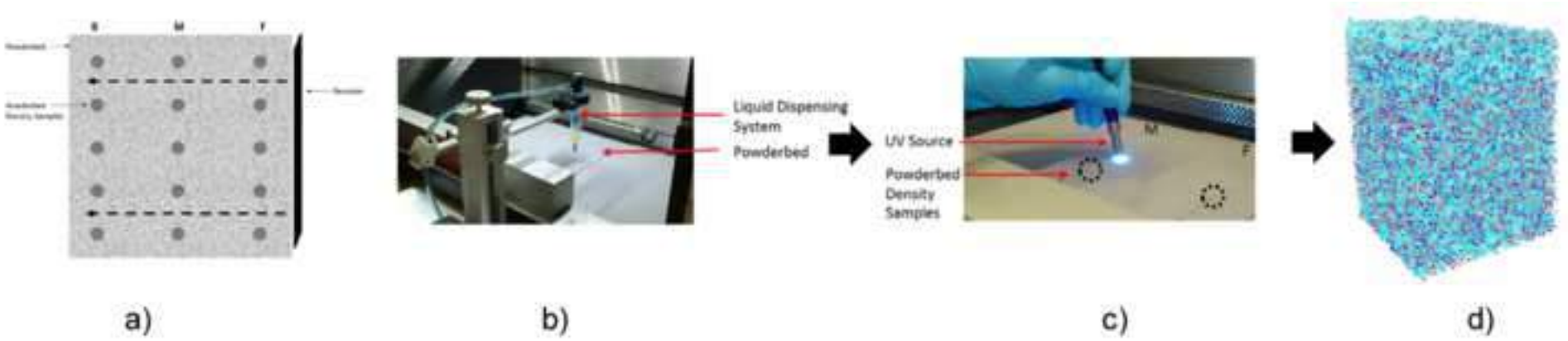

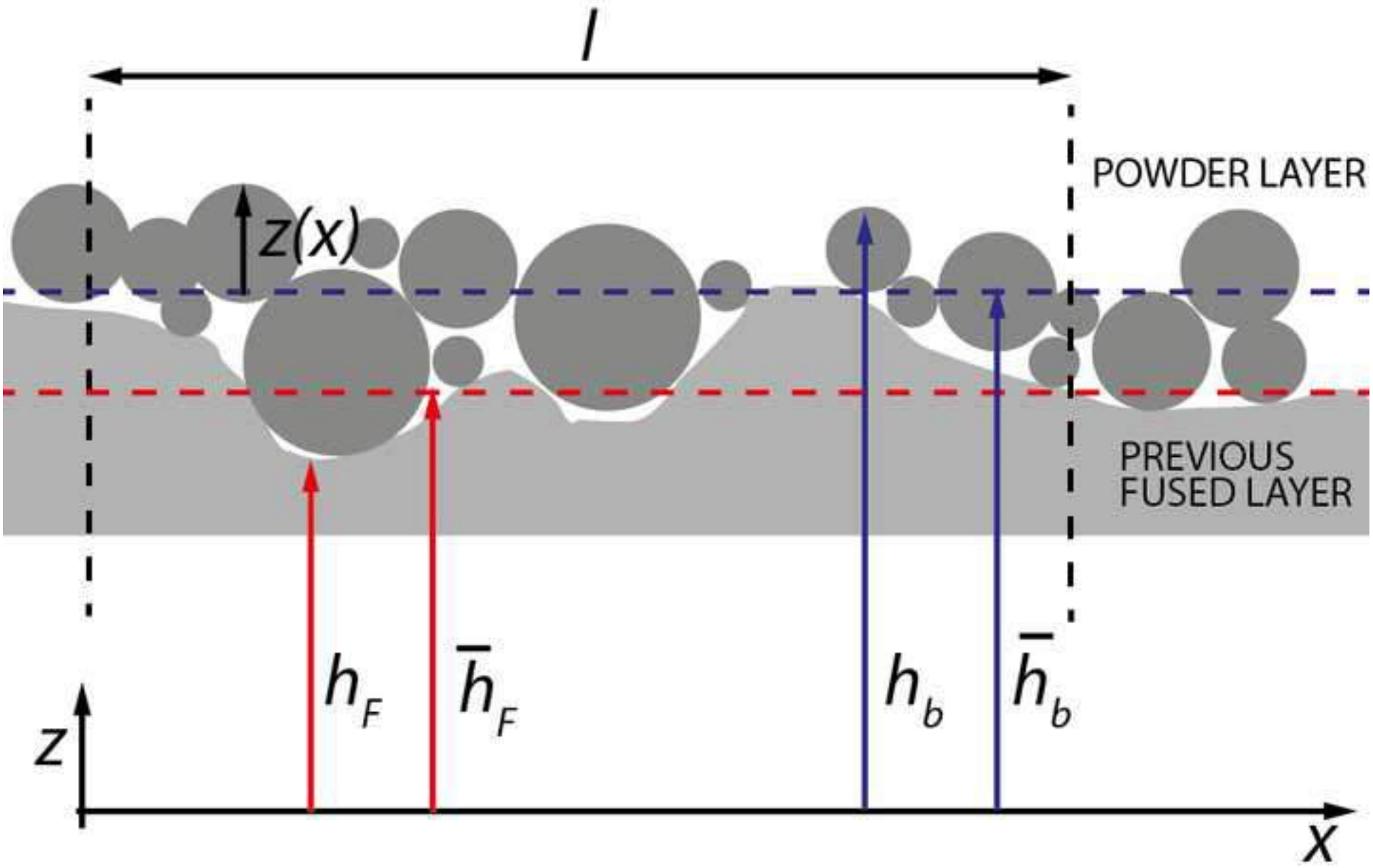

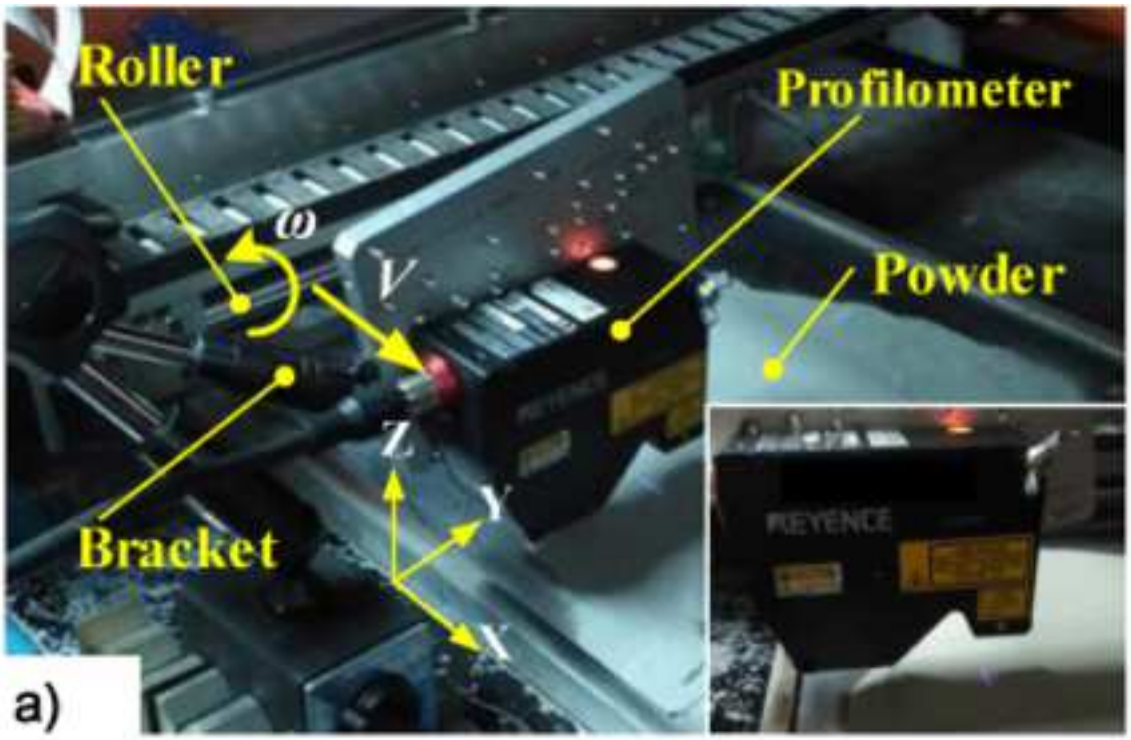

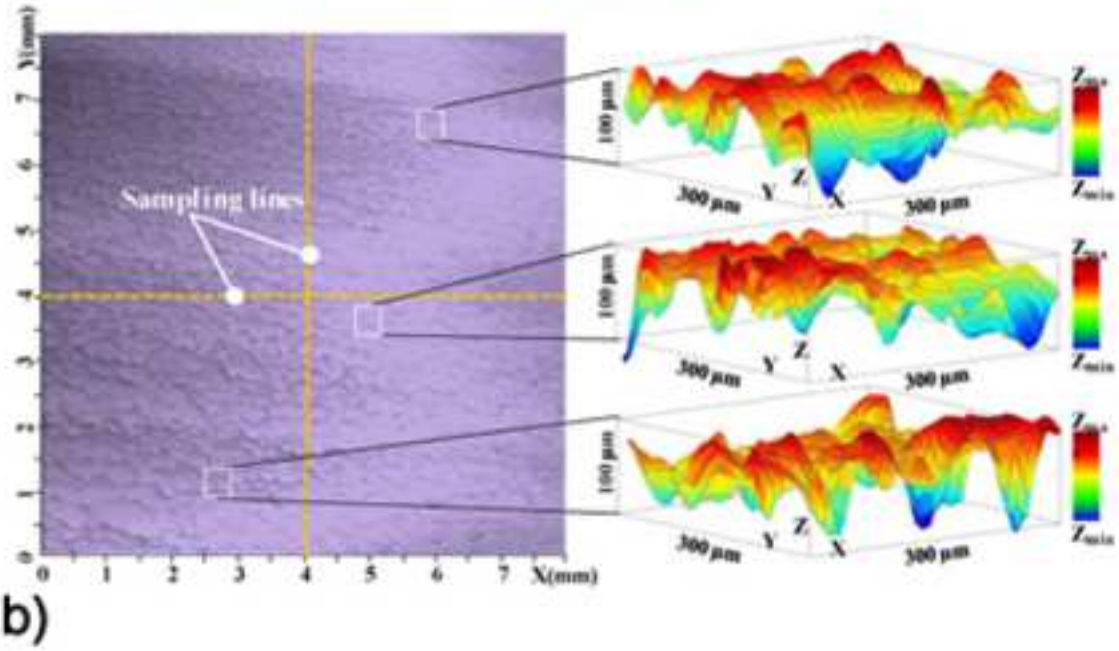

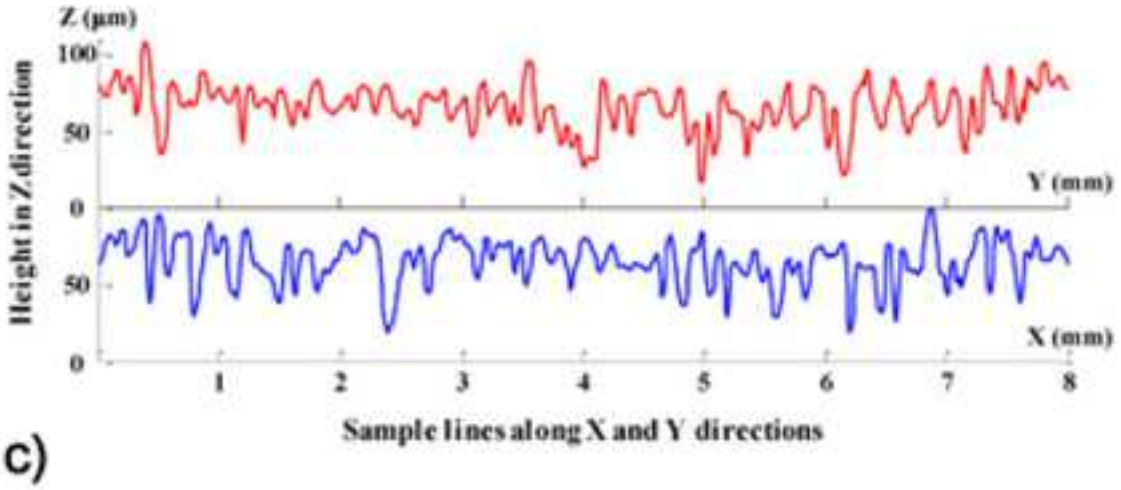

Fig_23

Click here to access/download;Figure;Figure 23.png

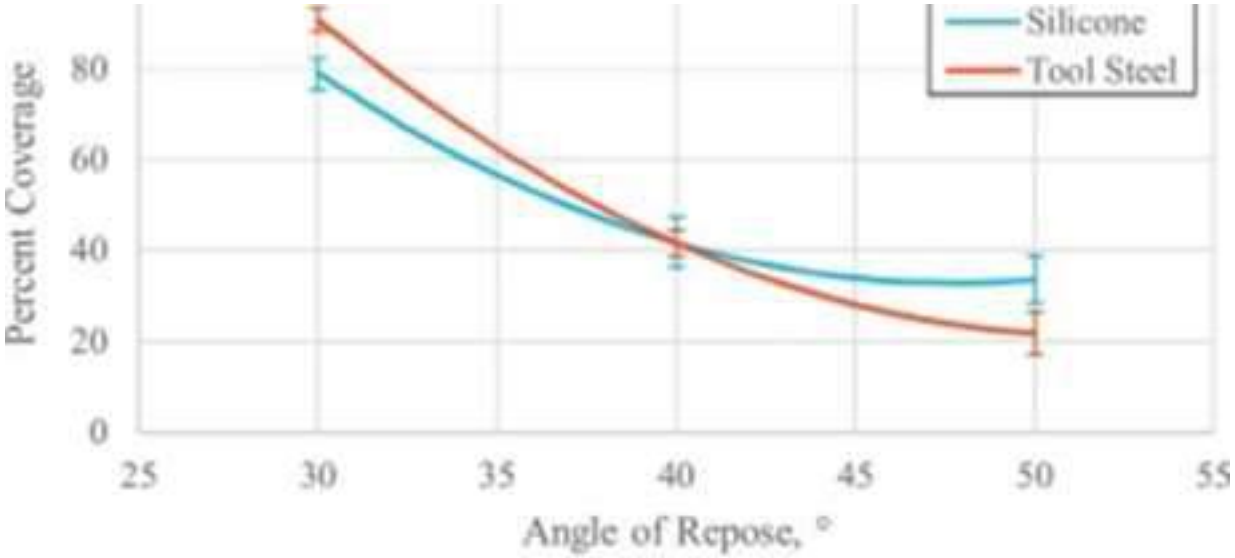

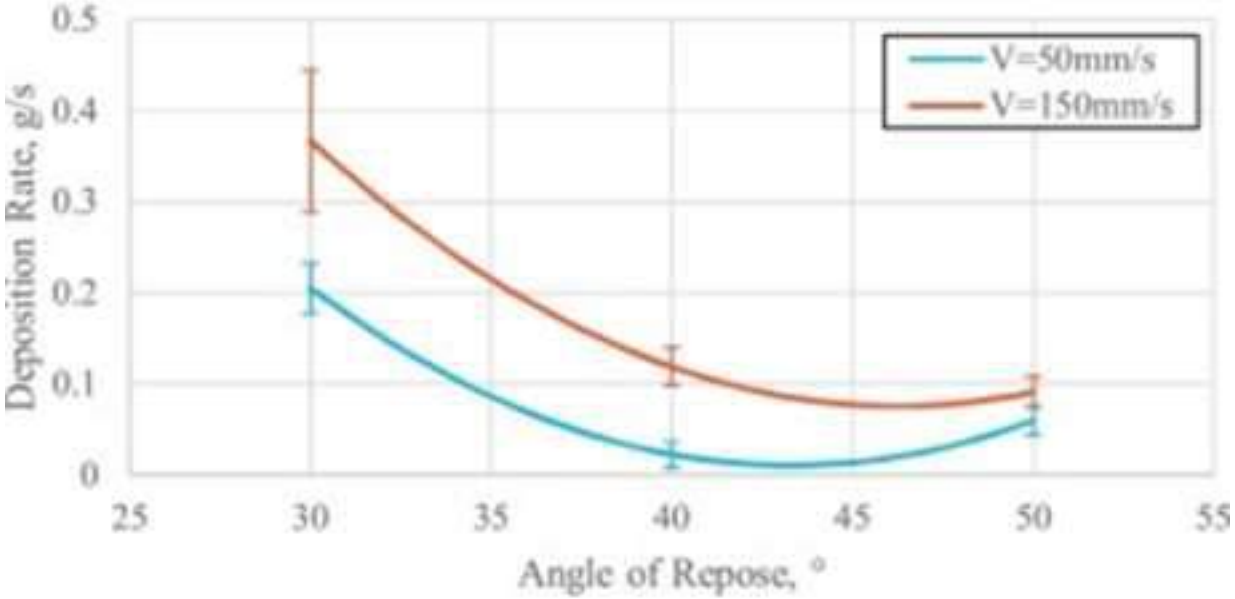

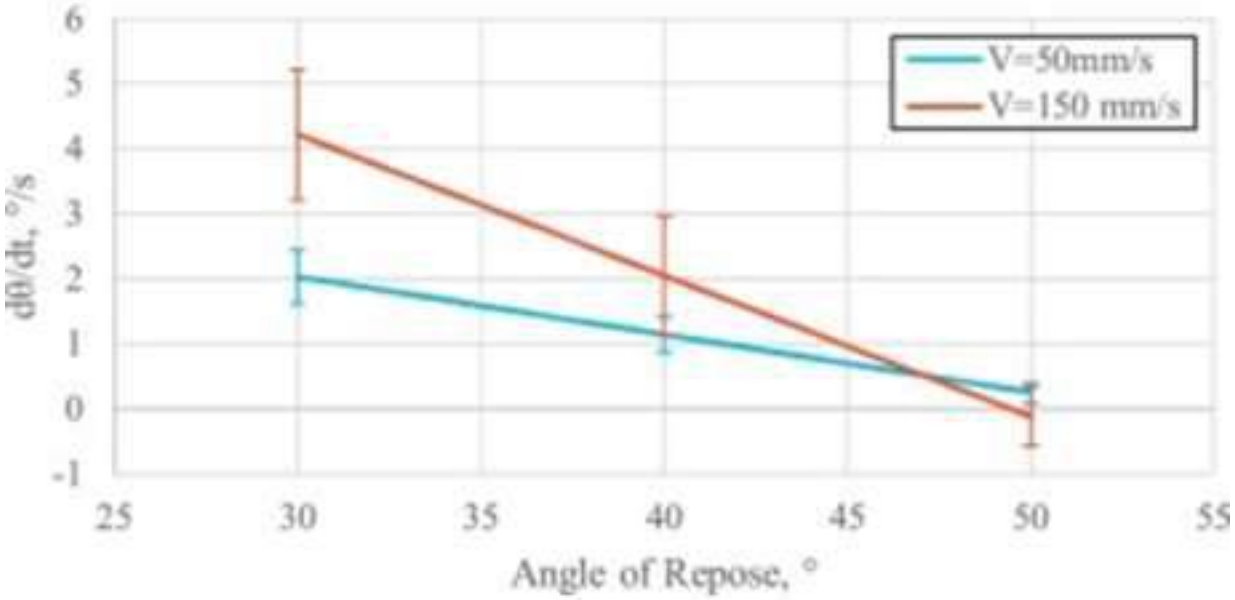

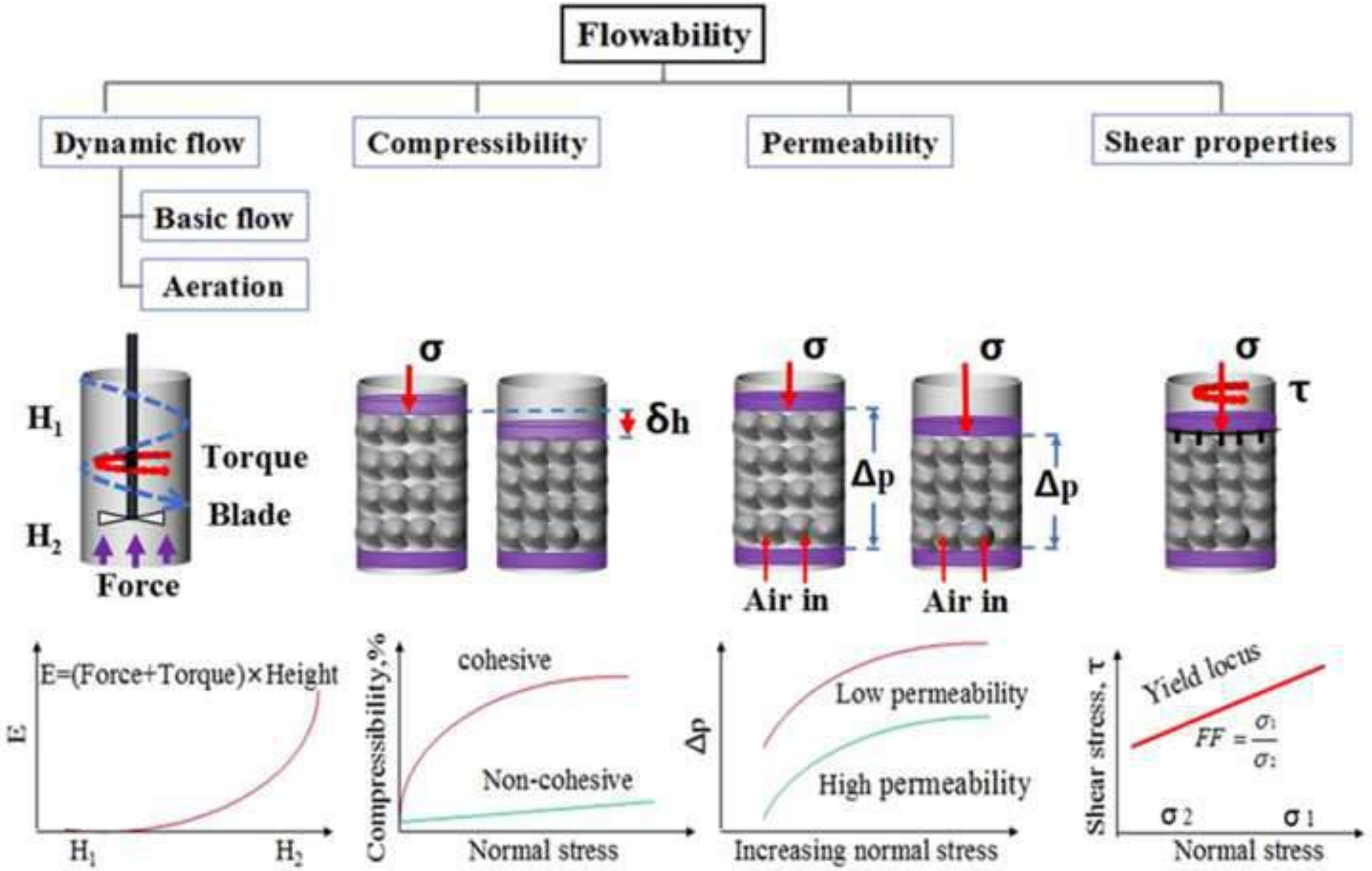

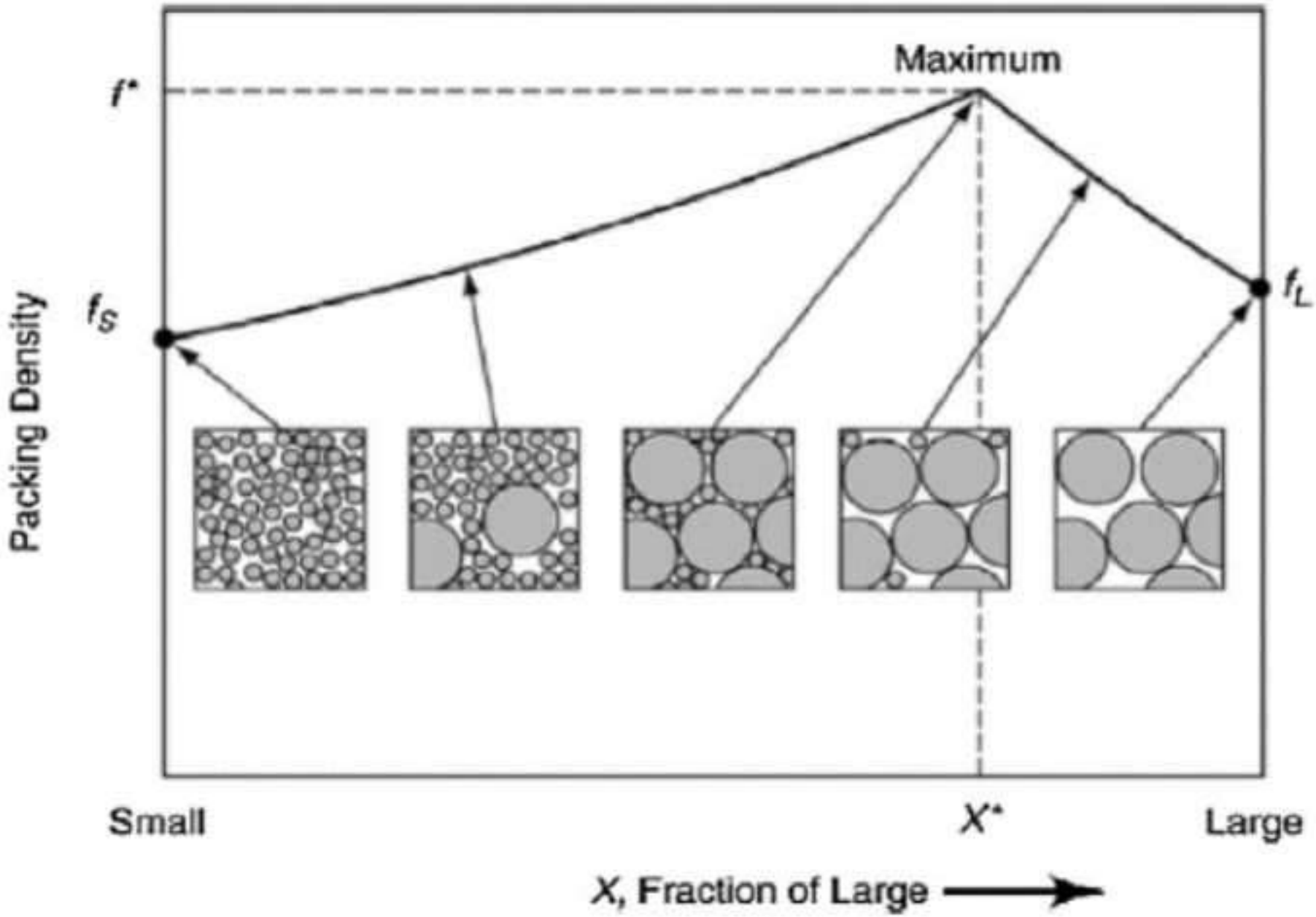

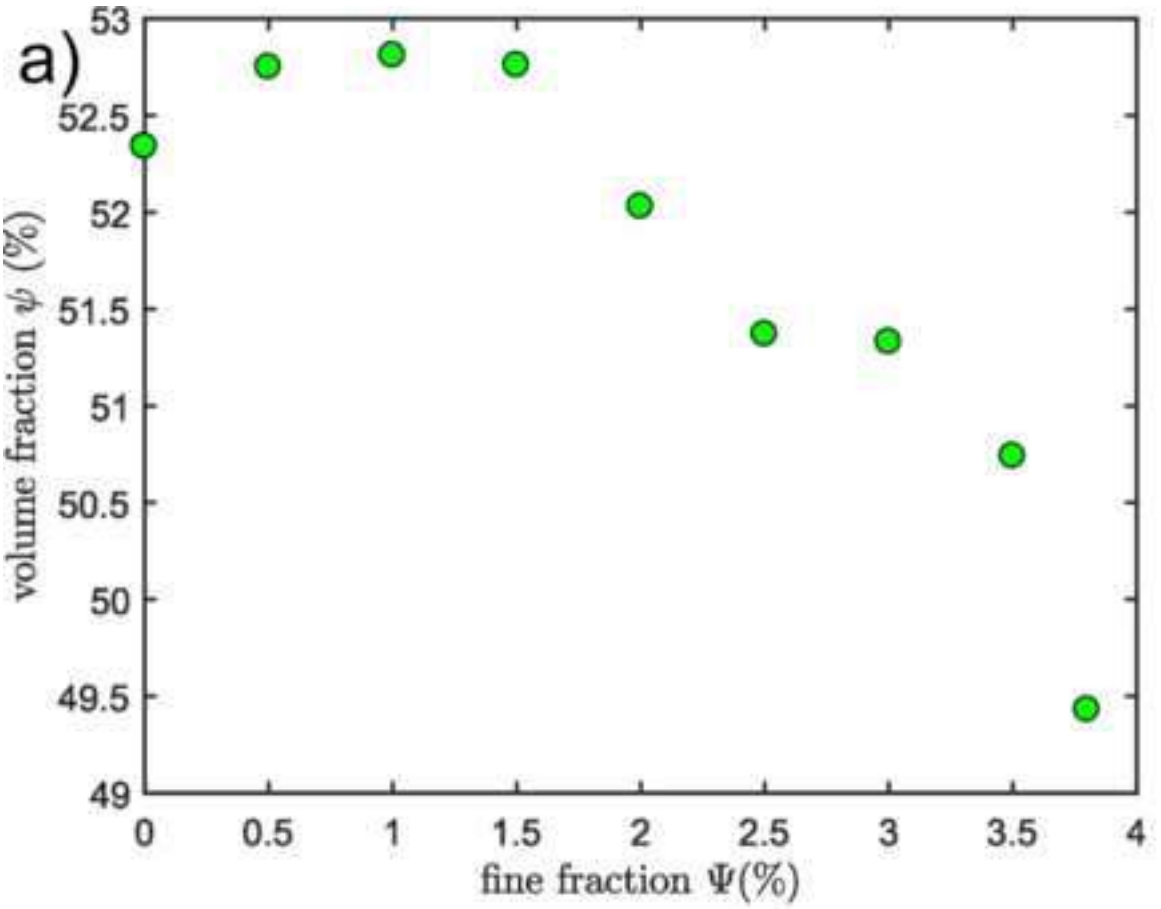

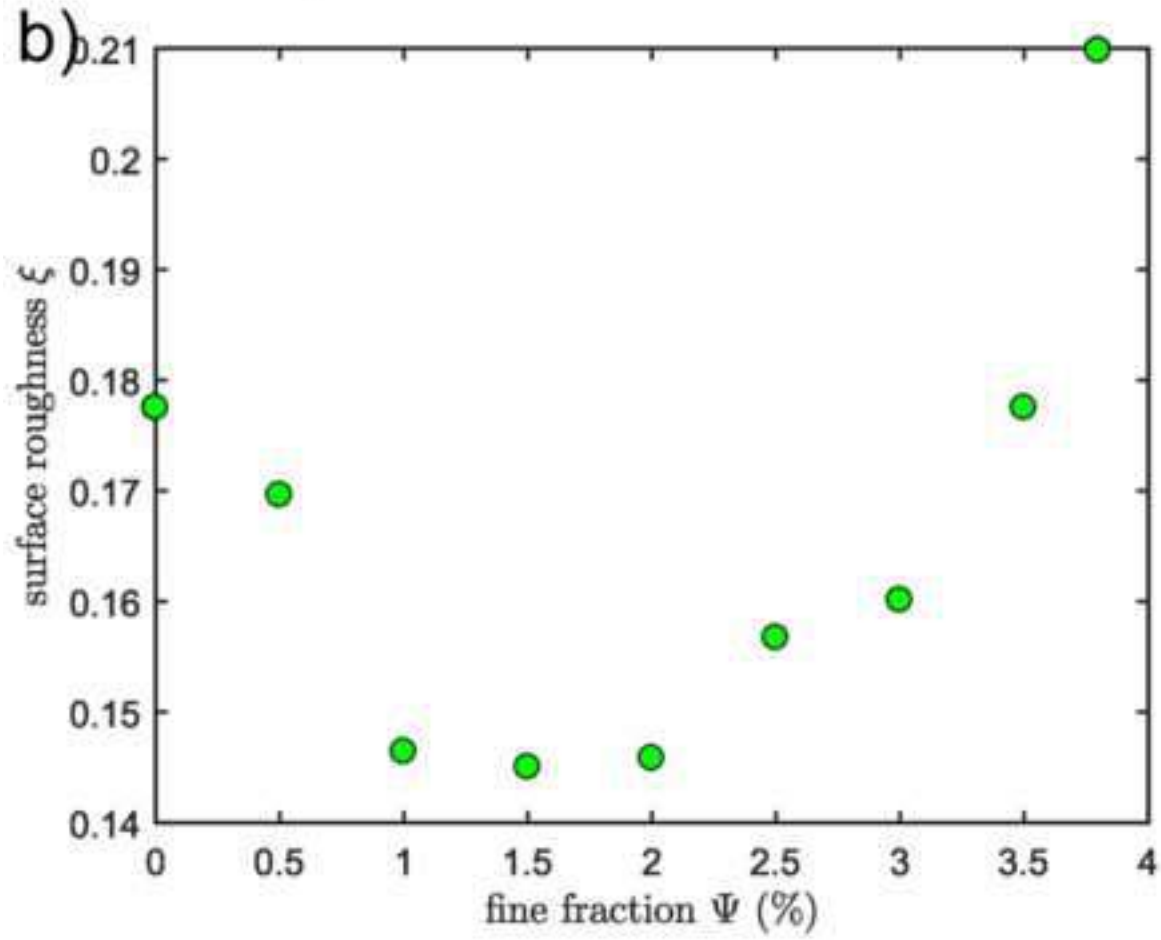

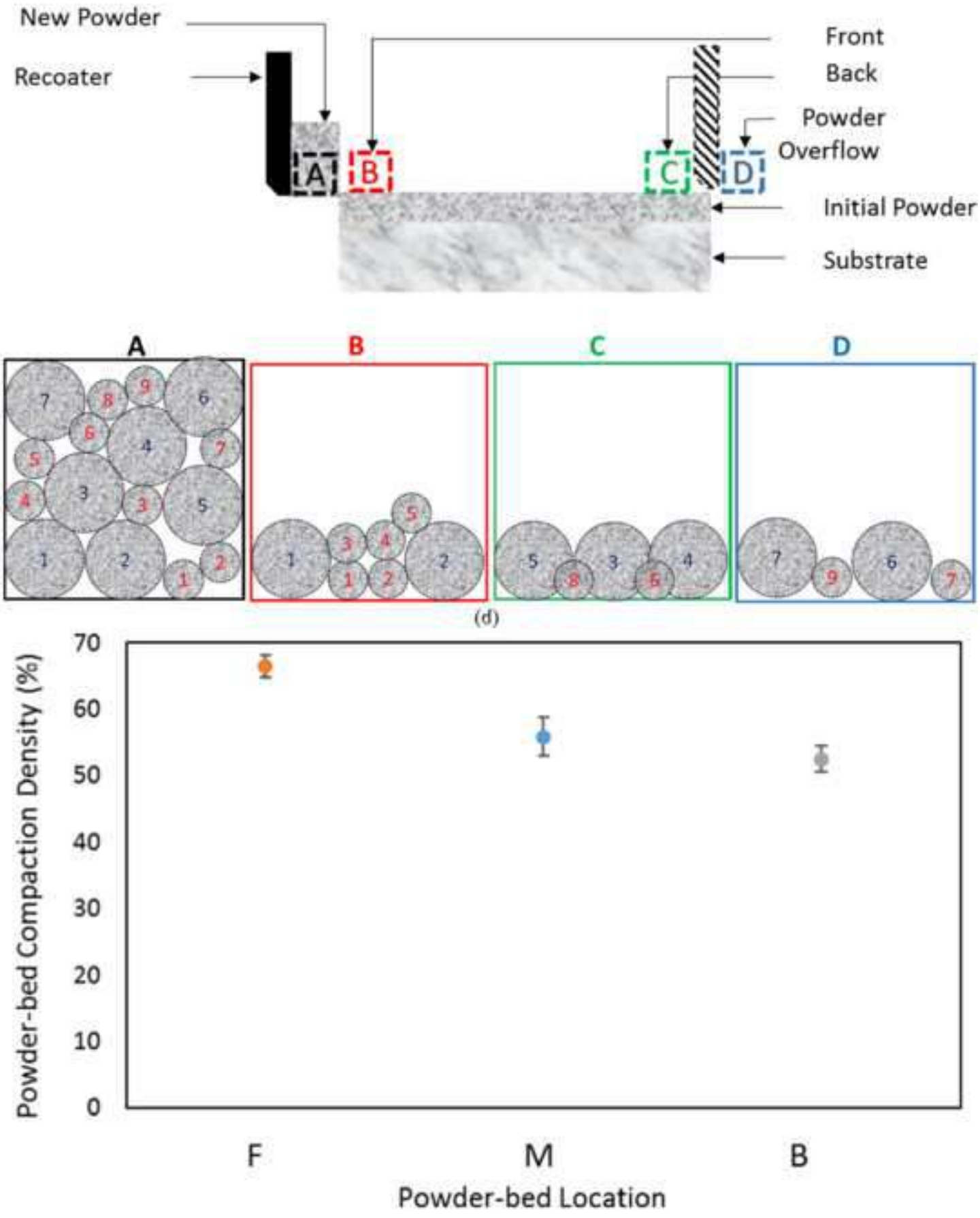

Fig_28

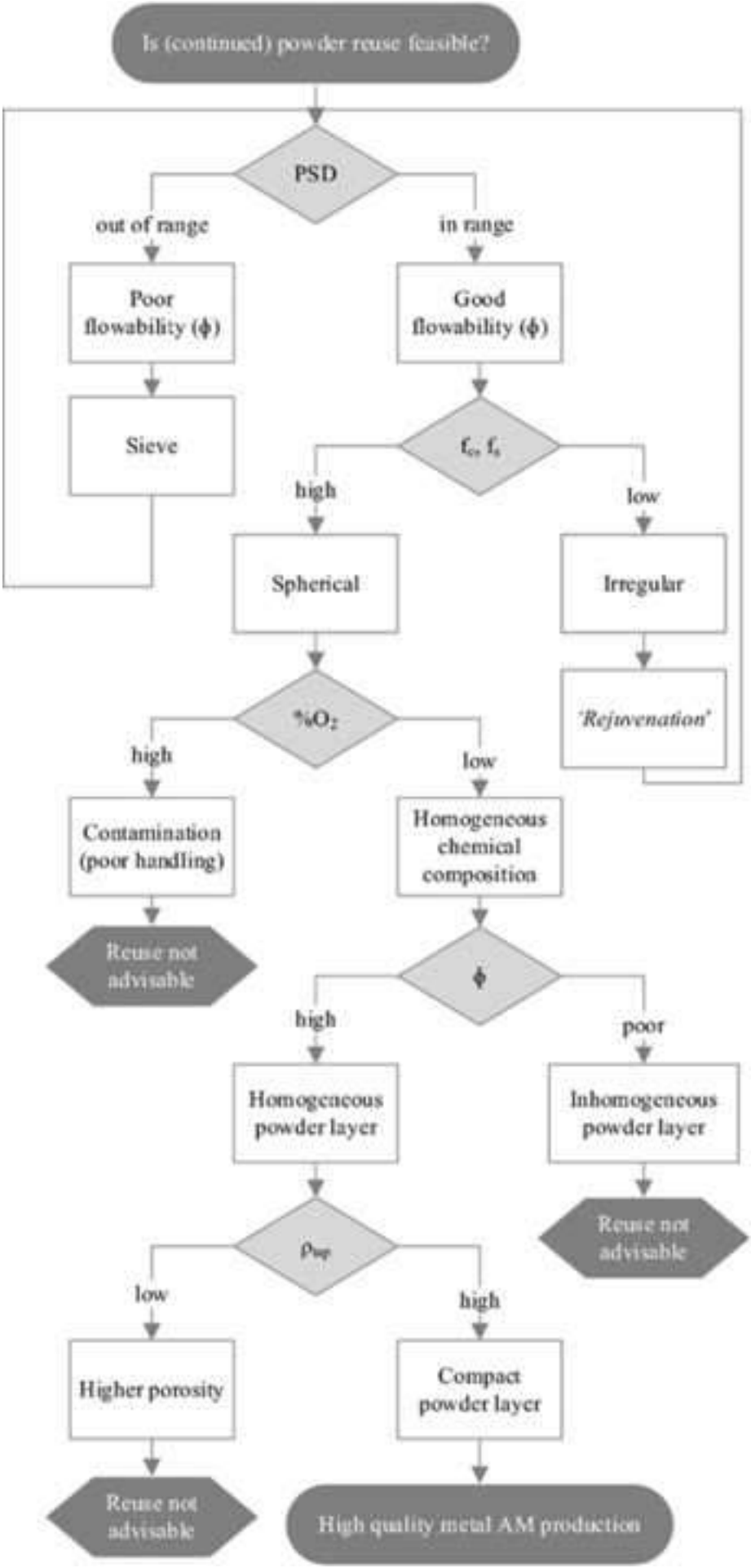

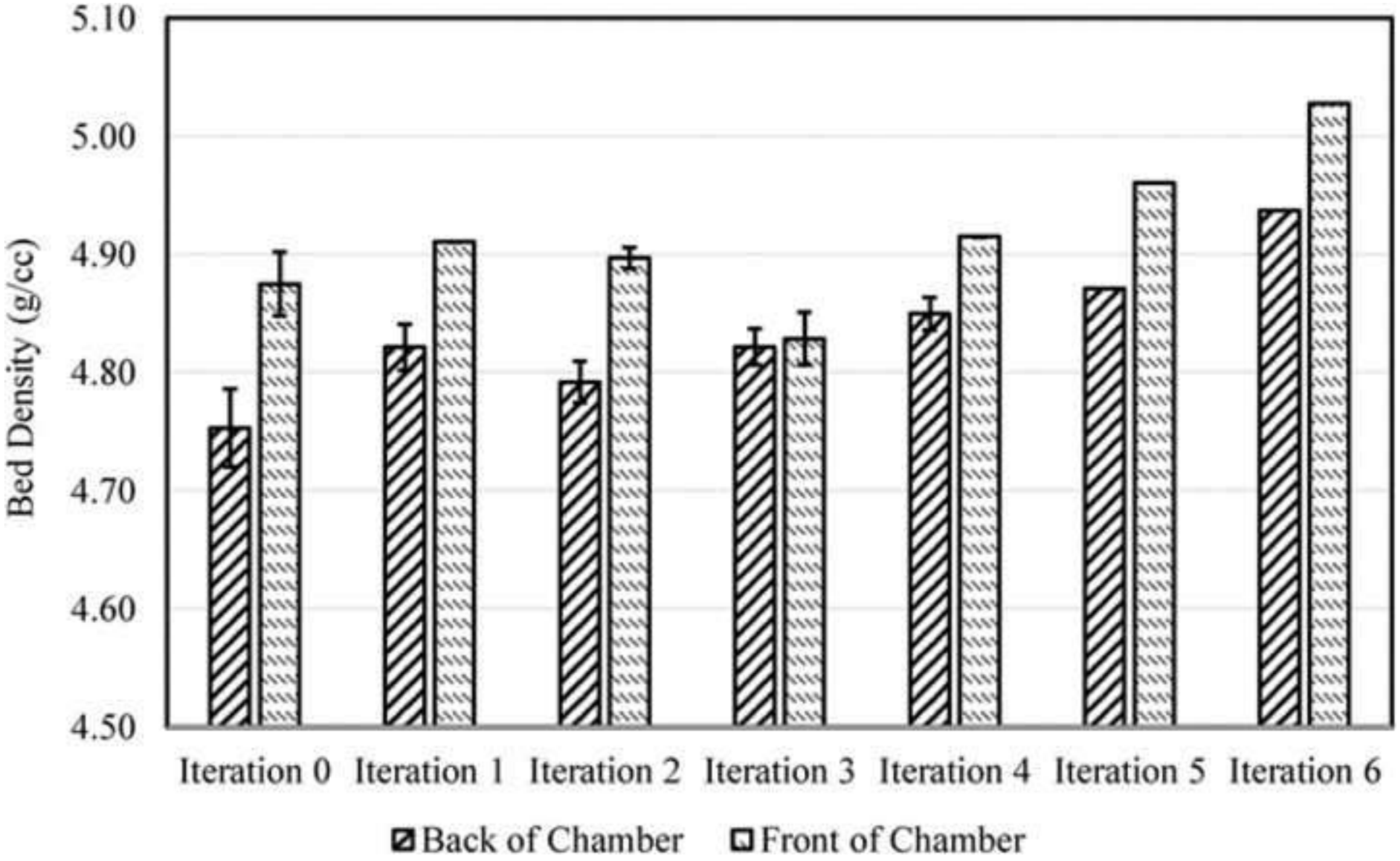

Fig_30

Click here to access/download;Figure;Figure 30.png

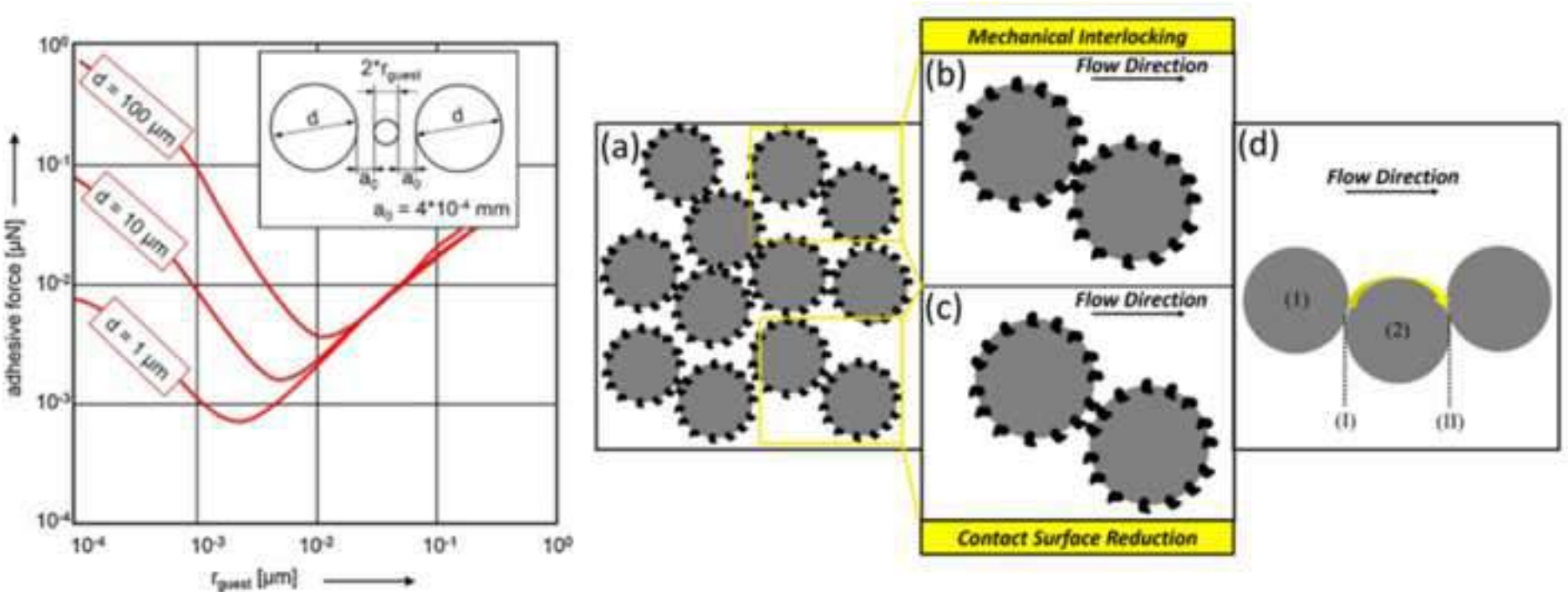

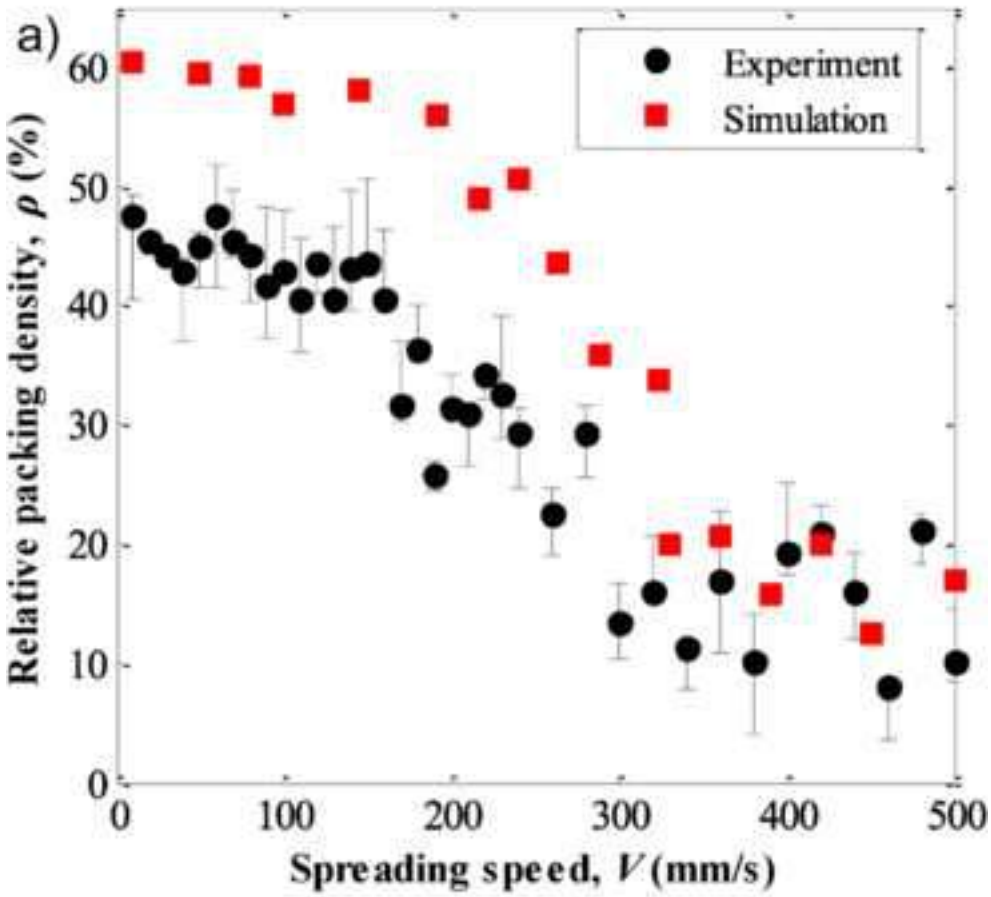

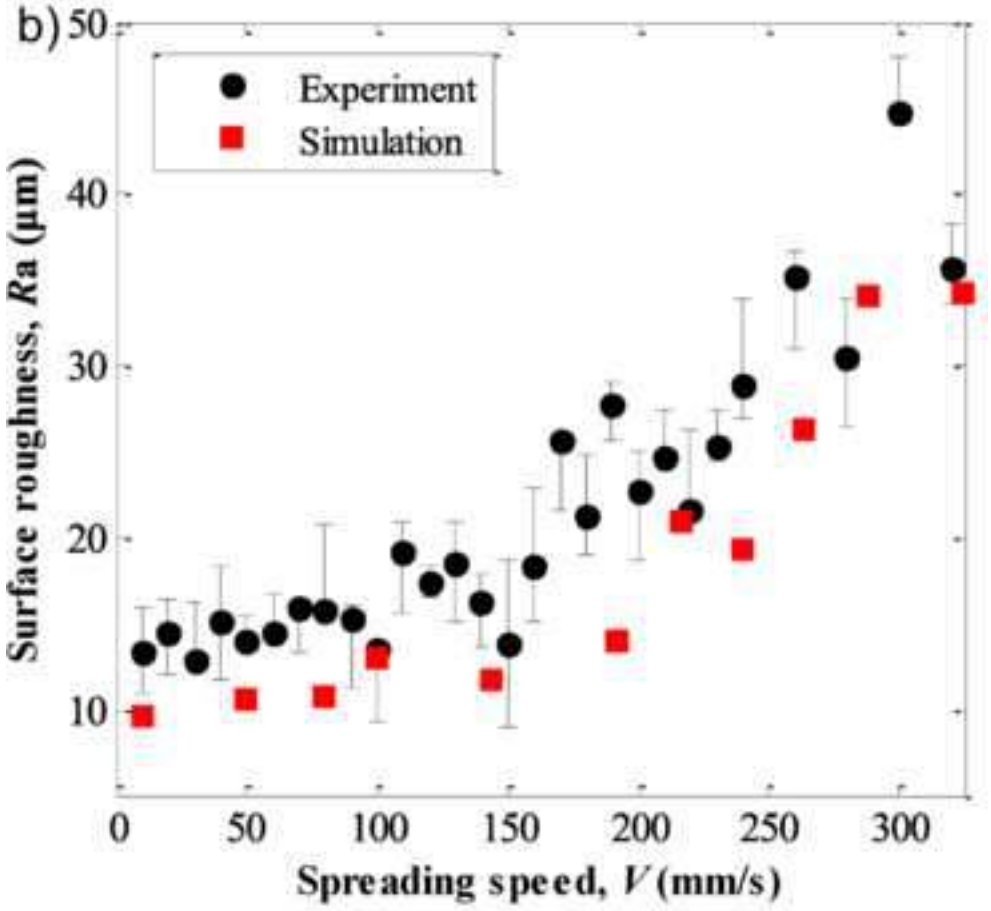

Fig_32

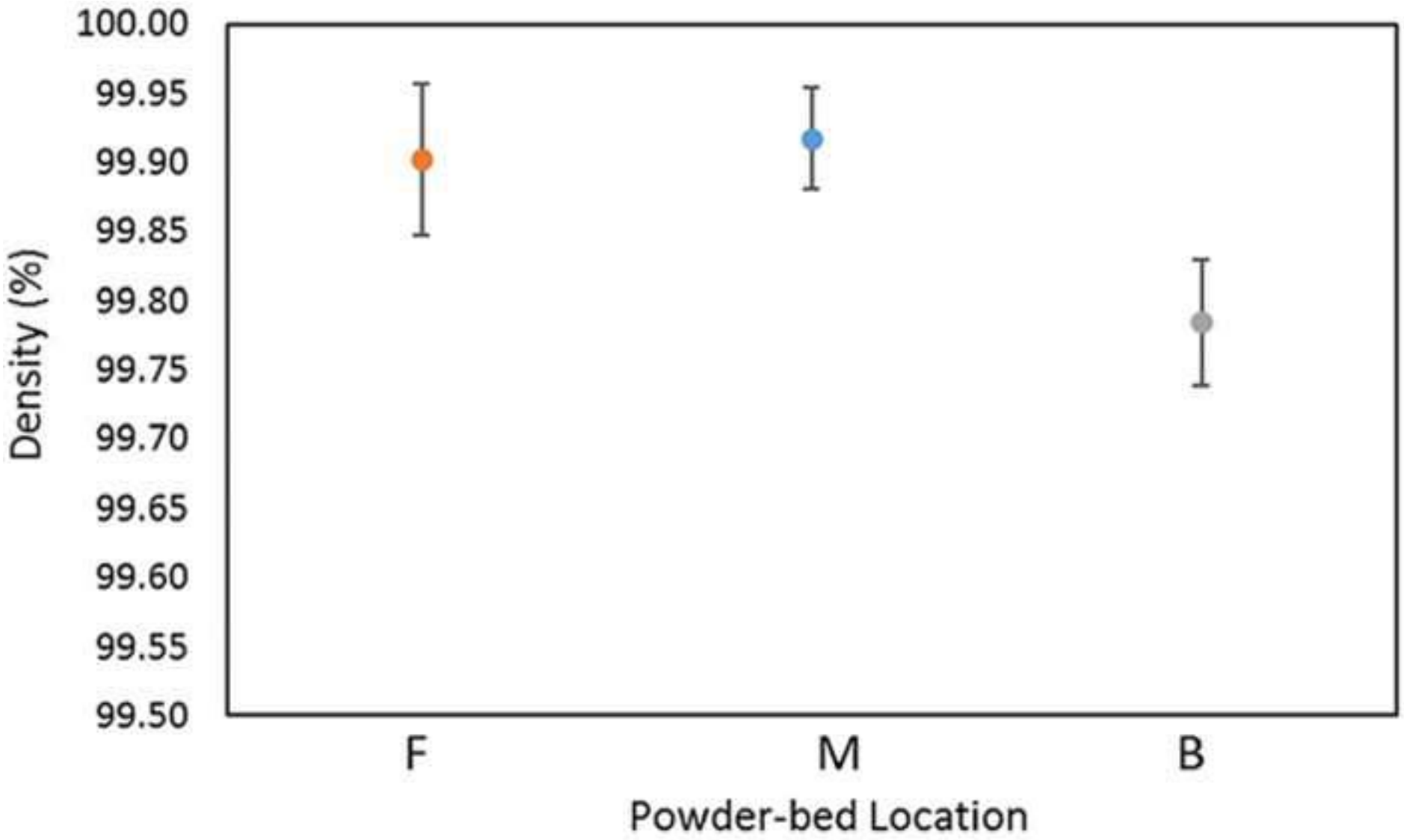

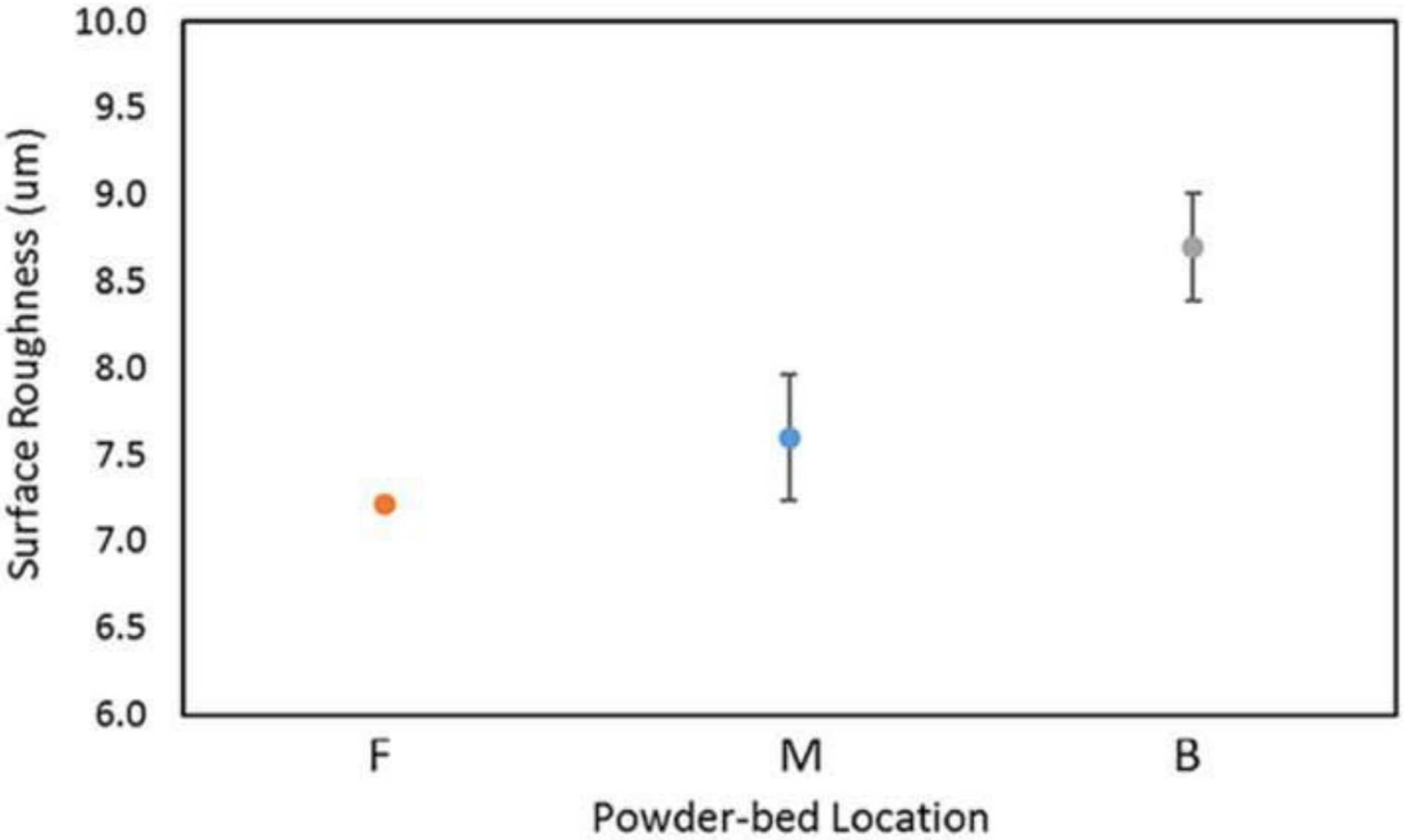

Table 1 - AM technologies used in processing metal powders.

Category	*Process*	*Heat source / temperature*	*Raw materials (metals)*	*Powder size distribution (approx.)*	*Layer thickness (approx.)*	*Ref.*
Powder-bed fusion	Selective Laser Melting (SLM)	high-intensity laser / above melting point	Iron-based (316L, 420, M2), titanium and titanium based (Ti6Al4V, TiAl), aluminium-based (AlSi, AlCu, AlZn), nickel-based (Inconel 625, 718), copper, niobium, tantalum, bio-material metals–polymers and metals–ceramics combinations	10 – 50 µm	20 – 100 µm	(Bo et al., 2020; Chin et al., 2020; Tiwari et al., 2015)
	Selective Laser Sintering (SLS)	high-intensity laser / below melting point				
	Electron Beam Melting (EBM)	Electron Beam / above melting point	Ti grade 2, Ti6Al4V, Inconel 718, CoCrMo; alloys having volatile constituents, e.g., Zn, Mg, Pb, Bi, are not advisable.	40 – 100 µm	50 – 200 µm	(Chin et al., 2020; Gokuldoss et al., 2017; Sames et al., 2016)
Directed energy deposition	Powder directed energy deposition	Laser, arc or e-beam / above melting point	Titanium alloy (Ti-22Al-23Nb, Ti-6Al-4V, Ti-6.5Al-3.5Mo-1.5Zr-0.3Si, Ti-5Al-5Mo-4V-1Cr-1Fe), Steel (10V, 15-5 PH, 410, AISI 309Aremet 10, A2, MM10), Nickel based superalloy (CMSX-3, Haynes188, Haynes230, IN600, IN690, IN713, Rene 142, Rene N5), Aluminum alloy (CP Al, 6061, 2024)	20–200 µm	200–800 µm	(Chin et al., 2020; Saboori et al., 2017; Sames et al., 2016)

Table 2 – Calibration method used for powders used in AM.

Authors	Material	Particles			Calibration method	
		Type	Polydispersity	Cohesion	Experimental	Simulation
Geer et al., 2018 (Geer et al., 2018)	Gas atomized stainless steel (17-4SS) powder	Spherical	20 – 75 μm	no	AOR obtained from the flow through a fixed funnel	AOR obtained from the flow through a fixed, down-scaled funnel and from clouds of powders
Meier et al, 2019 (Meier et al., 2019b)	Ti-6Al-4V	Spherical	20 – 160 μm	yes	AOR obtained from the flow through a fixed funnel	AOR obtained from the flow through a fixed, down-scaled funnel
Desai et al., 2019 (Desai et al., 2019)	Ti-6Al-4V	Spherical	Monosized 250 μm	no	AOR + powder rheometer	AOR + powder rheometer

Table 1 – Calibration method used for powders used in AM.

Authors	Material	Particles			Calibration method	
		Type	Polydispersity	Cohesion	Experimental	Simulation
Geer et al., 2018 (Geer et al., 2018)	Gas atomized stainless steel (17-4SS) powder	Spherical	20 – 75 μm	no	AOR obtained from the flow through a fixed funnel	AOR obtained from the flow through a fixed, down-scaled funnel and from clouds of powders
Meier et al, 2019 (Meier et al., 2019b)	Ti-6Al-4V	Spherical	20 – 160 μm	yes	AOR obtained from the flow through a fixed funnel	AOR obtained from the flow through a fixed, down-scaled funnel
Desai et al., 2019 (Desai et al., 2019)	Ti-6Al-4V	Spherical	Monosized 250 μm	no	AOR + powder rheometer	AOR + powder rheometer

Table 4 – Summary of the standardized tests to access spreadability

Table 1 – Simulation studies of powder spreading.

Authors	*Powders*	*Spreader*	*Variables studied*	*Metrics*
Mindt et al., 2016 (Mindt et al., 2016)	Spherical, polydisperse (15 – 70 µm), non-cohesive, Ti-6Al-4V particles	Flat spreader	Gap thickness	Bed particle fraction,
Haeri et al., 2016 (Haeri et al., 2016)	Rods (overlapping multi-sphere method), polydisperse, non-cohesive, polyether ether ketone (PEEK) particles	Roller spreader, flat spreader	Particle shape, gap thickness, roller velocity, blade velocity	Particle shape segregation, bed particle fraction, surface roughness, probability density function (PDF) for the spatial distribution of orientation
Parteli and Pöschel, 2016 (Parteli and Pöschel, 2016)	Non-spherical (overlapping multi-sphere method), polydisperse (30 – 100 µm) cohesive, Polymer PA12	Roller spreader	Roller velocity	Gap thickness
Chen et al. (Chen et al., 2017)	Spherical, polydisperse (9–140 µm), cohesive, 316L powder	Flat spreader	Cohesion, sliding and rolling friction, particle size, blade height, and velocity	Mass flow rate, dynamic repose angle
Gunasegaram et al., 2017 (Gunasegaram et al., 2017)	Elliptical, polydisperse (37 - 183 µm), non-cohesive, Ti-6Al-4V particles	Flat spreader		
Haeri, 2017 (Haeri, 2017)	Rods and irregular (overlapping multi-sphere method), polydisperse, non-cohesive, polyether ether ketone (PEEK) particles	From flat to rounded spreaders	Blade velocity, design of blade profile	Bed particle fraction, surface roughness
Nam et al., 2018 (Nan et al., 2018)	Non-spherical (overlapping multi-sphere method), polydisperse (15 – 55 µm) cohesive, gas-atomized 316 L stainless steel particles	Flat spreader	Gap thickness	Particle fraction, Frequency of empty patches, Frequency distribution of jamming
Chen et al., 2019 (Chen et al., 2019)	Spherical, polydisperse (5 – 80 µm), AISI 316L stainless steel powder	Flat spreader	Particle size, polydispersity, the effect of the wall, cohesion energy	Bed packing fraction, powder flow, percolation
Meier et al., 2019 (Meier et al., 2019a)	Spherical, polydispersed (20 - 44 µm), cohesive, titanium alloy (Ti-6Al-4V) particles	Flat spreader	Gap thickness, cohesion energy	Surface profile, bed packing fraction
Nam and Ghadiri, 2019 (Nan and Ghadiri, 2019)	Non-spherical (overlapping multi-sphere method), polydisperse (15 – 55 µm) cohesive, gas-atomized 316 L stainless steel particles	Flat spreader	Gap thickness, blade velocity	Mass flow rate through the gap, Shear band
Gu et al., 2019 (Gu et al., 2019)	Spherical, polydispersed, cohesive, WC/Inconel 718 composite powders	Flat spreader	Effect of powder bed on thermodynamics and laser processability	
Ma et al., 2020 (Ma et al., 2020)	Spherical, polydispersed, cohesive powder	Flat spreader	Presence of fine fraction	Packing fraction, coordination number, surface roughness
Fouda and Bayly, 2020 (Fouda and Bayly, 2020)	Spherical, mono-sized (50 µm), non-cohesive titanium alloy (Ti-6Al-4V) particles	Flat spreader	Gap thickness, blade velocity	Bed packing fraction
Chen et al., 2020 (Chen et al., 2020)	Spherical, polydisperse (5 – 80 µm), cohesive, 316 L stainless steel powder	Counter-rolling spreader	Gap thickness, blade velocity	Mass flow rate through the gap, normal stress on bed, surface profile, bed packing fraction
He et al., 2020 (He et al., 2020)	Spherical, mono-sized (50 µm), cohesive, plasma atomised Ti-6Al-4V particles	Flat spreader		Packing density, surface roughness, density pore, chamber pore

Nam et al., 2020 (Nan et al., 2020)	Non-spherical (overlapping multi-sphere method), polydisperse (15 – 55 μm) cohesive, gas-atomised 316 L stainless steel particles	Counter-rolling spreader	Roller rotational speed, gap thickness	Particle segregation, mass flow rate of particles through the gap, normalised spread particle volume
Lee et al., 2020 (Lee et al., 2020)	Spherical, polydisperse (30 - 100 μm), cohesive, Co–Cr powder	Flat spreader	Number of layers, spreader velocity,	Height of the layer, dynamic AOR, packing density, particle size distribution
Wang et al., 2020 (Wang et al., 2020)	Spherical, polydisperse (30 - 90 μm), cohesive, Hastelloy X (HX) powder	Roller spreader, flat spreader	Cohesiveness, particle size distribution,	Packing fraction, surface roughness, properties along spreading direction
Yao et al., 2021 (Yao et al., 2020)	Spherical, monosizes (34.8, 100, 123.2, 169.4 μm), cohesive, 316 L stainless steel powder	Flat spreader	Particle size, sprading velocity, gap heigh, blade angle	Packing density and its evolution, pore size, particle velocity distribution,

Table 1 list of in-situ, ex-situ and simulation techniques to determine powder spreadability.

Name	Pros	Cons
Open applicator	Imitate real AM equipment	requires a visual inspection of the layer
Funnel Applicator	Measures powder spreadability	Higher deviation
Modular powder spreading	Totally automated requires only a little powder	-
Hegman gauge	Fast measurement of spreadability	only qualitatively results are achieved
Visible light Camera	Measures the dynamic repose angle of powders	Only a limited amount of information can be obtained
X-ray imaging	Higher resolution, capable of identifying cluster formation	-
Continous approach	Evaluates powder behaviour based on fluid dynamic Models	Old equations. Not very widespread among researchers and end-users
Discrete approach	simulation of powder-powder interactions	requires a calibration process, high computing power demanding
AI/digital twins	Highly customizable	requires a calibration process, high computing power demanding

Table 1 – Summary of the standardized tests to access spreadability

Method	*Characterization parameter*	*Link with spreadability*
Rheometer (FT-4)	Basic flow energy (BFE)	Higher its value, lower the spreadability because of the higher flowing resistance (Brika et al., 2020; Clayton, 2014; Clayton et al., 2015). Exceptions have been shown (Balbaa et al., 2020).
Rheometer (FT-4)	Specific energy (SE)	Higher its value lower the spreadability because of the higher flowing resistance (Balbaa et al., 2020; Brika et al., 2020; Clayton et al., 2015)
Rheometer (FT-4)	Conditioned bulk density (CBD)	Higher its value, higher packing density (Balbaa et al., 2020; Brika et al., 2020)
Rheometer (FT-4)	Compressibility index (CI)	Lower its value, higher packing density (Brika et al., 2020)
Rheometer (FT-4)	Permeability (pressure drop, PD)	Higher permeability (lower PD), higher packing density because of the better ability to release entrapped air (Brika et al., 2020)
Rheometer (FT-4)	Aeration energy (AE)	Lower its value, higher powder bed uniformity because of a lower tendency to agglomerate (Brika et al., 2020)
Rheometer (FT-4)	Cohesion coefficient (c)	Lower its value, powder bed uniformity because of a lower mechanical interlocking and higher tendency to shear (Brika et al., 2020)
Rotating Drum (Revolution powder analyzer)	Avalanche angle (AA)	Higher its value, lower spreadability because of greater resistance to flow (Kiani et al., 2020; Snow et al., 2019)
Rotating Drum (Revolution powder analyzer)	Break energy (BE)	Higher its value, lower spreadability because of greater resistance to flow (Kiani et al., 2020)
Rotating Drum (Revolution powder analyzer)	Avalanche energy (AE)	Higher its value, lower spreadability because of greater resistance to flow (Snow et al., 2019)
Rotating Drum (Revolution powder analyzer)	Avalanche average angle	Higher its value, lower spreadability because of greater resistance to flow (Snow et al., 2019)
Rotating Drum (Revolution powder analyzer)	Avalanche surface fractal	Lower its value, better flowability with no agglomeration (Sillani et al., 2019)
Hall Flowmeter	Apparent/bulk density (ρ_B)	Poor connection with the lower limit of packing density in the powder layer
Hall Flowmeter	Tap density (ρ_T)	Poor connection with the upper limit of packing density in the powder layer
Hall Flowmeter	Hausner ratio (HR)	Succefful spreading with no lack-of-fusion porosity if HSR < 1.25 (Dobson and Starr, 2020)
Hall Flowmeter	Angle of repose (AOR)	Higher the AOR, higher powder cohesion and lower flowability (Tan et al., 2017). Higher the AOR, poorer the spreadability (Snow et al., 2019). AOR > 40° exhibited poor flowability for high spreading velocities
Hall Flowmeter	Hall flow rate (HF)	Unsuitable method: powders that were not able to flow freely through the funnel were spread without problems (Choi et al., 2017; Mitterlehner et al., n.d.); powders with the same flow rate presented different spreadability (Clayton et al., 2015).